A THEORETICAL INVESTIGATION

OF THE REMOVAL

OF ATMOSPHERIC TRACE CONSTITUENTS

BY MEANS OF A DYNAMIC MODEL

Dissertation

zur Erlangung des Grades

"Doktor der Naturwissenschaften"

am Fachbereich Physik

der Johannes Gutenberg-Universität in Mainz

Andrea Ilse Floßmann

geboren in Berlin

Mainz 1986

Abstract

A theoretical model is formulated which allows to study the wet removal of atmospheric pollutants during the cloud formation and precipitation stages of a convective cloud. For the first time the microphysical processes of condensation, collision-coalescence, impaction scavenging of aerosol particles, and gas scavenging are coupled with the dynamics of a cloud in such a manner that for a given uniform aerosol type and particle size distribution, and for a given pollutant gas concentration (chosen to be SO_2) in the air, the evolution in time of the drop size distribution, the pollutant mass inside the drops, the aerosol mass remaining in the air as drop-interstitial aerosol, and the environmental gas concentration can be determined during the cloud formation and precipitation stage. The dynamic behavior of the considered cloud is modeled by means of an entraining air parcel and in a more detailed manner by the two dimensional convective cloud model of Clark et al.

This study leads to the following conclusions: (1) Collision and coalescence causes among the various drop size categories a re-distribution of the scavenged pollutant mass in such a manner that the main pollution mass is always associated with the main water mass, i.e. is contained inside the larger drops which may reach the ground as precipitation. (2) In contrast to the pollution mass scavenged from aerosol particles which causes that smaller drops are always more contaminated than larger ones, the amount of SO_2 scavenged is a function of time, a function of the concentration of SO_2 in the air, and a function of the oxidation rate of the sulfur in the drops. (3) For in-cloud scavenging and for typical SO_2 and $(NH_4)_2SO_4$ particle concentrations in the atmosphere it is found that sulfur scavenging from SO_2 dominates sulfur scavenging from $(NH_4)_2SO_4$ particles, if the oxidation rate inside the cloud drops is high ($K' > 0.01\ sec^{-1}$) and vice versa. (4) A comparison of the results of in-cloud scavenging of SO_2 with below-cloud scavenging shows, that below-cloud scavenging contributes less than 30% to the total amount of sulfur scavenged from SO_2. (5) A comparison of the nucleation scavenging (=in-cloud

scavenging) of $(NH_4)_2SO_4$ particles to the impaction scavenging (=below-cloud scavenging) yields, that impaction scavenging contributes only about 20% to the overall scavenged aerosol mass. (6) Nucleation scavenging causes inside a cloud a drop-interstitial aerosol which consists of a particle population reduced significantly in number and mass as compared to the particle population outside the cloud. (7) A broadening of the original aerosol particle size distribution and a lowering of the total particle concentration results in an enhancement of the likelihood of a cloud to precipitate, if the $(NH_4)_2SO_4$ particles are allowed to go through several cloud forming, cloud evaporation cycles.

Acknowledgements

I would like to extend my deepest appreciation to Professor Dr. Hans R. Pruppacher, without whose guidance this dissertation would not have been possible.

I also would like to thank Renate Forkel, Andreas Bott and Wolfram Wobrock for their scientific advice, helpful discussions and friendship.

The one person I would like to single out for special recognition is Dr. William D. Hall from the National Center for Atmospheric Research (NCAR) in Boulder, Colorado. He introduced me to cloud modeling, provided me with his microphysical model, a lot of computer time and neverending help.
Furthermore I would like to express my deepest appreciation to Dr. Terry L. Clark, also from NCAR, who furnished me with one of the best cloud dynamic models in existence and greatly helped in installing it in Germany during his stay at the DFVLR.
And I would like to thank Dr. Piotr Smolarkiewicz from NCAR for explaining me how to handle the two dimensional model and his help in setting up a dynamic case.

Acknowledgements further go to Dr. Ulrich Schumann and Dr. Thomas Jank from the DFVLR in Oberpfaffenhofen and Michael Holzmeier from the CRAY company in providing assistance in our difficult undertaking in installing the model in Germany.

I also would like to express appreciation to Professor Dr. Paul Crutzen, Director of the Max-Planck-Institut of air chemistry in Mainz, for giving us access to their CRAY-1A computer and for furnishing us with computer time.
Finally I am very grateful to Dr. Lutz Schäfer, also from the Max-Planck-Institut, for his help with all my computer problems.

The numerical calculations were carried out with the computers BULL DPS8/70 of the computer center at the Johannes Gutenberg-Universität in Mainz, the CRAY-1A of the NCAR in Boulder, Colorado and the CRAY-1A of the Max-Planck-Institut für Plasmaphysik in Garching near Munich.

Table of contents: page

I Introduction

It has been well established that the loading of the atmosphere by pollutants is determined on the one hand by the rate at which these pollutants are introduced into the atmosphere and, on the other hand, by the rate at which they are removed by dry and wet deposition involving clouds and precipitation. These pollutants can be solid, i.e. aerosol particles, or gaseous. In warm clouds, with which we shall be exclusively concerned here, wet deposition of aerosol particles operates via the removal by condensation (nucleation scavenging), i.e., by transforming some of the aerosol particles into drops as a result of drop nucleation from the vapor, and via the removal by impaction (impaction scavenging), i.e. by attaching aerosol particles to cloud and rain drops through the mechanisms of Brownian diffusion, inertia, hydrodynamic forces and through phoretic and electric forces. Gaseous constituents are removed by convective diffusion into the drops where they may be oxidized. The scavenged material is then transported to the ground by the drops if the cloud precipitates.

Little is known of the relative efficiency of these mechanisms. Field observations of Radke(1983) and Hegg and Hobbs(1983) suggest, however, that nucleation scavenging is of considerable importance to the overall scavenging mechanism. From their field observations they concluded that a major amount of the sulfate mass inside a cloud enters a drop via drop nucleation on sulfate particles (about 60-70%), while a usually smaller amount of sulfate enters by gas scavenging via oxidation to sulfate of the scavenged SO_2, and a still smaller amount enters via impaction scavenging of sulfate particles. They also deduced that through nucleation scavenging the total number concentration of aerosol particles decreases by 80 to 92% across the cloud base as a result of nucleation scavenging, whereby the particles of radii larger than 0.1 μm are most efficiently reduced.

Since the results on nucleation scavenging are only based on relative crude estimates, further quantitative studies are needed to arrive at a general view of the relative importance of nucleation and impaction scavenging, both of which not only determine the amount of aerosol particle mass inside the cloud water but also control the aerosol par-

ticle population located in the air between the drops (cloud interstitial aerosol). Only Murakami et al.(1983) concluded from their field observations that 20% of the mass of sulfate particles in the rainwater resulted from below-cloud scavenging as compared to 80% from in-cloud scavenging.

The gas scavenging, however, is mainly determined by the governing oxidation rates in the drops. Unfortunately the results of Radke(1983) and Hegg and Hobbs(1983) scattered so widely that no clear dependence on the rate of oxidation inside the cloud water could be determined. Also, no information was obtained on the variation with time of the efficiency of the sulfur-uptake mechanisms.

A study of literature further illustrates that little is known of the fate of the scavenged pollutants once they have been captured by cloud drops through nucleation, impaction and gas scavenging. Thus, it is expected that during the growth of the cloud drops by the stochastic collision-coalescence process a substantial re-distribution of the uptaken mass would take place. This expectation raises the question of whether during this re-distribution the pollutant loading will prefer certain drop size classes.

In order to shed more light on these questions, numerical models are a feasible approach. But the few theoretical models that exist on the scavenging problem are based on the 'Kessler' parameterization (e.g. Chaumerliac(1984)), which only distinguishes between cloud water and rain water. However, the scavenging mechanisms are significantly size dependent. So theoretical studies need to model the aerosol particle and drop spectra.

In order to remedy these insufficiencies, we have extended the microphysical model of Hall (1980) to formulate a theoretical model in which the condensation process, the collision-coalescence process, the process of impaction scavenging of aerosol particles, and the process of gas scavenging are coupled in such a manner that for a given aerosol type and particle size distribution, and a given gas concentration in the air the evolution in time of the drop size distribution, the pollutant mass inside the drops, the aerosol mass remaining in the air as drop-interstitial aerosol, and the environmental gas concentration can be determined.

This scavenging model we have linked to an entraining air parcel model

and to the two dimensional dynamic cloud model which was developed by Clark et al. (i.e. Clark(1977,1979) and Clark, Farley(1984)). To be able to qualitatively compare our results to the field observations of Radke(1983), Hegg and Hobbs(1983) and Murakami et al.(1983) we confined ourselves to the study of the removal of sulfur. So the aerosol particles are assumed to consist mainly of ammonium sulfate $(NH_4)_2 SO_4$ and the gas is set to be sulfur dioxide SO_2.

In chapter II we have formulated our model for the study of the aerosol scavenging processes alone. The model starts from a given aerosol particle size distribution of uniform composition and enables studying the effects of condensation, nucleation and impaction scavenging, and the effects of the collision-coalescence process on the drop and aerosol particle distribution in the air, and on the aerosol particle mass distribution inside the drops. In chapter III we have added gas scavenging with oxidation processes to this model to study the relative importance of the scavenging mechanisms depending on various oxidation rates. Chapter IV describes how our scavenging model is incorporated in an entraining air parcel model, and in chapter V we present our model for pure aerosol scavenging linked with the two dimensional dynamic model of Clark et al. Chapter VI describes some numerical properties of the model. In the first part of chapter VII we present the results of the pure aerosol particle scavenging in the entraining air parcel model. The second part of chapter VII contains the results of aerosol particle and gas scavenging in the entraining air parcel model while the third part describes the results of pure aerosol particle scavenging in the two dimensional cloud model of Clark et al. In chapter VIII some final remarks and suggestions for future research are made.

In this presentation we do not adhere to the unit system MKS but rather use the units most appropriate for our study and also most commonly found in literature.

II Theoretical formulation of the scavenging of aerosol particles

In this chapter a theoretical model is formulated which describes the time evolution of a drop size distribution originating on aerosol particles of a given size distribution and of given uniform composition, and the subsequent growth of the drops by condensation and collision and coalescence. The model also describes the simultaneously occuring time evolution of the aerosol particle mass captured by and redistributed among the various cloud drop size categories, and the simultaneously taking place time evolution of the mass and size distribution of the aerosol particles left unactivated in the air as drop interstitial aerosol.

II.1 The general model equations

In order to model the state of the atmosphere we need a set of equations which describe the evolution in time of the main atmospheric variables. These have to meet certain conservation requirements.
As the equations will have to apply to a model of finite grid spacing we shall use them in a form where the values represent averages over the grid domain and the time step (Pielke(1984)).
From mass conservation we obtain an equation for the density ρ_a (all variables are defined in the list of symbols):

$$\frac{\partial \rho_a}{\partial t} = - \nabla \cdot (\rho_a w) \qquad \text{(II-1)}$$

In the present study we are exclusively concerned with warm clouds. Therefore, the water budget can be described by an equation for the moisture field w_v and one for the total liquid water content w_L^* :

$$\frac{\partial w_v}{\partial t} = - \nabla \cdot (w_v w) - \nabla \cdot \mathbb{J}^v - C_{Ph} \qquad \text{(II-2)}$$

$$\frac{\partial w_L^*}{\partial t} = - \nabla \cdot (w_L^* w) - \nabla \cdot \mathbb{J}^L + C_{Ph} + \frac{\partial}{\partial z} (V_\infty w_L^*) \qquad \text{(II-3)}$$

The first term on the right hand side of equation (II-2) and (II-3) represents the advection process. The second term describes the flux

due to subgrid scale perturbations. Other fluxes will be neglected in this study. The flux $\mathbb{J}^{\psi}$ is parameterized by the gradient of ψ:

$$\mathbb{J}(\psi) = - K_m(\psi) \nabla \psi \qquad \text{(II-4)}$$

K_m is called the turbulent eddy mixing coefficient and generally is a function of the transported quantity. The third term on the right hand side of eqs.(II-2) and (II-3) represents the rate of phase change due to condensation or evaporation. The last term of eq.(II-3) describes the sedimentation of the liquid water.

From Newton's second law we can derive the equation of motion in the system of the rotating earth:

$$\frac{\partial w}{\partial t} = - w \cdot \nabla w - \frac{1}{\rho_a} \nabla p + \frac{1}{\rho_a} \nabla \cdot \mathbb{J} - \nabla \phi - 2 \Omega \times w \qquad \text{(II-5)}$$

where the first term represents the advection, the second term the pressure gradient force, and the third term the dissipation stress due to subgrid scale perturbations. The fourth term describes the gravitational force, and the fifth term the coriolis force.

From the first law of thermodynamics we find for the heat transport:

$$c_{pa} \frac{\partial \rho_a T}{\partial t} = - c_{pa} \nabla \cdot (\rho_a T w) - \nabla \cdot \mathbb{J}^{\vartheta} + \frac{dp}{dt} + L_v C_{ph} \qquad \text{(II-6)}$$

where the first term represents the advection, the second term describes the flux due to subgrid scale temperature perturbation. Other fluxes and dissipation processes are neglected. The third term represents pressure changes, and the last term phase change induced heating rates due to condensation or evaporation. $\mathbb{J}^{\vartheta}$ as well as $\mathbb{J}$ can be parameterized similar to eq.(II-4).

Equation (II-3) offers a way to treat the liquid water content w_L^*. However, in cloud models this treatment is not satisfactory since it gives no clue on how the liquid water mass is distributed among the various possible drop sizes. For example, it gives us no information on how many precipitation-sized drops are formed.

To get this kind of information from a cloud model we have to include formulations which keep track of the drop size distribution. If we

want to model aerosol scavenging we also have to include formulations which keep track of the aerosol particle distribution.

II.2 The microphysical equations

In order to formulate the model which describes the microphysical processes, we introduce the number and mass density distribution functions f and g.

Commonly the cloud drop spectrum is represented by a one dimensional number density function $f_d(m)$. This function is defined such that $f_d(m)\,\delta m$ is the number of droplets per unit volume between the mass m and $m+\delta m$.

$f_d(m)$: cloud drop number density distribution function

Analogously we define:

$g_{APd}(m)$: mass density distribution function for aerosol particles in cloud water

$f_{APa}(m_{AP})$: unactivated aerosol particle number density distribution function in air

$g_{APa}(m_{AP})$: aerosol particle mass density distribution function in unactivated aerosol particles

In there m is the total mass of one drop (=water mass + aerosol particle mass), m_{AP} is the total mass of unactivated aerosol particles (= water mass + aerosol particle mass) and the subscripts AP, d and a stand for aerosol particle, drop and air, respectively.

The time rate of change of the drop number density distribution function may be expressed as:

$$\begin{aligned}\frac{\partial f_d(m)}{\partial t} = &- \nabla\cdot\left(\vec{v}\, f_d(m)\right) + \nabla\cdot\left(K_m \nabla f_d(m)\right) \\ &+ \frac{\partial}{\partial z}\left(V_\infty f_d(m)\right) + \left.\frac{\partial f_d(m)}{\partial t}\right|_{act} \\ &+ \left.\frac{\partial f_d(m)}{\partial t}\right|_{con/eva} + \left.\frac{\partial f_d(m)}{\partial t}\right|_{AP,\,coll} \\ &+ \left.\frac{\partial f_d(m)}{\partial t}\right|_{d,\,coal} + \left.\frac{\partial f_d(m)}{\partial t}\right|_{d,\,break}\end{aligned} \qquad \text{(II-7)}$$

the time rate of change of the mass density distribution function for aerosol particles in cloud water:

$$\frac{\partial g_{APd}(m)}{\partial t} = -\nabla\cdot\left(w\, g_{APd}(m)\right) + \nabla\cdot\left(K_m \nabla g_{APd}(m)\right) + \frac{\partial}{\partial z}\left(V_\infty g_{APd}(m)\right) + \left.\frac{\partial g_{APd}(m)}{\partial t}\right|_{act} + \left.\frac{\partial g_{APd}(m)}{\partial t}\right|_{con/eva} + \left.\frac{\partial g_{APd}(m)}{\partial t}\right|_{AP,\,coll} + \left.\frac{\partial g_{APd}(m)}{\partial t}\right|_{d,\,coal} + \left.\frac{\partial g_{APd}(m)}{\partial t}\right|_{d,\,break} \qquad \text{(II-8)}$$

the time rate of change of the unactivated aerosol particle number density distribution function in air:

$$\frac{\partial f_{APa}(m_{AP})}{\partial t} = -\nabla\cdot\left(w\, f_{APa}(m_{AP})\right) + \nabla\cdot\left(K_m \nabla f_{APa}(m_{AP})\right) + \left.\frac{\partial f_{APa}(m_{AP})}{\partial t}\right|_{act} + \left.\frac{\partial f_{APa}(m_{AP})}{\partial t}\right|_{con/eva} + \left.\frac{\partial f_{APa}(m_{AP})}{\partial t}\right|_{AP,\,coll} \qquad \text{(II-9)}$$

and the time rate of change of the aerosol particle mass density distribution function in unactivated aerosol particles:

$$\frac{\partial g_{APa}(m_{AP})}{\partial t} = -\nabla\cdot\left(w\, g_{APa}(m_{AP})\right) + \nabla\cdot\left(K_m \nabla g_{APa}(m_{AP})\right) + \left.\frac{\partial g_{APa}(m_{AP})}{\partial t}\right|_{act} + \left.\frac{\partial g_{APa}(m_{AP})}{\partial t}\right|_{con/eva} + \left.\frac{\partial g_{APa}(m_{AP})}{\partial t}\right|_{AP,\,coll} \qquad \text{(II-10)}$$

The first term on the right hand side of eqs.(II-7) to (II-10) describes the advection of the quantity while the second term refers to the turbulent mixing. The third term on the right hand side of (II-7) and (II-8) describes the sedimentation effect of drops. No such

term appears in eqs.(II-9) and (II-10) as we assume that the terminal velocity V_∞ of the aerosol particles can be neglected compared to the vertical velocity of the air.

The other terms are characterized by their subscripts. Thus:

$( )|_{act}$: activation of aerosol particles to form drops or deactivation of drops (represents the nucleation scavenging)

$( )|_{con/eva}$: size changes due to condensation or evaporation

$( )|_{AP,coll}$: changes due to drops collecting aerosol particles (represents impaction scavenging)

$( )|_{d,coal}$: collision and coalescence of drops

$( )|_{d,break}$: break up of big drops

We disregard here all collision and coalescence processes among aerosol particles themselves. Though we are aware that they modify the aerosol spectrum considerably during the course of time they are not the concern of this study.

II.3 Additional definitions

To formulate the time rates of change of the distribution functions introduced above, we assume that all drops between m and $m+\delta m$ are of the same size and carry the same amount of aerosol particle mass each. The same is assumed for the aerosol particles between m_{AP} and $m_{AP}+\delta m_{AP}$. We equivalently could have assumed a distribution of aerosol particle mass inside each category. The variables then would refer to the averaged quantity over one interval.

This enables us to define a mixing ratio of aerosol particle mass inside the drop mass interval:

$$Q_{APd}(m) = \frac{g_{APd}(m)}{m\, f_d(m)} \qquad \text{(II-11)}$$

$$= \frac{\text{mass of aerosol particles in one drop}}{\text{mass of the drop}}$$

Analogously the mixing ratio of aerosol particle mass inside the unactivated aerosol particle mass interval is:

$$Q_{APa}(m_{AP}) = \frac{g_{APa}(m_{AP})}{m_{AP}\, f_{APa}(m_{AP})} \qquad \text{(II-12)}$$

The water mass in one drop interval m,m+δm per unit volume is

$$g_w(m) = m\, f_d(m)\left(1 - Q_{APd}(m)\right) \qquad \text{(II-13)}$$

and the water mass in one unactivated aerosol particle category $m_{AP}, m_{AP}+\delta m_{AP}$ per unit volume is

$$g_{wa}(m_{AP}) = m_{AP}\, f_{APa}(m_{AP})\left(1 - Q_{APa}(m_{AP})\right) \qquad \text{(II-14)}$$

With these quantities we can rewrite

$$Q_{APd}(m) = \frac{g_{APd}(m)}{g_{APd}(m) + g_w(m)} \qquad \text{(II-15)}$$

$$Q_{APa}(m_{AP}) = \frac{g_{APa}(m_{AP})}{g_{APa}(m_{AP}) + g_{wa}(m_{AP})} \qquad \text{(II-16)}$$

Furthermore we can calculate

N_d : total number of drops per unit volume

$$N_d = \int_0^\infty f_d(m)\, dm \qquad \text{(II-17)}$$

N_{APa} : total number of unactivated aerosol particles in air per unit volume

$$N_{APa} = \int_0^\infty f_{APa}(m_{AP})\, d m_{AP} \qquad \text{(II-18)}$$

w_L : liquid water content of the drops

$$w_L = \int_0^\infty g_w(m)\, dm \qquad \text{(II-19)}$$

w_{LAP} : liquid water content of the unactivated aerosol particles

$$w_{LAP} = \int_0^\infty g_{wa}(m_{AP})\, dm_{AP} \qquad \text{(II-20)}$$

w_L^* : total liquid water content

$$w_L^* = w_L + w_{LAP} \qquad \text{(II-21)}$$

w_{APd} : total aerosol particle mass in drops

$$w_{APd} = \int_0^\infty g_{APd}(m)\, dm \qquad \text{(II-22)}$$

w_{APa} : total aerosol particle mass in unactivated aerosol particles

$$w_{APa} = \int_0^\infty g_{APa}(m_{AP})\, dm_{AP} \qquad \text{(II-23)}$$

$\overline{Q}_{APd}$: mean mixing ratio of aerosol mass in drops

$$\overline{Q}_{APd} = \frac{w_{APd}}{w_L + w_{APd}} \qquad \text{(II-24)}$$

$\overline{Q}_{APa}$: mean mixing ratio of aerosol mass in unactivated aerosol particles

$$\overline{Q}_{APa} = \frac{w_{APa}}{w_{LAP} + w_{APa}} \qquad \text{(II-25)}$$

We stated earlier that the mass of the drops m and the mass of the unactivated aerosol particles m_{AP} consist of both water mass and aerosol mass. Since in the model we often use the radius of the constituents instead of their mass a relationship is needed between the two quantities.

To get this relationship we have to assume that all drops and aerosol particles are spheres. This is not necessarily true as experiments on drops by Pruppacher and Beard (1970) and Pruppacher and Pitter(1971) showed. By convention this problem is circumvented by introducing what is known as the equivalent radius 'a'. This radius is defined as the radius of a sphere of the same mass as the deformed drop. Similarly we shall define the radius 'r' of an aerosol particle. With these definitions, the problem is reduced to finding the actual density ϱ of the drops or ϱ_{AP} of the aerosol particles, respectively.

For drops we therefore find the following three equations:

$$m = m_W + m_N \quad \Rightarrow \quad \varrho a^3 = \varrho_W a_W^3 + \varrho_N r_N^3$$

$$V = V_W + V_N \quad \Rightarrow \quad a^3 = a_W^3 + r_N^3 \qquad \text{(II-26)}$$

$$Q_{APd} = \frac{m_N}{m} \quad \Rightarrow \quad Q_{APd} = \frac{\varrho_N r_N^3}{\varrho a^3}$$

where:

ϱ : actual density of the drops

a_W : equivalent radius of the water mass m_W in the drop

r_N : equivalent radius of the dry aerosol particle nucleus of mass m_N in the drop

ϱ_W : density of the water

ϱ_N : density of the dry aerosol particle nucleus.

With these three relationships we can eliminate the unknowns and get:

$$\varrho = \frac{\varrho_W \varrho_N}{\varrho_N + Q_{APd}(m)(\varrho_W - \varrho_N)} \qquad \text{(II-27)}$$

and with eq.(II-11)

$$Q_{APd}(m) = \frac{g_{APd}(m)\,\varrho_N}{V f_d(m) \varrho_W \varrho_N - g_{APd}(m)(\varrho_W - \varrho_N)} \qquad \text{(II-28)}$$

Likewise we find for an aerosol particle:

$$\varrho_{AP} = \frac{\varrho_W \varrho_N}{\varrho_N + Q_{APa}(m_{AP})(\varrho_W - \varrho_N)} \qquad \text{(II-29)}$$

$$Q_{APa}(m_{AP}) = \frac{g_{APa}(m_{AP})\,\varrho_N}{V_{AP} f_{APa}(m_{AP}) \varrho_W \varrho_N - g_{APa}(m_{AP})(\varrho_W - \varrho_N)} \qquad \text{(II-30)}$$

Considering eq.(II-21) and the definition of g_W in (II-13) and g_{Wa} in (II-14) we have to make sure that the 'integration' of eq.(II-7) together with the 'integration' of eq.(II-9) gives us eq.(II-3).

In the following chapters we shall be concerned with the treatment of the terms with subscripts in eqs.(II-7) to (II-10), checking whether they meet this requirement.

II.4 Growth of unactivated aerosol particles by vapor diffusion

As nearly all aerosol particles contain some water soluble material they take up or lose water vapor in accordance with the governing relative humidity of the environmental air. This growth or evaporation by vapor diffusion causes a change in the number and mass density functions of the aerosol particles in air as described by the expressions:

$$\left.\frac{\partial f_{APa}(m_{AP})}{\partial t}\right|_{con/eva} = -\frac{\partial}{\partial m_{AP}}\left(\left.\frac{dm_{AP}}{dt}\right|_{con/eva} f_{APa}(m_{AP})\right) \qquad \text{(II-31)}$$

$$\left.\frac{\partial g_{APa}(m_{AP})}{\partial t}\right|_{con/eva} = -\frac{\partial}{\partial m_{AP}}\left(\left.\frac{dm_{AP}}{dt}\right|_{con/eva} g_{APa}(m_{AP})\right) \qquad \text{(II-32)}$$

where $(dm_{AP}/dt)|_{con/eva}$ represents the growth of a single aerosol particle. Integration of eqs.(II-31) and (II-32) over the aerosol particle spectrum reveals that, as required, the total number and the total aerosol particle mass of the unactivated aerosol particles is conserved (compare eqs.(II-18) and (II-23)). Pruppacher, Klett (1978) show that:

$$\left.\frac{dm_{AP}}{dt}\right|_{con/eva} = 4\pi r \frac{\ln\frac{e_a}{e_{sat,w}} - \frac{A}{r} + \frac{B r_N^3}{r^3 - r_N^3}}{\frac{L_v}{k_a^* T}\left(\frac{L_v M_w}{RT} - 1\right) + \frac{RT}{M_w e_{sat,w} D_v^*}} \qquad \text{(II-33)}$$

with

$$A = \frac{2\sigma_{w,a} M_w}{RT\rho_w} \qquad \text{(II-34)}$$

$$B = \frac{\nu \varepsilon \Phi_s M_w \rho_N}{M_s \rho_w} \qquad \text{(II-35)}$$

for the diffusional growth of a droplet containing water soluble material of fraction $\varepsilon = m_s/m_N$, where m_s is the mass of the water soluble compound in the aerosol particle nucleus of total mass m_N.
From eq.(II-33) follows that for equilibrium $(dm_{AP}/dt)|_{con/eva} = 0$ and

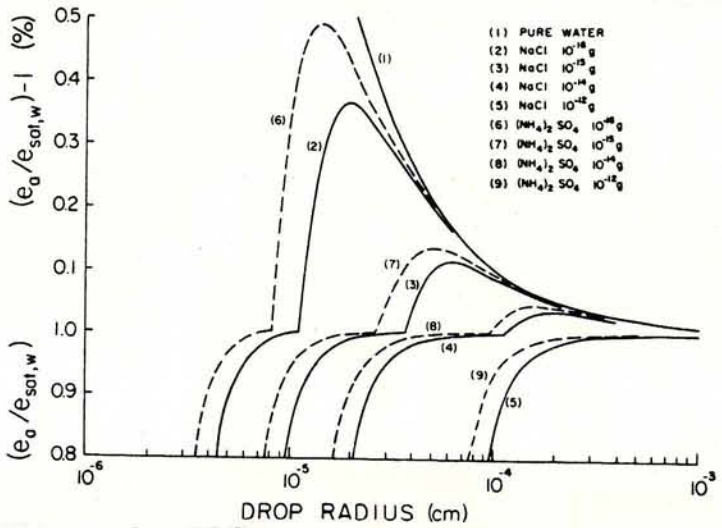

Fig.(II-1): Variations of the equilibrium vapor pressure over an aqueous solution drop with drop size, for various amount of NaCl (solid lines) and $(NH_4)_2SO_4$ (dashed lines) in solution, and for 20°C (Pruppacher and Klett (1978)).

therefore

$$\ln \frac{e_a}{e_{sat,w}} = \frac{A}{r} - \frac{B r_N^3}{r^3 - r_N^3} \qquad \text{(II-36)}$$

which is the well known Koehler equation for the equilibrium condition of an aqueous solution droplet of size r grown on an aerosol particle of size r_N.

If we introduce the new variable y=1/r, we get a fourth order equation

$$y^4 + y^3 \frac{B - \ln \frac{e_a}{e_{sat,w}}}{A} - \frac{1}{r_N^3} y + \frac{\ln \frac{e_a}{e_{sat,w}}}{A r_N^3} = 0 \qquad \text{(II-37)}$$

which can be solved analytically by known algorithms for fourth order equations. From the solution of this equation we obtain the equilibrium radius r_{eq} of a solution droplet as a function of the supersaturation in the environmental air, as represented by the curves in Fig.(II-1) for various values of m_N, i.e. r_N.

Aerosol particles which have acquired sufficient amounts of water so that they have reached sizes which are larger than the critical size represented by the maximum of the Koehler curve are said to have become 'activated' and shall henceforth be considered as 'drops'. These particles will be discussed in section II.5.

Aerosol particles which have acquired only little moisture and are therefore confined to sizes smaller than the critical size represented by the maximum of the Koehler curve are said to remain 'unactivated' and shall henceforth be considered as moist aerosol particles. The growth of these particles to their equilibrium size shall be considered below.

Unfortunately the formulation (II-33) for the particle growth is quite expensive to use in a cloud model since $(dm_{AP}/dt)|_{con/eva}$ becomes larger the smaller the aerosol particle radius. For small aerosol particles the CFL criterion for eqs.(II-31) and (II-32) would require time steps which assume values of 10^{-5} sec or smaller. Such small time steps are unsuitable for the present cloud model. But large growth rates also mean that the aerosol particles reach their equilibrium size very fast. The actual time for this depends on the relative humidity as well as on the size of the aerosol particle. Thus, the larger an aerosol particle the longer its time to reach its equilibrium size. In fact, if the air is supersaturated the time for a large aerosol particle to reach its equilibrium size may be considerably longer than the presently chosen model time step of 2-5 seconds (see Pruppacher and Klett (1978).

In order to remedy this situation we redefine the diffusion velocity in eqs.(II-31) and (II-32) by writing:

$$\frac{\Delta t}{\Delta m_{AP}} \left(\left. \frac{dm_{AP}}{dt} \right|_{con/eva} \right) = \frac{d m_{AP}}{\Delta m_{AP}} \qquad \text{(II-38)}$$

where Δm_{AP} is the spacing of the aerosol particle size intervals and dm_{AP} gives the amount an aerosol particle of starting mass m_{AP}^{τ} grows or shrinks to reach its equilibrium size $m_{APeq}^{\tau+1}$ (from eq.(II-37)), matching the new relative humidity, i.e.

$$d m_{AP} = m_{APeq}^{\tau+1} - m_{AP}^{\tau} \qquad \text{(II-39)}$$

Unfortunately this definition is restricted to relative humidities below 100% as the time for a particle to reach its equilibrium size for a relative humidity above 100% would be prohibitively long in comparison to the time step used in the present model. We therefore had to terminate our computations for the aerosol particle growth at a size

which corresponded to a relative humidity of 100%. This restriction of our model is not serious since it applies only to the very small particles which change very little in size between 100% relative humidity and the critical supersaturation so that the underestimate in the impaction scavenging efficiency can be assumed to be negligible. The large particles will mostly not be affected by this restriction since they will become activated, i.e. change into 'drops', anyway.
Considering now the growth of the small moist aerosol particles we must remember that the diffusion velocity in eqs.(II-31) and (II-32) applies to the boundary between two size interval categories. Thus, m_{AP}^{τ} is the aerosol size at this boundary and represents a staggered quantity (see also chapter VI.1). For calculating the nucleus radius r_N, i.e. the mass m_N , of the dry aerosol particle corresponding to the moist aerosol particle m_{AP}^{τ} we have open two ways. First, we may interpolate between the neighbouring values:

$$m_N = \frac{1}{2} \left\{ \left(\frac{g_{APa}(m_{AP})}{f_{APa}(m_{AP})} \right)_i + \left(\frac{g_{APa}(m_{AP})}{f_{APa}(m_{AP})} \right)_{i+1} \right\} \qquad \text{(II-40)}$$

Secondly, we can make use of the fact that a time step earlier equilibrium existed. Thus, eq.(II-36) was valid also for the staggered value which gives:

$$r_N^3 = \frac{r^3 \left(A - \ln \frac{e_a}{e_{sat,w}} + \tau \right)}{A + \tau \left(B - \ln \frac{e_a}{e_{sat,w}} \right)} \qquad \text{(II-41)}$$

For the sake of consistency with eq.(II-37) we shall use eq.(II-41) in our model, although eq.(II-40) would lead to the same results unless there are numerical effects interfering.
The above specifications enable us now to calculate the growth rates (dm_{AP}/dt) necessary for evaluating eqs.(II-31) and (II-32).

II.5 Activation of aerosol particles to drops, nucleation scavenging

We have already mentioned in section II.4 (see Fig.(II-1)) that for any given supersaturation in the environmental air only aerosol particles larger than a certain size will become activated to 'drops'. Once being 'drops', i.e. having reached sizes larger than the critical

size represented by the maxima in the Koehler curves, they continue to grow at a rate which is controlled by the diffusion of water vapor to the drop even though the relative humidity might decrease as long as it remains above saturation. Each activated aerosol particle on which a drop 'nucleated' must therefore be considered 'lost' to the population of aerosol particles in the air. Thus, the mechanism of activation to drops represents a removal mechanism for aerosol particles, called nucleation scavenging.

In eqs.(II-7) to (II-10) nucleation scavenging is represented by the terms:

$$\left.\frac{\partial f_d(m)}{\partial t}\right|_{act} = -\left.\frac{\partial f_{APa}(m_{AP})}{\partial t}\right|_{act} \qquad \text{(II-42)}$$

$$\left.\frac{\partial g_{APd}(m)}{\partial t}\right|_{act} = -\left.\frac{\partial g_{APa}(m_{AP})}{\partial t}\right|_{act} \qquad \text{(II-43)}$$

The critical aerosol particle size for nucleation is given by the maximum of the appropriate Koehler curve:

$$s_{v,w} = \frac{A}{r} - \frac{\mathcal{B} r_N^3}{r^3 - r_N^3} \qquad \text{(II-44)}$$

$$\frac{\partial s_{v,w}}{\partial r} = 0 = -\frac{A}{r^2} + \frac{3\mathcal{B} r^2 r_N^3}{(r^3 - r_N^3)^2} \qquad \text{(II-45)}$$

These two equations determine the critical radius for activation r_c and the critical nucleus radius r_{NC}:

$$r_c = -\frac{\mathcal{D}}{2} + \left\{\frac{\mathcal{D}^2}{4} - E\right\}^{1/2} \qquad \text{(II-46)}$$

$$r_{NC} = \left\{\frac{r_c^3 (A - s_{v,w} r_c)}{A + (\mathcal{B} - s_{v,w}) r_c}\right\}^{1/3} \qquad \text{(II-47)}$$

with:

$$\mathcal{D} = \frac{2\mathcal{B}^2 A - 6\mathcal{B} A s_{v,w}}{3\mathcal{B} s_{v,w}^2 - 3\mathcal{B}^2 s_{v,w}} \qquad \text{(II-48)}$$

$$E = \frac{3\mathcal{B} A^2}{3\mathcal{B} s_{v,w}^2 - 3\mathcal{B}^2 s_{v,w}} \qquad \text{(II-49)}$$

As stated in section II.4 the aerosol particle growth due to vapor diffusion is calculated only up to 100% relative humidity. To correct-

ly determine those aerosol particles which can be activated we further have to calculate the critical radius which the aerosol particle would have at 100% relative humidity:

$$\sigma = \frac{A}{r_{100}} - \frac{B\, r_{NC}^3}{r_{100}^3 - r_{NC}^3} \qquad \text{(II-50)}$$

which gives:

$$r_{100}^3 - \frac{B}{A} r_{NC}^3 r_{100} - r_{NC}^3 = \sigma \qquad \text{(II-51)}$$

This is a cubic equation which can be solved analytically by well known algorithms.

All aerosol particles which are larger than r_{100} are considered activated at the supersaturation $s_{v,w}$. They are taken out of the aerosol particle spectrum and put into the drop spectrum.

If the activation size of an aerosol particle doesn't lie at the boundary of one aerosol particle size category the fraction

$$(f_{APa})_i \; \frac{\ln r_{i+1/2} - \ln r_{100}}{\ln r_{i+1/2} - \ln r_{i-1/2}} \qquad \text{(II-52)}$$

becomes activated. For all larger particles the full number of aerosol particles inside the size intervals are considered to be activated and are put into the corresponding drop size categories (for the definition of the categories see chapter VI). If the aerosol particles to be activated are smaller than the smallest drop size interval they are transferred to this smallest drop size interval.

If the relative humidity decreases the air may become subsaturated. The drops then begin to evaporate and may become deactivated. This is true if the drop radius becomes smaller than the critical drop radius a_c necessary for activation. So for $s_{v,w}<0$ we calculate the nucleus of the drops:

$$r_N^3 = \frac{g_{APd}(m)}{\frac{4}{3}\pi \varrho_N f_d(m)} \qquad \text{(II-53)}$$

which gives us the critical radius a_c from:

$$\frac{\partial s_{v,w}}{\partial a} = 0 = -\frac{A}{a_c^2} + \frac{3B r_N^3 a_c^2}{(a_c^3 - r_N^3)^2} \qquad \text{(II-54)}$$

if we solve this sixth order equation numerically (e.g. by Newton's method):

$$a_c^6 - \frac{3B r_N^3}{A} a_c^4 - 2 r_N^3 a_c^3 + r_N^6 = 0 \qquad \text{(II-55)}$$

Thus, if the drop is smaller than a_c, it is considered to be deactivated and put back into the corresponding aerosol particle size category. If the drop radius is larger than the largest aerosol size category the drop is put into this largest aerosol size category while being 'chopped' in as many portions as necessary to fit the size of the class:

$$\Delta f_{APa} = f_d(m) \frac{a^3}{r^3} \qquad \text{(II-56)}$$

II.6 Growth and evaporation of drops by vapor diffusion

The time rate of change of the drop spectrum due to growth or evaporation of drops by vapor diffusion is:

$$\left.\frac{\partial f_d(m)}{\partial t}\right|_{con/eva} = -\frac{\partial}{\partial m}\left(\left.\frac{dm}{dt}\right|_{con/eva} f_d(m)\right) \qquad \text{(II-57)}$$

The corresponding time rate of change of the aerosol particle mass inside drops of a given size category is

$$\left.\frac{\partial g_{APd}(m)}{\partial t}\right|_{con/eva} = -\frac{\partial}{\partial m}\left(\left.\frac{dm}{dt}\right|_{con/eva} g_{APd}(m)\right) \qquad \text{(II-58)}$$

Integration of eqs.(II-57) and (II-58) over the drop spectrum reveals that the total number and the total aerosol particle mass of drops is conserved (compare eqs.(II-17) and (II-22)). Pruppacher and Klett (1978) state:

$$\left.\frac{dm}{dt}\right|_{con/eva} = 4\pi a \; \frac{\left\{ S_{v,w} - \frac{A}{a} + \frac{B r_N^3}{a^3 - r_N^3} \right\} F_v}{\frac{L_v}{k_a^* T}\left(\frac{L_v M_w}{RT} - 1\right) + \frac{RT}{M_w e_{sat,w} D_v^*}} \qquad \text{(II-59)}$$

with A and B as defined in eqs.(II-34) and (II-35). If for the chosen drop size intervals and time steps $(dm/dt)|_{con/eva}$ is too big to meet the CFL criterion the calculations are done in n iterations, where n is the number by which the time step is reduced to meet the CFL criterion (see also chapter VI.2).

$$\Delta t^* = \frac{\Delta t}{n} \qquad \text{(II-60)}$$

In the paragraphs above we explained how the nucleation and vapor diffusion processes have been treated mathematically. In our model these processes don't act alone but continuously interact with each other. Both are controlled by the relative humidity which is influenced by dynamical processes. In turn, however, both processes act back on the water vapor content.
How to treat this complex interactions has always been a crucial problem in cloud models. In the present study, we followed Hall(1980) and extended his treatment to meet our requirements. The details about the interactions between the dynamics and the condensation and evaporation are given in appendix A1.

In the following sections we shall describe the modeling of the effects which don't involve phase change.

II.7 Impaction scavenging

Due to Brownian diffusion, inertia, hydrodynamic forces and through phoretic and electric forces unactivated aerosol particles in the air are collected by drops. This is called impaction scavenging. The rate at which the number of unactivated aerosol particles in air is reduced due to capture by drops is

$$\left.\frac{\partial f_{APa}(m_{AP})}{\partial t}\right|_{AP,coll} = -\int_0^\infty f_{APa}(m_{AP})\, f_d(m)\, K_{AP}(m_{AP},m)\, dm \qquad \text{(II-61)}$$

and the rate at which the aerosol particle mass is reduced by capture is

$$\left.\frac{\partial g_{APa}(m_{AP})}{\partial t}\right|_{AP,coll} = -\int_0^\infty g_{APa}(m_{AP})\, f_d(m)\, K_{AP}(m_{AP},m)\, dm \qquad \text{(II-62)}$$

This capture process contributes aerosol particle mass and water mass to the drops. The resulting increase in mass of the drops changes the drop spectrum according to

$$\left.\frac{\partial f_d(m)}{\partial t}\right|_{AP,coll} = -\frac{\partial}{\partial m}\left(\left.\frac{dm}{dt}\right|_{AP,coll} f_d(m)\right) \qquad \text{(II-63)}$$

with

$$\left.\frac{dm}{dt}\right|_{AP,coll} = \int_0^\infty m_{AP}\, f_{APa}(m_{AP})\, K_{AP}(m_{AP},m)\, dm_{AP} \qquad \text{(II-64)}$$

The time rate of change of aerosol particle mass inside the drops resulting from the capture of unactivated aerosol particles is

$$\left.\frac{\partial g_{APd}(m)}{\partial t}\right|_{AP,coll} = f_d(m)\int_0^\infty g_{APa}(m_{AP})\, K_{AP}(m_{AP},m)\, dm_{AP} - \frac{\partial}{\partial m}\left(\left.\frac{dm}{dt}\right|_{AP,coll} g_{APd}(m)\right) \qquad \text{(II-65)}$$

wherein the first term on the right hand side of eq.(II-65) represents the contribution due to the collection of aerosol particles, and the second term represents the contribution due to the shift of the whole drop number distribution resulting from the drop growth by intake of aerosol particles.

During the process of impaction scavenging the aerosol particle mass is conserved and the number of drops doesn't change:

$$\int_0^\infty \left.\frac{\partial f_d(m)}{\partial t}\right|_{AP,coll} dm = 0 \qquad \text{(II-66)}$$

$$-\int_0^\infty \left.\frac{\partial g_{APa}(m_{AP})}{\partial t}\right|_{AP,coll} dm_{AP} = \int_0^\infty \left.\frac{\partial g_{APd}(m)}{\partial t}\right|_{AP,coll} dm \qquad \text{(II-67)}$$

$K_{AP}(m_{AP},m)$ in eqs.(II-61) to (II-67) is the collection kernel of unactivated aerosol particles and drops:

$$K_{AP}(m_{AP},m) = \pi (a+r)^2 E_{AP}(m_{AP},m) |V_\infty(m) - V_\infty(m_{AP})| \quad \text{(II-68)}$$
$$= \pi (a+r)^2 E_{AP}(m_{AP},m) V_\infty(m)$$

wherein we shall neglect the terminal velocity of the aerosol particles (compare eqs.(II-9) and (II-10)). $E_{AP}(m_{AP},m)$ is the collection efficiency of unactivated aerosol particles and drops. The collection efficiency has been discussed on the basis of theoretical studies and laboratory tests by Barlow and Latham(1985), Leong et al.(1982), Carstens and Martin(1982), Wang et al.(1978), Lai et al.(1978), Grover et al.(1977), Wang and Pruppacher(1977), Kerker and Hampl(1974) and Hampl et al.(1971). Due to the difficulties in controlling and measuring the ambient conditions, field studies, on the other hand, have thus far not yet led to quantitative data on the efficiency of impaction scavenging. An exception to this are the field observations of Radke et al.(1980) who deduced impaction scavenging efficiencies considerably larger than those theoretically predicted. To create a table of collection efficiencies for our model we assumed that there are no electrical forces present. We used the theoretical efficiencies from Wang et al.(1978) for four different relative humidities (100%, 95%, 75% and 50%). In their calculations the particle radius varies from 10^{-3} µm and 5 µm and the drop radius ranges from 8.6 µm to 438 µm. Unfortunately there is a lack of information on the efficiency for drops larger than 500 µm. To estimate these we used the experiments of Wang and Pruppacher(1977) for an aerosol particle size of .25 µm and drop radii up to 3000 µm. In addition, we used the interpolation formula proposed by Beard and Grover(1974) for aerosol particles larger than 2 µm.

To obtain complete tables for the four different relative humidities we interpolated linearly between these values and smoothed the curves five times. The tables are to be found in appendix B1. These tables are used in the model where the values given have to be interpolated again according to the actual size of the drops, the aerosol particles and the relative humidity.

II.8 Collision and coalescence of drops

The time rate of change of the drop number distribution function due to collision and coalescence between the drops is according to Berry and Reinhardt(1974a,b,c,d):

$$\left.\frac{\partial f_d(m)}{\partial t}\right|_{d,coal} = \int_0^{m/2} f_d(m-m')\, f_d(m)\, K_d(m-m', m')\, dm' - \int_0^{\infty} f_d(m)\, f_d(m')\, K_d(m, m')\, dm' \qquad \text{(II-69)}$$

The first term on the right hand side describes the gain of drops of mass m due to collision and coalescence of drops m' and m-m', while the second term gives the loss of drops of mass m due to collision with any drops m'.

Due to the collision and coalescence among the drops the aerosol particle mass spectrum inside the drops also changes. The loss of aerosol mass in a drop m is analogously to the second term in eq.(II-69)

$$\left.\frac{\partial q_{APd}(m)}{\partial t}\right|_{loss} = -q_{APd}(m)\int_0^{\infty} f_d(m')\, K_d(m, m')\, dm' \qquad \text{(II-70)}$$

Due to the collision of one drop of mass m' and one of mass m-m' a new drop of mass m is formed. The aerosol mass in this new drop is:

$$Q_{APd}(m')\, m' + Q_{APd}(m-m')\,\{m-m'\} \qquad \text{(II-71)}$$

So the total gain of aerosol particle mass in the category m due to the drop collision is:

$$\left.\frac{\partial q_{APd}(m)}{\partial t}\right|_{gain} = \int_0^{m/2} \left\{ Q_{APd}(m')\, m' + Q_{APd}(m-m')\,\{m-m'\}\right\} f_d(m')\, f_d(m-m')\, K_d(m-m', m)\, dm' \qquad \text{(II-72)}$$

The sum of the two eqs.(II-70) and (II-72) gives the total change of aerosol particle mass inside the drops

$$\left.\frac{\partial g_{APd}(m)}{\partial t}\right|_{d,coal} = \int_0^{m/2} \left\{ Q_{APd}(m')\, m' + Q_{APd}(m-m')\{m-m'\} \right\} \tag{II-73}$$

$$f_d(m-m')\, f_d(m')\, K_d(m-m', m')\, dm'$$

$$- g_{APd}(m) \int_0^{\infty} f_d(m')\, K_d(m, m')\, dm'$$

In order to avoid undue computation costs to evaluate these integrals we choose a slightly different way of computing them. According to eq.(II-11)

$$g_{APd}(m) = Q_{APd}(m)\, m\, f_d(m)$$

therefore

$$\frac{\partial g_{APd}(m)}{\partial t} = m\, f_d(m) \frac{\partial Q_{APd}(m)}{\partial t} + m\, Q_{APd}(m) \frac{\partial f_d(m)}{\partial t} \tag{II-74}$$

solving for $\frac{\partial Q_{APd}}{\partial t}$ with $\frac{\partial f_d(m)}{\partial t}$ from eq.(II-69) gives:

$$\left.\frac{\partial Q_{APd}(m)}{\partial t}\right|_{d,coal} = \frac{1}{m\, f_d(m)} \int_0^{m/2} \left\{ Q_{APd}(m')\, m' + Q_{APd}(m-m') \right. \tag{II-75}$$

$$\left. \cdot \{m-m'\} - Q_{APd}(m)\, m \right\} f_d(m')\, f_d(m-m')\, K_d(m-m', m')\, dm'$$

As expected, the mixing ratio of aerosol particles doesn't change due to the loss of particles. Therefore we calculate $\partial g_{APd} / \partial t$ with eqs.(II-75) and (II-74) which saves us from solving one more loss integral.

Due to the collision and coalescence of drops the aerosol particle mass inside the drop spectrum should not change:

$$\int_0^{\infty} \left.\frac{\partial g_{APd}(m)}{\partial t}\right|_{d,coal} dm = 0 \tag{II-76}$$

The proof for this is given in appendix A2.

The quantity $K_d(m,m')$ in the previous equations is the collection kernel of drops:

$$K_d(m, m') = \pi (a + a')^2\, E_d(m, m')\, \left| V_\infty(m) - V_\infty(m') \right| \tag{II-77}$$

where $E_d(m,m')$ is the collection efficiency of drops. This efficiency is a superposition of the coalescence efficiency and the collision efficiency.

Here the coalescence efficiency for drops was assumed to be unity, while the values for the collision efficiency of drops were assumed to be given by a combination of those computed by Davis(1972), Jonas(1972), Klett and Davis(1973), Lin and Lee(1975), Schlamp et al.(1976) and Shafrir and Gal-Chen(1971), in a selection of values given by Hall(1980). The table is to be found in appendix B2.

II.9 Break up of drops

The break up of drops is incorporated into eqs.(II-7) and (II-8) through the terms

$$\left.\frac{\partial f_d(m)}{\partial t}\right|_{d,break} \quad \text{and} \quad \left.\frac{\partial q_{APd}(m)}{\partial t}\right|_{d,break}$$

The procedure for evaluating these terms is due to Danielsen et al.(1972). The process is parameterized as a spontaneous break up of droplets larger than a specific size. Upon their appearance due to collision and coalescence the droplet mass is instantaneously redistributed according to a prescribed reference spectrum. The percentage of mass placed in each category is shown in the table in appendix B5 and is identical to the procedure described by Danielsen et al.(1972).

III Theoretical formulation of the gas scavenging

In this chapter we shall discuss an extension of our theory of scavenging to also include the scavenging of atmospheric gases. In doing so we had to confine ourselves to the removal of SO_2. The reason for this specification is that gas scavenging cannot be formulated as generally as the aerosol scavenging since it depends critically on the chemical properties of the gas.

III.1 The chemical reactions of SO_2 in water

For sulfur dioxide entering water the following equilibrium conditions exist (see e.g. Walcek et al.(1984)).

$$SO_2\,(g) + H_2O \overset{K_H}{\rightleftharpoons} SO_2 \cdot H_2O\,(\ell)$$

$$K_H = \frac{[SO_2 \cdot H_2O]_\ell}{[SO_2]_g} = 7.1\ 10^{-4} \exp\left\{\frac{3145}{T}\right\} \left(\frac{\text{Molar}}{\text{Molar}}\right) \qquad \text{(III-1)}$$

$$SO_2 \cdot H_2O\,(\ell) \overset{K_1}{\rightleftharpoons} H^+ + HSO_3^-$$

$$K_1 = \frac{[H^+][HSO_3^-]}{[SO_2 \cdot H_2O]} = 1.9\ 10^{-5} \exp\left\{\frac{2022}{T}\right\} \left(\frac{\text{moles}}{\text{liter}}\right) \qquad \text{(III-2)}$$

$$HSO_3^- \overset{K_2}{\rightleftharpoons} H^+ + SO_3^{2-}$$

$$K_2 = \frac{[H^+][SO_3^{2-}]}{[HSO_3^-]} = 2.4\ 10^{-10} \exp\left\{\frac{1671}{T}\right\} \left(\frac{\text{moles}}{\text{liter}}\right) \qquad \text{(III-3)}$$

where the values for K_H, K_1, K_2 were taken from Sillen(1964), and where henceforth the concentration of a chemical species is given in square brackets. Since under atmospheric conditions one may assume for cloud and rain water pH$\leq$5.5, the dissociation of $SO_2 \cdot H_2O$ stops

with eq.(III-2) so that we can disregard reaction (III-3).
The condition for electro-neutrality in this range is then given with sufficient accuracy by

$$[H^+] = [HSO_3^-] \qquad \text{(III-4)}$$

from which follows for the total sulfur concentration

$$[S(IV)] = [SO_2 \cdot H_2O] + [HSO_3^-] = \frac{[H^+]^2 + K_1[H^+]}{K_1} \qquad \text{(III-5)}$$

Known [S(IV)] eq.(III-5) gives us the pH=-log[H^+].
If an oxidizing agent, such as e.g. H_2O_2, or a catalyst, as e.g. a metal oxyde, is present inside the water, S(IV) becomes irreversibly converted to S(VI), where the roman numerals inside the brackets specify the valency of the sulfur. For simplicity one may assume for this process a linear conversion rate:

$$\frac{\partial [S(VI)]}{\partial t} = K' [S(IV)] \qquad \text{(III-6)}$$

Sulfur(VI) exists as two species related by the equilibrium condition:

$$HSO_4^- \overset{K_3}{\rightleftharpoons} SO_4^{2-} + H^+ \quad ; \quad K_3 = \frac{[SO_4^{2-}][H^+]}{[HSO_4^-]} = 0.012 \left(\frac{\text{moles}}{\text{liter}}\right) \qquad \text{(III-7)}$$

from which we find the concentration of S(VI) as

$$[S(VI)] = [HSO_4^-] + [SO_4^{2-}] \qquad \text{(III-8)}$$

The [H^+] is a function of [S(IV)] and [S(VI)]:

$$\begin{aligned} &[H^+]^3 + \{(K_1 + K_3) - [S(VI)]\}[H^+]^2 \\ &+ \{K_1K_3 - [S(IV)]K_1 - [S(VI)](K_1 + 2K_3)\}[H^+] \\ &- \{K_1K_3([S(IV)] + 2[S(VI)])\} = 0 \end{aligned} \qquad \text{(III-9)}$$

Since $pH=-\log[H^+]$ we may determine from eq.(III-9) the acidity of the solution from the knowledge of the total sulfur content of the solution. Thus, despite of the fact that in water sulfur dioxide exists in form of a variety of chemical species it is possible to determine the amount of SO_2 scavenged from air by water drops as well as the acidity of the drops by simply keeping track of the sulfur(IV) and sulfur(VI) concentration in the drops. An extension of our scavenging model for aerosol particles to include gas scavenging must include therefore the capability to follow the mass of S(IV) and S(VI) inside the drops of any size category. In order to meet this requirement we formulated the gas scavenging portion of our model as follows:

III.2 The model equations

By including the scavenging of gases into our model of aerosol scavenging presented in chapter II the general model equations (II-1) to (II-6) as well as the microphysical equations (II-7) to (II-10) remain unchanged. However, additional equations are needed for:

g_{Ga} : mass of sulfur dioxide in air

$g_{G4d}(m)$: mass density distribution function for sulfur (IV) in cloud water

$g_{G6d}(m)$: mass density distribution function for sulfur (VI) in cloud water

$g_{G4AP}(m_{AP})$: mass density distribution function for sulfur (IV) inside the water on the unactivated aerosol particles

$g_{G6AP}(m_{AP})$: mass density distribution function for sulfur (VI) inside the water on the unactivated aerosol particles

where m is the total mass of one drop (= water mass + aerosol particle mass + gas mass) and m_{AP} is total mass of unactivated aerosol particle (= water mass + aerosol particle mass + gas mass). Hereby we will assume that the uptaken gas does not change the mass or radius coordinate of the drop or aerosol particle. In the above equations the subscripts G, G4 and G6 stand for gas (sulfur dioxide), sulfur (IV) and sulfur (VI), respectively.

Henceforth all sulfur S(IV) and S(VI) was counted in terms of taken up SO_2.

Analogously to the equations found in chapter II for aerosol scavenging, the time rate of change of the mass of sulfur dioxide in air may be expressed as:

$$\frac{\partial g_{Ga}}{\partial t} = -\nabla\cdot\left(g_{Ga}\, w\right) + \nabla\cdot\left(K_m \nabla g_{Ga}\right) + \left.\frac{\partial g_{Ga}}{\partial t}\right|_{uptake} \qquad \text{(III-10)}$$

the time rate of change of the mass density distribution function for sulfur (IV) in cloud water as

$$\begin{aligned}\frac{\partial g_{G4d}(m)}{\partial t} = &-\nabla\cdot\left(w\, g_{G4d}(m)\right) + \nabla\cdot\left(K_m \nabla g_{G4d}(m)\right)\\ &+ \frac{\partial}{\partial z}\left(V_\infty\, g_{G4d}(m)\right) + \left.\frac{\partial g_{G4d}(m)}{\partial t}\right|_{act}\\ &+ \left.\frac{\partial g_{G4d}(m)}{\partial t}\right|_{con/eva} + \left.\frac{\partial g_{G4d}(m)}{\partial t}\right|_{AP,\,coll}\\ &+ \left.\frac{\partial g_{G4d}(m)}{\partial t}\right|_{d,coal} + \left.\frac{\partial g_{G4d}(m)}{\partial t}\right|_{d,break}\\ &+ \left.\frac{\partial g_{G4d}(m)}{\partial t}\right|_{uptake} + \left.\frac{\partial g_{G4d}(m)}{\partial t}\right|_{ox}\end{aligned} \qquad \text{(III-11)}$$

the time rate of change of the mass density distribution function for sulfur (VI) in cloud water as

$$\begin{aligned}\frac{\partial g_{G6d}(m)}{\partial t} = &-\nabla\cdot\left(w\, g_{G6d}(m)\right) + \nabla\cdot\left(K_m \nabla g_{G6d}(m)\right)\\ &+ \frac{\partial}{\partial z}\left(V_\infty\, g_{G6d}(m)\right) + \left.\frac{\partial g_{G6d}(m)}{\partial t}\right|_{act}\\ &+ \left.\frac{\partial g_{G6d}(m)}{\partial t}\right|_{con/eva} + \left.\frac{\partial g_{G6d}(m)}{\partial t}\right|_{AP,\,coll}\\ &+ \left.\frac{\partial g_{G6d}(m)}{\partial t}\right|_{d,coal} + \left.\frac{\partial g_{G6d}(m)}{\partial t}\right|_{d,break}\\ &+ \left.\frac{\partial g_{G6d}(m)}{\partial t}\right|_{ox}\end{aligned} \qquad \text{(III-12)}$$

the time rate of change of the mass density distribution function for sulfur (IV) in unactivated aerosol particles in air as

$$\frac{\partial g_{G4AP}(m_{AP})}{\partial t} = -\nabla\cdot\left(\mathbf{v}\, g_{G4AP}(m_{AP})\right) + \nabla\cdot\left(K_m \nabla g_{G4AP}(m_{AP})\right)$$
$$+ \left.\frac{\partial g_{G4AP}(m_{AP})}{\partial t}\right|_{act} + \left.\frac{\partial g_{G4AP}(m_{AP})}{\partial t}\right|_{con/eva} \qquad \text{(III-13)}$$
$$+ \left.\frac{\partial g_{G4AP}}{\partial t}\right|_{AP,coll} + \left.\frac{\partial g_{G4AP}}{\partial t}\right|_{uptake} + \left.\frac{\partial g_{G4AP}}{\partial t}\right|_{ox}$$

and the time rate of change of the mass density distribution function for sulfur (VI) in unactivated aerosol particles in air as

$$\frac{\partial g_{G6AP}(m_{AP})}{\partial t} = -\nabla\cdot\left(\mathbf{v}\, g_{G6AP}(m_{AP})\right) + \nabla\cdot\left(K_m \nabla g_{G6AP}(m_{AP})\right)$$
$$+ \left.\frac{\partial g_{G6AP}(m_{AP})}{\partial t}\right|_{act} + \left.\frac{\partial g_{G6AP}(m_{AP})}{\partial t}\right|_{con/eva} \qquad \text{(III-14)}$$
$$+ \left.\frac{\partial g_{G6AP}(m_{AP})}{\partial t}\right|_{AP,coll} + \left.\frac{\partial g_{G6AP}(m_{AP})}{\partial t}\right|_{ox}$$

The first term on the right hand side of eqs.(III-10) to (III-14) describes the advection while the second term refers to the turbulent mixing. The third term on the right hand side of each of eqs.(III-11) and (III-12) describes the sedimentation effect of drops. The other terms, characterized by their subscripts, describe the processes already discussed in chapter II, with the exception of the two newly introduced processes:

$\left.( )\right|_{uptake}$: uptake of sulfur dioxide into the drops and aerosol particles

$\left.( )\right|_{ox}$: oxidation process converting S(IV) into S(VI)

III.3 Additional definitions

In order to formulate the time rate of change of the above introduced distribution functions we assume that all drops between m and $m+\delta m$ carry the same amount of sulfur. The same is assumed for the moist aerosol particles in m_{AP} and $m_{AP}+\delta m_{AP}$. This implies that over any particular drop mass interval the gas mass is uniformly distributed. We equivalently could have assumed a distribution of gas mass inside each category. The values then would refer to the averaged quantity over one interval.

We are able now to define the mixing ratio of sulfur(IV) mass inside a drop mass interval as:

$$Q_{G4d}(m) = \frac{g_{G4d}(m)}{m\, f_d(m)} \qquad \text{(III-15)}$$

and the mixing ratio of sulfur(VI) mass inside the drop mass interval as:

$$Q_{G6d}(m) = \frac{g_{G6d}(m)}{m\, f_d(m)} \qquad \text{(III-16)}$$

m includes now the taken up gas, water and aerosol particle mass. To eliminate m in eq.(III-16)

$$m = \varrho V \qquad \text{(III-17)}$$

we have to compute a mean density analogously to eq.(II-27):

$$\varrho = \frac{\varrho_W \varrho_N}{\varrho_N + (Q_{APd}(m) + Q_{G4d}(m) + Q_{G6d}(m))(\varrho_W - \varrho_N)} \qquad \text{(III-18)}$$

and with this

$$Q_{APd}(m) = \frac{g_{APd}(m)\,\varrho_N}{V f_d(m) \varrho_W \varrho_N - (g_{APd}(m) + g_{G4d}(m) + g_{G6d}(m))(\varrho_W - \varrho_N)} \qquad \text{(III-19)}$$

$$Q_{G4d}(m) = \frac{g_{G4d}(m)\,\varrho_N}{V f_d(m) \varrho_W \varrho_N - (g_{APd}(m) + g_{G4d}(m) + g_{G6d}(m))(\varrho_W - \varrho_N)} \qquad \text{(III-20)}$$

$$Q_{G6d}(m) = \frac{g_{G6d}(m)\,\varrho_N}{V f_d(m) \varrho_W \varrho_N - (g_{APd}(m) + g_{G4d}(m) + g_{G6d}(m))(\varrho_W - \varrho_N)} \qquad \text{(III-21)}$$

Furthermore, we can calculate the following quantities:

g_{Gd} : mass density distribution function for sulfur in cloud water

$$g_{Gd}(m) = g_{G4d}(m) + g_{G6d}(m) \qquad \text{(III-22)}$$

w_{G4d} : total mass of sulfur (IV) in drops

$$w_{G4d} = \int_0^\infty g_{G4d}(m)\, dm \qquad \text{(III-23)}$$

w_{G6d} : total mass of sulfur (VI) in drops

$$w_{G6d} = \int_0^\infty g_{G6d}(m)\, dm \qquad \text{(III-24)}$$

w_{Gd} : total mass of sulfur in drops

$$w_{Gd} = \int_0^\infty g_{Gd}(m)\, dm \qquad \text{(III-25)}$$

$c_4(m)$: concentration of S(IV) in drops in moles/liter

$$c_4(m) = \frac{g_{G4d}(m)}{V f_d(m) M_{SO_2}} \qquad \text{(III-26)}$$

where $V = 4/3\ \pi a^3$ is the volume of the drop, and M_{SO_2} is the molecular weight of sulfur dioxide.

$c_6(m)$: concentration of S(VI) in drops in moles/liter

$$c_6(m) = \frac{g_{G6d}(m)}{V f_d(m) M_{SO_2}} \qquad \text{(III-27)}$$

$c_G(m)$: concentration of S in drops in moles/liter

$$c_G(m) = c_4(m) + c_6(m) \qquad \text{(III-28)}$$

In the following chapters we shall be concerned with the evaluation of the terms with subscripts in eqs.(III-10) to (III-14).

III.4 The gas scavenging terms for the processes of chapter II

The microphysical processes considered here were already discussed in detail in chapter II and shall only be summarized in their important features as they apply to the scavenging of gases.

III.4.1 Diffusional growth of aerosol particles

In chapter II we have stated that also unactivated aerosol particles have taken up water in accordance with the relative humidity. The thus

resulting water film can also take up gases. Although this effect is very small it shall be included into the model for the sake of completeness. The gas mass inside the water of the aerosol particles follows the growth behavior of the aerosol particles. That's why we can write analogously to eq.(II-32):

$$\left.\frac{\partial g_{G4AP}(m_{AP})}{\partial t}\right|_{con/eva} = -\frac{\partial}{\partial m_{AP}}\left(\left.\frac{dm_{AP}}{dt}\right|_{con/eva} g_{G4AP}(m_{AP})\right) \quad \text{(III-29)}$$

$$\left.\frac{\partial g_{G6AP}(m_{AP})}{\partial t}\right|_{con/eva} = -\frac{\partial}{\partial m_{AP}}\left(\left.\frac{dm_{AP}}{dt}\right|_{con/eva} g_{G6AP}(m_{AP})\right) \quad \text{(III-30)}$$

with the diffusion velocity given by eq.(II-38).
Since we assumed that the uptake of gas doesn't change the mass and the radius coordinate of the aerosol particles or drops but only affects the density, we also can neglect the influence of the uptaken gas onto the diffusion velocity through the solute effect. This may underestimate the growth of the aerosol particles in their equilibrium stage and it also may underestimate the growth of drops in the early stages of their life time. However, the results of our computations will show that the amount of gas taken up by aerosol particles and drops in the early stages of growth is relatively small. The major amount is taken up by the drops through the oxidation process predominant in the later stages of growth and slowly builds up in the drops. So it seems justified to neglect the contribution of uptake of gas on the solute effect in the diffusion growth of the aerosol particles and drops.

III.4.2 Nucleation scavenging

It was mentioned in chapter II that some of the aerosol particles become activated to drops. This process causes that the gas mass contained in those moist aerosol particles which become activated is transferred to the drop spectrum:

$$\left.\frac{\partial g_{G4d}(m)}{\partial t}\right|_{act} = -\left.\frac{\partial g_{G4AP}(m_{AP})}{\partial t}\right|_{act} \quad \text{(III-31)}$$

$$\left.\frac{\partial g_{G6d}(m)}{\partial t}\right|_{act} = - \left.\frac{\partial g_{G6AP}(m_{AP})}{\partial t}\right|_{act} \qquad \text{(III-32)}$$

III.4.3 Condensation and evaporation of drops

The time rate of change of the drop spectrum due to condensation or evaporation of drops affects the gas mass contained in the drop categories:

$$\left.\frac{\partial g_{G4d}(m)}{\partial t}\right|_{con/eva} = - \frac{\partial}{\partial m}\left(\left.\frac{dm}{dt}\right|_{con/eva} g_{G4d}(m)\right) \qquad \text{(III-33)}$$

$$\left.\frac{\partial g_{G6d}(m)}{\partial t}\right|_{con/eva} = - \frac{\partial}{\partial m}\left(\left.\frac{dm}{dt}\right|_{con/eva} g_{G6d}(m)\right) \qquad \text{(III-34)}$$

with $(dm/dt)|_{con/eva}$ given by eq.(II-59).
For the reasons already mentioned in chapter III.4.1 we also neglect here the effect of the uptake of gas on the solute effect.

III.4.4 Impaction scavenging

Due to Brownian motion, inertia, hydrodynamic forces and through phoretic and electric forces unactivated aerosol particles are captured by drops. Through this process the gas mass taken up by the moist aerosol particles is transferred to the drop spectrum (compare chapter II.7).

$$\left.\frac{\partial g_{G4AP}(m_{AP})}{\partial t}\right|_{AP,coll} = - \int_0^\infty g_{G4AP}(m_{AP})\, f_d(m)\, K_{AP}(m_{AP}, m)\, dm \qquad \text{(III-35)}$$

$$\left.\frac{\partial g_{G6AP}(m_{AP})}{\partial t}\right|_{AP,coll} = - \int_0^\infty g_{G6AP}(m_{AP})\, f_d(m)\, K_{AP}(m_{AP}, m)\, dm \qquad \text{(III-36)}$$

and the gas mass in the drops increases by

$$\left.\frac{\partial g_{G4d}(m)}{\partial t}\right|_{AP,coll} = f_d(m) \int_0^\infty g_{G4AP}(m_{AP})\, K_{AP}(m_{AP}, m)\, dm_{AP} - \frac{\partial}{\partial m}\left(\left.\frac{dm}{dt}\right|_{AP,coll} g_{G4d}(m)\right) \qquad \text{(III-37)}$$

$$\left.\frac{\partial q_{G6d}(m)}{\partial t}\right|_{AP,coll} = f_d(m)\int_0^\infty q_{G6d}(m)\, K_{AP}(m_{AP}, m)\, dm_{AP} - \frac{\partial}{\partial m}\left(\left.\frac{dm}{dt}\right|_{AP,coll} q_{G6d}(m)\right) \qquad \text{(III-38)}$$

with $(dm/dt)|_{AP,coll}$ given by eq.(II-64).

III.4.5 Collision and coalescence of drops

The time rate of change of the gas mass distribution functions due to collision and coalescence between drops is calculated according eqs.(II-74) and (II-75)

$$\left.\frac{\partial q_{G4d}(m)}{\partial t}\right|_{d,coal} = m f_d(m)\frac{\partial Q_{G4d}(m)}{\partial t} + m Q_{G4d}(m)\left.\frac{\partial f_d(m)}{\partial t}\right|_{d,coal} \qquad \text{(III-39)}$$

with:

$$\left.\frac{\partial Q_{G4d}(m)}{\partial t}\right|_{d,coal} = \frac{1}{m f_d(m)}\int_0^{m/2}\Big\{Q_{G4d}(m')\,m' + Q_{G4d}(m-m')\cdot\{m-m'\} - Q_{G4d}(m)\,m\Big\} f_d(m') f_d(m-m') K_d(m-m', m')\, dm' \qquad \text{(III-40)}$$

and

$$\left.\frac{\partial q_{G6d}(m)}{\partial t}\right|_{d,coal} = m f_d(m)\frac{\partial Q_{G6d}(m)}{\partial t} + m Q_{G6d}(m)\left.\frac{\partial f_d(m)}{\partial t}\right|_{d,coal} \qquad \text{(III-41)}$$

with:

$$\left.\frac{\partial Q_{G6d}(m)}{\partial t}\right|_{d,coal} = \frac{1}{m f_d(m)}\int_0^{m/2}\Big\{Q_{G6d}(m')\,m' + Q_{G6d}(m-m')\cdot\{m-m'\} - Q_{G6d}(m)\,m\Big\} f_d(m') f_d(m-m') K_d(m-m', m')\, dm' \qquad \text{(III-42)}$$

and $(\partial f_d(m)/\partial t)|_{d,coal}$ is given by eq.(II-69).

III.4.6 Break up of drops

Through the break up of drops also the gas mass included in the drops is redistributed. That's why

$$\left.\frac{\partial q_{Gud}(m)}{\partial t}\right|_{d,break} \quad \text{and} \quad \left.\frac{\partial q_{Gbd}(m)}{\partial t}\right|_{d,break}$$

are treated as described in chapter II.9.

III.5 The physics of gas uptake into the liquid phase

The amount of gas entering a drop depends on the one hand on the amount of gas which the atmosphere can supply, and on the other hand on what happens to the gas once it has entered the drop, i.e. how it's distributed, and whether there are chemical reactions taking place. The process of gas uptake was modeled explicitly by Walcek, Pruppacher(1984a) who solved the complete convective diffusion equation:

$$\frac{\partial c}{\partial t} = - v \cdot \nabla c + D \nabla^2 c \qquad \text{(III-43)}$$

for sulfur outside and inside the drop. At the boundary of the drop Henry's law was assumed to hold. This law states that a gas over a pure water surface enters the water until a saturation value is

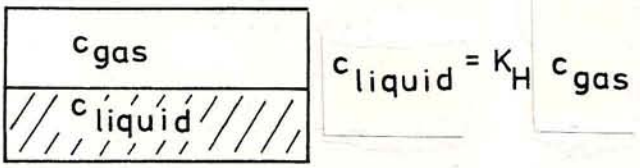

Fig.(III-1): Illustration of Henry's law.

reached (Fig.(III-1)). For the case that the gas does not undergo chemical reactions in water the saturation concentration is proportional to the concentration of the gas in the gas phase. The proportionality factor is called the Henry constant K_H (compare eq.(III-1)).

If the gas is sulfur dioxide which undergoes chemical reactions with water (compare chapter III.1) Henry's law must be modified according

$$c_{Liquid} = K_H' \, c_{gas} \qquad \text{(III-44)}$$

with

$$K_H' = \frac{K_H c_{gas} + \sqrt{K_1 K_H c_{gas}}}{c_{gas}}$$

where K_H' is now called the partition coefficient.

Walcek, Pruppacher(1984a) applied this modified Henry's law as a boundary condition to their model and calculated the uptake of SO_2 into the drops by solving the complete convective diffusion equation with the help of solutions to the Navier-Stokes equation of motion for the flow inside and outside of a drop.

Unfortunately their detailed approach was, from a computational point of view, not suitable for inclusion in our scavenging model. However, based on some of the results obtained with the detailed model they suggested a simplified model, which we employed. Thus, Fig.(II-2) illustrates the time needed for a pure water drop as a function of the environmental SO_2 concentration to reach 63% of its saturation value. We can see from this figure that drops with radii smaller than 50μm reach 63% of their saturation value within a time span much shorter than the time step of our model (2-5sec) if the atmospheric SO_2 concentration ranges between 10 and 100 ppb(v). Drops larger than 50μm take considerably longer to reach their saturation value. This suggests that in our model we can treat small droplets and aerosol particles as being in equilibrium with the environmental SO_2 concentration.

Fig.(III-3) displays another important consequence of Walcek and Pruppacher's calculations. The figure shows that two extreme domains have to be considered:

1. In the first domain the resistance to diffusion lies entirely in the liquid phase. This implies that the environment is assumed to supply sulfur dioxide infinitely fast. The amount of gas taken up by a drop therefore depends only on the internal transportation and mixing of the gas.

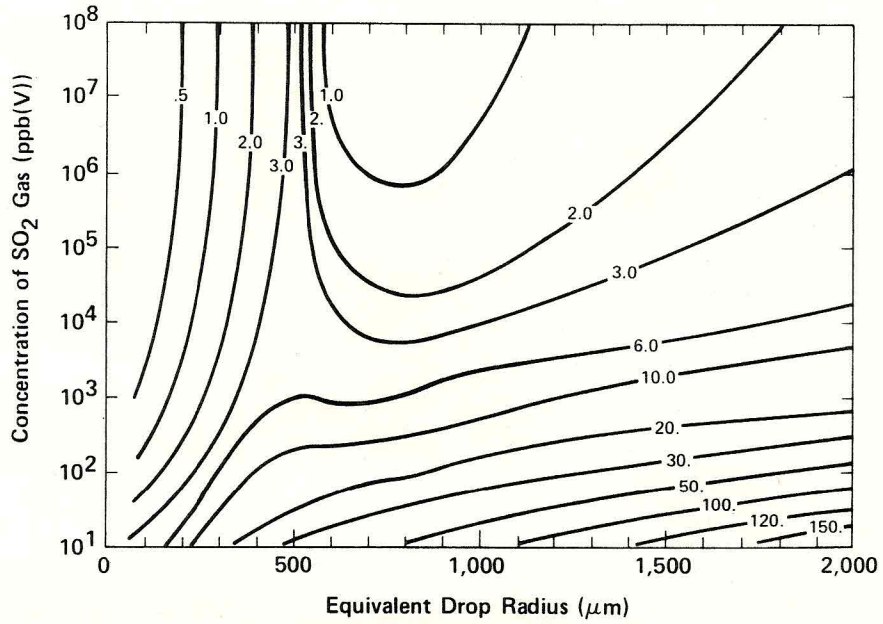

Fig.(III-2): Time (seconds) it takes a drop falling through an environment of given SO_2 concentration to reach 63% of saturation, as a function of drop size and SO_2 concentration (taken from Walcek, Pruppacher(1984a)).

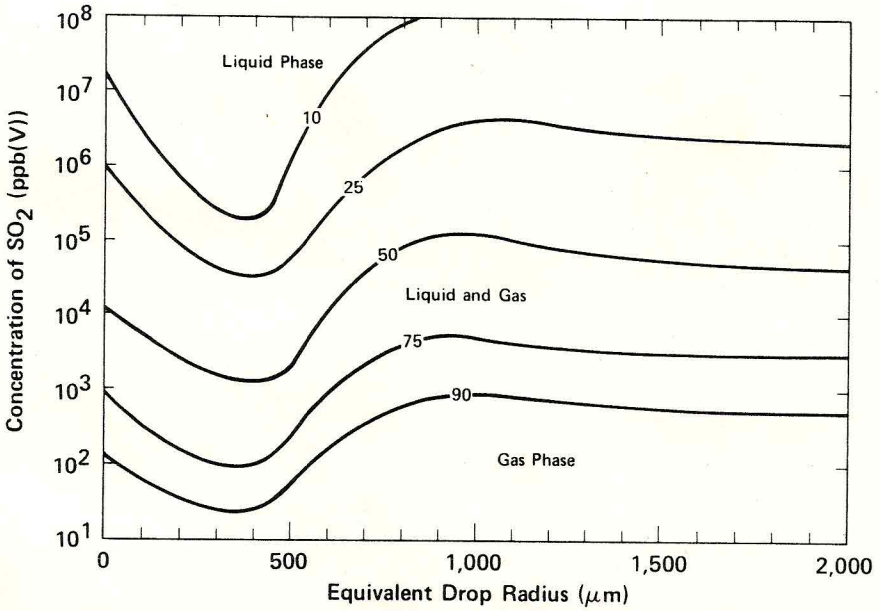

Fig.(III-3): Proportion of resistance to diffusion in the gas phase as percentage of the total resistance, for drops of various sizes falling through various concentrations of SO_2 in the gas phase (taken from Walcek, Pruppacher(1984a)).

2. In the second domain the resistance to diffusion lies entirely in the gas phase. This implies that the drop acts as a perfect sink and the taken up gas is immediately evenly distributed inside the drop. The amount of gas taken up therefore only depends on how fast the environment can deliver the sulfur dioxide to the drop.

From Fig.(III-3) we see that under atmospheric SO_2 conditions (10 to 100 ppb(v)) the resistance to diffusion lies in the gas phase. This enables us to use the simple film theory approach to describe the uptake of sulfur dioxide into large drops (see Walcek and Pruppacher (1984a)). This theory is summarized below.
Applying Fick's first law of diffusion to the present problem, we may approximate that the change of solute concentration inside a drop is given by the product of the gradient of the concentration, the drop surface and the diffusion coefficient. This gradient can be found from the difference between the gas concentration at the surface and the gas concentration in the undisturbed environment divided by a characteristic length $\delta_g = a/F_v$ which is called the gas film thickness. Thus

$$\frac{dN_m}{dt} = D_g \, 4\pi a^2 \, \nabla C$$
$$= D_g \, 4\pi a^2 \, \frac{c_{g,\infty} - c_{g,surf}}{\delta_g} \qquad \text{(III-45)}$$

where the surface concentration is coupled to the concentration in the drop through Henry's law. F_v is the ventilation coefficient for water vapor in air, which approximates the ventilation coefficient of most other atmospheric gases (Balboolal et al.(1981)).
For the case that the gas is assumed not to undergo chemical reaction with water, the drop will become saturated with gas after a sufficiently long time.

If, however, the drop is contaminated with oxidizing agents or catalysts, oxidation processes will take place. The uptaken S(IV) will be irreversibly converted to S(VI) and thus the drop will never become saturated but takes up sulfur dioxide continuously. The amount of uptaken sulfur is then determined by the governing oxidation rate K' (compare section III.1).

The above results shall now be incorporated in our model.

III.6 Uptake of SO_2 without oxidation processes

From section III.5 we learn that without oxidation small drops are in immediate equilibrium with the environmental gas concentration while the larger ones obey the film theory. Furthermore, without oxidation

$$g_{G6d}(m) = g_{G6AP}(m_{AP}) = 0 \tag{III-46}$$

and

$$\left.\frac{\partial g_{G4d}(m)}{\partial t}\right|_{ox} = -\left.\frac{\partial g_{G6d}(m)}{\partial t}\right|_{ox} = 0$$
$$\left.\frac{\partial g_{G4AP}(m_{AP})}{\partial t}\right|_{ox} = -\left.\frac{\partial g_{G6AP}(m_{AP})}{\partial t}\right|_{ox} = 0 \tag{III-47}$$

III.6.1 Uptake of SO_2 by moist unactivated aerosol particles

For unactivated aerosol particles with a thin water layer we can assume that the water is in immediate equilibrium with the environmental gas concentration. This implies that if the ambient gas concentration changes the wet aerosol particles adjust themselves at once, so that the gas mass in the environment and the mass inside an aerosol particle size category is conserved, i.e.

$$g_{Ga} + g_{G4AP}(m_{AP}) = \text{const} \tag{III-48}$$

Further, the gas mass inside the water layer of the aerosol particle is given by Henry's law:

$$g_{G4AP}(m_{AP}) = \sqrt{K_1 K_H M_{SO_2}}\, V_{AP}\, f_{APa} \sqrt{g_{Ga}} + K_H f_{APa} V_{AP} g_{Ga} \tag{III-49}$$

With this we can now calculate:

$$\left.\frac{\partial g_{Ga}}{\partial t}\right|_{uptake} = \frac{g_{Ga}^{\tau+1} - g_{Ga}^{\tau}}{\Delta t} \tag{III-50}$$

with $$g_{Ga}^{\tau+1} = \frac{C_1}{C_2} + \frac{C_3}{2C_2^2}\left(C_3 - \sqrt{C_3^2 + 4C_1C_2}\right)$$

$$C_1 = g_{Ga}^{\tau} + g_{G+AP}^{\tau}(m_{AP})$$

$$C_2 = 1 + V_{AP}\, f_{APa}(m_{AP})\, K_H$$

$$C_3 = V_{AP}\, f_{APa}(m_{AP}) \sqrt{K_1 K_H M_{SO_2}}$$

and

$$\left.\frac{\partial g_{G+AP}(m_{AP})}{\partial t}\right|_{uptake} = -\left.\frac{\partial g_{Ga}}{\partial t}\right|_{uptake} \qquad \text{(III-51)}$$

III.6.2 Uptake of SO_2 by drops

It was stated in chapter III.5 that only drops smaller than 50μm can be assumed to be in immediate equilibrium with the ambient gas concentration. The SO_2 uptake by larger drops has to be described by the film theory. As threshold between the two domains we chose, however, 30μm instead of 50μm. This threshold is somewhat arbitrary. The results in chapter VII.2 will show, however, that the transition between one domain and the other is smooth, if 30μm are used as the transition size.

III.6.2.1 Uptake of SO_2 by drops smaller than 30μm

The theory for the uptake of sulfur dioxide by drops smaller than 30μm is the same as for the unactivated aerosol particles in chapter III.6.1. Thus,

$$g_{Ga} + g_{G+d}(m) = \text{const} \qquad \text{(III-52)}$$

From Henry's law follows:

$$g_{G+d}(m) = \sqrt{K_1 K_H M_{SO_2}}\, V\, f_d(m) \sqrt{g_{Ga}} + K_H f_d(m) V g_{Ga} \qquad \text{(III-53)}$$

and therefore

$$\left.\frac{\partial g_{Ga}}{\partial t}\right|_{uptake} = \frac{g_{Ga}^{\tau+1} - g_{Ga}^{\tau}}{\Delta t} \qquad \text{(III-54)}$$

with $$g_{Ga}^{\tau+1} = \frac{C_1}{C_2} + \frac{C_3}{2C_2^2}\left(C_3 - \sqrt{C_3^2 + 4C_1C_2}\right)$$

$$C_1 = g_{Ga}^{\tau} + g_{G4d}^{\tau}(m)$$

$$C_2 = 1 + V f_d(m) K_H$$

$$C_3 = V f_d(m) \sqrt{K_1 K_H M_{SO_2}}$$

and

$$\left.\frac{\partial g_{G4d}(m)}{\partial t}\right|_{uptake} = -\left.\frac{\partial g_{Ga}}{\partial t}\right|_{uptake} \qquad \text{(III-55)}$$

III.6.2.2 Uptake of SO_2 by drops larger than 30μm

To model the uptake of sulfur dioxide by drops larger than 30μm we apply the film theory (eq.(III-45)):

$$\left.\frac{\partial g_{G4d}(m)}{\partial t}\right|_{uptake} = D_g f_d(m) 4\pi a^2 \frac{g_{Ga} - g_{Ga,surf}}{\delta g} \qquad \text{(III-56)}$$

with $\delta g = a/F_v$ and with $g_{Ga,surf}$ at the surface of the drop from Henry's law given by:

$$g_{Ga,surf} = \frac{M_{SO_2}}{2K_H}\left(K_1 + 2\frac{g_{G4d}}{V f_d M_{SO_2}}\right) - \frac{M_{SO_2}}{2K_H}\sqrt{K_1\left(K_1 + 4\frac{g_{G4d}}{V f_d M_{SO_2}}\right)} \qquad \text{(III-57)}$$

The loss of SO_2 in the gas phase through one drop size category is

$$\left.\frac{\partial g_{Ga}}{\partial t}\right|_{uptake} = -\left.\frac{\partial g_{G4d}(m)}{\partial t}\right|_{uptake} \qquad \text{(III-58)}$$

The pH of the water on the unactivated aerosol particles, as well as of the water in the drops can be calculated from eq.(III-5).

If oxidation agents or catalysts are present in the drops, as often is the case under atmospheric conditions, the uptake of sulfur dioxide

becomes significantly enhanced.

III.7 Uptake of SO_2 in the presence of oxidation processes

If sulfur is converted from S(IV) to S(VI) by oxidation processes in the drops the amount of uptaken SO_2 depends mainly on the rate with which this oxidation reaction is proceeding, while for the uptake of S(IV) the theory of section III.6 still stays valid.

III.7.1 Uptake of SO_2 by unactivated wet aerosol particles

For the unactivated wet aerosol particles we can assume that the sulfur (IV) is always in equilibrium with the environmental gas concentration no matter how fast the oxidation process is converting S(IV) in S(VI). Thus, the total gas mass in the aerosol particles is given through

$$g_{GAP}(m_{AP}) = g_{G4AP}(m_{AP}) + g_{G6AP}(m_{AP}) \qquad \text{(III-59)}$$

This total gas mass increases through the uptake of sulfur dioxide from the gas phase

$$\frac{\partial g_{GAP}(m_{AP})}{\partial t} = D_g f_{APa}(m_{AP}) 4\pi r^2 \frac{g_{Ga} - g_{Ga,surf}}{\delta g} = \frac{\partial g_{G6AP}}{\partial t} \qquad \text{(III-60)}$$

since $\partial g_{G4AP}(m_{AP})/\partial t = 0$, which implies that the aerosol particles are always saturated with sulfur (IV).
If we assume a linear oxidation rate (compare eq.(III-6)) converting sulfur (IV) in sulfur (VI) we may write:

$$\left.\frac{\partial g_{G4AP}(m_{AP})}{\partial t}\right|_{ox} = -K' g_{G4AP}(m_{AP}) = -\left.\frac{\partial g_{G6AP}(m_{AP})}{\partial t}\right|_{ox} \qquad \text{(III-61)}$$

Substitution of eq.(III-61) in eq.(III-60) yields:

$$K' g_{G4AP}(m_{AP}) = D_g f_{APa}(m_{AP}) 4\pi r^2 \frac{g_{Ga} - g_{Ga,surf}}{\delta g} \qquad \text{(III-62a)}$$

and from Henry's law we get:

$$g_{G4AP}(m_{AP}) = \sqrt{K_1 K_H M_{SO_2}}\, V_{AP} f_{APa} \sqrt{g_{Ga,surf}} + K_H V_{AP} f_{APa} g_{Ga,surf} \quad \text{(III-62b)}$$

Eqs.(III-62a) and (III-62b) represent two equations with the two unknowns $g_{G4AP}(m_{AP})$ and $g_{Ga,surf}$. We therefore find:

$$\left.\frac{\partial g_{G4AP}(m_{AP})}{\partial t}\right|_{uptake} = \frac{g_{G4AP}^{\tau+1}(m_{AP}) - g_{G4AP}(m_{AP})}{\Delta t} \quad \text{(III-63)}$$

with

$$g_{G4AP}^{\tau+1}(m_{AP}) = \sqrt{K_1 K_H M_{SO_2}}\, V_{AP} f_{APa} \sqrt{g_{Ga,surf}^{\tau+1}} + K_H V_{AP} f_{APa} g_{Ga,surf}^{\tau+1}$$

and

$$g_{Ga,surf}^{\tau+1} = \frac{C_1}{C_2} + \frac{C_3}{2C_2^2}\left(C_3 - \sqrt{C_3^2 + 4C_1C_3}\right)$$

with

$$C_1 = D_g\, 4\pi r^2\, g_{Ga}$$

$$C_2 = K' K_H \delta_g V_{AP} + D_g 4\pi r^2$$

$$C_3 = K' \delta_g V_{AP} \sqrt{K_1 K_H M_{SO_2}}$$

and

$$\left.\frac{\partial g_{G6AP}(m_{AP})}{\partial t}\right|_{ox} = K' g_{G4AP}(m_{AP}) \quad \text{(III-64)}$$

and further for one aerosol particle size

$$\left.\frac{\partial g_{Ga}}{\partial t}\right|_{uptake} = -\left.\frac{\partial g_{G4AP}(m_{AP})}{\partial t}\right|_{uptake} - \left.\frac{\partial g_{G6AP}(m_{AP})}{\partial t}\right|_{ox} \quad \text{(III-65)}$$

III.7.2 Uptake of SO_2 by drops

As before we distinguish between two drop size regions, i.e. drops with radii less than 30μm where the S(IV) concentration is in equilibrium with the environment, and drops larger 30μm.

III.7.2.1 Uptake of SO_2 by drops smaller than 30µm

The theory for the uptake of SO_2 by drops smaller than 30µm is the same as for the unactivated wet aerosol particles in section III.7.1. The total gas mass in the drops is therefore given by

$$g_{Gd}(m) = g_{G4d}(m) + g_{G6d}(m) \qquad \text{(III-66)}$$

This total gas mass increases by the uptake of SO_2 from the gas phase

$$\frac{\partial g_{Gd}(m)}{\partial t} = \frac{\partial g_{G6d}(m)}{\partial t} = D_g f_d(m) 4\pi a^2 \frac{g_{Ga} - g_{Ga,surf}}{\delta_g} = K' g_{G4d}(m) \qquad \text{(III-67)}$$

Together with Henry's law for the gas concentration at the surface of the drop (see eq.(III-53)) we find:

$$\left.\frac{\partial g_{G4d}(m)}{\partial t}\right|_{uptake} = \frac{g_{G4d}^{\tau+1}(m) - g_{G4d}^{\tau}(m)}{\Delta t} \qquad \text{(III-68)}$$

with

$$g_{G4d}^{\tau+1}(m) = \sqrt{K_1 K_H M_{SO_2}}\, V f_d(m) \sqrt{g_{Ga,surf}^{\tau+1}} + K_H V f_d(m)\, g_{Ga,surf}^{\tau+1}$$

and

$$g_{Ga,surf}^{\tau+1} = \frac{C_1}{C_2} + \frac{C_3}{2C_2^2}\left(C_3 - \sqrt{C_3^2 + 4C_1C_2}\right)$$

with

$$C_1 = D_g\, 4\pi a^2\, g_{Ga}$$

$$C_2 = K' K_H \delta_g V + D_g 4\pi a^2$$

$$C_3 = K' \delta_g V \sqrt{K_1 K_H M_{SO_2}}$$

and

$$\left.\frac{\partial g_{G6d}(m)}{\partial t}\right|_{ox} = K' g_{G4d}(m) \qquad \text{(III-69)}$$

and further for one drop size

$$\left.\frac{\partial g_{Ga}}{\partial t}\right|_{uptake} = -\left.\frac{\partial g_{G4d}(m)}{\partial t}\right|_{uptake} - \left.\frac{\partial g_{G6d}(m)}{\partial t}\right|_{ox} \qquad \text{(III-70)}$$

III.7.2.2 Uptake of SO_2 by drops larger than 30μm

To model the uptake of sulfur dioxide by drops larger than 30μm we apply the film theory approach and assume a linear oxidation rate. Therefore:

$$\left.\frac{\partial g_{G4d}(m)}{\partial t}\right|_{uptake} = D_g\, 4\pi a^2 f_d \frac{g_{Ga} - g_{Ga,surf}}{\delta g} - \left.\frac{\partial g_{G6d}(m)}{\partial t}\right|_{ox} \qquad \text{(III-71)}$$

with $g_{Ga,surf}$ from Henry's law

$$g_{Ga,surf} = \frac{M_{SO_2}}{2K_H}\left(K_1 + 2\frac{g_{G4d}}{V_{fd} M_{SO_2}}\right) - \frac{M_{SO_2}}{2K_H}\sqrt{K_1\left(K_1 + 4\frac{g_{G4d}}{V_{fd} M_{SO_2}}\right)} \qquad \text{(III-72)}$$

and

$$\left.\frac{\partial g_{G6d}(m)}{\partial t}\right|_{ox} = K'\, g_{G4d}(m) \qquad \text{(III-73)}$$

and further for one drop size category:

$$\left.\frac{\partial g_{Ga}}{\partial t}\right|_{uptake} = -D_g\, 4\pi a^2 f_d(m) \frac{g_{Ga} - g_{Ga,surf}}{\delta g} \qquad \text{(III-74)}$$

The pH of the water on the unactivated wet aerosol particles, as well as of the water in the drops can be calculated from eq.(III-9).

IV The entraining air parcel model

Before linking our scavenging model to a two dimensional cloud model, we decided to test it under simplified conditions. For this purpose we linked our scavenging model to a simple entraining air parcel model. Although the simplified dynamics prohibited us from getting some detailed results on the rate at which a precipitating cloud is able to scavenge aerosol particles and gases, our model was able to point to some very important effects of the scavenging mechanisms. In the following chapters the entraining air parcel model is described and the initial conditions for the cases, chosen for evaluation are given.

IV.1 The model equations

In order to model the inside of an entraining air parcel a set of equations is required which describes the evolution in time of the main atmospheric variables. They can be derived from the general model equations in chapter II.1 (see Pruppacher, Klett(1978)). From eq.(II-6) we obtain for the temperature changes due to adiabatic cooling, entrainment and phase changes:

$$\frac{dT}{dt} = -\frac{g\,u}{c_{pa}} - \mu\,(T - T^e)\,u + \frac{L_v}{c_{pa}}\,C_{Ph} \qquad \text{(IV-1)}$$

where the quantities with subscript 'e' refer to the parcel's environment and have to be specified. The quantity μ is the entrainment parameter which is chosen after Mason and Jonas(1974) to be:

$$\mu = \frac{0.6}{R} \qquad \text{(IV-2)}$$

R being the radius of the air parcel. According eq.(II-3):

$$C_{Ph} = \frac{dw_L^*}{dt} + \mu\,(w_L^* - w_L^{*e})\,u \qquad \text{(IV-3)}$$

and from eq.(II-2) we get:

$$\frac{dw_v}{dt} = -\mu (w_v - w_v^e) u - C_{Ph} \qquad \text{(IV-4)}$$

From the equation of motion we get an equation for the vertical velocity U in the parcel:

$$\frac{du}{dt} = \frac{g}{1+\gamma} \left\{ \frac{T_v - T_v^e}{T_v^e} - w_L^* \right\} - \frac{\mu}{1+\gamma} u^2 \; ; \quad \gamma = 0.5 \qquad \text{(IV-5)}$$

where T_v is the virtual temperature. The radius of the air parcel changes according to:

$$\frac{d \ln R}{dt} = \frac{1}{3} \left(\mu u - \frac{d \ln \varrho_a}{dt} \right) \qquad \text{(IV-6)}$$

The ideal gas law gives:

$$\varrho_a = \frac{p M_a}{R T} \qquad \text{(IV-7)}$$

$$\frac{d \ln p}{dt} = - \frac{g u M_a}{R T} \qquad \text{(IV-8)}$$

In order to link our aerosol scavenging model to an entraining air parcel model the first three terms on the right hand side of eq.(II-7) have to be replaced by

$$-\mu f_d(m) u \qquad \text{(IV-9)}$$

and the first three terms on the right hand side of eq.(II-8) by

$$-\mu g_{APd}(m) u \qquad \text{(IV-10)}$$

Also the first two terms of eqs.(II-9) and (II-10) have to be replaced by

$$-\mu \{ f_{APa}(m_{AP}) - f_{APa}^e(m_{AP}) \} u \qquad \text{(IV-11)}$$

and

$$-\mu \{ g_{APa}(m_{AP}) - g_{APa}^e(m_{AP}) \} u \qquad \text{(IV-12)}$$

respectively.
In order to model the simultaneous uptake of aerosol particles as well as SO_2 we also have to replace the first two terms on the right hand side of eqs.(III-10), (III-13) and (III-14) by

$$-\mu \{ g_{Ga} - g_{Ga}^{e} \} u \qquad \text{(IV-13)}$$

$$-\mu\, g_{G4AP}(m_{AP})\, u \qquad \text{(IV-14)}$$

$$-\mu\, g_{G6AP}(m_{AP})\, u \qquad \text{(IV-15)}$$

respectively. This implies that we entrain SO_2 in the gas phase, however, none in the liquid phase. Furthermore we have to replace the first three terms on the right hand side of eqs.(III-11) and (III-12) by

$$-\mu\, g_{G4d}(m)\, u \qquad \text{(IV-16)}$$

and

$$-\mu\, g_{G6d}(m)\, u \qquad \text{(IV-17)}$$

respectively.
The equations given above represent a closed system provided the values with subscript 'e' referring to the environment of the parcel are specified. In addition, some initial conditions have to be assumed.

IV.2 Initial conditions

The entraining air parcel model is initialized as a bubble of radius R=350m starting to ascend with an initial updraft velocity U=1m/sec from a height of 1km. The relative humidity inside the bubble at its starting point is set to 99%. The parcel ascends through an atmosphere given by the sounding of Lee et al.(1980) (Fig.(IV-1)). The quantities given by the sounding are set to be the values with

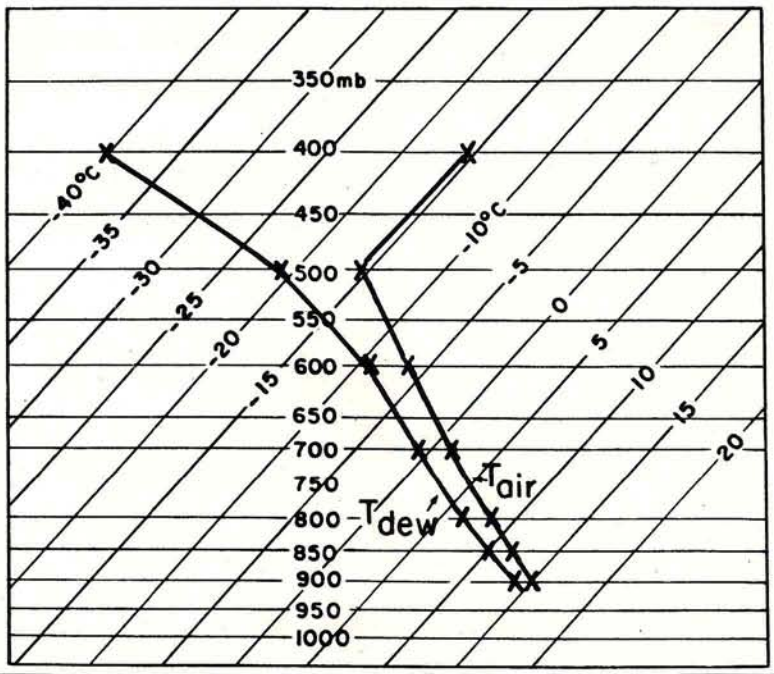

Fig.(IV-1): Initial sounding for the entraining air parcel model calculations (Lee et al. (1980)).

subscript 'e' in eq.(IV-1) to (IV-6) and are entrained during the lifetime of the parcel. The quantities D_v^*, M_w, $e_{sat,w}$, Φ_s, $\sigma_{w,a}$, L_v, F_v were assumed to have the values given by Pruppacher and Klett(1978). In all cases the dry aerosol particles were assumed to have a density $\rho_N = 2 g\ cm^{-3}$. The time step of these runs was set to 2 seconds and the smallest drop radius was assumed to be 1 µm (compare chapter VI.1).

IV.2.1 Initial conditions for the aerosol scavenging

By considering aerosol particle scavenging only, we attempted to determine: (1) the relative importance of the scavenging of aerosol particles by the nucleation mechanism as compared to the impaction mechanism, (2) the conditions necessary for a drop-interstitial aerosol to be formed, (3) the manner in which the scavenged aerosol material becomes redistributed in the cloud water during the collision and coalescence growth of the cloud drops, and (4) the manner by which

aerosol particles become processed during successive cloud evaporation/condensation cycles.

In order to make these determinations we initialized our model with three different aerosol particle distributions which all follow a modified gamma distribution of the form described by Deirmendjian(1969):

$$f_{APa}(\ln r_N) = A_D\, r_N^{\alpha_D+1} \exp\left(-B_D\, r_N^{\gamma_D}\right) \qquad \text{(IV-18)}$$

where r_N is the radius of the dry aerosol nucleus. To get a continental type of aerosol spectrum we chose the variables according to Deirmendjian(1969) to be:

$$\begin{aligned} A_D &= 4.9759\ 10^7\ \text{cm}^{-3}\,\mu\text{m}^{-3} \\ B_D &= 15.1186\ \mu\text{m}^{-0.5} \\ \alpha_D &= 2 \\ \gamma_D &= 0.5 \end{aligned} \qquad \text{(IV-19)}$$

This continental type spectrum with a total number concentration of $N_{APa}=1000\text{cm}^{-3}$ we assumed in one set of runs to consist entirely of ammonium sulfate $(NH_4)_2SO_4$ (i.e. $\varepsilon=1.0$) with a molecular weight of $M_s=132$. This assumption implies an ammonium sulfate concentration of 230 $\mu g/m^3$.

In another set of runs we assumed the continental aerosol type distribution to have a composition of $\varepsilon=0.01$ with the water insoluble portion to consist of silicate. This assumption implies an ammonium sulfate concentration of 2.3 $\mu g/m^3$.

In a third set of runs we assumed a maritime-type aerosol with $N_{APa}=100\text{cm}^{-3}$ and $\varepsilon=1$ and

$$\begin{aligned} A_D &= 5.333\ 10^4\ \text{cm}^{-3}\,\mu\text{m}^{-2} \\ B_D &= 8.9443\ \mu\text{m}^{-0.5} \\ \alpha_D &= 1 \\ \gamma_D &= 0.5 \end{aligned} \qquad \text{(IV-20)}$$

This assumption implies an initial ammonium sulfate concentration of 88 $\mu g/m^3$. To get the initial aerosol distribution we let the dry aerosol particles grow to an equilibrium size at 99% relative humidity inside the bubble as described in chapter II.4. This also defines the environmental aerosol spectrum that is entrained during the parcel's ascent.

Looking critically at these 3 cases by comparing them with field observations, which show that the mass concentration of particulate sulfate typically ranges between 0.3 and 20 $\mu g/m^3$ (Meszaros(1978), Hidy et al.(1978), Hegg et al.(1984), Georgii et al.(1971), Brosset(1978), Meszaros(1981), Junge(1963), Shaw, Paur(1983), Hegg et al.(1980), and Hegg and Hobbs(1981,1983)), we notice that only case 2 is based on a realistic value for the mass concentration of $(NH_4)_2 SO_4$, while the values for case 1 and 3 are much too large. It is obvious that these large values are a result of the fact that we assumed the aerosol particles to entirely consist of the same water soluble material $(NH_4)_2 SO_4$. Such is rarely the case. Rather, under atmospheric conditions aerosol particles only contain 1 to 10% sulfate (Brosset(1978), Meszaros(1981), Junge(1963)). Unfortunately our model did not allow to consider mixtures of different water soluble and insoluble substances in the aerosol particles. This neglect implies that the amount of sulfur scavenged in the model represents an upper limit to the amount of sulfur scavenged in the atmosphere. However, it is easy to see that the determinations listed in section IV.2.1 are not affected by the overestimate of the mass concentration of the sulfur content of the air.

The results of these runs are discussed in chapter VII.1.

IV.2.2 Initial conditions for simultaneous aerosol and gas scavenging

By considering aerosol and gas scavenging simultaneously in an entraining air parcel model we attempted to determine: (1) the relative importance of sulfur scavenging from SO_2 as compared to sulfur scavenging from $(NH_4)_2 SO_4$ particles, (2) the re-distribution which the sulfur, scavenged by the cloud drops from SO_2, experiences during the collision and coalescence growth of cloud drops, (3) the amount of ac-

id formed inside the cloud water, (4) the influence of gas scavenging on the processed aerosol particle distribution, and (5) the relative importance of the in-cloud scavenging of SO_2 as compared to

Case	amount of $(NH_4)SO_4$ mass in air ($\mu g/m^3$)	amount of SO_2 mass in air $\mu g/m^3$	ppb	K' (sec^{-1})
A	88*	88	31	$5x10^{-3}$
B	88*	44	15	$5x10^{-3}$
C	88*	44	15	0.1
D	88*	44	15	1.0
E	88*	100	35	0.1
F	230**	44	15	0.1
G	13+	44	15	1.0
H	13+	44	15	0.5
I	13+	44	15	0.1

Table IV-1: Input data for the nine cases chosen for comparing aerosol and gas scavenging (* aerosol particle distribution given by eq.(IV-18) and parameters (IV-20) (same as in chapter VII.1, case 3), ** aerosol particle distribution given by eq.(IV-18) and parameters (IV-19) (same as in chapter VII.1, case 1), + aerosol particle distribution given by eq.(IV-18) and parameters (IV-20) but truncated at the large drops).

below-cloud scavenging of SO_2. In order to make these determinations we evaluated nine different cases. In these the aerosol particle size distributions used were the same as those used for the cases where aerosol particle scavenging alone was considered. The SO_2 concentrations were chosen either to be larger than, equal to or less than the ammonium sulfate concentration. Also the influence of the oxidation rate K' was tested. Table IV-1 contains a summary of the input date for the nine cases chosen.

Atmospheric SO_2 concentrations assume values between 1 and 30$\mu g/m^3$ (Meszaros(1978), Hidy et al.(1978), Hegg and Hobbs(1981, 1982, 1983), Shaw and Paur(1983), and Hegg et al.(1984)) with maxima as high as 200

$\mu g/m^3$ in extremely polluted regions (Perseke et al.(1980), Georgii(1985)). So the SO_2 concentrations for the nine cases lie within the range of the atmospheric values. Measurements of the acidity in rain made by Georgii(1982), Perseke(1982), Kins(1982) and others yields values between 3 and 6. For this range of pH Hegg and Hobbs(1982) and Martin(1984) suggested K' values ranging from $0.5\ 10^{-2}$ to 10 sec^{-1}. So the assumed oxidation rates for the nine cases also lie within the range of the atmospheric values.
The results of these runs are discussed in chapter VII.2.

V The two dimensional cloud model of Clark et al.

After successfully testing our scavenging model with a simple entraining air parcel model we felt encouraged to link it to a more complete dynamic model for convective clouds. For that purpose we chose the cloud model of Clark et al. This model may be used for the simulation of either two or three dimensional flows. The model also allows for several models to be nested into each other for finer resolution of interesting portions of the dynamic domain. The model is described in detail by Clark(1977, 1979), Clark and Farley(1984) and Hall(1980).

Since our scavenging model already requires considerable amounts of computer time and space we were forced to use the Clark et al. model in its two dimensional, non-nested version. For the same reason we confined ourselves for the present to aerosol scavenging only. The results of this study will be presented in chapter VII.3.

In the following chapters we shall briefly summarize the important features of the two dimensional version of the cloud model of Clark et al. and describe the initial conditions used for evaluating the model.

V.1 The model equations

The basic dynamic framework employed in the present study is a two dimensional, slab-symmetric version of the three dimensional model of Clark et al. The model utilizes the anelastic form of the equations of motion, continuity and first law of thermodynamics.

The anelastic framework requires that the thermodynamic and dynamic variables be divided into the basic state of the environment, which is in hydrostatic balance and is only a function of height (denoted by overbars), and the deviation from the basic state (denoted by primed values):

$$\begin{aligned} \rho_a &= \bar{\rho}_a(z) + \rho_a'(x,z,t) \\ p &= \bar{p}(z) + p'(x,z,t) \\ T &= \bar{T}(z) + T'(x,z,t) \\ \theta &= \bar{\theta}(z) + \theta'(x,z,t) \end{aligned} \qquad \text{(V-1a)}$$

where Θ is the potential temperature defined as

$$\Theta = T \left(\frac{p_0}{p} \right)^{R_d/c_{pd}} \qquad (V\text{-}2)$$

Furthermore

$$w_v = \bar{w}_v(z) + w_v'(x,z,t)$$

$$w_L^* = \bar{w}_L^*(z) + w_L^{*\prime}(x,z,t) = w_L^{*\prime}(x,z,t) \; ; \; \bar{w}_L^* = 0 \qquad (V\text{-}1b)$$

$$w = \bar{w}(z) + w'(x,z,t) = w'(x,z,t) \; ; \; \bar{w} = 0$$

So the basic state is assumed to be at rest and cloud-free.
We substitute these relations into the equations of chapter II.1 and neglect density variations except when they are coupled to the gravitational acceleration in the buoyancy force. This filters the acoustic modes from the model. If we also subtract from these equations the ones valid for the basic state of the environment, neglect products of primed quantities as small and assume that fluctuations in density only result from thermal (as opposed to pressure) effects we obtain the anelastic equations for deep convection (compare Spiegel, Veronis(1960) and Ogura, Phillips(1962)).
The equation of motion (II-5) then transforms into:

$$\bar{\rho}_a \left(\frac{\partial w}{\partial t} + w \cdot \nabla w \right) = - \nabla p' - g \rho_a' \mathbb{k} + \nabla \cdot \mathbb{J} \qquad (V\text{-}3)$$

if we neglect the coriolis force for cumulus clouds.
We next have to rewrite the buoyancy term. For this purpose we assume that the density of moist air and the liquid water content contribute to the total air density.

$$\rho_a = \rho_{moist} + w_L^* \qquad (V\text{-}4)$$

Therefore $\bar{\rho}_a = \bar{\rho}_{moist}$ and $\rho_a' = \rho'_{moist} + w_L^*$
With this we can rewrite the term:

$$\frac{\rho_a'}{\bar{\rho}_a} = \frac{\rho'_{moist}}{\bar{\rho}_{moist}} + \frac{w_L^*}{\bar{\rho}_a} \qquad (V\text{-}5)$$

For moist air we assume the ideal gas law:

$$\rho_{moist} = \frac{p}{R_d T_v} \tag{V-6}$$

T_v is the virtual temperature of moist air and is defined as:

$$T_v = T \left(\frac{R_d}{R_v} + q_v \right) \left\{ \frac{R_d}{R_v} (1 + q_v) \right\}^{-1} \tag{V-7}$$

where q_v is the water vapor mixing ratio. With the definition of the potential temperature (V-2) we can eliminate T and so we can rewrite eq.(V-5):

$$\frac{\rho_a'}{\bar{\rho}_a} = \frac{p'}{\bar{p}} \left(1 - \frac{R_d}{c_{pd}} \right) - \frac{\theta'}{\bar{\theta}} + \left(\frac{R_d}{R_v} - 1 \right) \frac{R_v}{R_d} q_v' + \frac{w_L^*}{\bar{\rho}_a} \tag{V-8}$$

and with the anelastic hypothesis:

$$\frac{\rho_a'}{\bar{\rho}_a} = - \frac{\theta'}{\bar{\theta}} + \left(1 - \frac{R_v}{R_d} \right) q_v' + \frac{w_L^*}{\bar{\rho}_a} \tag{V-9}$$

If we further assume $\mathbb{III} = \sum_{ij} \tau_{ij} e_i e_j$ we get the horizontal and vertical momentum equations:

$$\bar{\rho}_a \left(\frac{\partial u}{\partial t} + u \frac{\partial u}{\partial x} + w \frac{\partial u}{\partial z} \right) = - \frac{\partial p'}{\partial x} + \frac{\partial \tau_{11}}{\partial x} + \frac{\partial \tau_{13}}{\partial z}$$

$$\bar{\rho}_a \left(\frac{\partial w}{\partial t} + u \frac{\partial w}{\partial x} + w \frac{\partial w}{\partial z} \right) = - \frac{\partial p'}{\partial z} + \frac{\partial \tau_{31}}{\partial x} + \frac{\partial \tau_{33}}{\partial z} \tag{V-10}$$

$$+ \bar{\rho}_a g \left\{ \frac{\theta'}{\bar{\theta}} + 0.608 q_v' - \frac{w_L^*}{\bar{\rho}_a} \right\}$$

The anelastic form of the continuity equation (II-1) is expressed as

$$\frac{\partial}{\partial x} \left(\bar{\rho}_a u \right) + \frac{\partial}{\partial z} \left(\bar{\rho}_a w \right) = 0 \tag{V-11}$$

The first law of thermodynamics is expressed by

$$\bar{\rho}_a \left\{ \frac{\partial}{\partial t} \left(\frac{\theta'}{\bar{\theta}} \right) + w \cdot \nabla \left(\frac{\theta'}{\bar{\theta}} \right) \right\} = \frac{L_v}{c_{pd} \bar{T}} C_{ph} + \nabla \cdot \left(\bar{\rho}_a K_m \nabla \left(\frac{\theta'}{\bar{\theta}} \right) \right) \tag{V-12}$$

The eddy mixing coefficient K_m is set to be independent of the transported quantity and thus the same in every equation. So eqs.(II-2) and (II-3) become:

$$\frac{\partial w_v'}{\partial t} = -\nabla\cdot\left(w_v' w\right) + \nabla\cdot\left(K_m \nabla w_v'\right) - C_{Ph}$$

$$\frac{\partial w_L^*}{\partial t} = -\nabla\cdot\left(w_L^* w\right) + \nabla\cdot\left(K_m \nabla w_L^*\right) + C_{Ph} + \frac{\partial}{\partial z}\left(V_\infty w_L^*\right) \qquad \text{(V-13)}$$

The components of the stress tensor τ_{ij} are taken proportional to the deformation D_{ij} according to the first-order theory of Lilly(1962) and Smagorinsky(1963) where

$$\tau_{ij} = \bar{\rho}_a K_m D_{ij} \qquad \text{(V-14)}$$

and the deformation tensor D_{ij} and eddy mixing coefficient K_m are expressed as

$$D_{ij} = \frac{\partial u_i}{\partial x_j} + \frac{\partial u_j}{\partial x_i} - \frac{2}{3}\delta_{ij}\frac{\partial u_k}{\partial x_k} \qquad \text{(V-15)}$$

$$K_m = \begin{cases} \dfrac{C\Delta^2}{\sqrt{2}} |Def| \left(1 - Ri\right)^{1/2} & Ri < 1 \\ 0 & Ri \geq 1 \end{cases} \qquad \text{(V-16)}$$

where C=0.2 and $\Delta = \sqrt{\Delta x \Delta z}$ with Δx and Δz being the model grid spacing for the horizontal and the vertical directions respectively. Def is the total deformation in two dimensions and Ri the local Richardson number. Their definitions are

$$Def = \frac{1}{2}\left\{\left(D_{11}^2 + D_{33}^2\right) + D_{13}^2\right\}^{1/2} \qquad \text{(V-17)}$$

$$Ri = g\frac{\partial}{\partial z}\left\{\frac{\theta'}{\bar{\theta}} + 0.608\, q_v' - \frac{w_L^*}{\bar{\rho}_a}\right\} Def^{-2} \qquad \text{(V-18)}$$

V.2 Initial conditions for evaluating the model

The main purpose for evaluating our scavenging model in conjunction with the more realistic two dimensional cloud model of Clark et al. is to verify our conclusions from our scavenging model as used in conjunction with the entraining air parcel model. In doing so we are fully aware that we are not able to completely simulate a real atmospheric cloud with this model. The reason is that a two dimensional cloud model does not describe the real three dimensional dynamics of the atmosphere since it allows divergence in one direction to be

compensated only by convergence in the other direction, since it does not allow a vortex in three dimensions. However, even a three dimensional model is never able to exactly simulate a real cloud as it predicts the mean field of a cloud neglecting the random effects of nature.

Given these facts it is interesting to ask oneself why two dimensional and even one dimensional cloud models successfully can predict the formation of a cloud and the rainfall (e.g. Silverman and Glass (1973)). The reason for this is that cloud formation and thus all scavenging related processes are mainly determined by the atmospheric sounding and by the surface heating, while any accurate dynamics is only of secondary importance to these special features. That's why we felt justified to apply the two dimensional version of the Clark et al. model to our scavenging problems.

The main goals of our study are to determine (1) the possibility of integrating aerosol scavenging in a cloud dynamic model (2) the total amount of uptaken aerosol material into the drops (3) the relative importance of the scavenging of aerosol particles by the nucleation mechanism as compared to the impaction mechanism (4) the concentration of aerosol material in the rainwater (5) the efficiency of aerosol scavenging as compared to the rain efficiency.

To achieve this goal we initialized the model with a sounding from the CCOPE experiment on June 20,1981 at 11 o'clock local time. The change with height of two of the input parameters, potential temperature θ and relative humidity RH, are displayed in Fig.(V-1). As our model at present is only designed to simulate warm clouds, we applied the above sounding to the equator (0° latitude) and chose further as input a maritime type of aerosol spectrum with a total number concentration of $N_{APo}=100\ cm^{-3}$ at the surface. The initial dry aerosol particle spectrum was assumed to be given by the distribution of Deirmendjian(1969) eq.(IV-18) and the parameters listed in (IV-20). The aerosol particle number concentration was assumed to decrease with increasing height according to the governing air density. This means that the number per kg air remained constant. The aerosol particles were assumed to consist only of ammonium sulfate $(NH_4)_2SO_4$, $\varepsilon=1$, in order to determine the maximum possible amount of sulfur scavenged via the uptake of $(NH_4)_2SO_4$ particles. As already stated in section IV.2.1 this results

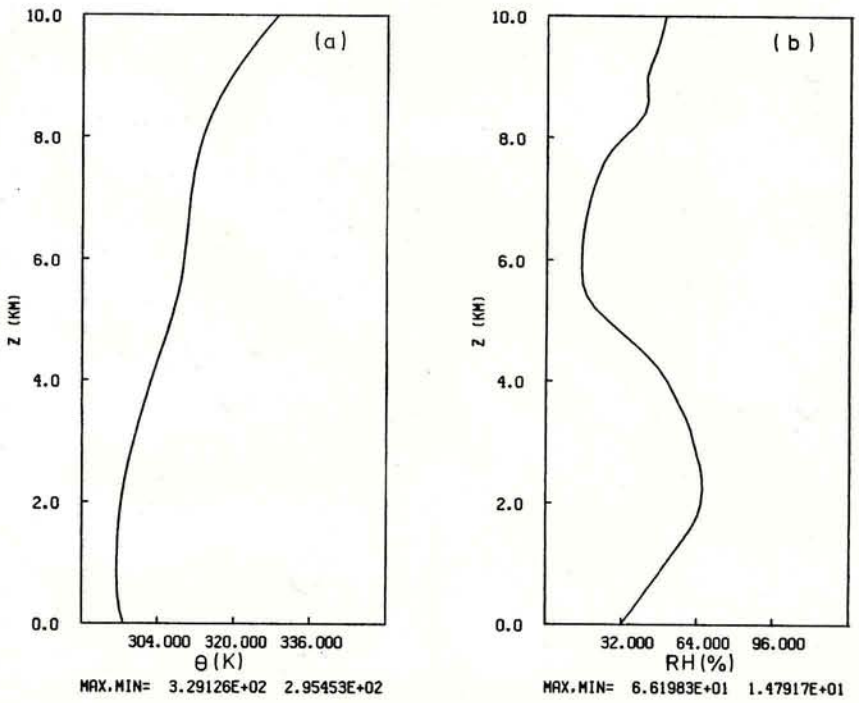

Fig.(V-1): Change with height of the input data for the 2-D run (a) potential temperature θ in K, (b) relative humidity RH in %.

in an ammonium sulfate mass content in air of 88 $\mu g/m^3$. This value is about 10 to 100 times too large as compared to sulfate contents in the air measured by field observations. We therefore expect that the amount of sulfate scavenged by the cloud also will exceed the field observations by a similar factor. In actuality, as shown by Junge(1963) and others aerosol particles are mixed and consist of various water soluble and insoluble materials of which sulfate in only a small fraction. The amount of sulfate to be scavenged by a cloud will therefore be comparably less. Thus, for the chosen conditions, our model will overestimate the actual amount of sulfur to be scavenged by a cloud.

The density of the aerosol particles considered was assumed to be 2 $g\ cm^{-3}$. In order to get the initial moist aerosol particle distribution we allowed the dry aerosol particles to grow to their equilibrium size they have at the governing relative humidity.

The present model covers a domain of 10km in the vertical and 20km in the horizontal. The space increments are set to be Δz=200m and Δx=400m. The time step was chosen to be Δt=5sec and the minimum drop radius was set to be 4μm (compare chapter VI).

The initialization of the model was designed by Smolarkiewicz(1984) to also allow the simulation of whole cloud fields randomly generated and is described in the following paragraph.
The model is driven by a sensible heat flux and a moisture flux from the surface. These fluxes are assumed to be proportional to the incoming shortwave solar flux S (Clark, Gall(1982)):

$$S = S_o \cos Z \tag{V-19}$$

S_o is the solar constant taken as 1395 W m^{-2} and Z the sun's zenith angle is given as

$$\cos Z = \sin \varphi \sin \lambda + \cos \varphi \cos \lambda \cos \phi_r \tag{V-20}$$

where the latitude φ was taken as 0°, the sun's declination angle λ was calculated as:

$$\lambda = \frac{23.45}{180} \pi \cos \left(\frac{2\pi (n_d - 172)}{365} \right) \tag{V-21}$$

n_d: number of this day of the year
and the hour angle ϕ_r is given as

$$\phi_r = \frac{\pi (12 - h_d)}{12} \tag{V-22}$$

h_d: hour of the day.
The average surface sensible heat flux was then assumed to be P =58% and the latent heat flux to be P =2% of the incoming solar flux. These heat fluxes were assumed to consist of a background value and a

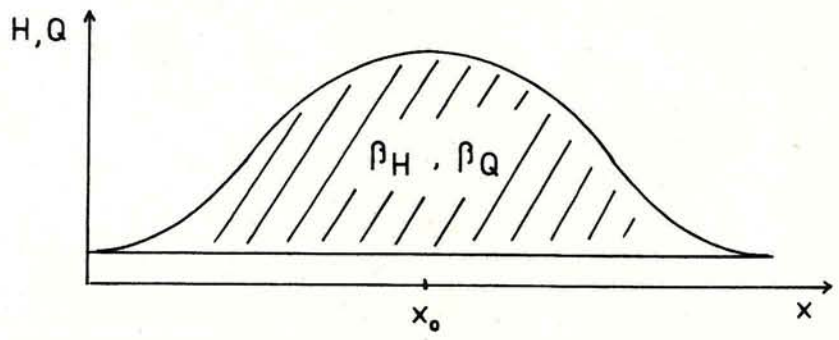

Fig.(V-2): Schematic display of the surface sensible and latent heat flux.

Gaussian perturbation fraction (compare Fig.(V-2)). The size of these fractions determined the location and strength of the cloud. To force a fast developing cloud in the middle of the domain we set the fraction of the total energy that goes into the Gaussian perturbation of the sensible heat flux to be β_H=99.5% and the fraction that goes into the Gaussian perturbation of the latent heat flux to be β_Q=99.5%.
The surface sensible heat flux is then calculated to be:

$$H = \frac{P_H S}{1 + \frac{\alpha_H \sqrt{2\pi}}{6}} \left(1 + \alpha_H \exp\left\{ - \frac{(x - x_o)^2}{2\sigma_H^2} \right\} \right) \qquad (V\text{-}23)$$

and the surface latent heat flux:

$$Q = \frac{P_Q S}{1 + \frac{\alpha_Q \sqrt{2\pi}}{6}} \left(1 + \alpha_Q \exp\left\{ - \frac{(x - x_o)^2}{2\sigma_Q^2} \right\} \right) \qquad (V\text{-}24)$$

with

$$\alpha_H = \frac{6\beta_H}{\sqrt{2\pi}(1 - \beta_H)} \qquad (V\text{-}25)$$

$$\alpha_Q = \frac{6\beta_Q}{\sqrt{2\pi}(1 - \beta_Q)} \qquad (V\text{-}26)$$

σ_H=3600m and σ_Q=3600m being the half-width of the two Gaussian perturbations, and x_o locates the middle of the domain in the horizontal. These heat and moisture sources were assumed to have their maximum at the ground and attenuate exponentially with height, so that at 150m they have decreased to 1/e of their surface value.
This present run took 4.5h on a CRAY-1A computer and the results are presented in chapter VII.3.

VI The numerics of the scavenging model

To code the presented equations for aerosol particle and gas scavenging in a numerical model they need to be discretized. The transformation of the equations in a discrete form and their numerical evaluation will be described in the following sections.
The numerics of the two dimensional cloud model of Clark et al. will not be described here as we only use it in its present form and don't alter it. For the description of the numerics we refer to Clark(1977, 1979) and to Clark and Farley(1984).

VI.1 The discretion of radius

The drop spectrum is discretized onto a logarithmic radius grid, according Berry and Reinhardt(1974a-d), where the grid spacing interval is a constant with mass doubling every JRS category. JRS is the resolution parameter and is equal to 2 for the present study. The radius of each grid value is:

$$a(J) = a(1)\, 2^{\frac{J-1}{3\,JRS}} \qquad \text{(VI-1)}$$

with a(1): minimum droplet radius.
a(1) is assumed to 1μm in the calculation with the air parcel model and 4μm in the calculation with the two dimensional model of Clark et al. J ranges from 1 to the maximum number of drop categories:

$$J_{max} = 69 \text{ for the air parcel model}$$

$$J_{max} = 57 \text{ for the two dimensional model} \qquad \text{(VI-2)}$$

In both cases we end up with a maximum drop size of 2580.3μm.
For the drop sizes given by eq.(VI-1) the cloud drop number density distribution function f_d, the mass density distribution function for aerosol particles in cloud water g_{APd} and other related distribution functions are defined. Their values represent averages over the drop size categories. The boundaries of these drop size categories are

staggered values and given by:

$$a_s(J) := a(J+1/2) = a(1)\, 2^{\frac{J-1/2}{3\,JRS}} \qquad \text{(VI-3)}$$

The discretion of the aerosol particle radius is carried out in a way similar to the discretion of the drop radius:

$$r(K) = r(1)\, 2^{\frac{K-1}{3\,KRS}} \qquad \text{(VI-4)}$$

The resolution parameter is assumed again to be KRS=2. The minimum aerosol particle radius was set to be near 10^{-3} µm, while the maximum radius was set to be about 10µm, as bigger aerosol particles tend to fall out due to sedimentation.
So there is a certain range between 1µm and 10µm where the drop spectrum and the aerosol particle spectrum overlap. In this range we require the categories to be aligned such that each aerosol particle size category ranges over the same size interval as the corresponding drop size category. This prevents a considerable amount of bookkeep-

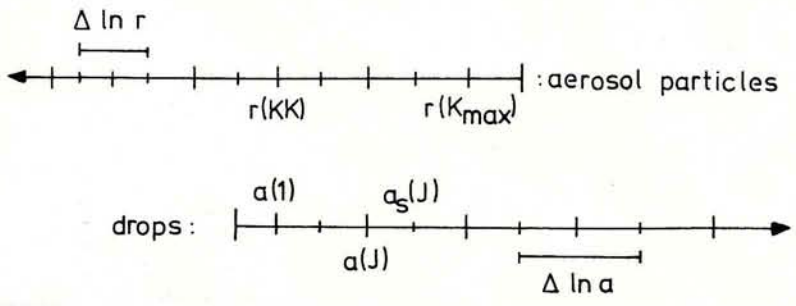

Fig.(VI-1): Schematic display of the alignment of aerosol particle and drop size categories.

ing during the activation and deactivation processes. Fig.(VI-1) illustrates this behavior schematically. In this manner a constraint is obtained for the minimum aerosol category radius. We set:

$$\tilde{r}(1) = 10^{-3}\,\mu m$$

and calculate the KK integer value next to a(1):

$$a(1) = \tilde{r}(1)\, 2^{\frac{KK-1}{3\,KRS}}$$

so:

$$KK = INT\left\{ \left(\ln \frac{a(1)}{r(1)} \Big/ \ln 2 \right) \cdot 3\,KRS + 1.5 \right\} \qquad \text{(VI-5)}$$

then we set r(KK)=a(1) and solve for r(1):

$$a(1) = r(1)\; 2^{\frac{KK-1}{3\,KRS}}$$

This gives us:

$$r(1) = 9.76\;\; 10^{-4}\;\mu m \qquad \text{(VI-6)}$$

The other radii are given by eq.(VI-4). In this manner the categories are now aligned, and the maximum value for the aerosol particle radii considered lies at 10.08μm for K_{max}=81.

The unactivated aerosol particle number density distribution function in air f_{APa}, the aerosol particle mass density distribution function in unactivated aerosol particles g_{APa} and other related distribution functions are defined for the aerosol particle sizes given by eq.(VI-4). Their values represent averages over the aerosol particle size categories. The boundaries of these aerosol particle size categories are staggered values given by

$$r_s(K) := r(K + 1/2) = r(1)\; 2^{\frac{K-1/2}{3\,KRS}} \qquad \text{(VI-7)}$$

The grid spacing intervals for the drops and for the aerosol particles have therefore the same constant width:

$$\Delta \ln a := \ln \frac{a(J+1)}{a(J)} = \frac{\ln 2}{3\,JRS} \qquad \text{(VI-8)}$$

$$\Delta \ln r := \ln \frac{r(K+1)}{r(K)} = \frac{\ln 2}{3\,KRS} \qquad \text{(VI-9)}$$

VI.2 Treatment of the advection equation

In numerous parts of the calculations equations of the form:

$$\frac{\partial \psi}{\partial t} + \frac{\partial}{\partial x} (u \psi) = 0 \qquad \text{(VI-10)}$$

have to be solved (compare e.g. chapter II.4, II.6, II.7), where ψ is a scalar quantity and u is the transport velocity. These advection equations have long time been a problem to numeric modelers. Either the applied numeric schemes are very costly because of the excessive computer time they require and/or they produce negative values during their solution and suffer from excessive numerical diffusion.
To remedy this problem Smolarkiewicz(1983) developed a simple positive definite advection scheme with small implicit diffusion which we used in the model with very satisfying results.
As a base for the construction of the scheme, Smolarkiewicz chose the 'upstream' advection scheme on a staggered grid:

$$\psi_i^{\tau+1} = \psi_i^{\tau} - \left\{ F(\psi_i^{\tau}, \psi_{i+1}^{\tau}, u_{i+1/2}^{\tau}) - F(\psi_{i-1}^{\tau}, \psi_i^{\tau}, u_{i-1/2}^{\tau}) \right\} \qquad \text{(VI-11)}$$

where

$$F(\psi_i, \psi_{i+1}, u) = \left\{ (u + |u|) \cdot \psi_i + (u - |u|) \psi_{i+1} \right\} \cdot \frac{\Delta t}{2 \Delta x} \qquad \text{(VI-12)}$$

ψ_i^{τ} is the value of ψ at the 'i' grid point for 'τ' time steps; Δt, Δx are the time and space increments, and the fluxes F are defined at the same staggered points as the velocity values.
The stability condition for this scheme is given by the CFL criterion:

$$\max_i \left(\frac{|u_{i+1/2}^{\tau}| \cdot \Delta t}{\Delta x} \right) \leq 1 \qquad \text{(VI-13)}$$

If this condition is not met the calculations are done in n iterations, where 'n' is the number by which the time step has to be reduced to meet the CFL criterion:

$$\Delta t^* = \frac{\Delta t}{n} \qquad \text{(VI-14)}$$

As the 'upstream' advection scheme has a strong implicit diffusion after each iteration we have to correct for this entirely numerical effect. This is done by running the same scheme again for several correction steps while the transport velocity u is replaced by a diffusion velocity:

$$\tilde{u}_{i+1/2} = \frac{(|u_{i+1/2}|\,\Delta x - \Delta t\, u_{i+1/2}^2)(\eta_{i+1} - \eta_i)}{(\eta_i + \eta_{i+1} + \varepsilon_s)\,\Delta x} - \frac{1}{4}\frac{\Delta t}{\Delta x}\, u_{i+1/2}\,(u_{i+3/2} - u_{i-1/2}) \qquad \text{(VI-15)}$$

where ε_s is a small value e.g. 10^{-15}.
The second term on the right hand side of eq.(VI-15) was proposed by Smolarkiewicz(1984) to correct for divergence effects. The more correction steps are run with this scheme the better the results get. Though for our purposes normally one or two steps lead to sufficiently good results.

The time derivatives are treated with a forward difference scheme:

$$\frac{\partial \eta}{\partial t} = \frac{\eta^{\tau+1} - \eta^{\tau}}{\Delta t} \qquad \text{(VI-16)}$$

where the time increment Δt is set to 2 sec in the parcel model case and to 5 sec in the two dimensional model.

The numerical treatment of the kinetic equations of chapter II.8 is done in the way described by Berry, Reinhardt(1974a-d).

VII Results

VII.1 Aerosol scavenging in an entraining air parcel model

To study some effects of aerosol scavenging we have linked the aerosol scavenging model described in chapter II to the entraining air parcel model of chapter IV. This gives us a very simplified dynamic framework that enables us to look closely at the effects of the microphysics of a cloud on the scavenging processes. The initial conditions and the boundary values are given in chapter IV.2. In the rising air parcel a cloud forms on three different aerosol particle spectra as given by eqs.(IV-18) to (IV-20). We now shall look at the results of these cases:

VII.1.1 Case 1

In these computations the aerosol particle spectrum is given by eq.(IV-18) and the parameters (IV-19). This represents a continental type spectrum and the particles shall only consist of ammonium sulfate (ε=1). Fig.(VII-1) displays the behavior of the dynamic variables inside the air parcel during its ascent. The parcel starts at a height of 1km and stops at about 4.2 km. The radius of the bubble increases from 350m to about 2500m due to the expansion of air in higher altitudes. The vertical velocity U increases with height from 1m/sec to about 2.5m/sec in 2.3km and then decreases again until the parcel stops at 4.2 km. This is due to the friction produced by the entrainment. The total liquid water content w_L^* increases during the whole period of integration to about 2g/kg. The supersaturation $s_{v,w}$ shows a very distinct overshooting in the first hundred meters of the cloud resulting from the fact that the system first has to activate the necessary amount of particles before they can grow through condensation and thus the supersaturation can drop again.
Fig.(VII-2a) represents the evolution in time of the aerosol particle distribution function which is represented by the variable f_{APa}.
We note here that in all forthcoming figures the density distribution functions are expressed per logarithmic radius interval $\Delta \ln a$ or $\Delta \ln r$

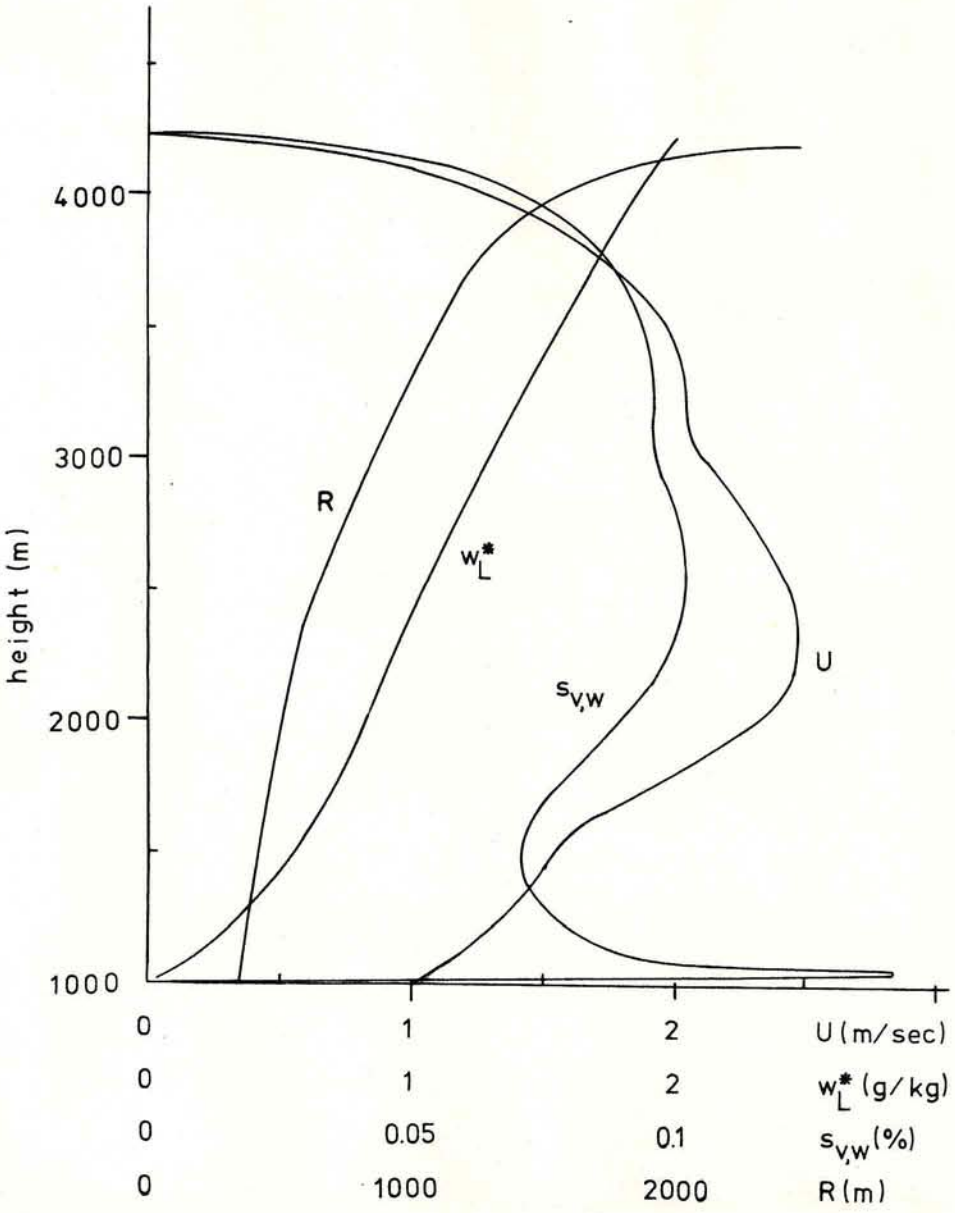

Fig.(VII-1): Variations with height of total liquid water content w_L^*, updraft radius R, supersaturation $s_{v,w}$ and updraft velocity U in the entraining air parcel for case 1 (continental aerosol particle spectrum, $\varepsilon = 1$).

as given in eqs.(VI-8) and (VI-9). The ordinates are linear and always adjusted to the occuring maximum of the curve. The aerosol particle spectrum ranges from 10^{-3} µm to 10 µm. The graphs are drawn with a time spacing of 200 seconds. The actual time is given by the first number in the graph. The second number gives the current updraft velocity and the following two numbers give the total aerosol number concentration per m^3 and per kg. At time t=0 seconds we see the full aerosol particle spectrum in a cloud free air parcel (compare

Fig.(VII-2b)). Then the air parcel rises and the air becomes supersaturated. According to chapter II.5 a major part of the aerosol particle spectrum becomes activated. Within 200 seconds the total number of aerosol particles decreases by 84%. The sharp cut-off in the spectrum is due to the fact that we only treat one species of aerosol particles. This implies that all particles of a certain size category either get activated or do not get activated. In the real atmosphere the aerosol represents not only an 'inner' but also an 'outer' mixture which implies that aerosol particles of different chemical composition are side by side suspended in the air. Thus, as the air becomes supersaturated some particles of a certain size category become activated while others stay unactivated. We further note from Fig.(VII-2a) that the supersaturation must have decreased since some of the previously activated categories fill up again due to entrainment and are not activated (compare Fig.(VII-1)). The rest of the time the total number of aerosol particles changes only little. We note that after t=600 seconds the total number of aerosol particles in air N_{APa} continues to slightly decrease in time due to further nucleation scavenging. During this time the supersaturation increases a little. After t=1000 seconds, however, N_{APa} increases again due to a lowering of $s_{v,w}$ on account of the entrained air which increases in dryness with height. Consequently fewer aerosol particles become activated, i.e., more remain as interstitial aerosol.

Fig.(VII-2b) shows the corresponding drop number density distribution function f_d. The drop spectrum ranges from 1 μm to 2580 μm. At the beginning the total number of drops N_d=0. Then at 200 seconds about 800 drops cm^{-3} have been activated. Through condensation this peak slowly migrates to larger drop sizes. Entrainment provides new aerosol particles which can be activated and form new drops. The constraint of activation on the entrained nuclei has as a consequence that new drops only appear after a critical time has elapsed, a time after which the vapor pressure again is large enough to raise the supersaturation in the parcel above that required for activating new aerosol particles to drops. During this 'recovery' of the vapor field, the previously formed group of drops has had time to grow by diffusion and thus to 'detach' itself somewhat from the next following group of aerosol particles activated to drops. This is the explanation for the multiple peaks in the drop size spectrum in Fig.(VII-2b). We expect

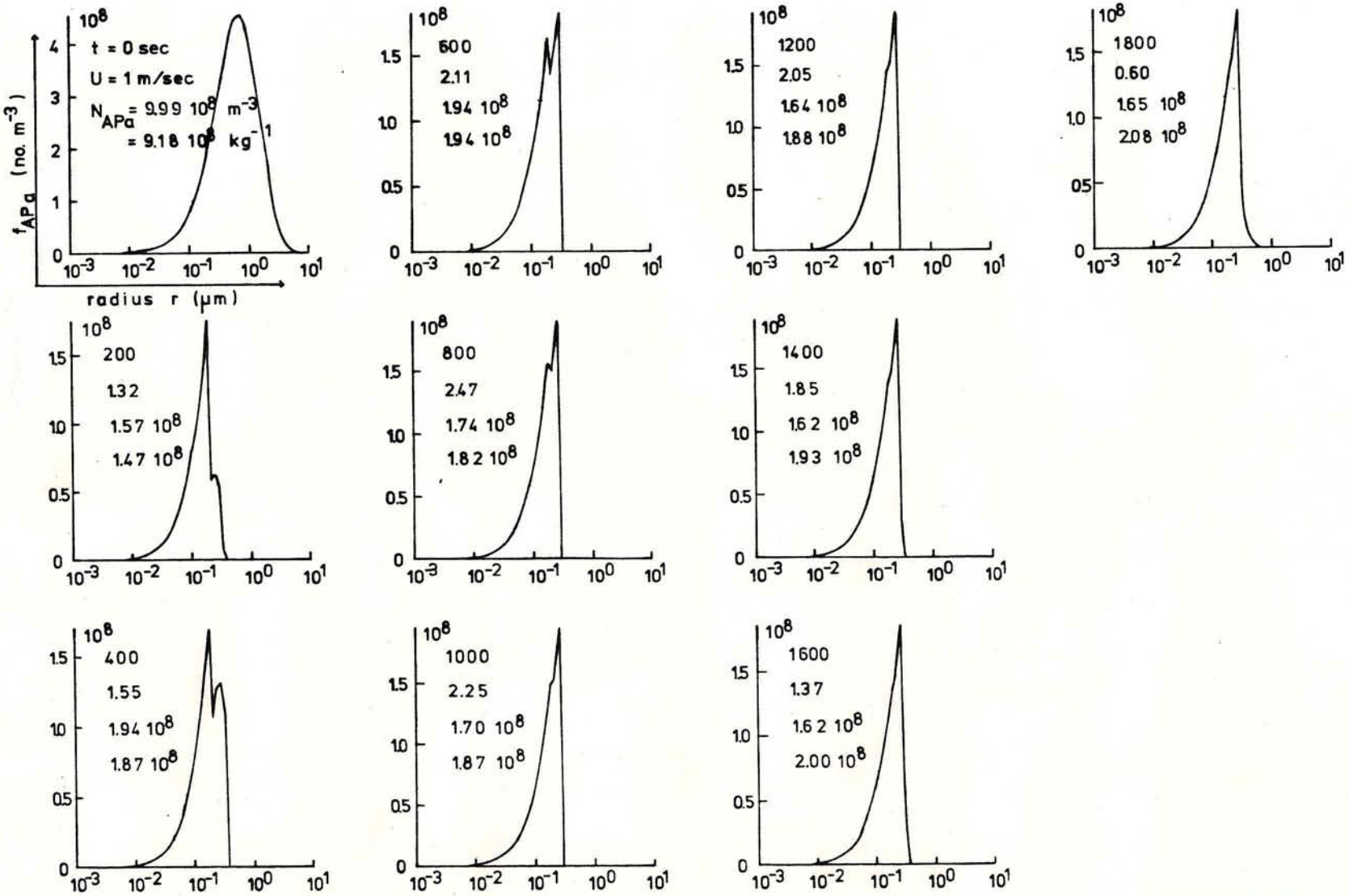

Fig.(VII-2a): Time evolution of aerosol particle number density distribution function f_{APa} for aerosol particles of radius r in air between cloud drops (interstitial aerosol) for case 1 (continental aerosol particle spectrum, $\varepsilon = 1$).

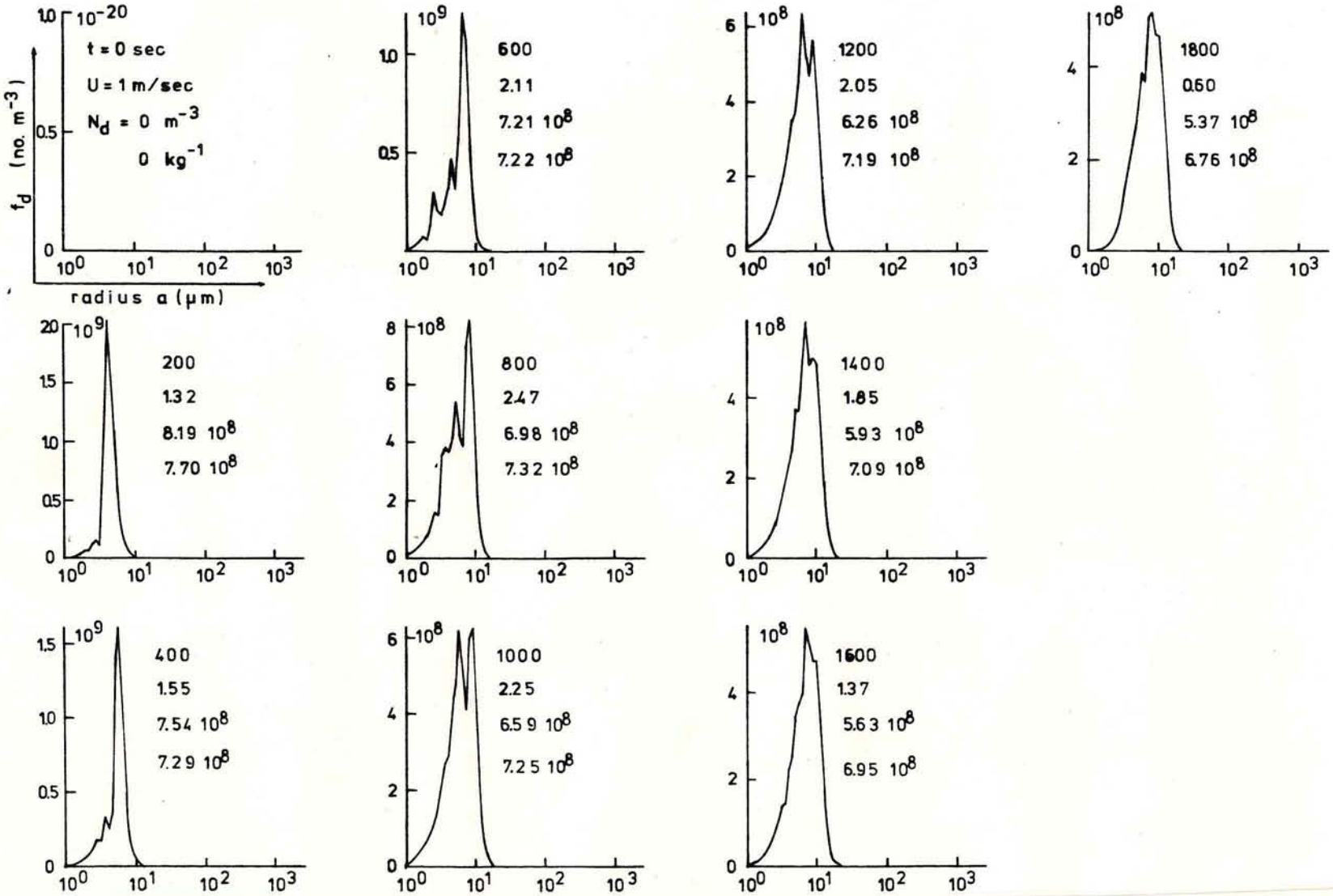

Fig.(VII-2b): Time evolution of drop number density distribution function f_d as a function of drop radius for case 1 (continental aerosol particle spectrum, ε=1).

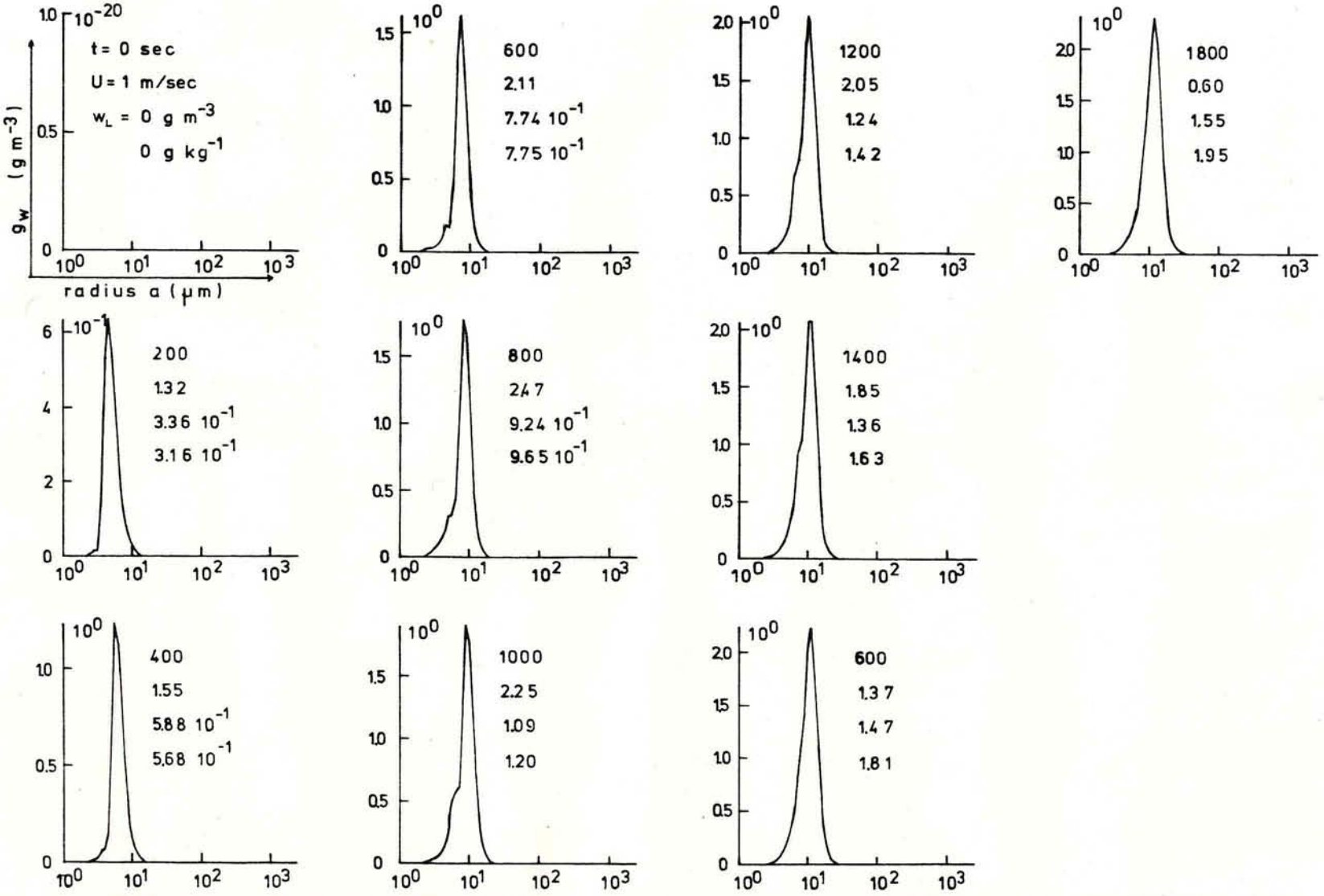

Fig.(VII-2c): Time evolution of the drop water mass density distribution function g_w as a function of drop radius for case 1 (continental aerosol particle spectrum, $\varepsilon = 1$).

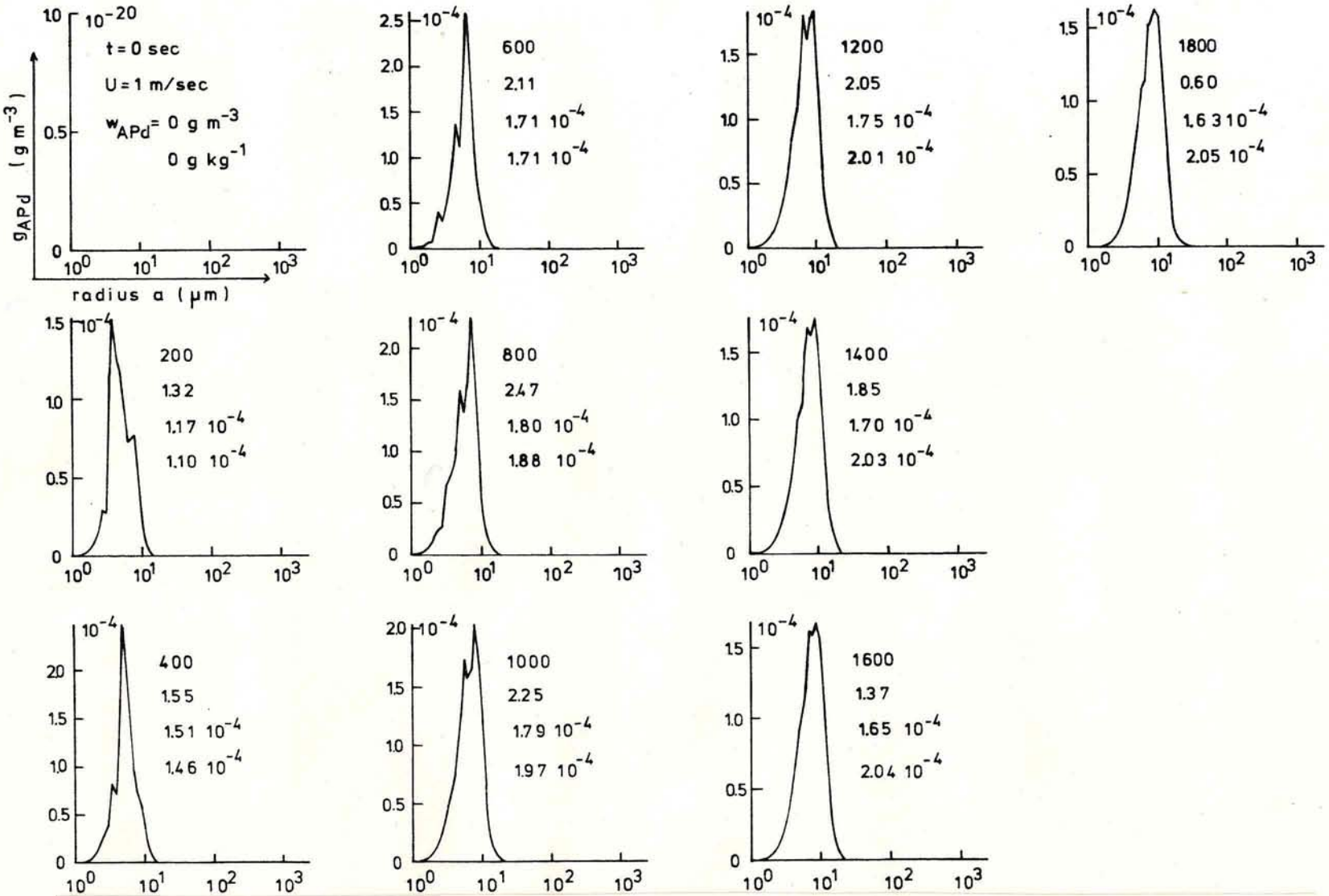

Fig.(VII-2d): Time evolution of aerosol particle mass density distribution function g_{APd} for aerosol particle mass inside drops of radius a, captured through nucleation and impaction scavenging by drops of size spectrum evolving in time as given in Fig.(VII-2b) and Fig.(VII-2c) for case 1 (continental aerosol particle spectrum, $\varepsilon = 1$).

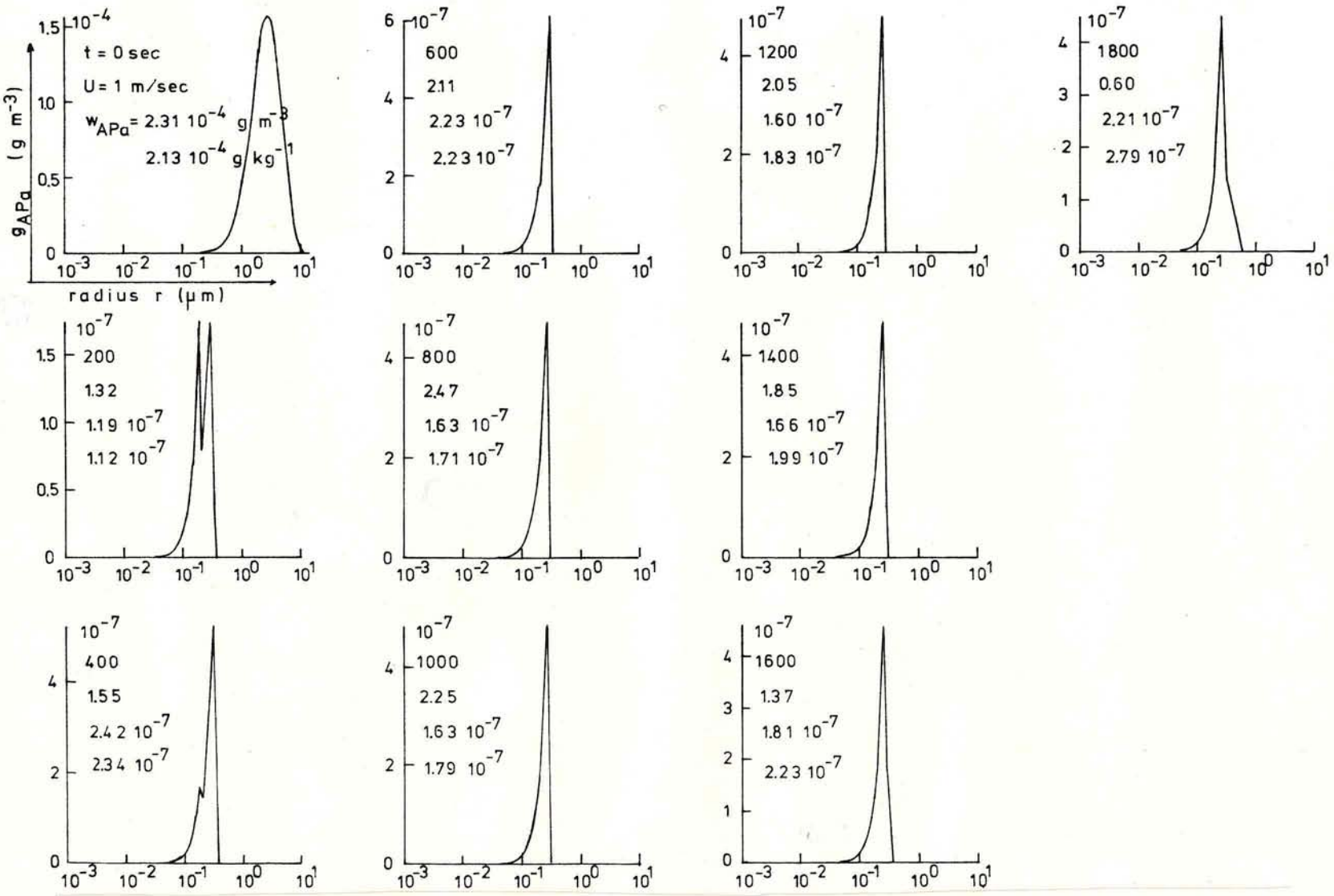

Fig.(VII-2e): Time evolution of aerosol particle mass density distribution function g_{APa} for aerosol mass in air between cloud drops (interstitial aerosol) as a function of radius r of aerosol particles for case 1 (continental aerosol particle spectrum, $\varepsilon = 1$).

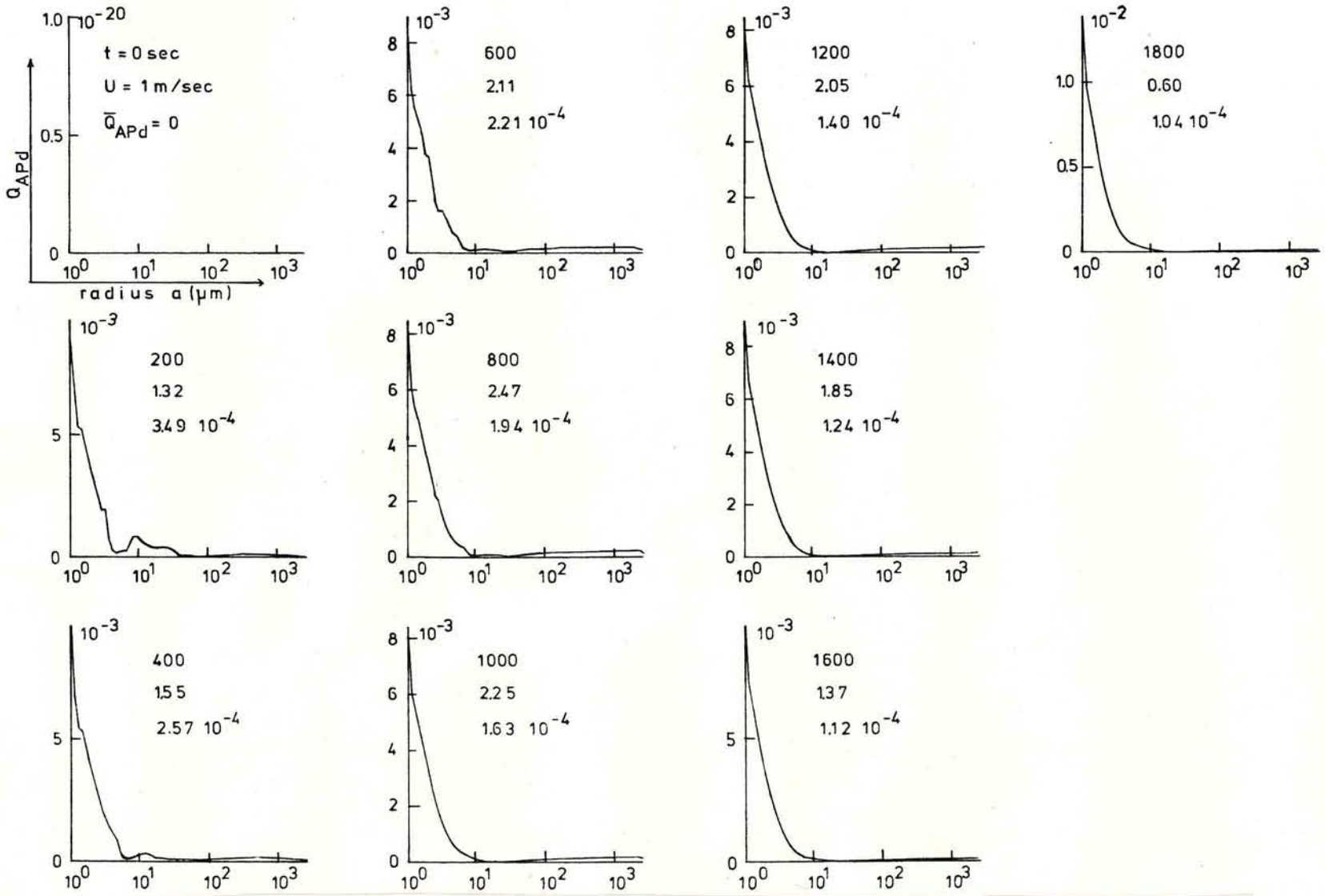

Fig.(VII-2f): Time evolution of aerosol particle mass mixing ratio Q_{APd} in cloud drops as a function of drop radius for case 1 (continental aerosol particle spectrum, $\varepsilon = 1$).

that the multiple peaks will disappear if the atmospheric aerosol represents an external mixture of particles in the air and if the turbulence in the cloud is allowed to mix the drops formed. We also should emphasize that the disappearance of the multiple maxima in the drop size distribution is a result of the choice of increasingly broader drop size categories which 'swallow up' the different peaks. Fig.(VII-2c) displays the total water mass g_w attached to the drop spectrum. We note here that the collision-coalescence process which is responsible for producing big drops can't work efficiently. No 2nd maximum - indicating precipitation-sized drops - is formed. The main water mass stays confined to the small drops. The reason for that is that so many drops were nucleated that they could not grow efficiently by condensation to that point where collision and coalescence can become effective. This also becomes clear from Table VII-1 which displays the number concentration of drops larger than 30μm, 50μm, 100μm, 500μm and 1000μm. The solid line separates the region where most drops are from the one with only little drop numbers. We can see here that the spectrum does not develop enough large drops for them to

a(μm) / t(sec)	30	50	100	500	1000
200	0.552E-4	0.278E-4	0.184E-4	0.252E-5	0.117E-5
400	0.645E-3	0.449E-4	0.219E-4	0.189E-5	0.918E-6
600	0.169E-1	0.518E-4	0.219E-4	0.151E-5	0.880E-6
800	0.443E+0	0.717E-4	0.204E-4	0.128E-5	0.989E-6
1000	0.863E+1	0.639E-2	0.190E-4	0.176E-5	0.924E-6
1200	0.112E+3	0.549E+0	0.136E-3	0.486E-5	0.115E-5
1400	0.970E+3	0.210E+2	0.769E-1	0.899E-5	0.315E-5
1600	0.557E+4	0.374E+3	0.844E+1	0.158E-4	0.909E-5
1800	0.223E+5	0.341E+4	0.267E+3	0.140E-1	0.201E-4

Table VII-1: Number of drops per m^3 larger than 30μm, 50μm, 100μm, 500μm and 1000μm as a function of time for case 1 (continental aerosol particle spectrum, ϵ =1).

grow efficiently by collision and coalescence of drops.

The same behavior can be found in Fig.(VII-2d) for the aerosol mass

inside the drops g_{APd}. The main aerosol mass stays with the small drops. What strikes here is that the amount of captured aerosol mass inside the drops does increase only little after the first 200 seconds as a result of continued nucleation of aerosol particles transported into the parcel by entrainment, impaction scavenging of the aerosol particles left unactivated during condensation, and detrainment of drops.

The reason for that becomes clear if we look at the spectrum of aerosol particle mass in the air g_{APa} in Fig.(VII-2e). This figure displays the aerosol particle spectrum remaining in the air not by its number - as in Fig.(VII-2a) - but by the aerosol mass attached to the aerosol particles. We notice from this figure that in the first 200 seconds the total aerosol mass w_{APa} is reduced by three orders of magnitude. That is because all the large particles which contain the major part of the mass become activated. Only the small particles with little mass are left behind as drop-interstitial aerosol. Therefore impaction scavenging doesn't have any chance to contribute a noticeable amount to the captured aerosol mass inside the drops.

The last figure of this series -Fig.(VII-2f)- illustrates the mixing ratio Q_{APd}, which is the ratio of aerosol mass to cloud drop mass, as a function of drop radius. We note that this mixing ratio strongly increases with decreasing drop size, implying that the smallest drops are also the most contaminated ones. However, we have to recall that the mass associated with the aerosol particles in these small drops is very small indeed. Thus, although the large drops are characterized by very small values of Q_{APd}, they still carry the main aerosol mass. We also note from Fig.(VII-2f) that the total mass mixing ratio $\overline{Q}_{APd}$ of aerosol particle mass in the cloud water decreases with time as a result of continued 'dilution' of the captured aerosol material due to the diffusion growth of the drops.

As we have seen such an aerosol particle spectrum determines a drop spectrum that doesn't develop precipitation-sized drops. However, the aerosol particle spectrum becomes processed during the life time of the cloud in a way illustrated by Fig.(VII-3). Curve (1) represents the initial dry aerosol particle spectrum as given at the beginning of the computations. Curve (2) illustrates the dry interstitial aerosol particle spectrum after 30 min of cloud life time. We see here that the aerosol particle spectrum is reduced in its larger particles due

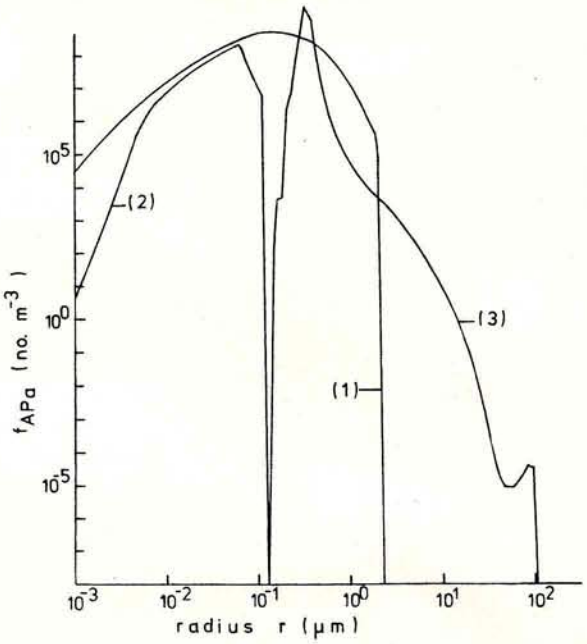

Fig.(VII-3): Aerosol particle number density distribution function f_{APa} as a function of radius r of aerosol particles for case 1 (continental aerosol particle spectrum, $\varepsilon = 1$).
(1): initial dry aerosol particle spectrum
(2): dry interstitial aerosol particle spectrum after 30 min of cloud life time
(3): aerosol particle spectrum from dried-off cloud drops after 30 min of cloud life time, if all material inside one drop becomes one single particle

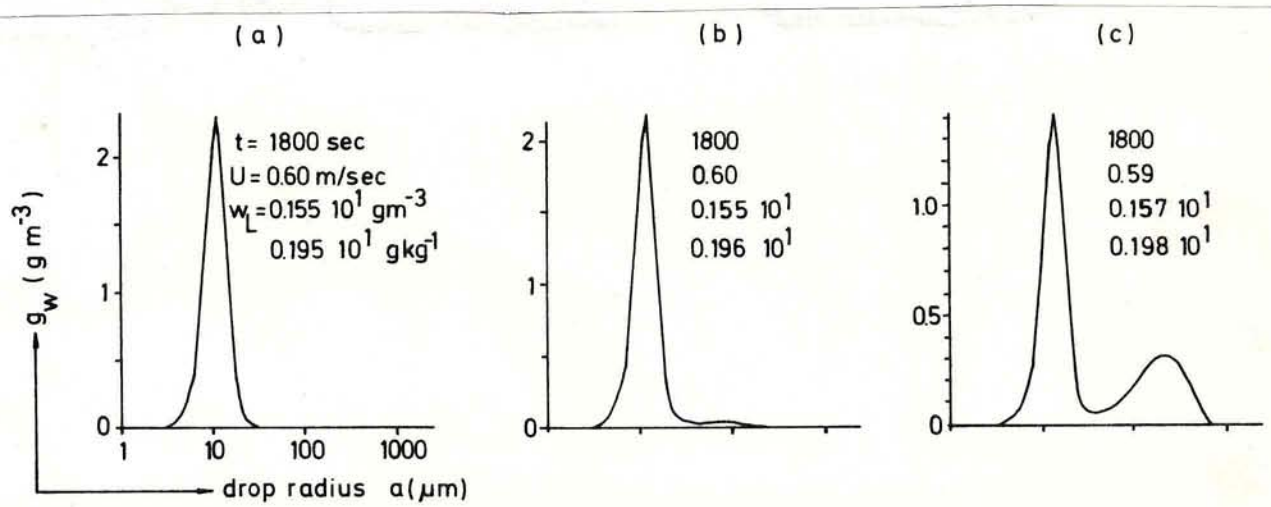

Fig.(VII-4): Drop water mass density distribution function g_w as a function of drop radius after 30 min of cloud life time.
(a): for the initial conditions of case 1
(b): as initial conditions served the interstitial and the dried-off aerosol particle spectrum of (a) after 30 min
(c): as initial conditions served the interstitial and the dried-off aerosol particle spectrum of (b) after 30 min

to nucleation scavenging and in its small particles by impaction scavenging as the efficiencies for impaction scavenging are large for the small aerosol particles due to the Brownian motion.
Curve (3) represents the size spectrum of the aerosol particles formed from the dried-off cloud drops. This is equivalent to the spectrum that would be released if the cloud would instantaneously completely evaporate and if it is assumed that all water soluble and insoluble material inside a drop becomes one single particle. We notice that the drops indeed have processed the aerosol particles in a way that a broadening of the aerosol size spectrum has taken place, increasing the number concentration of giant cloud condensation nuclei (CCN) and simultaneously reducing the number of small CCN around 1μm by 2 to 3 orders of magnitude.
We used this new aerosol particle spectrum consisting of curve (2) and curve (3) up to 2.2μm as an input for the same air parcel model run. The dry 2.2μm aerosol particles assume at the initial relative humidity of 99% a wet size of 10μm. All larger aerosol particles are assumed to have fallen out due to sedimentation or due to precipitation during their 'drop'-stage and are not considered as input into the new run. But they are so few that they don't matter much anyway. We notice that, as a result, the number of precipitation-sized drops has increased now. If we use the dried-off spectrum of this run once again as an input of a third condensation process, a distinct second maximum develops in the liquid water content g_w as displayed in Fig.(VII-4). Thus, we conclude that even if the effect of collision and coalescence between drops is relatively small the aerosol particle spectrum is processed during one cloud life time with the effect of producing rain drops after three condensation cycles.

VII.1.2 Case 2

In these computations the aerosol particle spectrum is given by the eq.(IV-18) and the parameters (IV-19). This is the same continental-type aerosol spectrum as in case 1 except that $\varepsilon = 0.01$ which means the aerosol particles consist of 1% ammonium sulfate and 99% insoluble silicate. Fig.(VII-5) displays again the behavior of the dynamic variables inside the air parcel during its ascent. The

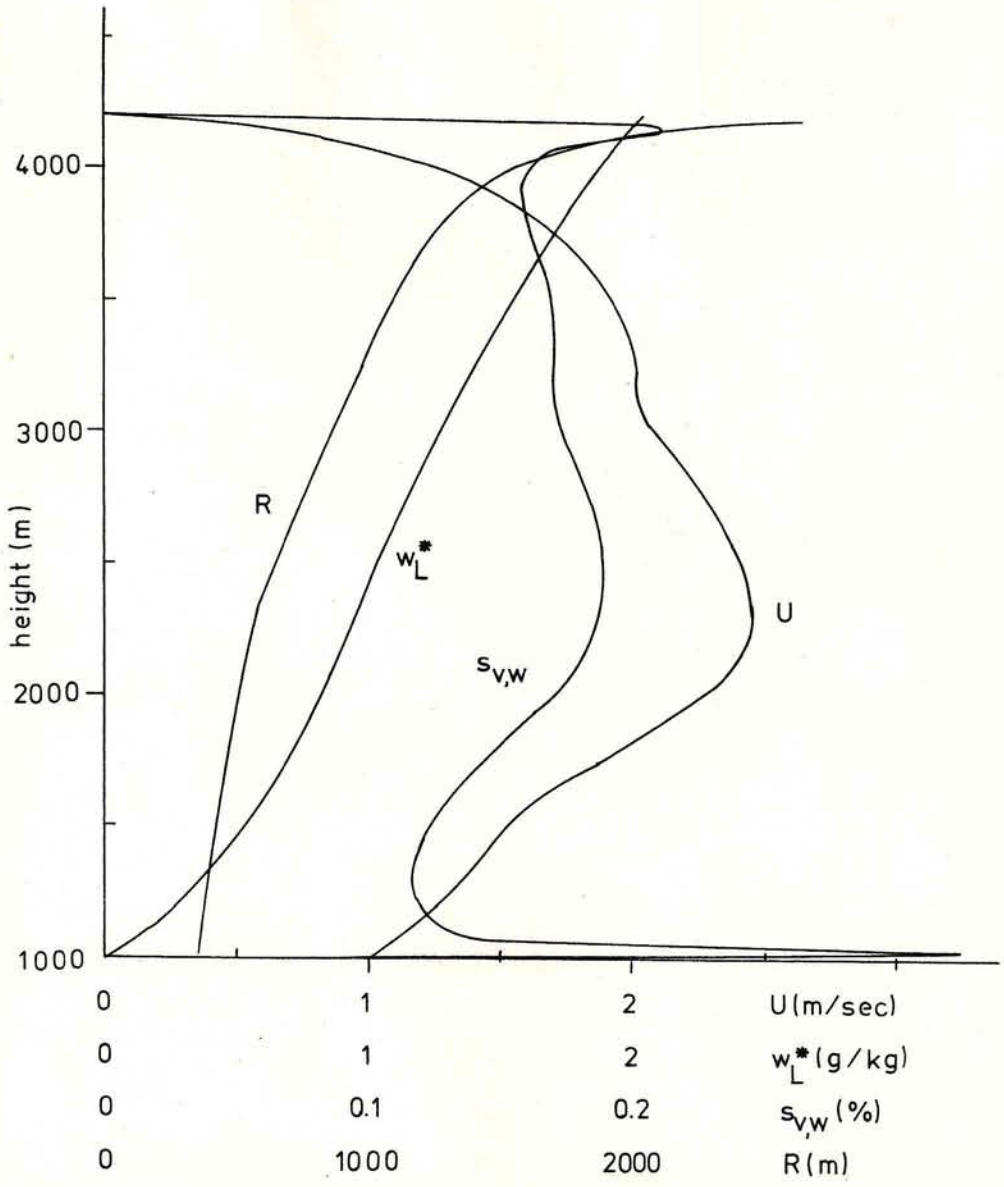

Fig.(VII-5): Variations with height of total liquid water content w_L^*, updraft radius R, supersaturation $s_{v,w}$ and updraft velocity U in the entraining air parcel for case 2 (continental aerosol particle spectrum, ε =.01).

curve for the bubble radius R, the one for the total liquid water content w_L^* and the one for the updraft velocity U are very similar to the same curves of case 1 since these variables are mainly determined by the dynamics. Only the curve for the supersaturation $s_{v,w}$ looks different and $s_{v,w}$ is about a factor of two larger than in case 1. This is due to the fact that fewer particles have now been activated due to their smaller soluble fraction, and thus the water vapor can't be so efficiently deposited on the fewer drops.

The Figures(VII-6a) to (VII-6f) display the same quantities as Figs.(VII-2a) to (VII-2f) for case 1.

Fig.(VII-6a) shows that the total number concentration of aerosol particles becomes reduced by 45%. Furthermore in the first 200 seconds the supersaturation has decreased considerably since some of the larger aerosol categories fill up again due to entrainment and these particles are not activated (compare Fig.(VII-5)).

From Fig.(VII-6b) we see that after 200 seconds about 420 drops per cm^3 have formed. In the first part of the computation these grow mainly by condensation. After 1600 seconds, however, the total number concentration of drops has decreased significantly. The reason for that is the collision-coalescence process dominating the later stages of the run. This also becomes clear if we look at Table VII-2 which displays the number concentration of drops larger than 30μm, 50μm, 100μm, 500μm and 1000μm. We can see here that collision and coalescence of drops has formed significantly more big drops than in case 1. This also becomes clear from Fig.(VII-6c) which displays the water mass attached to the drops and thus points to the precipitation-sized drops that have formed through collision and coalescence of drops. They contain the main water mass and in 'real' clouds correspond to rain drops.

Fig.(VII-6d) displays the behavior of the aerosol mass captured inside the drops. Here we see that they are transported along with the water mass to the large drop size categories. So the main aerosol mass is associated with the main water mass, thus insuring that if a cloud develops rain drops they carry with them the main pollution mass.

Fig.(VII-6e) illustrates the aerosol particle mass in the drop-interstitial aerosol. Here again it becomes clear that the main aerosol mass enters the drop via the nucleation process in the first stages of the cloud reducing the aerosol mass in the air by two orders of magnitude.

Fig.(VII-6f) displays the same behavior for the mixing ratio Q_{APd} as in case 1. Fig.VII-7 illustrates how strongly the aerosol particle spectrum is processed during the cloud life time. Curve (3) represents the size spectrum of the aerosol particles formed by the drying of cloud drops. We notice that a considerably larger number of large aerosol particles were formed than in case 1. This is due to the stronger collision-coalescence effect working.

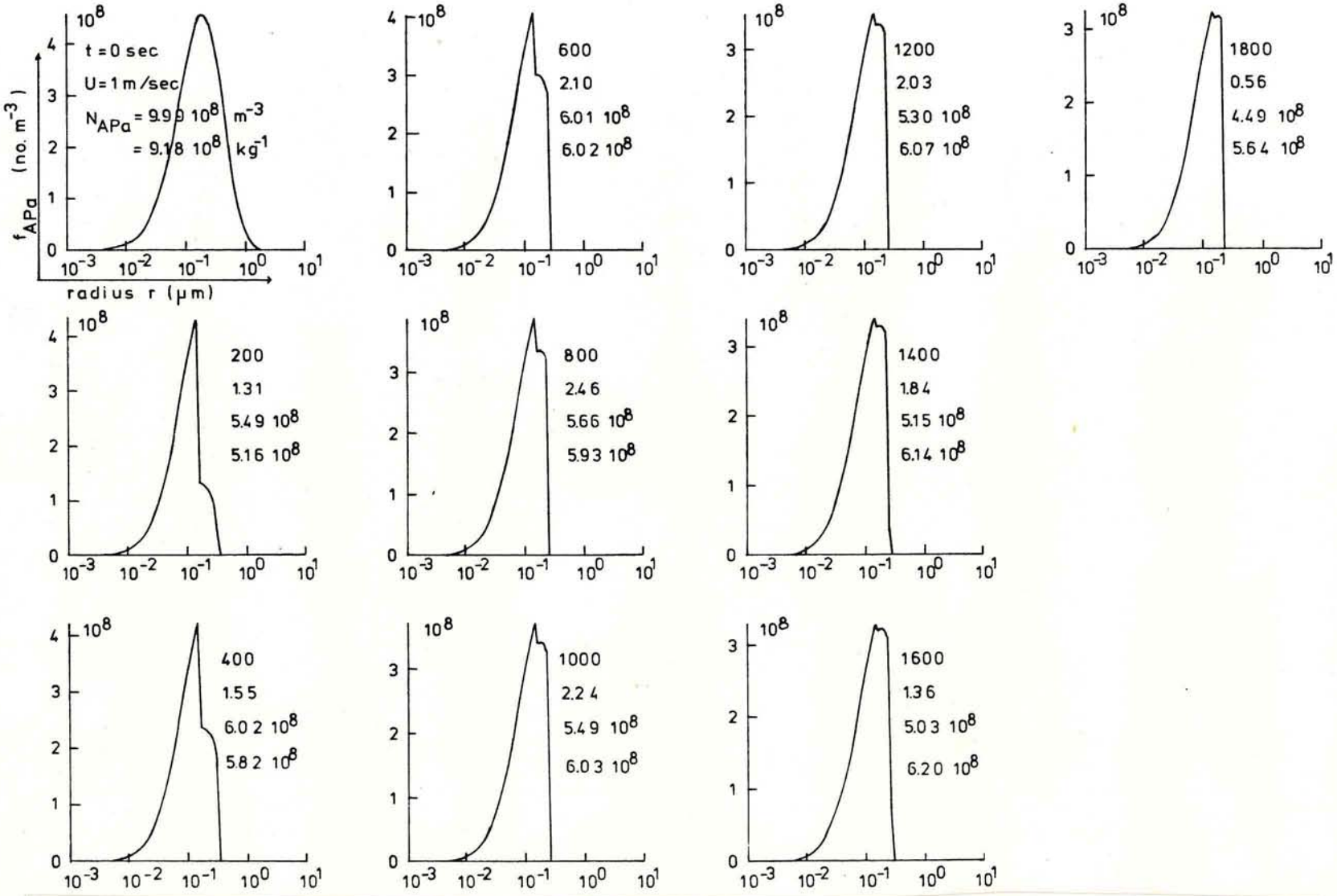

Fig.(VII-6a): Time evolution of aerosol particle number density distribution function f_{APa} for aerosol particles of radius r in air between cloud drops (interstitial aerosol) for case 2 (continental aerosol particle spectrum, ϵ=.01).

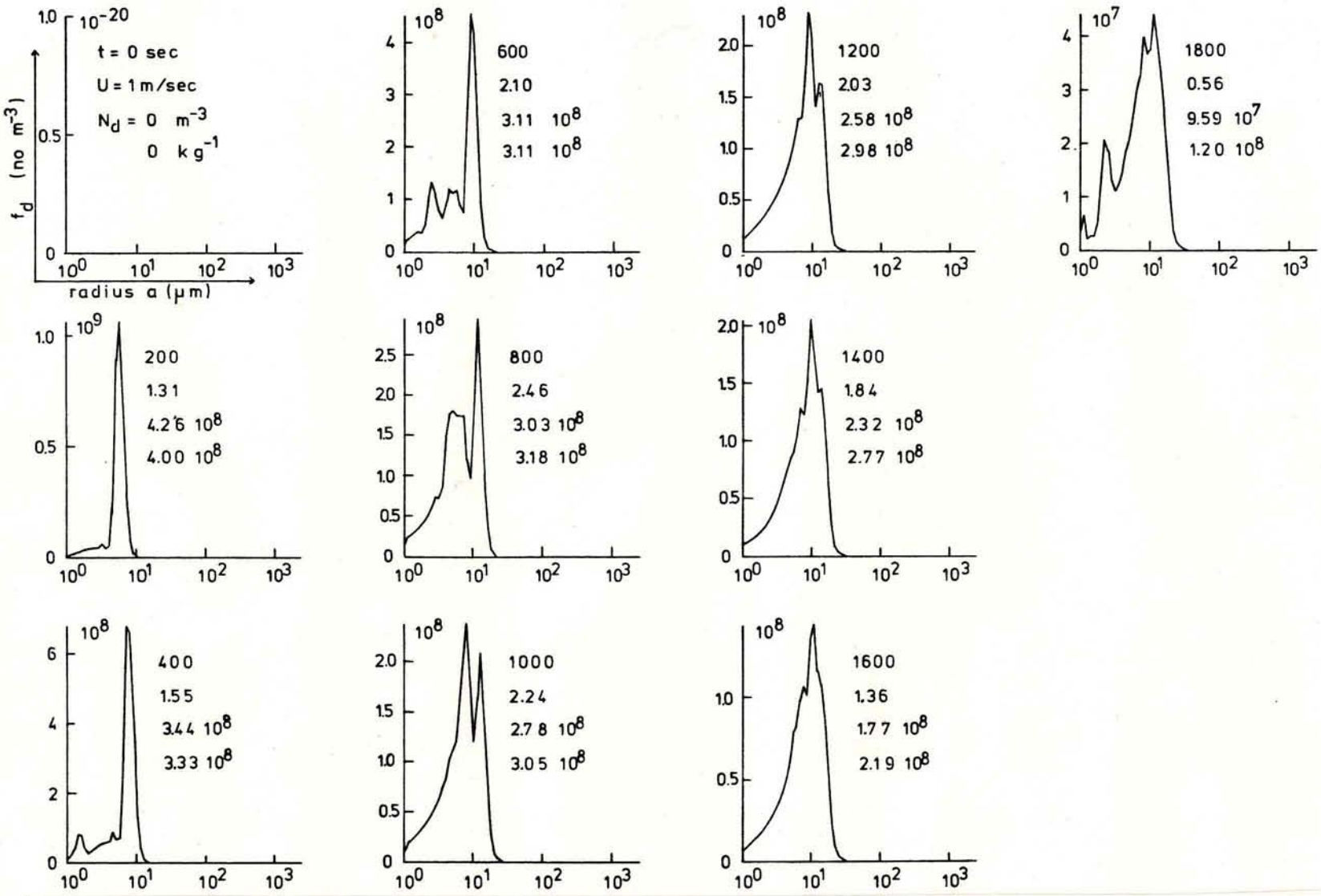

Fig.(VII-6b): Time evolution of drop number density distribution function f_d as a function of drop radius for case 2 (continental aerosol particle spectrum, $\varepsilon = .01$).

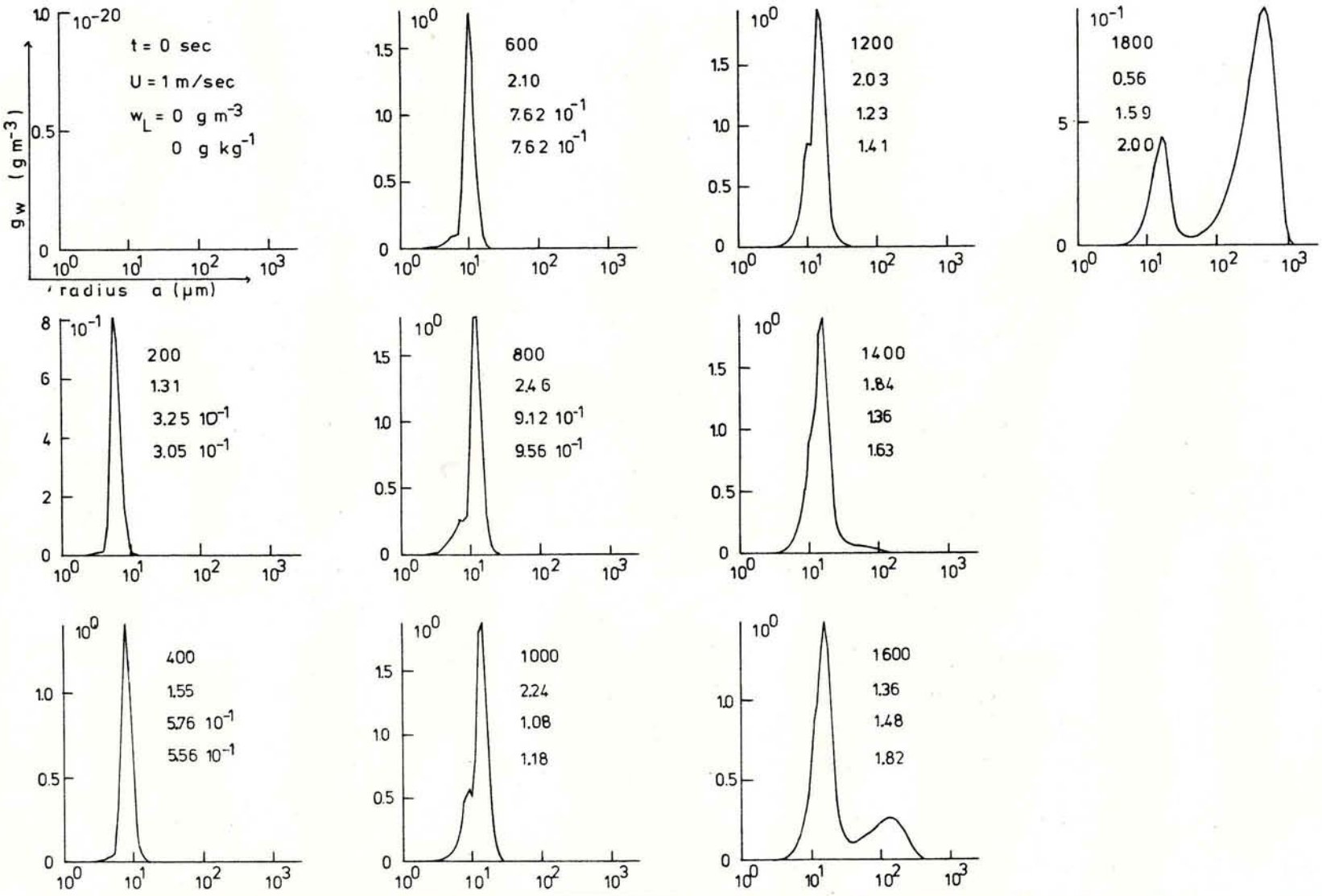

Fig.(VII-6c): Time evolution of the drop water mass density distribution function g_w as a function of drop radius for case 2 (continental aerosol particle spectrum, $\varepsilon = .01$).

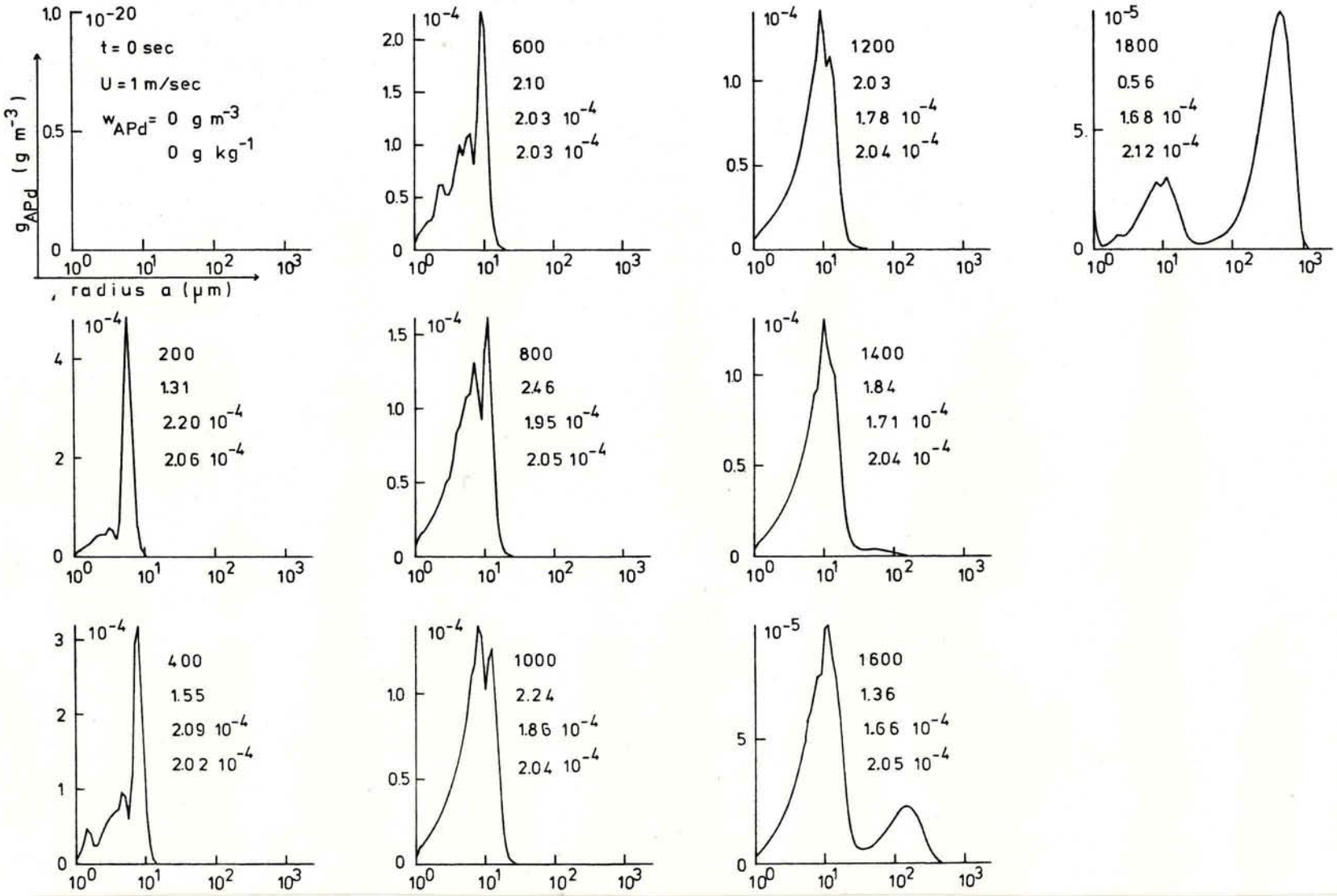

Fig.(VII-6d): Time evolution of aerosol particle mass density distribution function g_{APd} for aerosol particle mass inside drops of radius a, captured through nucleation and impaction scavenging by drops of size spectrum evolving in time as given in Fig.(VII-6b) and Fig.(VII-6c) for case 2 (continental aerosol particle spectrum, $\epsilon = .01$).

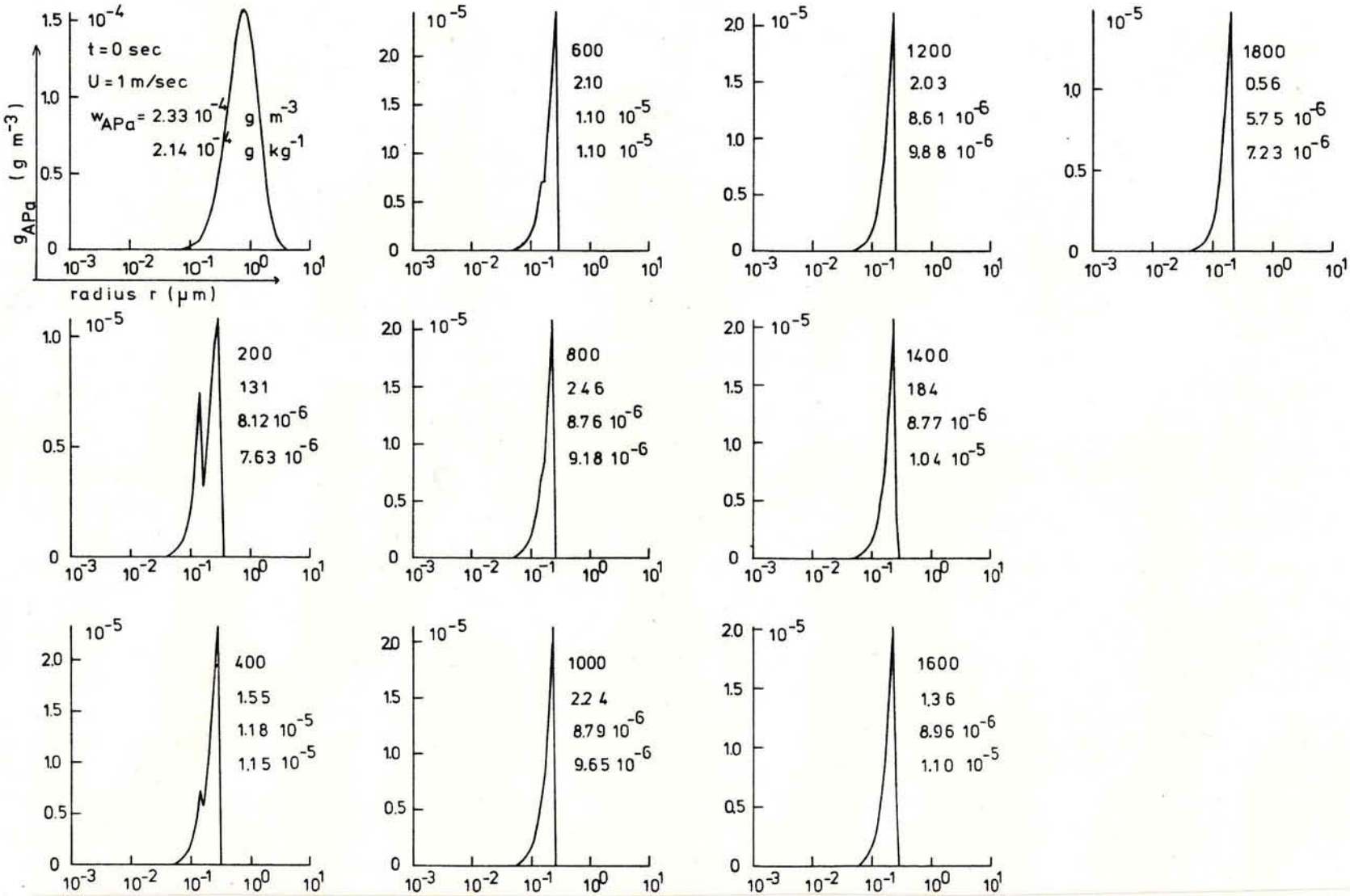

Fig.(VII-6e): Time evolution of aerosol particle mass density distribution function g_{APa} for aerosol mass in air between cloud drops (interstitial aerosol) as a function of radius r of aerosol particles for case 2 (continental aerosol particle spectrum, $\epsilon = .01$).

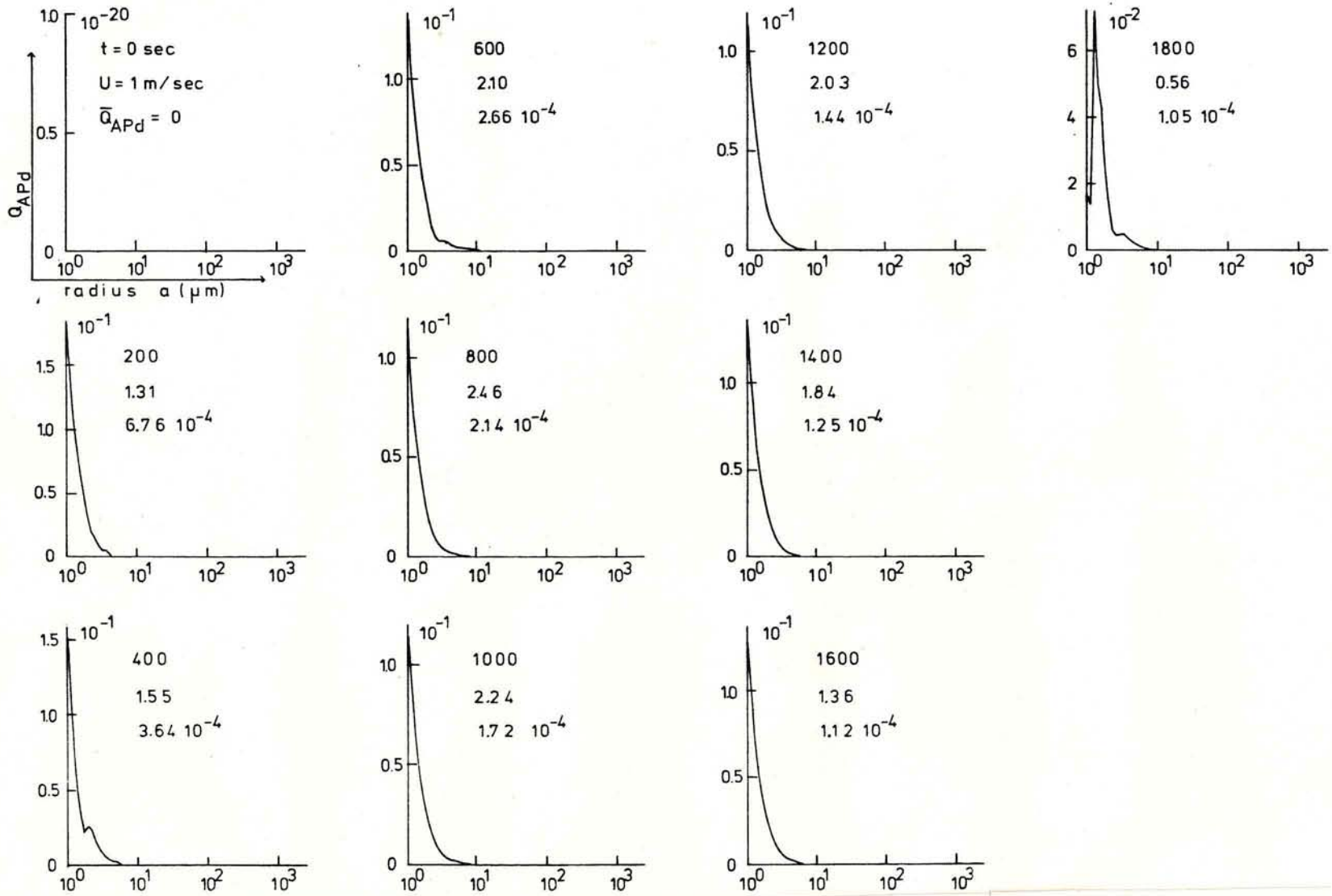

Fig.(VII-6f): Time evolution of aerosol particle mass mixing ratio Q_{APd} in cloud drops as a function of drop radius for case 2 (continental aerosol particle spectrum, ε=.01).

a(μm) / t(sec)	30	50	100	500	1000
200	0.399E-4	0.298E-4	0.221E-4	0.165E-5	0.891E-7
400	0.342E-3	0.273E-4	0.134E-4	0.187E-5	0.169E-6
600	0.493E+0	0.336E-4	0.123E-4	0.224E-5	0.402E-6
800	0.123E+3	0.205E-1	0.114E-4	0.178E-5	0.754E-6
1000	0.473E+4	0.206E+2	0.124E-3	0.270E-5	0.107E-5
1200	0.462E+5	0.207E+4	0.250E+1	0.326E-5	0.180E-5
1400	0.193E+6	0.308E+5	0.112E+4	0.559E-5	0.211E-5
1600	0.368E+6	0.114E+6	0.208E+5	0.177E+0	0.426E-5
1800	0.137E+6	0.554E+5	0.207E+5	0.432E+3	0.558E+0

Table VII-2: Number of drops per m^3 larger than 30μm, 50μm, 100μm, 500μm and 1000μm as a function of time for case 2 (continental aerosol particle spectrum, ϵ=.01).

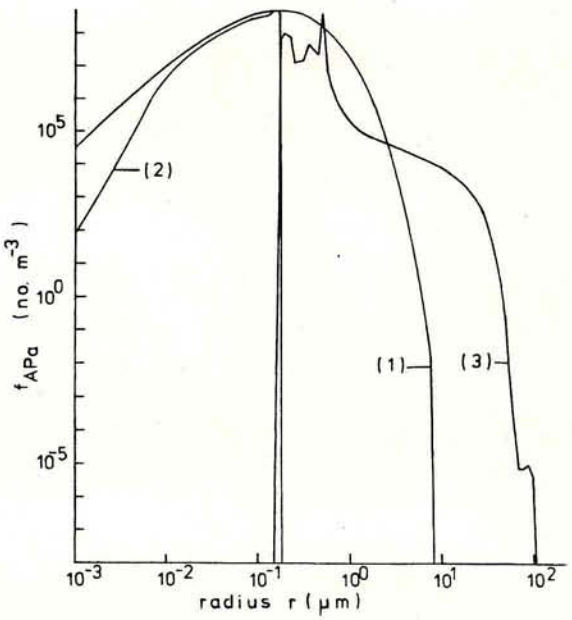

Fig.(VII-7): Aerosol particle number density distribution function f_{APa} as a function of radius r of aerosol particles for case 2 (continental aerosol particle spectrum, ϵ=.01).
(1): initial dry aerosol particle spectrum
(2): dry interstitial aerosol particle spectrum after 30 min of cloud life time
(3): aerosol particle spectrum from dried-off cloud drops after 30 min of cloud life time, if all material inside one drop becomes one single particle

VII.1.3 Case 3

In these computations the aerosol particle spectrum is given by eq.(IV-18) and the parameters (IV-20). This corresponds to a

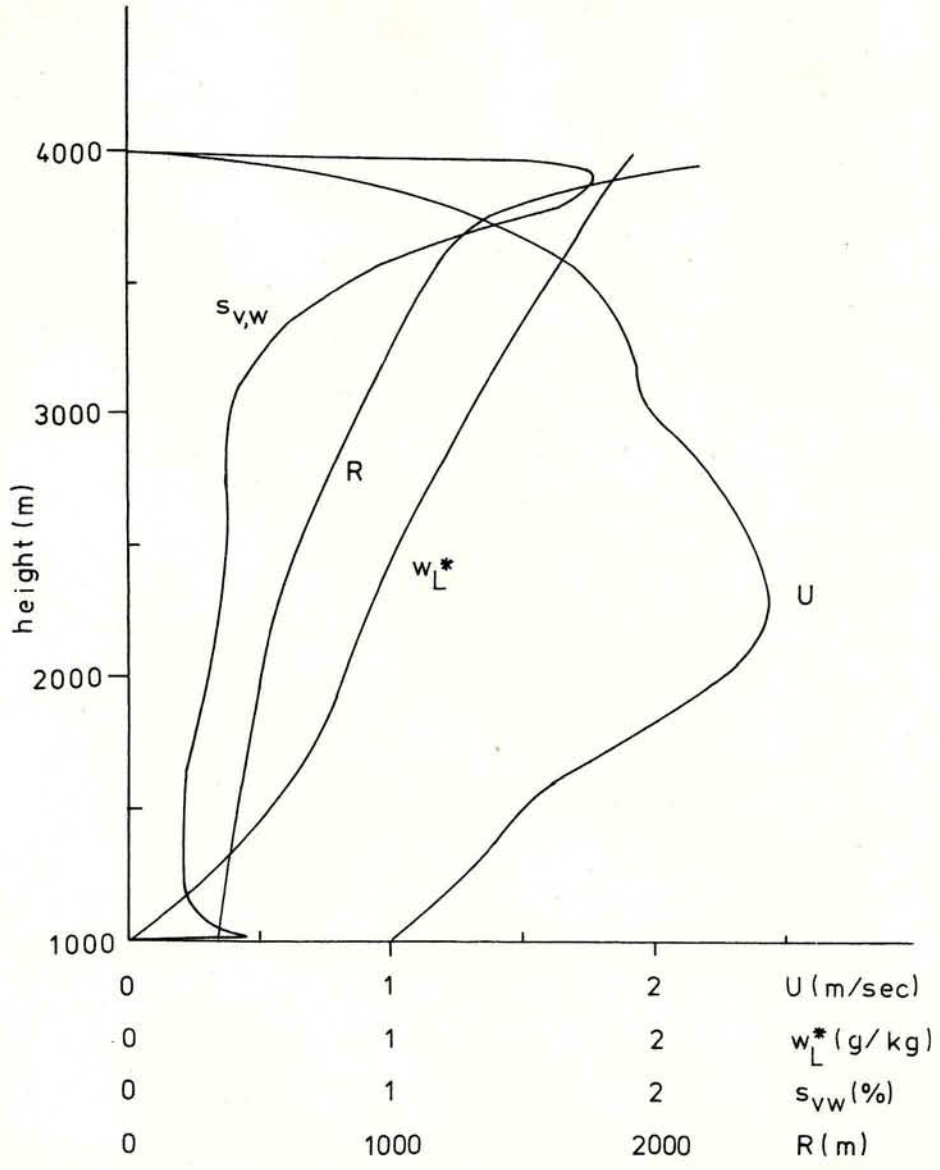

Fig.(VII-8): Variations with height of total liquid water content w_L^*, updraft radius R, supersaturation $s_{v,w}$ and updraft velocity U in the entraining air parcel for case 3 (maritime aerosol particle spectrum, $\varepsilon = 1$).

maritime-type aerosol particle spectrum with a total number concentration of 100 particles per cm^3. The particles were assumed to consist solely of ammonium sulfate, i.e. $\varepsilon = 1.0$.

Fig.(VII-8) displays the behavior of the dynamic variables inside the

air parcel during its ascent. Again the curves for the bubble radius R, the one for the total liquid water content w_L^* and the one for the vertical velocity U are similar to the same curves in Fig.(VII-1) of case 1 only the parcel stops a little earlier, that is at 4km. This is due to the smaller drop number concentration in this case. This results in a higher supersaturation $s_{v,w}$ and thus in less condensation than before and so the cooler air parcel develops less buoyancy.

The Figures (VII-9a) to (VII-9f) display the same quantities as in Figs.(VII-2a) to (VII-2f) for case 1.

Fig.(VII-9a) illustrates that the total number concentration of aerosol particles gets reduced by 94% in the first 200 seconds.

Fig.(VII-9b) shows that about 90 drops per cm^3 have formed. Because of their smaller number they grew by condensation even more efficient than the drops in case 2. Thus, the drop spectrum has become broader. Within a few minutes the mean radius of the spectrum reaches the threshold size (~ 13 µm) where collision and coalescence can become effective. As a result the total drop number concentration decreases significantly in the later stages of the 'cloud'.

This behavior is also illustrated in Table VII-3 which displays the total number concentration of drops larger than 30µm, 50µm, 100µm, 500µm and 1000µm. Here many big drops are formed.

Fig.(VII-9c) illustrates also the rapid formation of the precipitation-sized drops which again carry the main pollution mass along with them, as Fig.(VII-9d) displays.

We further note that the total aerosol mass w_{APd} in $g\ kg^{-1}$ contained in the cloud water continues to increase with time, although this increase is much smaller in comparison to the increase during the initial condensation period. Unfortunately, however, the present data do not allow any conclusion concerning the effects of impaction scavenging on the total amount of material scavenged, as these effects are completely overpowered by the effects of nucleation scavenging.

Fig.(VII-9e) illustrates the dominating effects of nucleation scavenging very clearly. As in case 1 and 2 the main decrease of the interstitial aerosol mass (5 orders of magnitude) happens in the first 200 seconds. A further noticeable decrease occurs after 1400 seconds until the end of the calculation. This is due to the fact that the strong collision and coalescence effect decreases the number of drops so drastically that the supersaturation rises again (compare

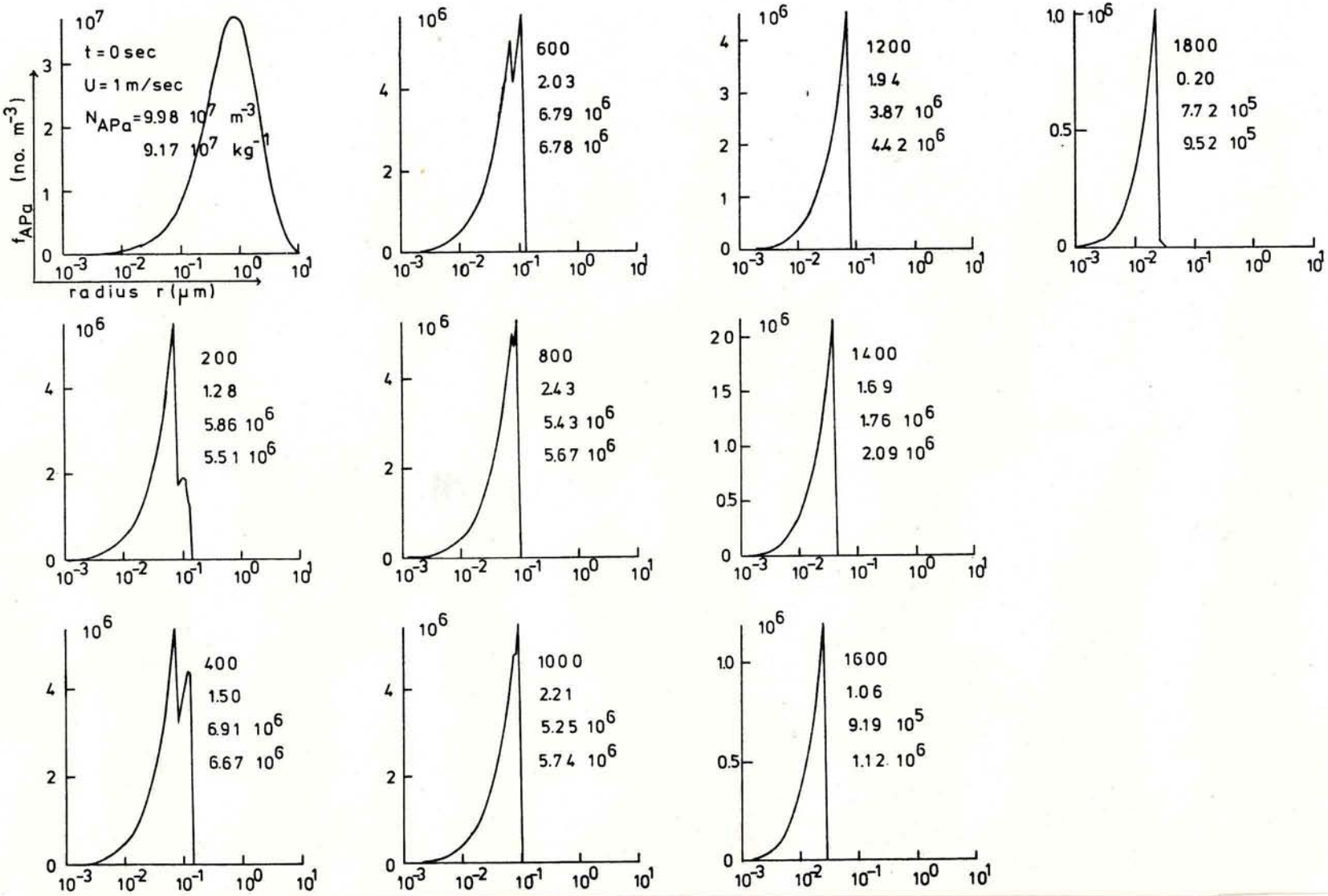

Fig.(VII-9a): Time evolution of aerosol particle number density distribution function f_{APa} for aerosol particles of radius r in air between cloud drops (interstitial aerosol) for case 3 (maritime aerosol particle spectrum, $\varepsilon = 1$).

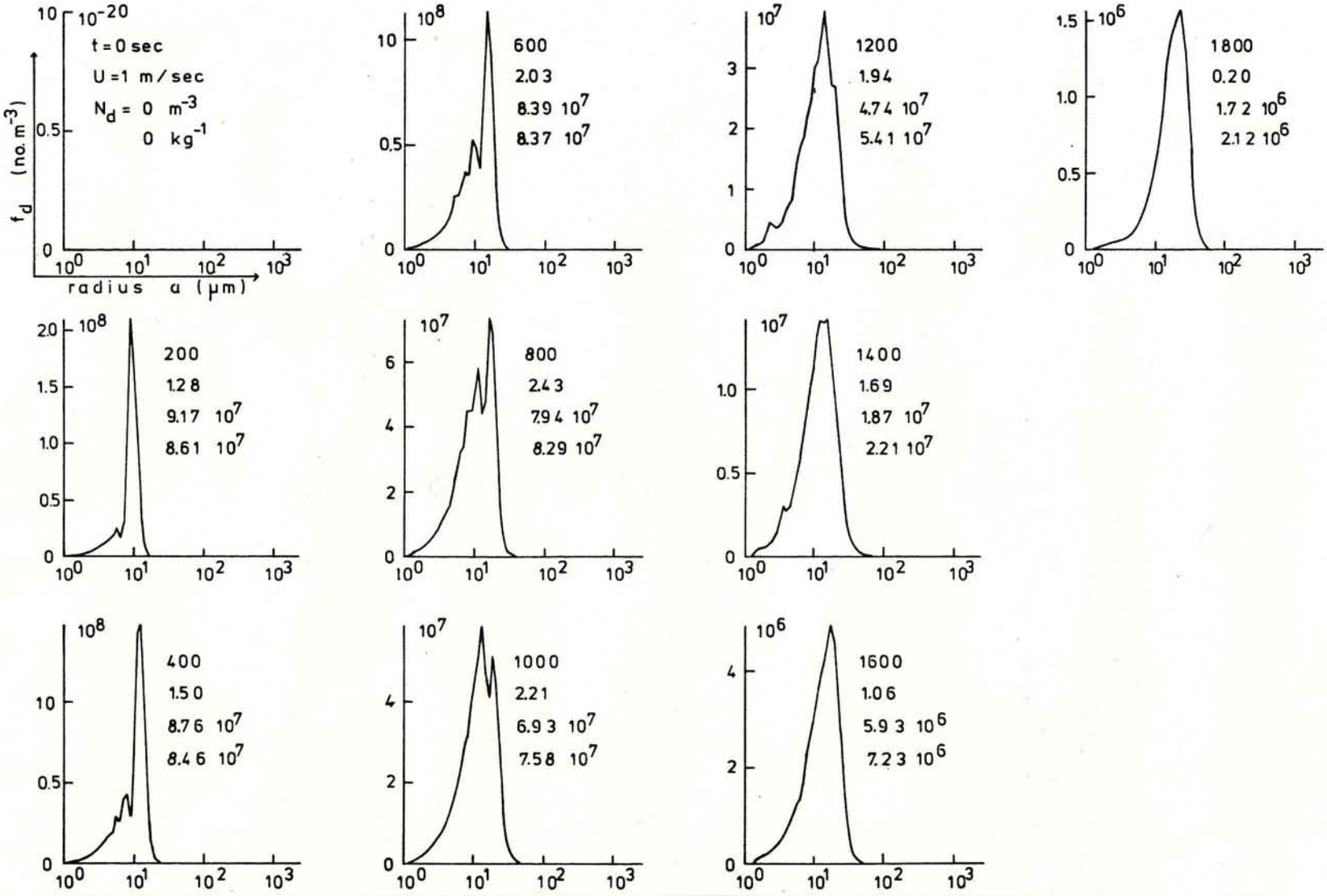

Fig.(VII-9b): Time evolution of drop number density distribution function f_d as a function of drop radius for case 3 (maritime aerosol particle spectrum, $\varepsilon = 1$).

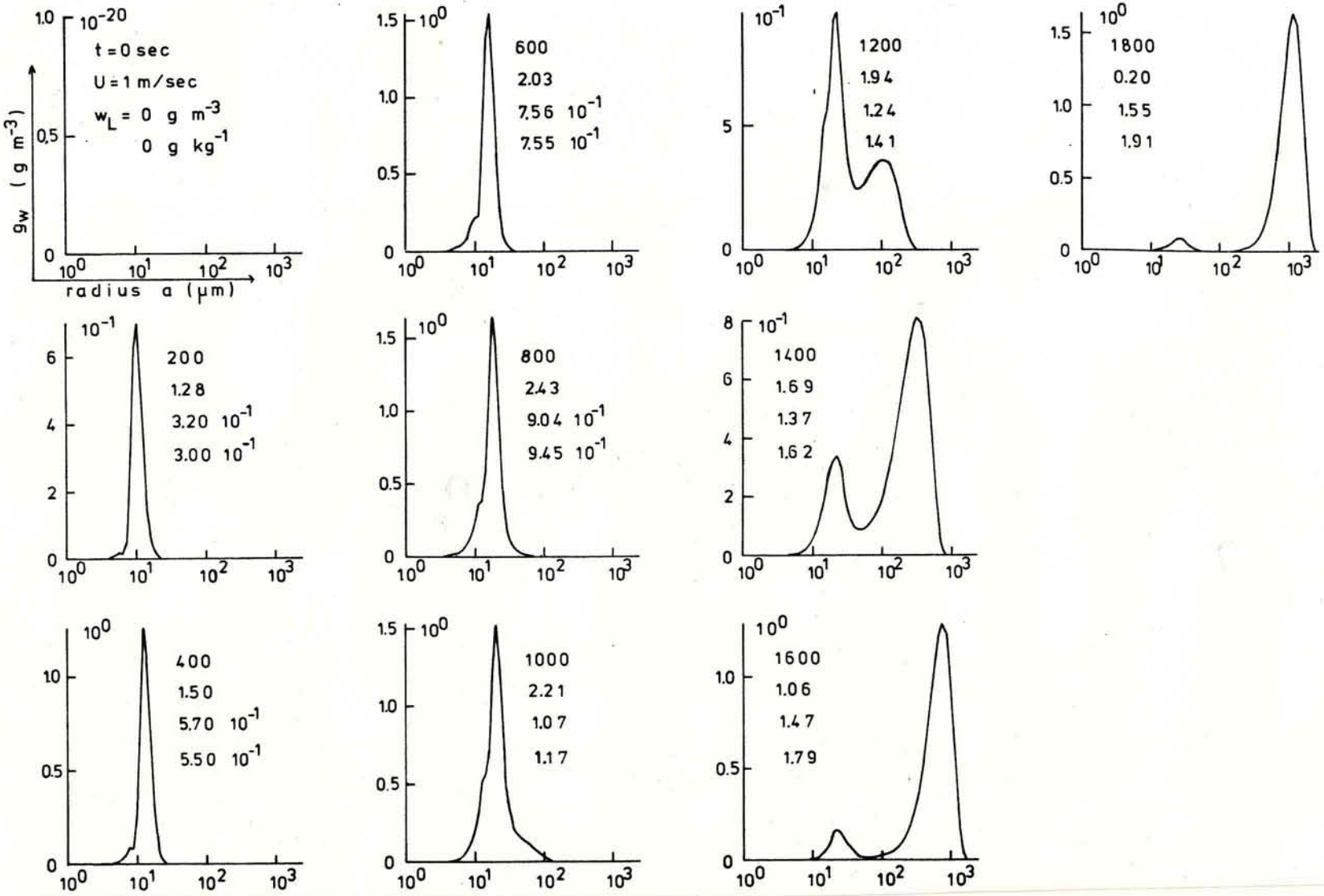

Fig.(VII-9c): Time evolution of the drop water mass density distribution function g_w as a function of drop radius for case 3 (maritime aerosol particle spectrum, $\varepsilon = 1$).

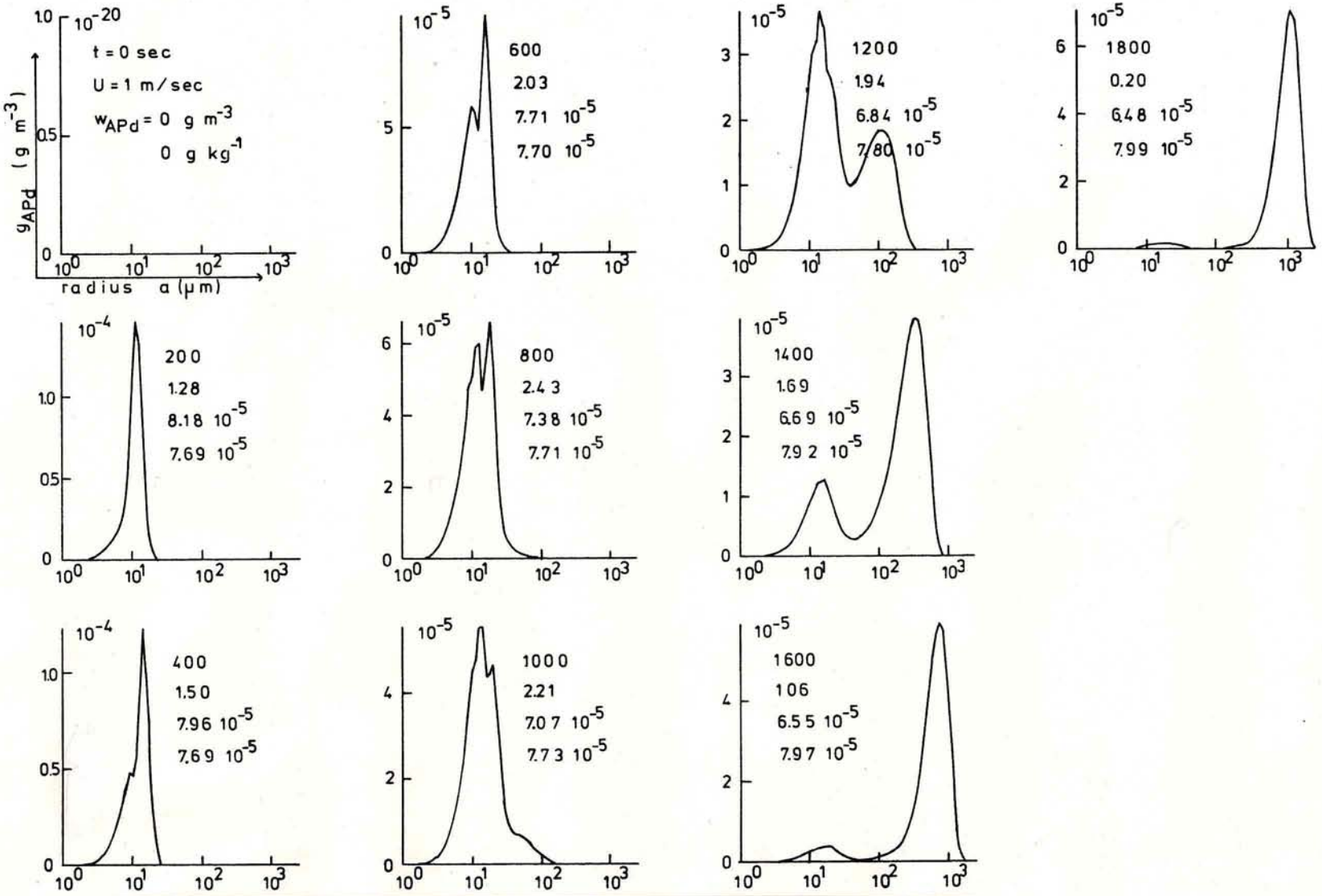

Fig.(VII-9d): Time evolution of aerosol particle mass density distribution function g_{APd} for aerosol particle mass inside drops of radius a, captured through nucleation and impaction scavenging by drops of size spectrum evolving in time as given in Fig.(VII-9b) and Fig.(VII-9c) for case 3 (maritime aerosol particle spectrum, $\varepsilon = 1$).

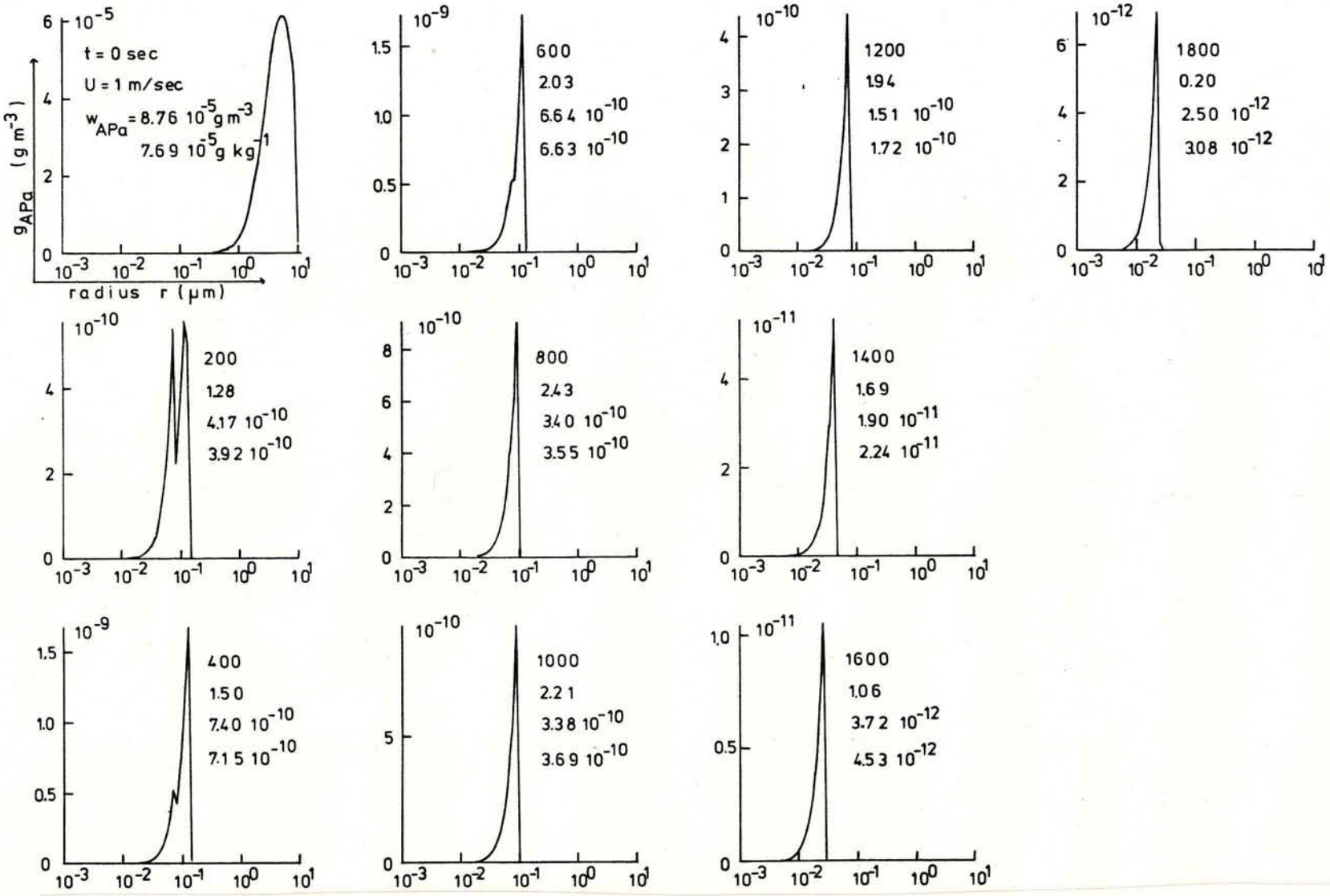

Fig.(VII-9e): Time evolution of aerosol particle mass density distribution function g_{APa} for aerosol mass in air between cloud drops (interstitial aerosol) as a function of radius r of aerosol particles for case 3 (maritime aerosol particle spectrum, ε =1).

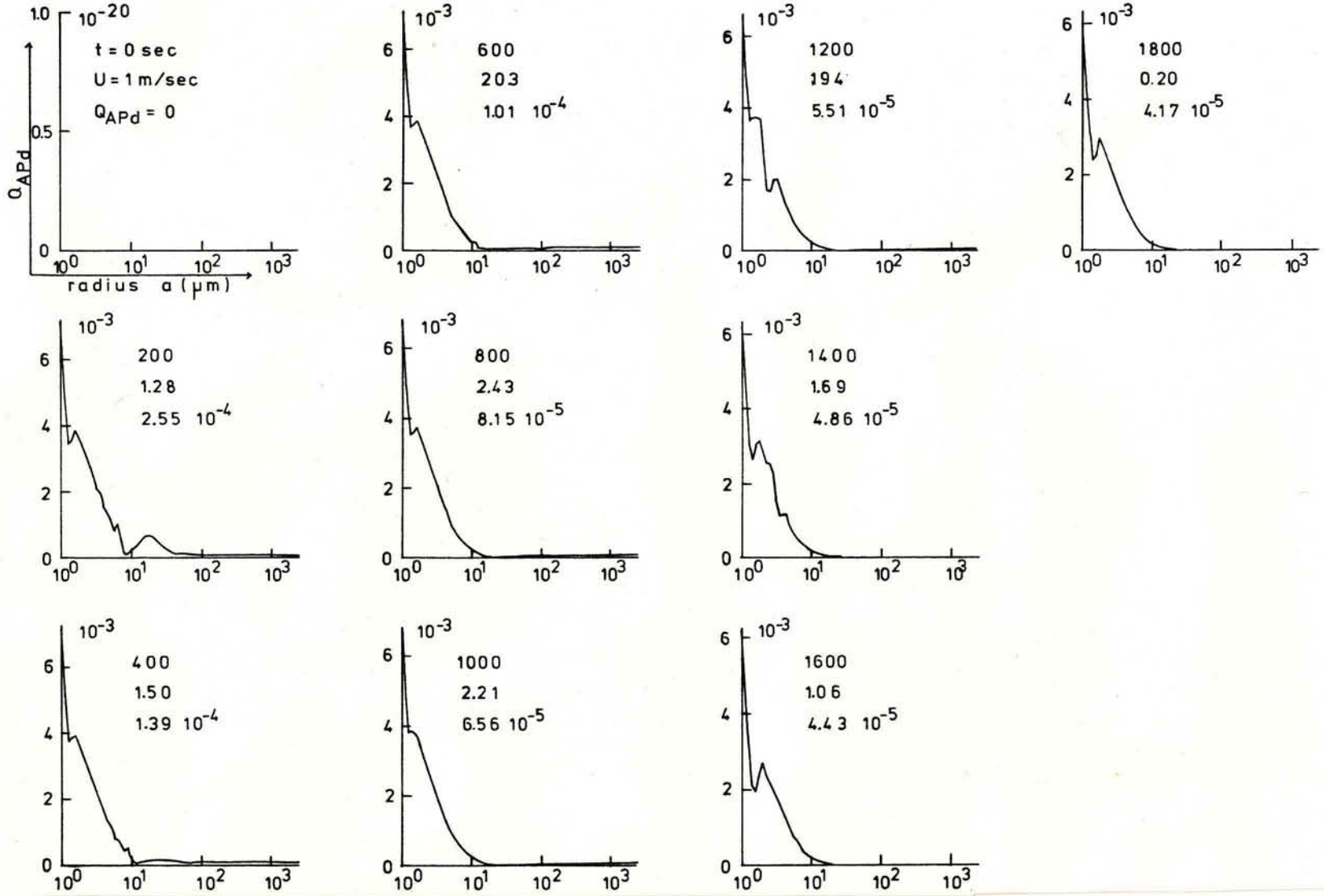

Fig.(VII-9f): Time evolution of aerosol particle mass mixing ratio Q_{APd} in cloud drops as a function of drop radius for case 3 (maritime aerosol particle spectrum, $\varepsilon = 1$).

a(μm) / t(sec)	30	50	100	500	1000
200	0.215E+1	0.139E-4	0.407E-5	0.672E-7	0.351E-7
400	0.482E+3	0.464E-1	0.434E-5	0.665E-7	0.312E-7
600	0.165E+5	0.497E+2	0.229E-4	0.138E-6	0.244E-7
800	0.155E+6	0.484E+4	0.914E+0	0.553E-6	0.226E-7
1000	0.580E+6	0.682E+5	0.108E+4	0.692E-6	0.963E-7
1200	0.852E+6	0.202E+6	0.274E+5	0.707E-4	0.360E-6
1400	0.369E+6	0.928E+5	0.293E+5	0.140E+3	0.442E-4
1600	0.152E+6	0.171E+5	0.625E+4	0.703E+3	0.307E+2
1800	0.108E+6	0.500E+4	0.137E+4	0.474E+3	0.109E+3

Table VII-3: Number of drops per m^3 larger than 30μm, 50μm, 100μm, 500μm and 1000μm as a function of time for case 3 (maritime aerosol particle spectrum, $\varepsilon = 1$).

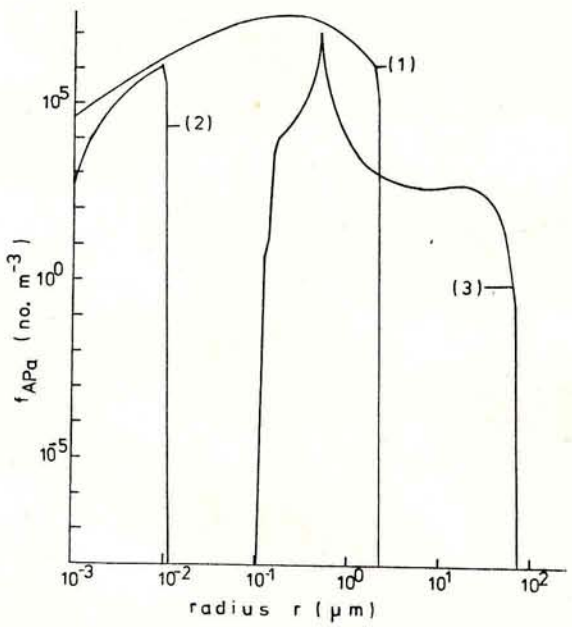

Fig.(VII-10): Aerosol particle number density distribution function f_{APa} as a function of radius r of aerosol particles for case 3 (maritime aerosol particle spectrum, $\varepsilon = 1$).
(1): initial dry aerosol particle spectrum
(2): dry interstitial aerosol particle spectrum after 30 min of cloud life time
(3): aerosol particle spectrum from dried-off cloud drops after 30 min of cloud life time, if all material inside one drop becomes one single particle

Fig.(VII-8)). So a further significant nucleation process occurs reducing the mass of the interstitial aerosol again by 2 orders of magnitude.

Fig.(VII-9f) displays the same behavior for the mixing ratio Q_{APd} as in case 1.

Fig.(VII-10) illustrates again how efficiently the aerosol particle spectrum is processed during the cloud life time. We notice that a large gap separates curve (2), which represents the dry interstitial aerosol particle spectrum, from curve (3), which represents the aerosol particle spectrum resulting from the dried-off drops. On the one hand this gap is due to the large supersaturation affecting the nucleation scavenging, and due to the collision and coalescence of drops. On the other hand it is also due to the artificiality of separating aerosol particles and drops in two different spectra.

VII.1.4 Conclusions

In order to study the effects of cloud microphysical processes on aerosol scavenging we have linked our aerosol scavenging model described in chapter II to the entraining air parcel model described in chapter IV. We evaluated this model for three different aerosol particle distributions and studied the time evolution of the aerosol particle mass scavenged by the drops, and of the aerosol particle mass left unactivated in the air as drop-interstitial aerosol.

Our study allows to identify five facts:

1.) The collision-coalescence process is responsible for a re-distribution of the scavenged aerosol particle mass inside the cloud water in such a manner that the main aerosol particle mass is always associated with the main water mass, thus ensuring that if a cloud reaches the precipitation stage it also will return to the ground the main scavenged aerosol particle mass. This result has yet to be verified by field observations.

2.) Although the main aerosol particle mass is contained in the large drops, the mass mixing ratio of the captured aerosol in the cloud water is larger inside small drops, implying that smaller drops are more contaminated than larger ones. This result is in good qualitative agreement with field studies of Georgii and Woetzel(1970).

3.) Inside a cloud a drop-interstitial aerosol exists which consists of a particle population reduced in number concentration through nucleation scavenging by up to 94%, and reduced in mass by several orders of magnitude, as compared to the aerosol particle population outside the cloud. This result is in qualitative good agreement with the field studies of Radke(1983, his Fig.2), if his approximate data for aerosol particles larger than 0.3 µm are disregarded due to his admittedly still unresolved experimental difficulties, and if it is recalled that our computations were carried out for aerosol particles which all had the same composition; this is in contrast to the heterogeneous composition of natural aerosols.

4.) The aerosol particle spectrum is processed during the life cycle of a cloud in the way that the total number of small cloud condensation nuclei (CCN) is reduced and that more giant aerosol particles are formed thus enabling an aerosol particle distribution which did not develop rain drops in the first cloud cycle to develop precipitation-sized drops in a second or third cloud cycle. This is in good agreement with the conclusions of Hindman et al.(1977) that an increase in the concentration of large and giant CCN only then leads to an increased formation of precipitation-sized drops if it is accompanied by a decrease in concentration of small CCN. Our result, however, is restricted to the uniform composition of the aerosol particles in the present study. In a heterogeneous cloud the processed aerosol spectrum may end up with more and better CCN than before due to the collision and coalescence process mixing soluble with insoluble particles and uptake of gases. This result is in agreement with the field observations of Hegg et al.(1980).

5.) Although the amount of aerosol mass scavenged by impaction cannot completely be neglected in accounting for the total aerosol particle mass removed by clouds, our results show further that independent of the composition the aerosol particle mass removed by nucleation scavenging is larger by several orders of magnitude than the aerosol particle mass removed by impaction scavenging inside clouds. This conclusion has been qualitatively verified by the field studies of Radke(1983) and Hegg and Hobbs(1983).

At this point it must be stressed that the values existing in literature for the efficiencies with which aerosol particles are scavenged by impaction with drops are quite tentative. In fact it has been

suggested (Radke et al.(1980), Barlow and Latham (1983)) that various factors existing in atmospheric clouds may cause the scavenging efficiencies to be considerably larger than those found in theoretical and laboratory studies. However, the present study shows quite convincingly that impaction scavenging contributes but little to the total amount of aerosol mass removed by nucleation scavenging. Thus, computations with an efficiency as large as near unity for all drops and aerosol sizes have yielded results which altered the present ones by less than 0.5%. This finding is physically reasonable, as nucleation scavenging removes the main aerosol mass, leaving for impaction scavenging drop-interstitial aerosol particles quite large in number but quite small in total mass. Even if this small mass would be removed by impaction scavenging with an efficiency of unity, the removed mass would still not contribute significantly to the total mass removed.

Though we must emphasize that the present study only applies to aerosol particles of uniform composition. Impaction scavenging may be considerably more prominent in removing aerosol particles of very different chemical composition.

Also, we must stress that the air parcel model only applies to in-cloud scavenging and does not consider below-cloud scavenging. In below-cloud scavenging, impaction scavenging will take a more prominent role than in in-cloud scavenging. For the discussion of this problem we refer to chapter VII.3 where we have linked the aerosol scavenging model to a two dimensional cloud model.

VII.2 Results of aerosol and gas scavenging in an entraining air parcel model

In this section we shall present the results of an evaluation of our aerosol and gas scavenging models described in chapter II and III linked to the entraining air parcel model described in chapter IV, with the initial conditions and the boundary values given in chapter IV.2.

VII.2.1 Case A

The initial conditions for case A are given in section IV.2.2. For the aerosol scavenging these are the same initial conditions as in case 3 of chapter VII.1. But this time also SO_2 is offered to the aerosol particles and drops to be simultaneously scavenged during the evolution of the 'cloud'. The evolution in time of the dynamic parameters and of the aerosol particle and drop spectrum is not affected by the inclusion of gas scavenging and therefore remains the same as that discussed in section VII.1.3. There, we showed that within about 17 minutes precipitation-sized drops developed. The evolution in time of the uptaken SO_2 is displayed in Figs.(VII-11a) to (VII-11d).

Fig.(VII-11a) exhibits the mass distribution function for sulfur which entered the cloud water via SO_2 uptake. We notice the rapid re-distribution of the entering sulfur mass inside the cloud water. This re-distribution proceeds such that the main sulfur mass, wether it entered by uptake of $(NH_4)_2 SO_4$ particles (compare Fig.(VII-9d)) or by uptake of SO_2, becomes associated with the main water mass, i.e. with the large precipitable drops. In Fig.(VII-11b) the concentration c_4 of S(IV) which entered the cloud water by SO_2 uptake is given as a function of time and drop size. We notice from this figure that all the drops smaller than 50µm are in gas equilibrium with the environment and therefore contain a S(IV) concentration c_4 equal to the equilibrium concentration. By further growth due to condensation and collision and coalescence the drops reach sizes at which, according to Fig.(III-3), they don't take up the equilibrium concentration of sul-

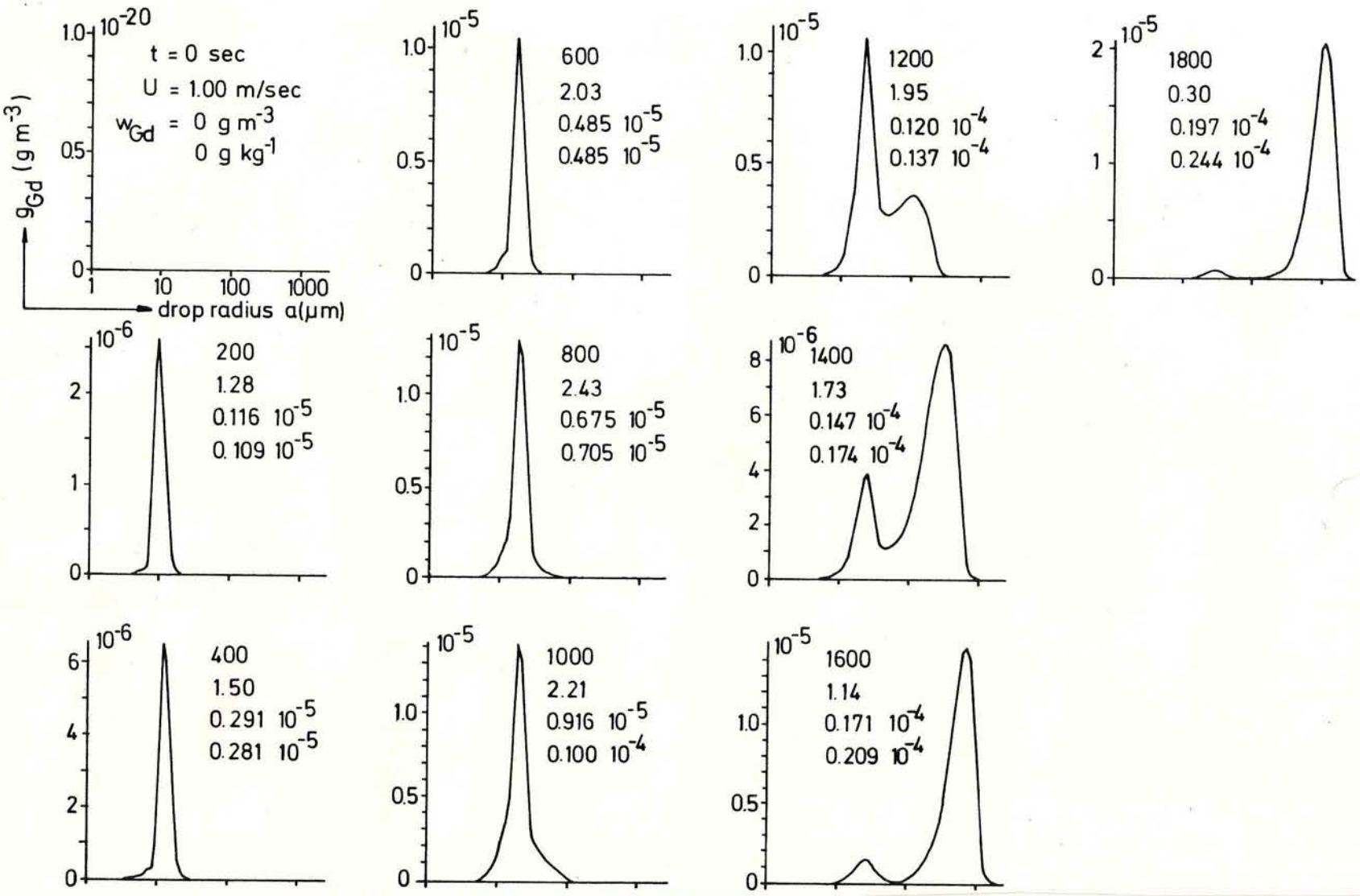

Fig.(VII-11a): Time evolution of the sulfur mass density distribution function g_{Gd} for gas mass inside drops of radius a taken up through convective diffusion by drops of size spectrum evolving in time as given in Fig.(VII-9b) and Fig.(VII-9c) for case A.

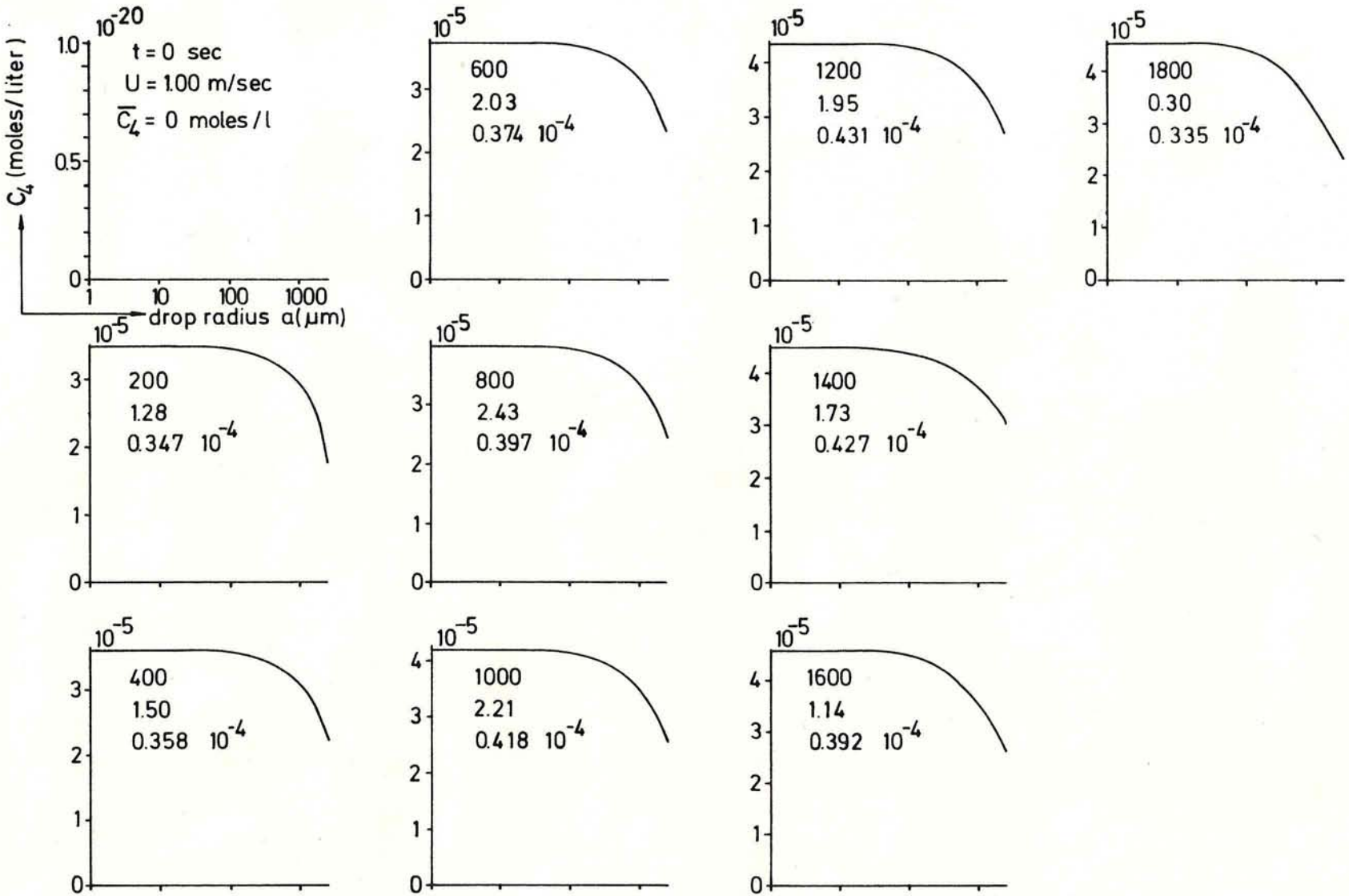

Fig.(VII-11b): Time evolution of the concentration c_4 of S(IV) inside drops of radius a for case A.

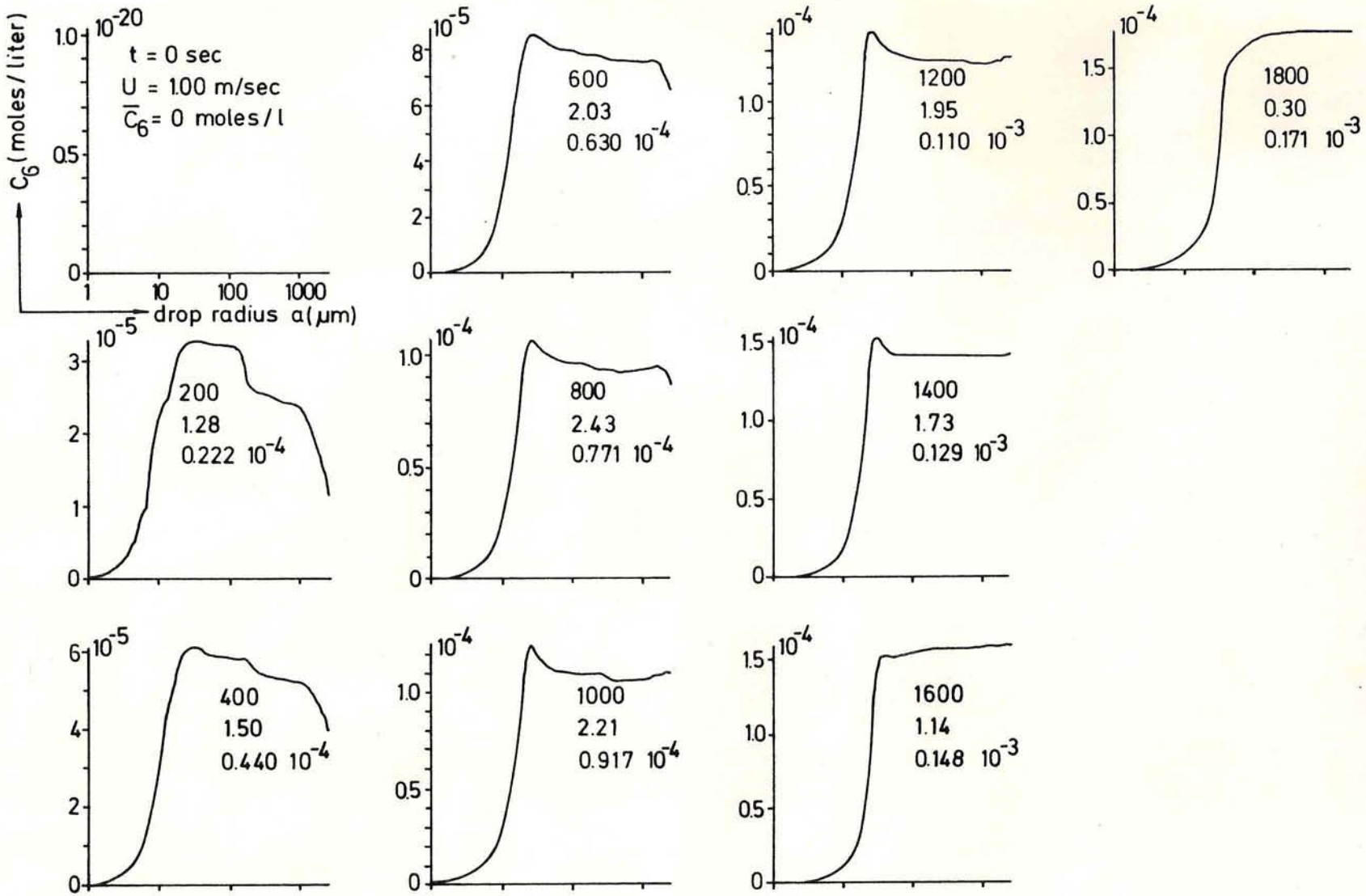

Fig.(VII-11c): Time evolution of the concentration c_6 of S(VI) inside drops of radius a for case A.

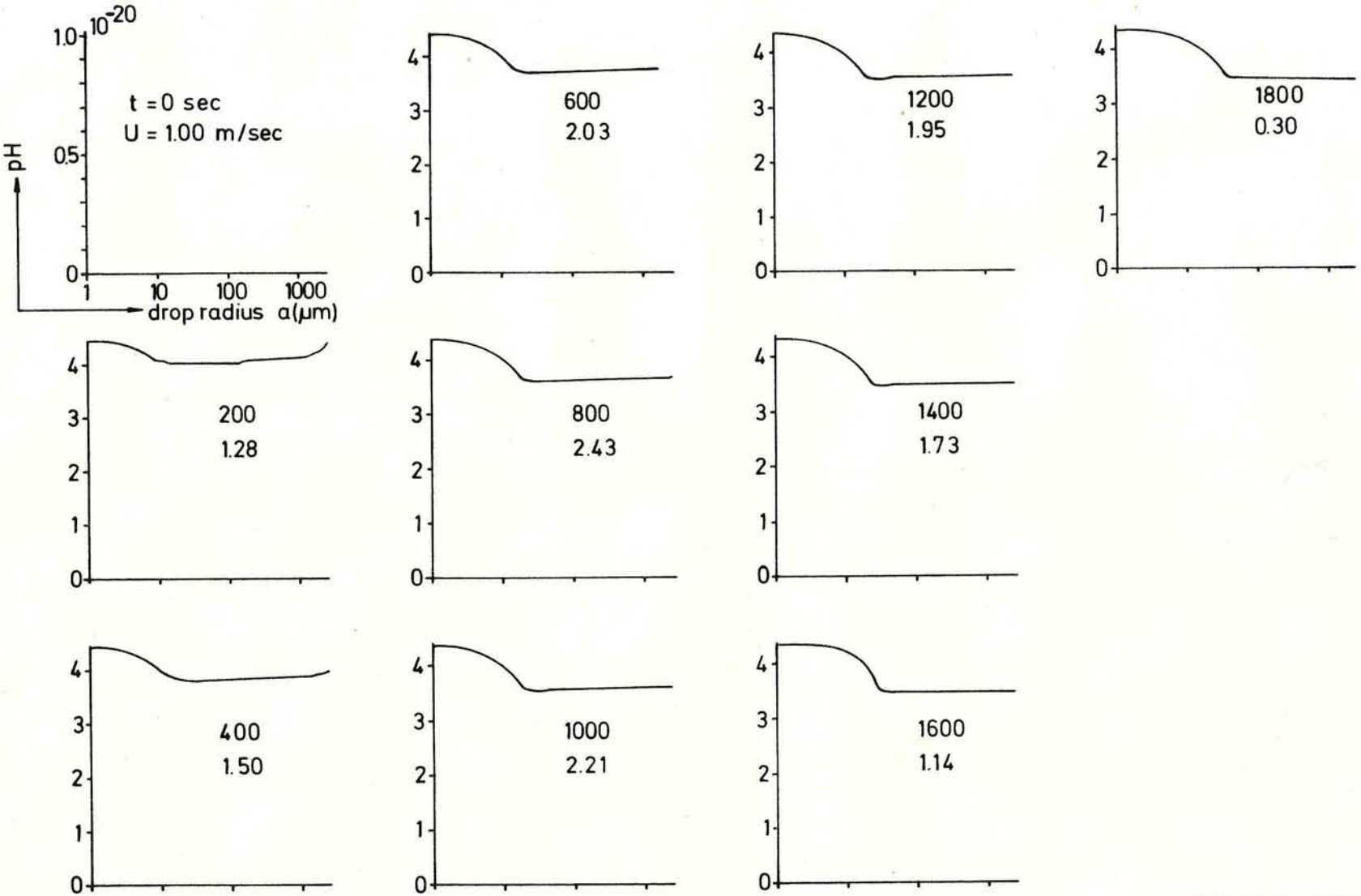

Fig.(VII-11d): Time evolution of the pH=-log[H^+] inside drops of radius a for case A.

fur within the time step interval of 2 seconds. This 'lag' becomes the more pronounced, i.e. c_4 becomes smaller, the larger the drop size. And even at the end of the computation these drops have not reached their equilibrium concentration which they would have had without oxidation since part of the uptaken S(IV) becomes irreversibly converted to S(VI) as it enters the drop.

From Fig.(VII-11c) we notice a totally different behavior for the concentration c_6 of the sulfur (VI). In the first 10 min of the cloud life time c_6 passes through a maximum. This maximum is due to the fact that the small drops grow faster through condensation than they take up sulfur (IV) and convert it to sulfur (VI). Therefore the small drops always have the smallest S(VI) concentration. The decrease of c_6 for the large drops in the first 10 min, however, is due to the lag in the c_4 concentration. With increasing time this minimum gradually fills up as the ageing drops mix through collision and coalescence.

Due to the dissociation of the various sulfur species in water, hydrogen ions $[H^+]$ are formed. These determine the $pH=-\log[H^+]$ of the cloud water. We note from Fig.(VII-11d) that the pH of the drops decreases with increasing 'drop age' and drop size. For this case, which assumed a moderate value for the oxidation rate $K'=5\ 10^{-3}\ sec^{-1}$, our model predicts a pH range from 3.5 to 4.5. These values are reasonable with regard to the measurements of the acidity in rain made by Georgii(1982), Perseke (1982), Kins(1982) and others.

In Fig.(VII-12) we have plotted the variation with time of the total sulfur per kilogram air which entered the drop via nucleation scavenging and via the convective diffusion of SO_2. We notice the immediate rise of the amount of sulfur due to nucleation scavenging. This amount is only unnoticeably affected by condensation on aerosol particles which subsequently entered the cloud by entrainment or entered the drop by impaction scavenging. In contrast, the amount of sulfur entering via SO_2 rises gradually with time as diffusion and oxidation proceeds. In this case, however, the amount of sulfur entering via SO_2 never reaches the amount which entered due to nucleation scavenging. This latter fact is also illustrated in Fig.(VII-13) which describes the time variation of the proportion which nucleation scavenging and gas scavenging contribute to the total sulfur scavenging. We note that for this case gas scavenging at all times

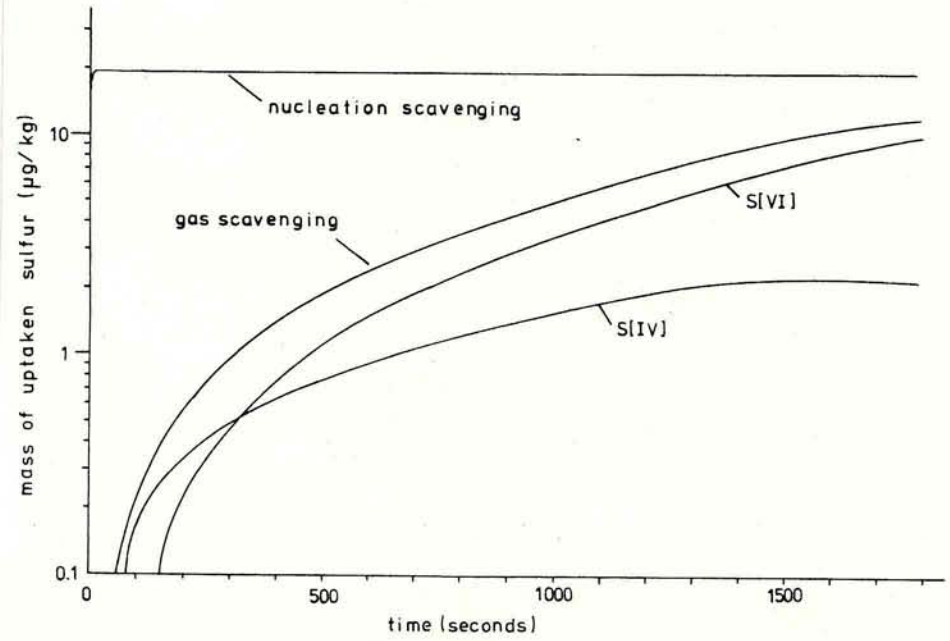

Fig.(VII-12): Time variation of mass of uptaken sulfur through aerosol scavenging of $(NH_4)_2SO_4$ and gas scavenging of SO_2 for case A.

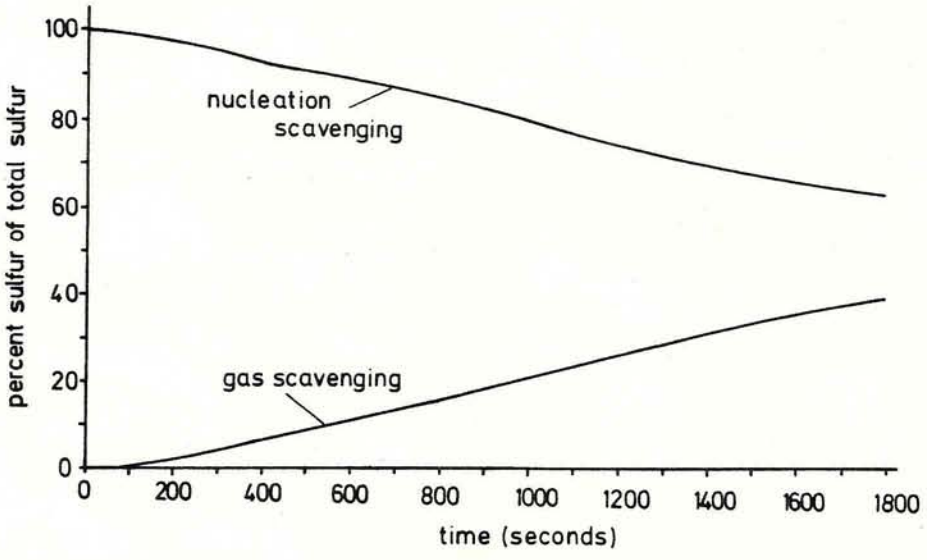

Fig.(VII-13): Time variation of percent sulfur of total sulfur taken up by aerosol scavenging of $(NH_4)_2SO_4$ and by gas scavenging of SO_2 for case A.

contributes less to the total sulfur scavenging than does nucleation scavenging, although the difference in the proportions decreases with time.

VII.2.2 Case B, C and D

While in case A the same amount of $(NH_4)_2SO_4$ mass and SO_2 mass was offered to the drops by the environmental air, equal amounts of sulfur are assumed to be offered to the drops in case B, C and D (see Table IV-1). We notice from Fig.(VII-14) that in case B less sulfur enters the cloud water via SO_2 than in case A due to the smaller amount offered. Thus, as expected, the contribution made by sulfur from SO_2 to the total sulfur taken up by the cloud is even lower than for case A. The contribution from SO_2 amounts to 25% after 1500 seconds in case B (Fig.(VII-15)) as compared to 35% in case A (Fig.(VII-13)).
In case C, as in case B, the same amounts of sulfur are offered to the drops via SO_2 and aerosol particles. However, the oxidation rate $K'=0.1sec^{-1}$ is now larger than in case B. While the behavior of the sulfur uptake from $(NH_4)_2SO_4$ aerosol particles remains the same as in case B the amount of sulfur from SO_2 rises now quickly and, after 650 seconds, becomes larger than the amount of sulfur taken up from the aerosol. This is also expressed by Fig.(VII-15) which shows that the percentage contribution of both scavenging mechanisms becomes equal at 650 seconds, after which gas scavenging dominates the aerosol uptake. As expected, the trend described for case C is found to continue in case D for which the amounts of sulfur offered to the drops via SO_2 and aerosol are the same as in case C. However, $K'=1.0sec^{-1}$ was further increased. Fig.(VII-14) shows that for this situation the amount of sulfur taken up by the cloud rises now very rapidly with time and surpasses the amount taken up from the aerosol already after 200 seconds. Thus, as expected, Fig.(VII-15) shows that the percentage contribution of SO_2 uptake to the total sulfur uptake dominates the sulfur uptake from aerosol particles at all times after 200 seconds. We further note from Fig.(VII-14) that the mass of uptaken sulfur from gas scavenging seems to converge for the cases C and D towards some value. This is due to the fact that the drops scavenged all the gas

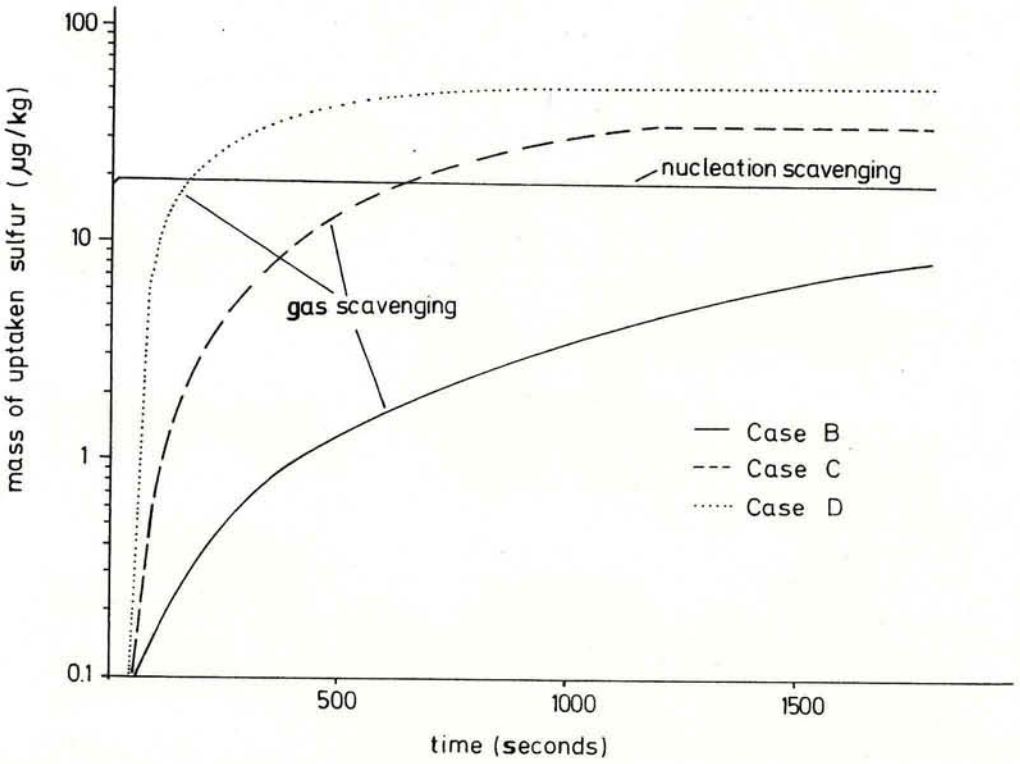

Fig.(VII-14): Time variation of mass of uptaken sulfur through aerosol scavenging of $(NH_4)_2SO_4$ and gas scavenging of SO_2 for case B, C and D.

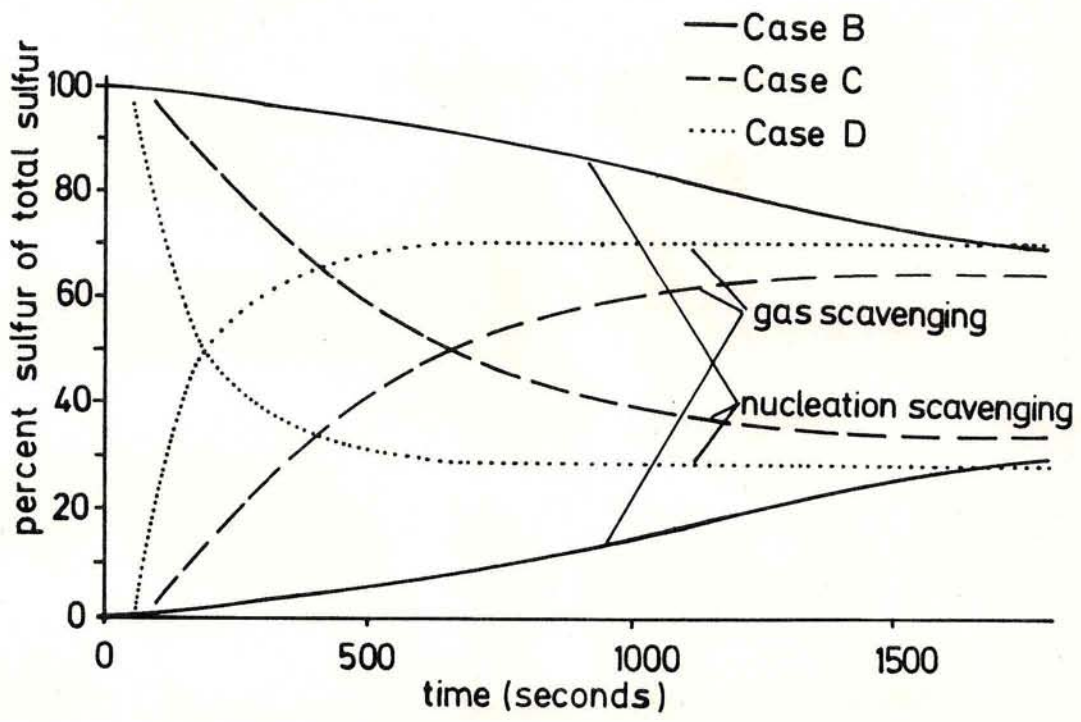

Fig.(VII-15): Time variation of percent sulfur of total sulfur taken up by aerosol scavenging of $(NH_4)_2SO_4$ and by gas scavenging of SO_2 for case B, C and D.

available in the parcel. And the entrainment can't supply the gas fast enough. Case D ends up with a higher gas mass scavenged because of the larger oxidation rate. The gas was faster depleted from the parcel and the entrainment had a stronger gradient to work with, thus supplying more gas mass for the scavenging.

VII.2.3 Case E

In the previous cases A, B, C and D the relative importance of the aerosol and gas uptake mechanisms was determined solely by the value of the oxidation rate. The effect of the amount of aerosol and gas available in the environmental air was studied by case E (see Table IV-1). We note that in this case the amount of sulfur from the gas is over 4 times higher than the amount of sulfur from the aerosol. The oxidation rate was assumed to be $K'=0.1\ sec^{-1}$. Fig.(VII-16) displays the amount of sulfur entering the drop through aerosol and gas scavenging, and Fig.(VII-17) gives the percent of sulfur due to aerosol and gas scavenging of the total uptaken sulfur. We note that the general behavior of the curves is similar to case C which had the same oxidation rate. However, due to the high amount of gas offered gas scavenging dominates aerosol scavenging already at 500 sec and overall takes up more gas than in case C.

VII.2.4 Case F

Analogously to case E, case F was chosen to study the effect of the amount of aerosol and gas available for scavenging in the surrounding air. In contrast to case E, however, we chose in case F that more sulfur was offered to the drop via aerosol scavenging than via gas scavenging (see Table IV-1). This increase in the amount of aerosol over and above the amount considered in cases A to E made it necessary to adjust the aerosol particle distribution to this new total aerosol mass concentration. The new distribution is chosen to be the continental type spectrum already used as initial condition for case 1 of section VII.1 and the evolution in time of the dynamic parameters and

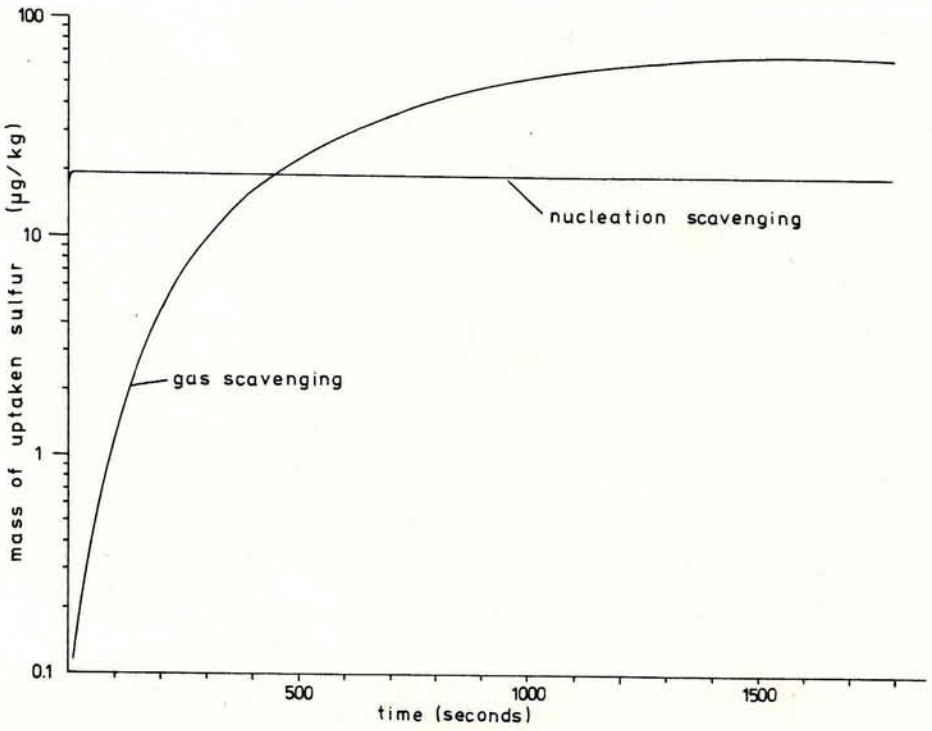

Fig.(VII-16): Time variation of mass of uptaken sulfur through aerosol scavenging of $(NH_4)_2 SO_4$ and gas scavenging of SO_2 for case E.

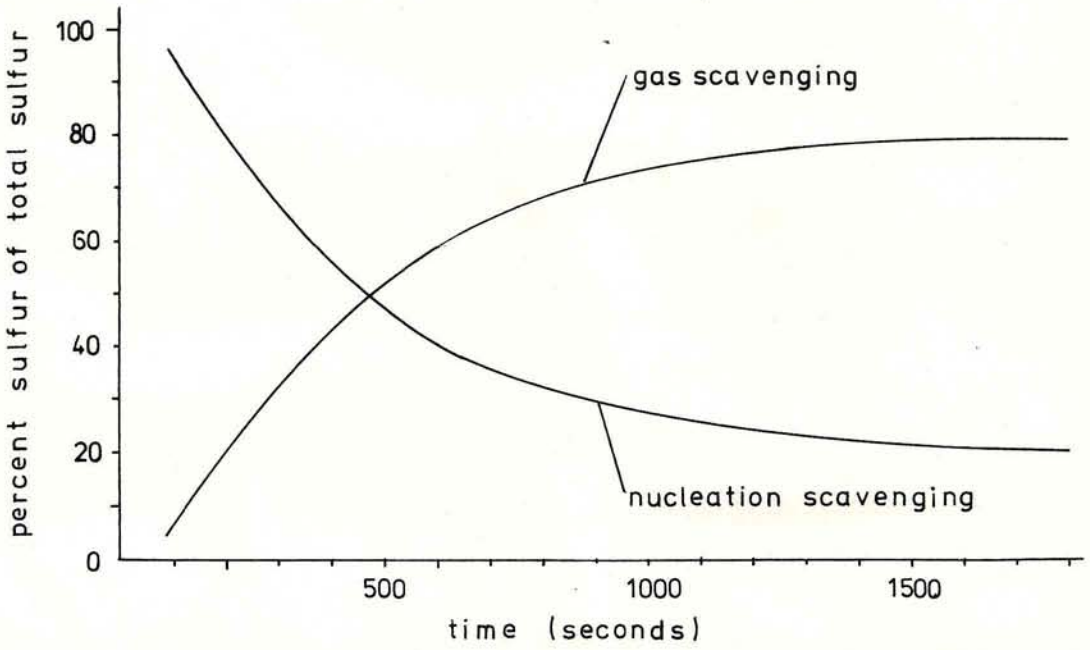

Fig.(VII-17): Time variation of percent sulfur of total sulfur taken up by aerosol scavenging of $(NH_4)_2 SO_4$ and by gas scavenging of SO_2 for case E.

of the aerosol particle and drop spectrum stays the same as that discussed in section VII.1.1. We note that for these initial conditions the drop spectrum doesn't develop rain.

For case F the oxidation rate K' was set to be $0.1 sec^{-1}$. Fig.(VII-18) displays for this case the amount of sulfur entering the drop through aerosol and gas scavenging. It is striking in this figure that, as in case C, after 650 sec gas scavenging dominates aerosol scavenging despite the fact that the amount of aerosol offered is now nearly 3 times higher than in case C. This is due to the fact that in case F many drops have formed through nucleation. These grow only very little by condensation and collision and coalescence so that they remain in the range where they are always saturated with respect to S(IV). This allows that in the cloud water the maximum possible amount of S(VI) is oxidized to S(VI). This has as a consequence that as time goes on more sulfur is taken up through gas scavenging than in case C although the amount of gas offered and the oxidation rate is the same in case F as in case C. This behavior is also reflected in Fig.(VII-19) which displays the percent of sulfur due to aerosol and gas scavenging of the total uptaken sulfur.

Case F was also used to determine the effect of gas scavenging on the processing of the aerosol particle spectrum, which was already discussed in section VII.1 for the aerosol scavenging alone. Fig.(VII-20) illustrates how the aerosol particle spectrum is processed during the life time of the cloud not only as a result of nucleation and impaction scavenging and collision and coalescence of the drops but also through the gas scavenging. This figure essentially contains the same information as Fig.(VII-3). However, curve (3) now represents the size of the aerosol particles which result after the complete evaporation of the drops in a cloud which was allowed to scavenge $(NH_4)_2SO_4$ particles and SO_2 for about 30 minutes. Curve(4) results if the drops were only allowed to scavenge aerosol particles but no SO_2. We notice from the curves in Fig.(VII-20) that through evaporation of drops, which were allowed to scavenge aerosol particles and gases during their life time, aerosol particles result with characteristics quite different from those aerosol particles on which the drops originated. Thus, the size distribution is broader and the number of aerosol particles which are able to become activated to

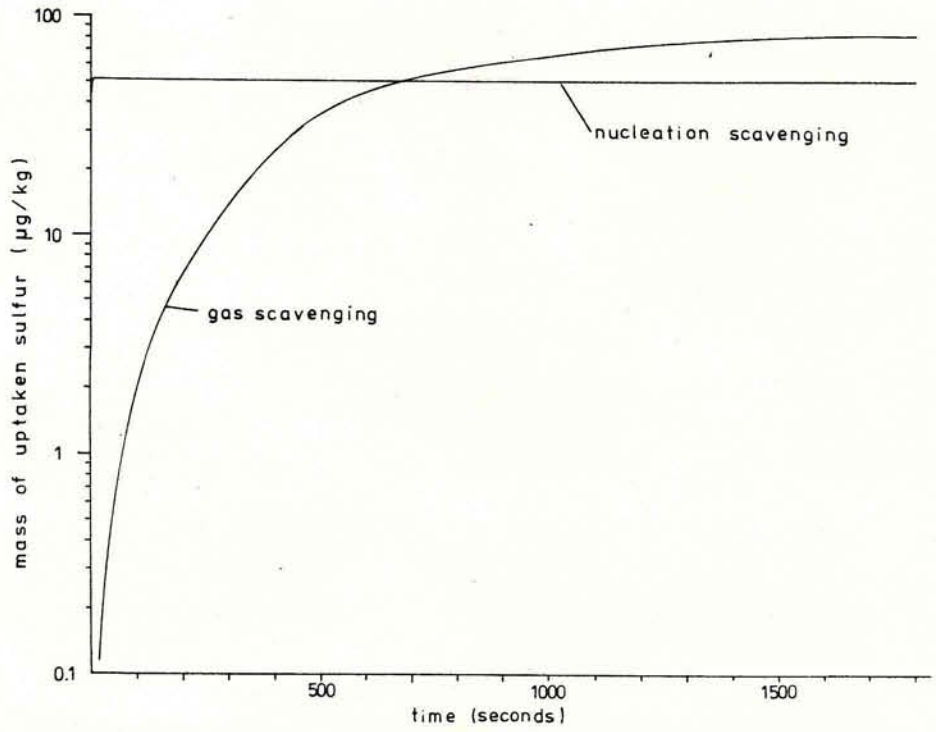

Fig.(VII-18): Time variation of mass of uptaken sulfur through aerosol scavenging of $(NH_4)_2SO_4$ and gas scavenging of SO_2 for case F.

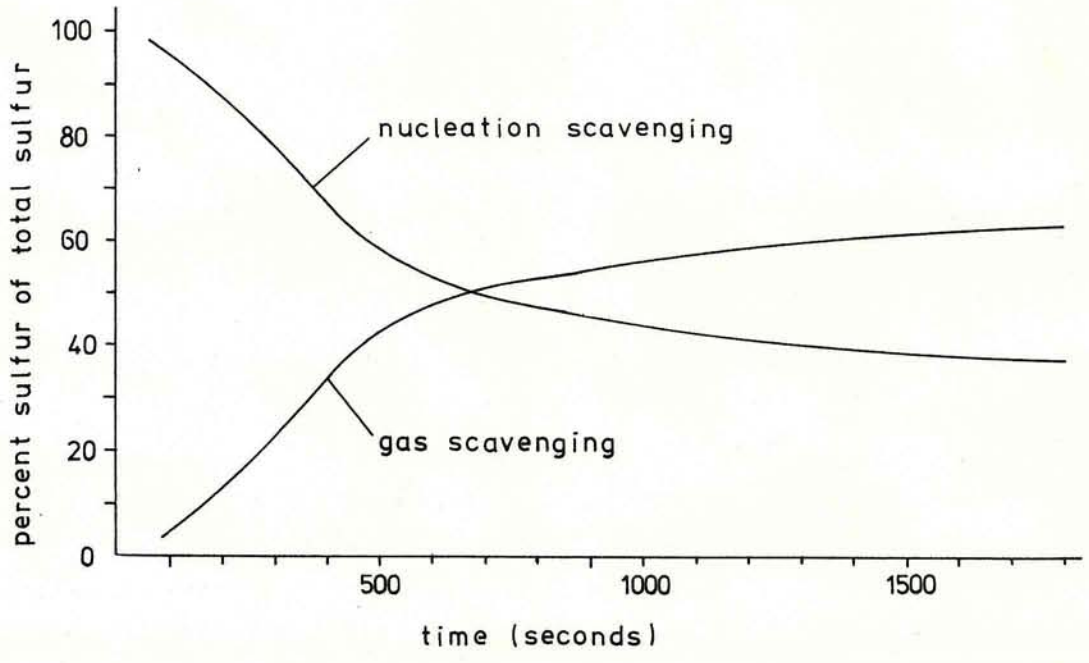

Fig.(VII-19): Time variation of percent sulfur of total sulfur taken up by aerosol scavenging of $(NH_4)_2SO_4$ and by gas scavenging of SO_2 for case F.

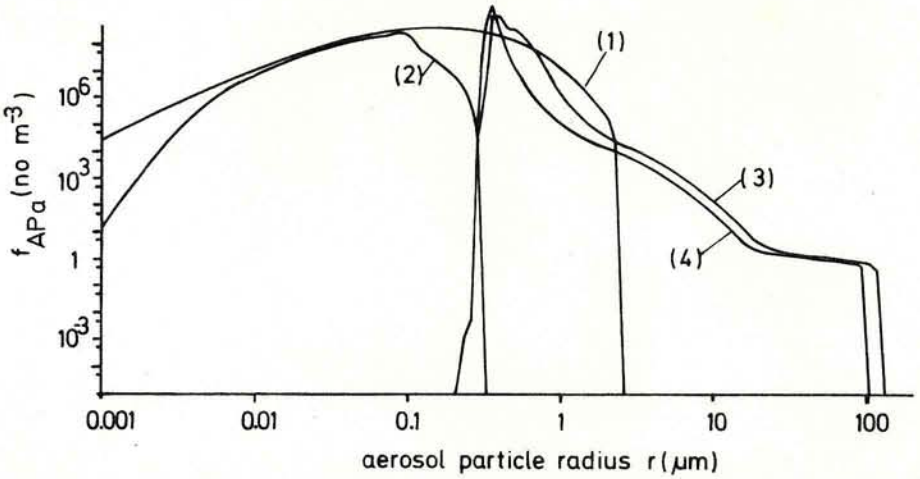

Fig.(VII-20): Aerosol particle number density distribution function f_{APa} as a function of radius r of aerosol particles for case F.
(1): initial dry aerosol particle spectrum
(2): dry interstitial aerosol particle spectrum after 30 min of cloud life time
(3): aerosol particle spectrum from dried-off cloud drops after 30 min of cloud life time, if all scavenged aerosol and gas material inside one drop becomes one single aerosol particle
(4): aerosol particle spectrum from dried-off cloud drops after 30 min of cloud life time, if only aerosol mass was scavenged

drops in a following cloud cycle is larger than that of the spectrum on which the drops originated. This effect is particularly pronounced if $(NH_4)_2 SO_4$ as well as SO_2 is allowed to be scavenged. We notice that with gas scavenging we gain larger CCN than without and if the initial particle spectrum would have consisted of bad CCN, i.e. insoluble material, the processed spectrum now would have far better CCN in a new cloud cycle.

VII.2.5 Case G, H and I

Case G, H and I were chosen to make a comparison between our theoretical results and the field observations of Hegg and Hobbs(1982, 1983). The mass concentrations of $(NH_4)_2 SO_4$ particles and of SO_2 offered for uptake by the cloud were chosen in accordance with the concentrations observed by Hegg and Hobbs and had the values given in Table IV-1. The low aerosol mass concentration was achieved by assuming that the

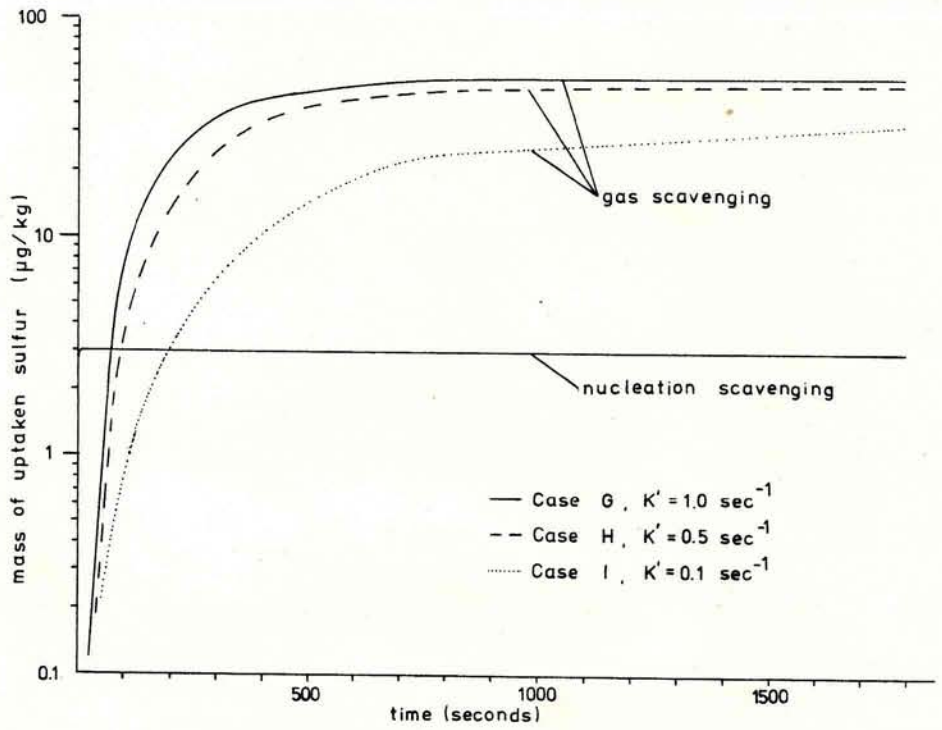

Fig.(VII-21): Time variation of mass of uptaken sulfur through aerosol scavenging of $(NH_4)_2SO_4$ and gas scavenging of SO_2 for case G, H and I.

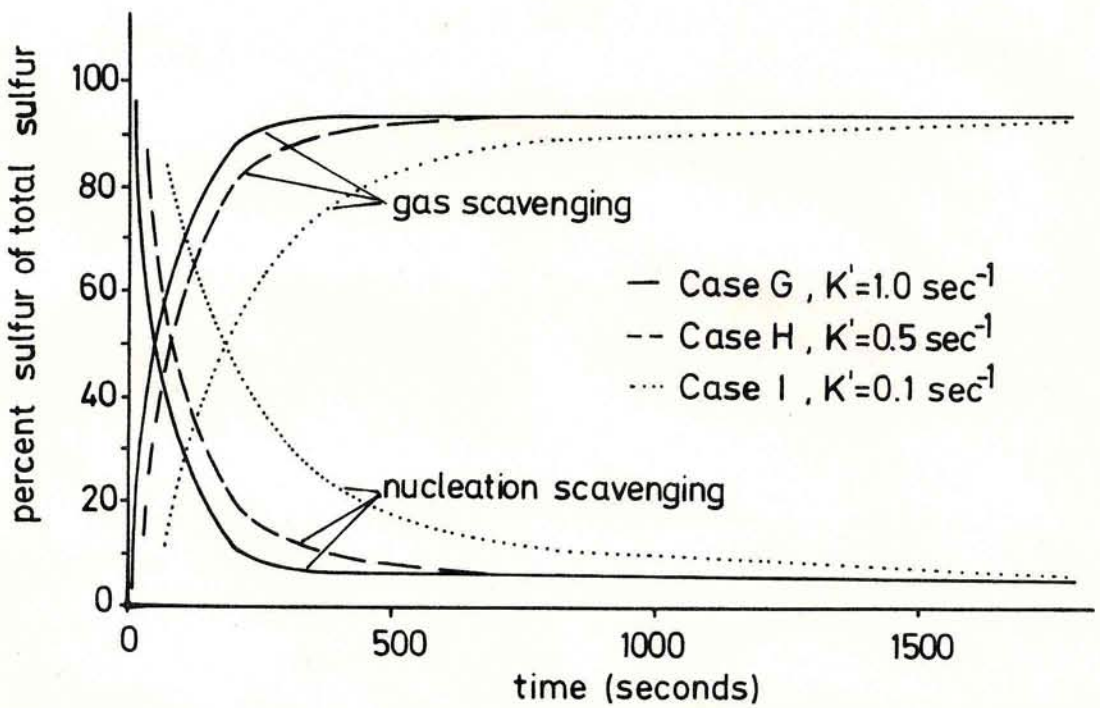

Fig.(VII-22): Time variation of percent sulfur of total sulfur taken up by aerosol scavenging of $(NH_4)_2SO_4$ and by gas scavenging of SO_2 for case G, H and I.

maritime-type aerosol spectrum of case A to E was truncated at the lower end to represent a total number concentration of $90cm^{-3}$. On such an aerosol particle spectrum the cloud develops in the manner described in case 3 of chapter VII.1. Fig.(VII-21) displays the variation with time of the total sulfur per kilogram air which entered the drop via aerosol and gas scavenging. As expected the oxidation rate determines the relative importance of the two mechanisms. Analogously Fig.(VII-22) gives for this case the percentage contribution of $(NH_4)_2SO_4$ particles and SO_2 to the total sulfur uptake for the oxidation rates K'=0.1, 0.5 and 1.0 sec^{-1}. As expected the domination of one or the other scavenging mechanisms depends on the value of K'. A comparison of the results for this case with the results of case B, C and D shows that gas scavenging dominates aerosol scavenging much sooner in the present case because of the lower amounts of $(NH_4)_2SO_4$ mass offered.

For the range of pH values between 4.5 and 5 measured in the cloud water, Hegg and Hobbs (1982) estimated the oxidation rate K' to be between 0.1 and 0.5 sec^{-1}. For this situation and a distance above cloud base, which is equivalent to a computation time of about 100 seconds in our model, they estimated the percentage contribution of aerosol nucleation scavenging to the total scavenging to be about 70%. This agrees qualitatively with our theoretical predictions, as seen from Fig.(VII-22), if we interpolate between the lines.

VII.2.6 Comparison of our results for in-cloud scavenging with the results by Walcek, Pruppacher(1984b) for below-cloud scavenging

It is tempting to make a brief comparison between the results of in-cloud scavenging studied in the present work and the results of below-cloud scavenging studied by Walcek and Pruppacher(1984b). For below-cloud scavenging and no oxidation Walcek and Pruppacher found that the concentration of S(IV) due to the uptake of SO_2 by the rain water, falling from cloud base through a pollution plume, was maximum for drops of sizes near 1200μm (Fig.(VII-23)). Larger drops fell too fast through the pollution layer for taking up much SO_2, while smaller

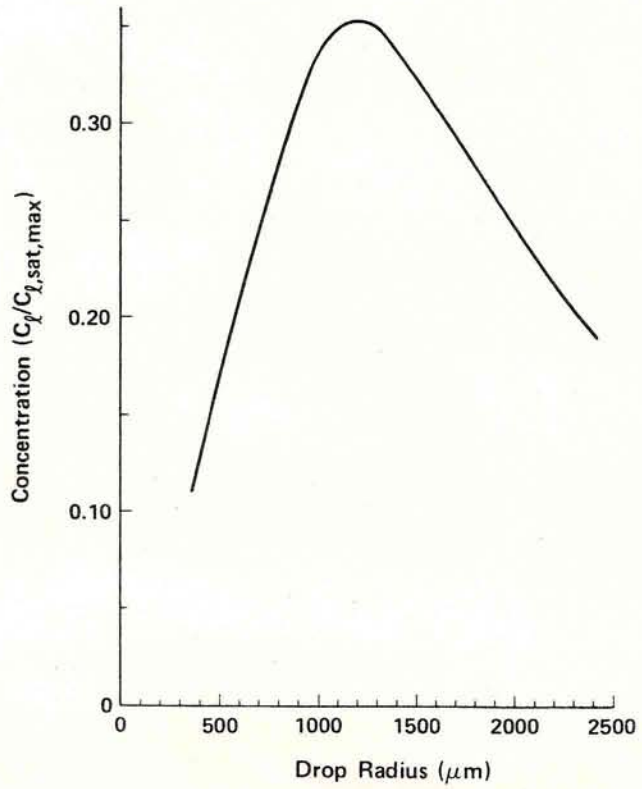

Fig.(VII-23): Variation of sulfur concentration in rain drops of Best (1950) distribution, assumed to be collected at the ground, as a function of drops size; no oxidation in the drops (taken from Walcek, Pruppacher(1984b)).

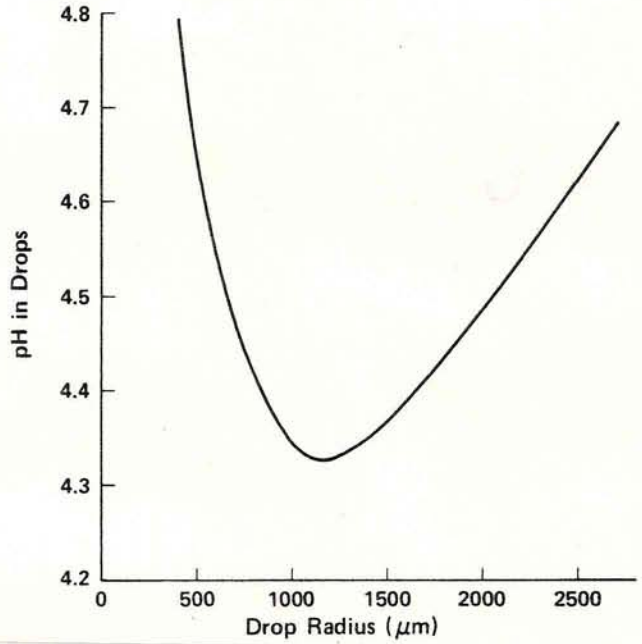

Fig.(VII-24): Variation of pH=-log[H^+] in rain drops of Best(1950) distribution, assumed to be collected at the ground, as a function of drop size; no oxidation in the drops (taken from Walcek, Pruppacher (1984b)).

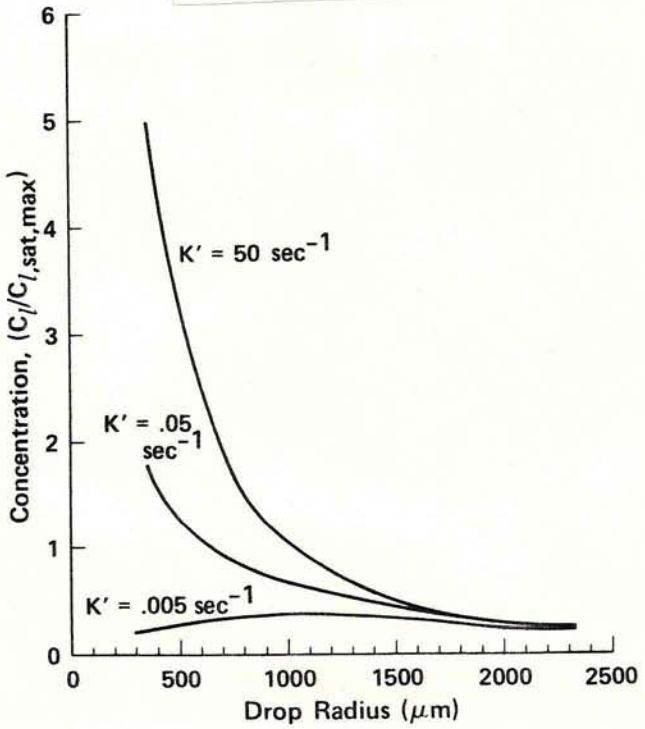

Fig.(VII-25): Variation of sulfur concentration in rain drops of Best (1950) distribution, assumed to be collected at the ground, as a function of drops size; with oxidation in the drops, for various values of K' (taken from Walcek, Pruppacher(1984b)).

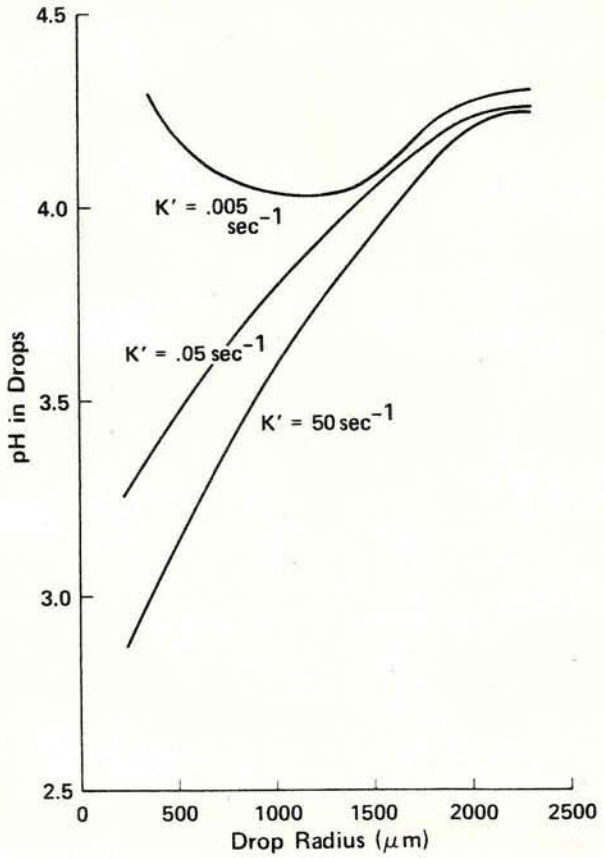

Fig.(VII-26): Variation of pH=-log[H^+] in rain drops of Best(1950) distribution, assumed to be collected at the ground, as a function of drop size; with oxidation in the drops, for various values of K' (taken from Walcek, Pruppacher(1984b)).

drops fell slowly enough to lose most of the taken up SO_2 by desorption below the plume. Accordingly, the pH of the acid, formed by dissociation of the sulfur species in the rain water, was also maximum near the mentioned drop size (compare Fig.(VII-24)). If oxidation was allowed to take place inside the falling rain drops Walcek and Pruppacher found that the sulfur concentration taken up by the rain drops from SO_2 increased with decreasing rain drop size, and accordingly, the pH decreased with decreasing rain drop size (Fig.(VII-25) and Fig.(VII-26)). This is due to the fact that the smaller the drops the longer is the time they are exposed to the pollution and during which oxidation can act. This behavior is in sharp contrast to the behavior shown in Fig.(VII-11a) and (VII-11d) for inside-cloud scavenging of SO_2. As mentioned above, below the cloud, drops have a fixed distance to cover for which they require a fixed time depending on their size, when falling individually from cloud base through various pollution layers to the ground. Thus, for below-cloud scavenging, the larger the drops the shorter the time needed to fall to the ground, and therefore the shorter the exposure time to SO_2. Inside a cloud, however, the drops are sustained in the air and continue to grow by condensation and by collision and coalescence. Under this condition the largest drops are also the 'oldest' ones and, after sufficient cloud time has elapsed and oxidation has taken place, have also the highest sulfur concentration from SO_2 uptake, and therefore the lowest pH.

A comparison between in-cloud scavenging and below-cloud scavenging is also made in Table VII-4 where for various oxidation rates the amount of sulfur taken up from SO_2 for our cases A to I inside the cloud are listed. These values are compared with the amounts of SO_2 taken up by a rain of 25mm/hr after 1mm rain had fallen through a Gaussian pollution plume of SO_2 with a maximum concentration of 500ppb(v) (from Walcek, Pruppacher(1984b), Fig.(VII-25)). We notice from this table that, except for exceptionally large oxidation rates in rain, below-cloud scavenging of SO_2 contributes less than 30% to the total scavenging of SO_2, even for the case of a very pronounced pollution layer below the cloud.

Table VII-4a

case	initial SO_2 concentration in air (ppb)	K' sec^{-1}	mass of SO_2 scavenged (mg S/liter)
A	31	$5x10^{-3}$	6.5
B	15	$5x10^{-3}$	4.5
C	15	0.1	20.0
D	15	1.0	30.0
E	35	0.1	41.0
F	15	0.1	45.5
G	15	1.0	30.2
H	15	0.5	27.1
I	15	0.1	19.6

Table VII-4b

case	initial SO_2 concentration in air (ppb)	K' sec^{-1}	mass of sulfur scavenged (mg S/liter)
(1)	for all cases:	$5x10^{-3}$	1.4
(2)	Gaussian distribution of	$5x10^{-2}$	3.0
(3)	SO_2 with 500 ppb conc max.	50	5.6

Table VII-4: Comparison between inside-cloud scavenging (Table VII-4a: our results after 30 minutes of cloud life time) and below-cloud scavenging (Table VII-4b: data of Walcek, Pruppacher(1984b) for a precipitation rate of 25 mm/hr and a drop size distribution given by Best(1950) after 1mm of rainfall).

VII.2.7 Conclusion

By linking our aerosol and gas scavenging models described in chapter II and III to the entraining air parcel model described in chapter IV we attempted to study: the evolution with time of the mass of the total sulfur as S(IV) and S(VI) inside the drops, the evolution with time of the acidity of the cloud water as a function of various oxidation rates and as a function of drop size, the relative importance of sulfur scavenging from SO_2 as compared to sulfur scavenging from $(NH_4)_2SO_4$ particles, and the contribution of inside-cloud scavenging and below-cloud scavenging to the total uptake of pollutants, all as a function of aerosol particle and gas concentration in the surrounding air.

Our study suggests for inside-cloud scavenging:

1.) Collision and coalescence causes among the various drop size categories a re-distribution of the sulfur scavenged from SO_2 and from $(NH_4)_2SO_4$. This re-distribution takes place such that the main sulfur mass is always associated with the main water mass in the cloud, i.e. is contained in the larger drops which may reach the ground as precipitation. This result has yet to be verified by measurements.

2.) In contrast to the sulfur scavenged from aerosol particles which causes that the smaller drops are always more contaminated than the larger ones, the concentration of sulfur scavenged from SO_2 is a function of time, a function of concentration of SO_2 in the air and a function of the oxidation rate of the sulfur in the drops. For the case that only S(IV) is present in the drops (no oxidation), the concentration at the beginning is lower in the larger drops than in the smaller ones due to the time lag of the former in absorbing SO_2. After a longer time all drops are saturated.

For the case that S(VI) is present in the drops (oxidation), the sulfur concentration is generally larger in the large drops than in the small ones due to the age of the former, due to a longer time over which oxidation could be active. This causes also that generally the pH is lower in the large drops than in the small ones.

3.) For the typical SO_2 and $(NH_4)_2SO_4$ particle concentrations in the atmosphere it is found that sulfur scavenging from SO_2 dominates sulfur scavenging from $(NH_4)_2SO_4$ particles, if the oxidation rate inside

the cloud drops is relatively high ($K' > 0.01$ sec^{-1}). If the oxidation rate inside the cloud drops is relatively low ($K' < 0.01$ sec^{-1}) sulfur scavenging from $(NH_4)_2SO_4$ particles dominates the scavenging from SO_2.

4.) After the complete evaporation of a drop spectrum that scavenged gas and aerosol particles the resulting aerosol particle spectrum contains larger particles than with only aerosol scavenging active. And through the uptaken gas the solubility of the aerosol particles is enhanced. This enhances the effectivity of the spectrum to produce rain in a second cloud cycle. This result is in agreement with field observations of Hegg et al.(1980).

5.) A comparison of the results of inside-cloud scavenging of SO_2 considered in this paper with the results of Walcek and Pruppacher (1984b) for below-cloud scavenging of SO_2 shows that, for typical atmospheric conditions, below-cloud scavenging contributes less than 30% to the total amount of sulfur scavenged from SO_2 by a cloud formation and precipitation event.

VII.3 Results of aerosol scavenging in the two dimensional cloud model of Clark et al.

To study aerosol scavenging by a more realistic description of a convective cloud we linked the aerosol scavenging model described in chapter II to the cloud model described in chapter V. This model provided a two dimensional framework and enabled us to verify the conclusions we obtained with the simple entraining air parcel model. The initial conditions are given in chapter V.2.

VII.3.1 Discussion of the model results

The cloud simulations start in a very stable atmosphere (compare Fig.(V-1)). But the incoming shortwave solar flux is high (0° latitude, June 20, 11o'clock) and drives the fluxes at the surface (compare chapter V.2); heat and moisture are introduced at the lower boundary of the domain. This results in a growing instability.

Figs.(VII-27a) to (VII-27f) display the situation inside the considered domain after 20 minutes of simulation time. Fig.(VII-27a) represents the field of the relative humidity. Comparison to the initial profile in Fig.(V-1b) shows that the introduced moisture raised the relative humidity in the lower 3km of the domain. Also the potential temperature, displayed in Fig.(VII-27b), increased due to the surface sensible heat flux in the lower portion of the domain. This increase is most distinct in the center of the x-direction at 10km as 99.5% of the total energy contributes to a bell shaped surface heating (compare Fig.(V-2)). The strong sensible and latent heat flux at the surface force the air to rise. Fig.(VII-27c) shows a starting updraft with a maximum of 2.5m/sec in the middle of the domain. Yet it still covers only a region up to 3km in the vertical. Left and right of the updraft center weak compensating downdrafts start to develop. Fig.(VII-27d) displays the field of the horizontal velocity field u. Solid lines represent positive values of u in direction of the x-axis and dashed lines represent the corresponding negative values. We see here that at the surface the air converges at the center of the x-axis

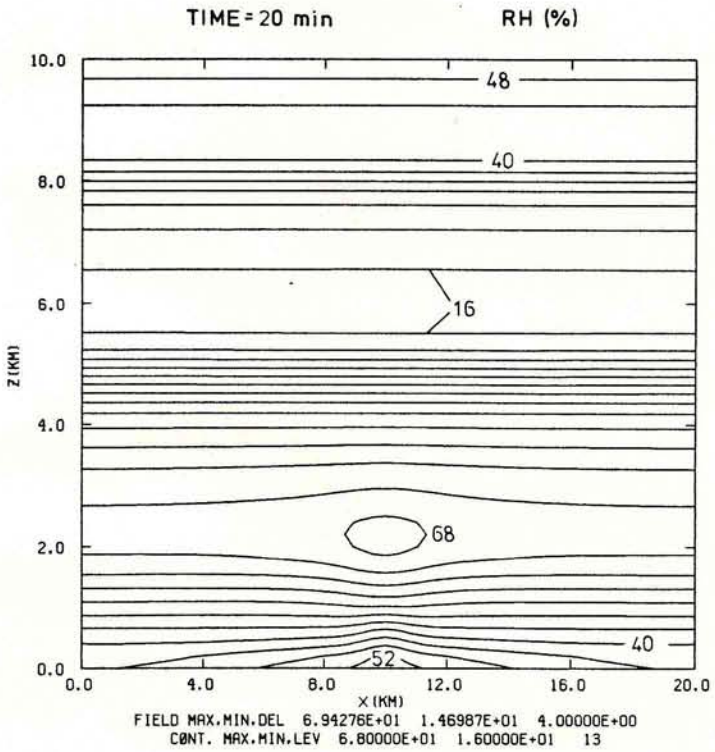

Fig.(VII 27a): Field of the relative humidity RH in % after 20 minutes (spacing of the curves: 4%).

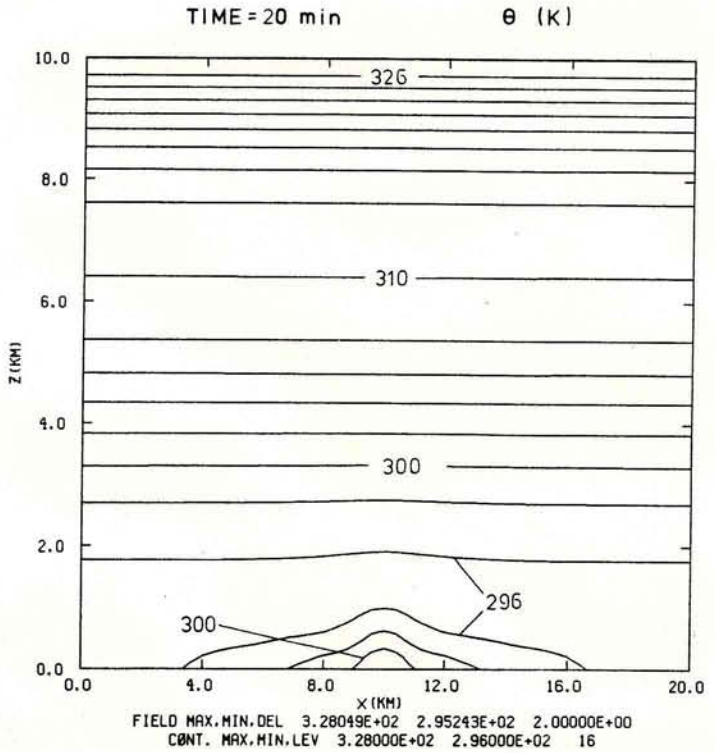

Fig.(VII-27b): Field of the potential temperature θ in K after 20 minutes (spacing of the curves: 2K).

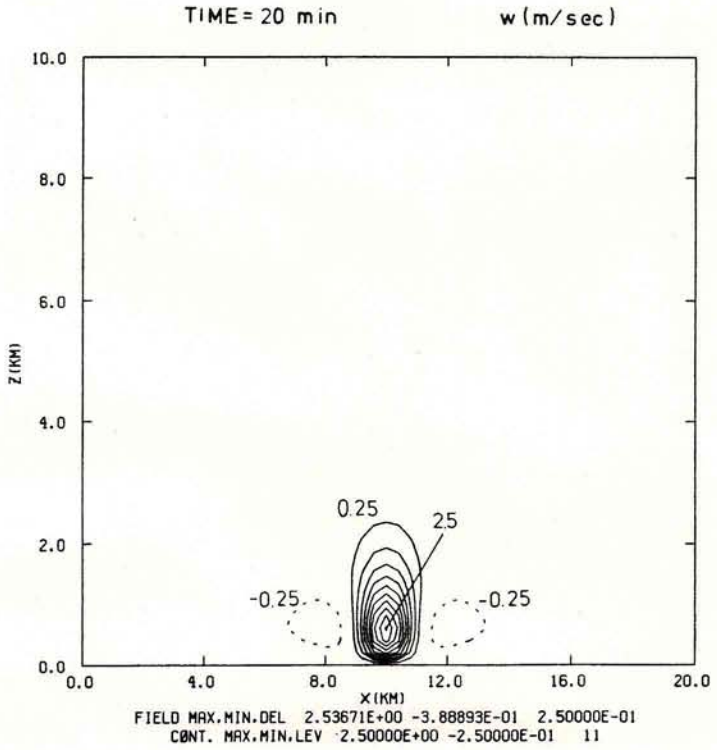

Fig.(VII-27c): Field of the vertical velocity w in m/sec after 20 minutes (solid lines: updraft, dashed lines: downdraft, spacing of the curves: 0.25m/sec).

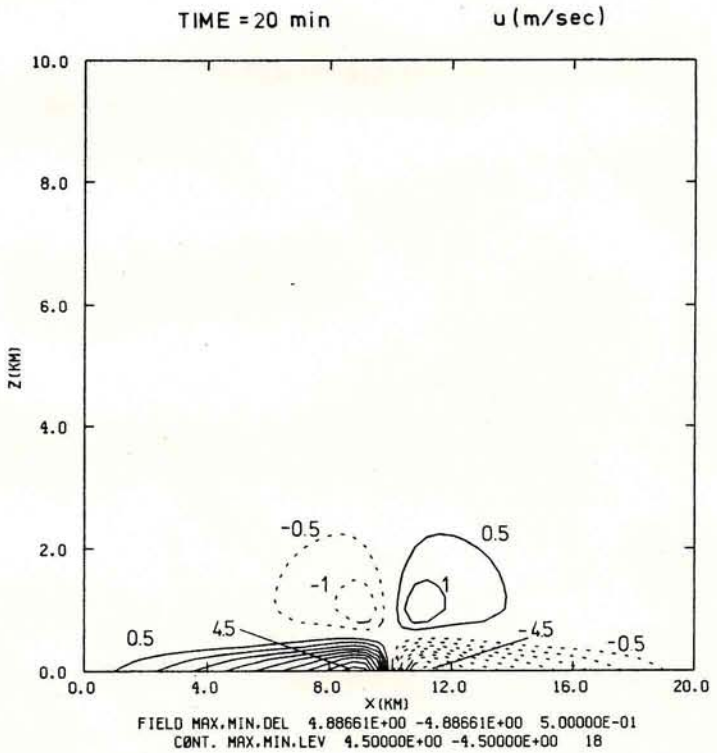

Fig.(VII-27d): Field of the horizontal velocity u in m/sec after 20 minutes (solid lines: u in positive x-direction, dashed lines: u in negative x-direction, spacing of the curves: 0.5 m/sec).

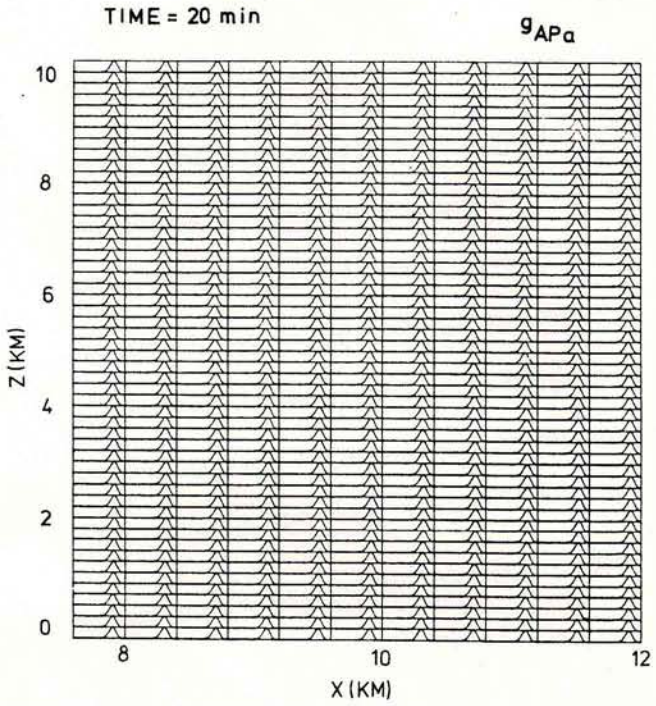

Fig.(VII-27e): Spectra of aerosol particle mass density distribution function in unactivated aerosol particles g_{APa} as a function of particle radius at each grid point in the middle section of the computational domain after 20 minutes (spectra are adjusted to the maximum occuring value).

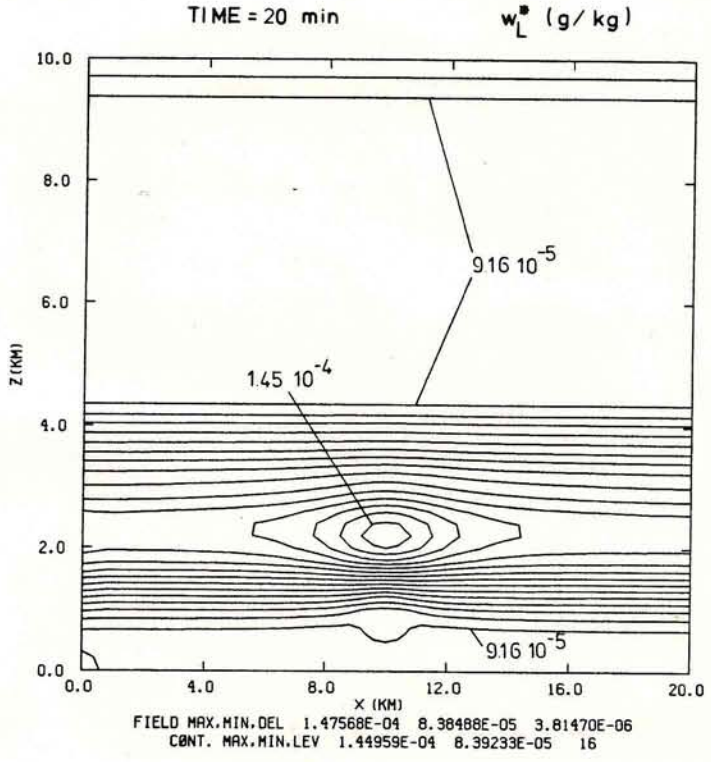

Fig.(VII-27f): Field of the total liquid water content w_L^* in g/kg after 20 minutes (spacing of the curves: 3.8 10^{-6} g/kg).

and diverges between 1 and 2 km height. Figs.(VII-27c) and (VII-27d) together indicate that two rotors are developing pumping the warm, moist air from the surface into the upper atmosphere. The convection cell starts to develop, however, no cloud has yet formed. The relative humidity (Fig.(VII-27a)) is still way below 100% and Fig.(VII-27e) still displays a complete aerosol particle spectrum at every grid point. As already stated in section V.2 we use as input the maritime type spectrum of case 3 (compare chapter VII.1.3). These aerosol mass spectra shifted slightly to larger particle sizes only in the region around x=10km and z=2km due to the increased ambient relative humidity. This is also displayed in Fig.(VII-27f) for the field of the total liquid water content w_L^*. As drops have not yet formed w_L^* represents only the water taken up by the aerosol particles. We see a maximum around x=10km and z=2km.

Figs.(VII-28a) to Fig.(VII-28k) display the situation 10 minutes later at which time a small cloud has formed. Fig.(VII-28a) displays the field of the relative humidity. We see there that in an area between 2 and 6km in the vertical and 8 and 12km in the horizontal the air is supersaturated. The maximum value of the relative humidity is around 103%. Moisture is still entering the domain at the lower boundary as the sensible and latent heat flux still continue. Fig.(VII-28b) of the potential temperature field θ also shows that warm air is transported from the surface into the upper atmosphere. The circulation inside the computational domain is illustrated by Figs.(VII-28c) and (VII-28d), which display the vertical velocity field w and the horizontal velocity field u. We notice that the updraft assumes values as high as 16m/sec. The compensating downdraft has its maximum value around -6m/sec. The horizontal inflow and outflow complete the picture of the two rotors working. In Fig.(VII-28e) we see that a small cloud has formed. It's maximum liquid water content is now around 5 g/kg. This time the major contribution to w_L^* is due to the liquid water content of the cloud to which the water attached to the aerosol particles only contributes negligibly. Fig.(VII-28f) exhibits the distribution of the liquid water in form of different drop spectra. The quantity g_w represents the water mass density distribution function in the center 4km of the domain. We notice from the behavior of this function that

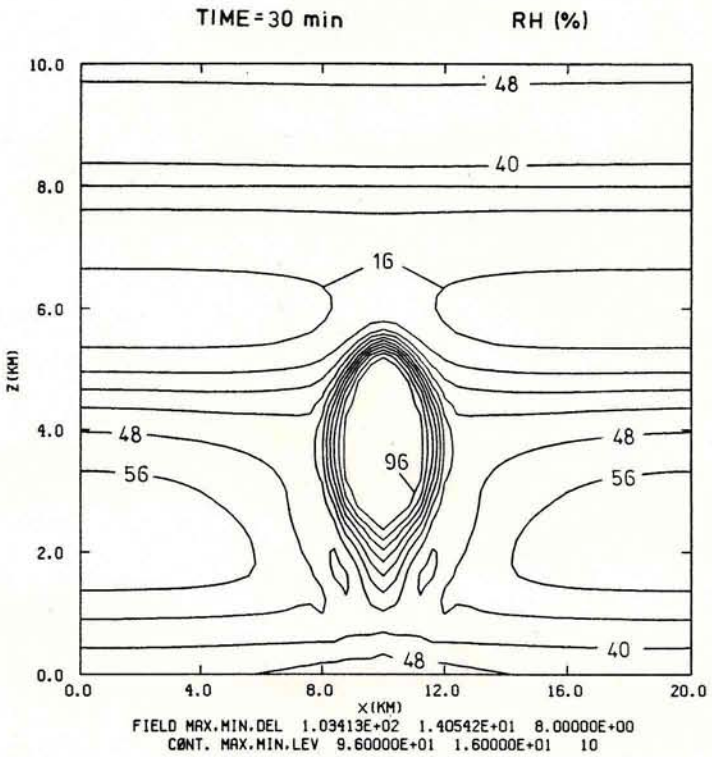

Fig.(VII-28a): Field of the relative humidity RH in % after 30 minutes (spacing of the curves: 8%).

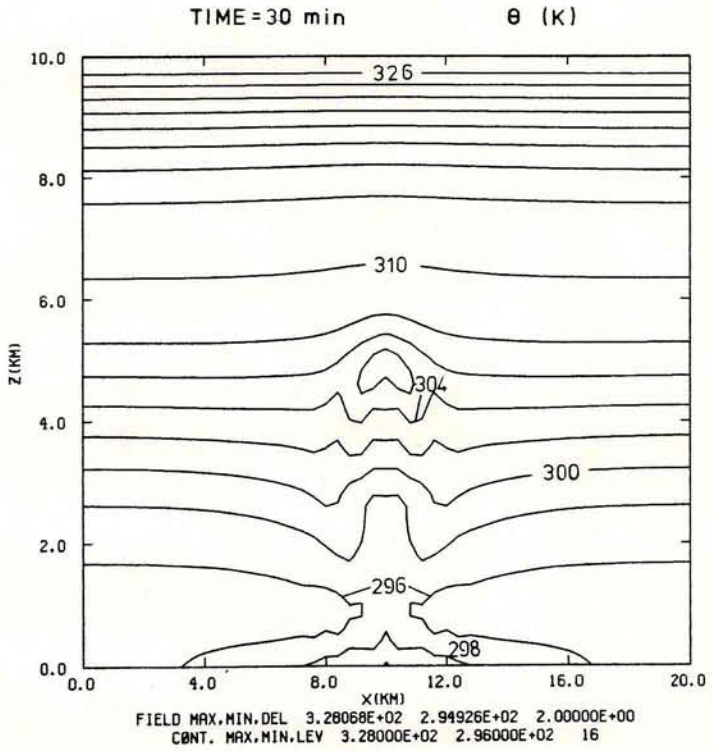

Fig.(VII-28b): Field of the potential temperature θ in K after 30 minutes (spacing of the curves: 2K).

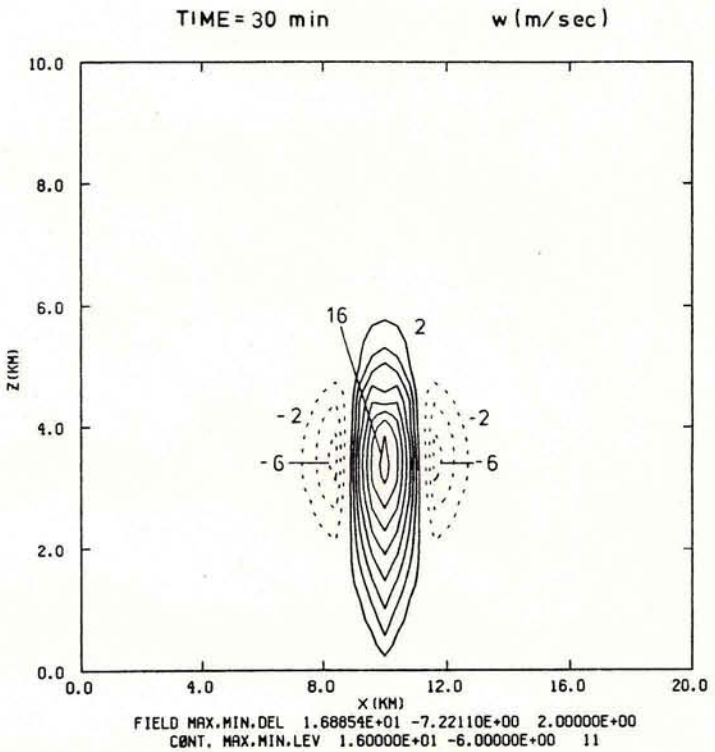

Fig.(VII-28c): Field of the vertical velocity w in m/sec after 30 minutes (solid lines: updraft, dashed lines: downdraft, spacing of the curves: 2m/sec).

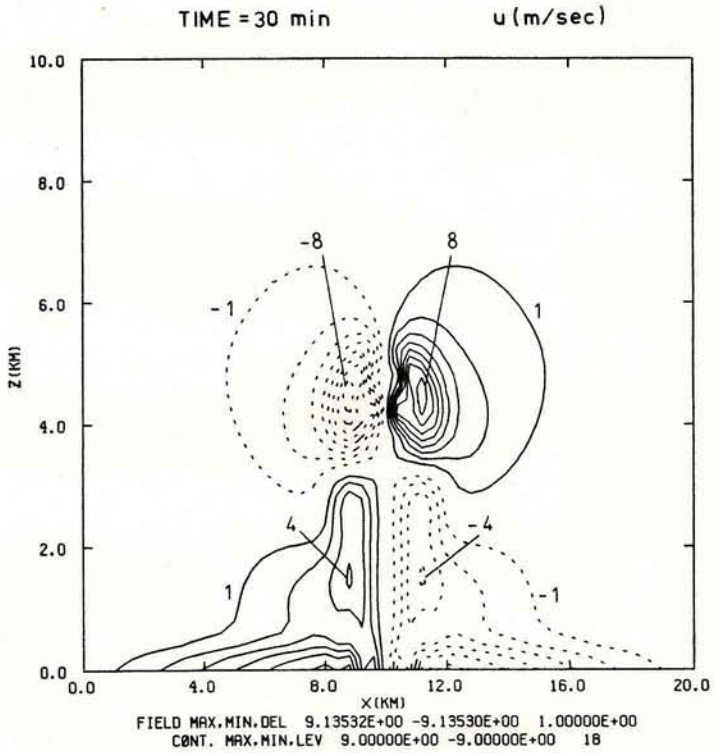

Fig.(VII-28d): Field of the horizontal velocity u in m/sec after 30 minutes (solid lines: u in positive x-direction, dashed lines: u in negative x-direction, spacing of the curves: 1 m/sec).

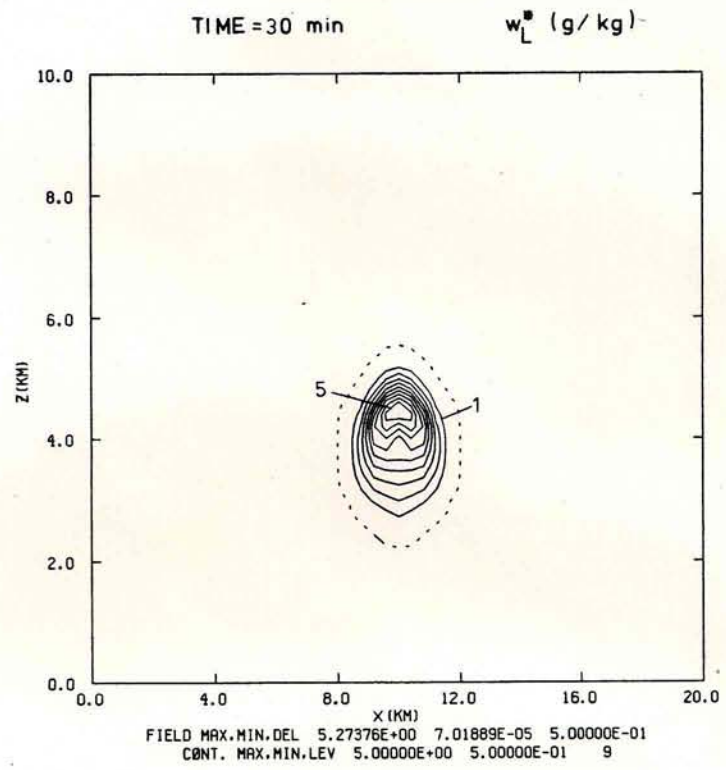

Fig.(VII-28e): Field of the total liquid water content w_L^* in g/kg after 30 minutes (dashed line: outer boundary of liquid water region = 10^{-2} g/kg, spacing of the curves: 0.5 g/kg).

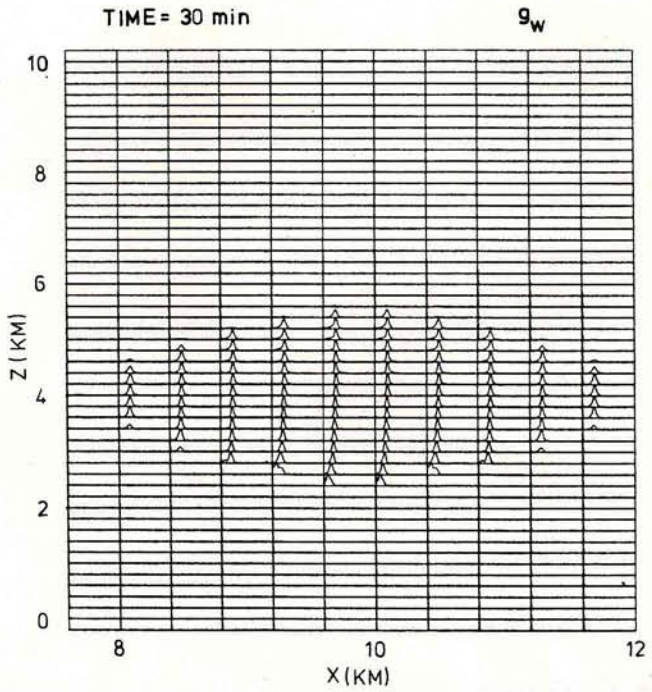

Fig.(VII-28f): Spectra of the drop water mass density distribution function g_w as a function of drop radius at each grid point in the middle section of the computational domain after 30 minutes (spectra adjusted to the maximum occuring value).

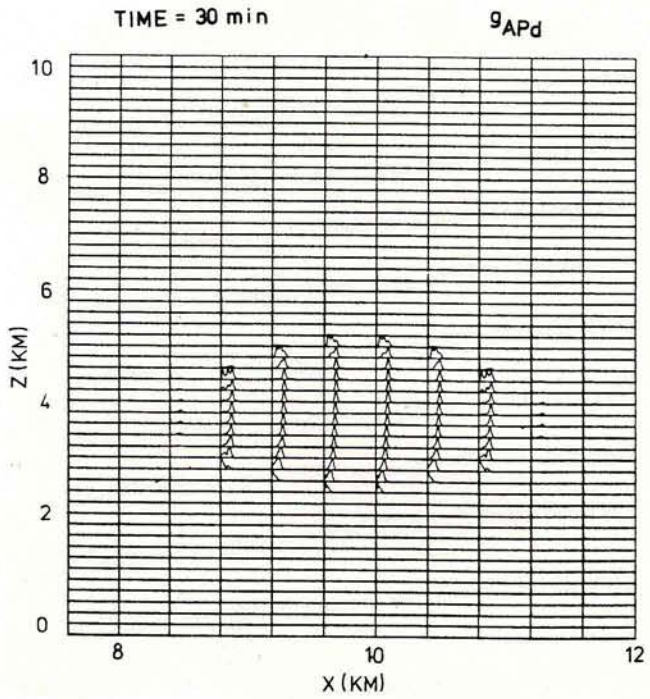

Fig.(VII-28g): Spectra of the aerosol particle mass density distribution function g_{APd} for aerosol material inside the drops as a function of drop radius at each grid point in the middle section of the computational domain after 30 minutes (spectra are adjusted to the maximum occuring value).

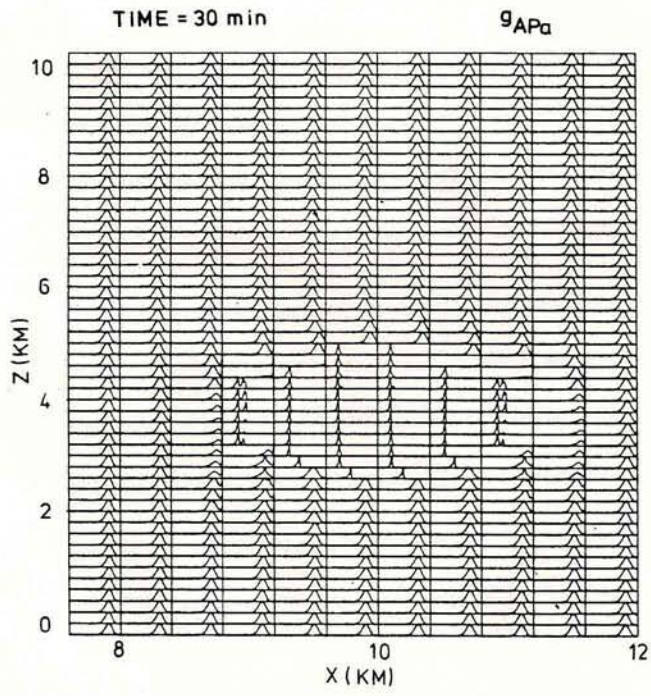

Fig.(VII-28h): Spectra of aerosol particle mass density distribution function in unactivated aerosol particles g_{APa} as a function of particle radius at each grid point in the middle section of the computational domain after 30 minutes (spectra are adjusted to the maximum occuring value).

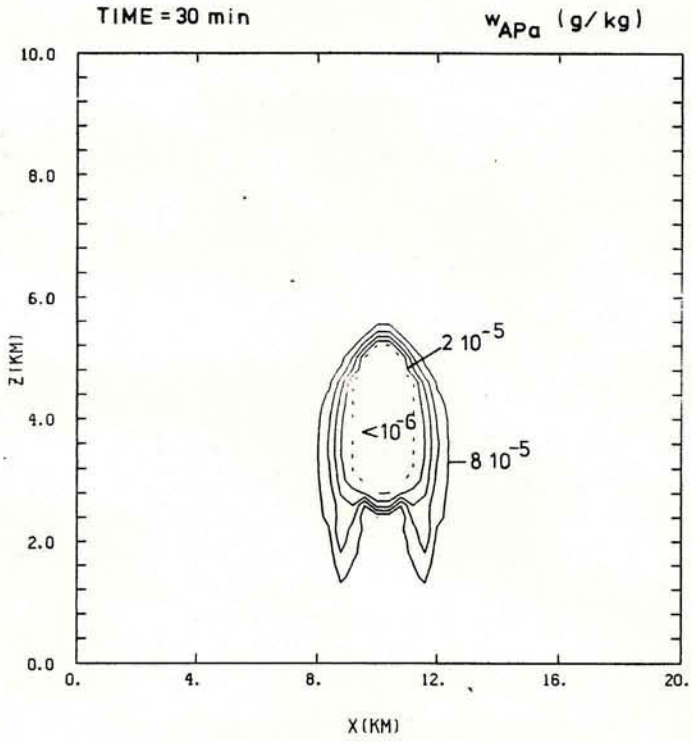

Fig.(VII-28i): Field of the total unactivated aerosol particle mass w_{APa} in air in g/kg after 30 minutes (dashed line: 10^{-6} g/kg, spacing of the curves: $2\ 10^{-5}$ g/kg).

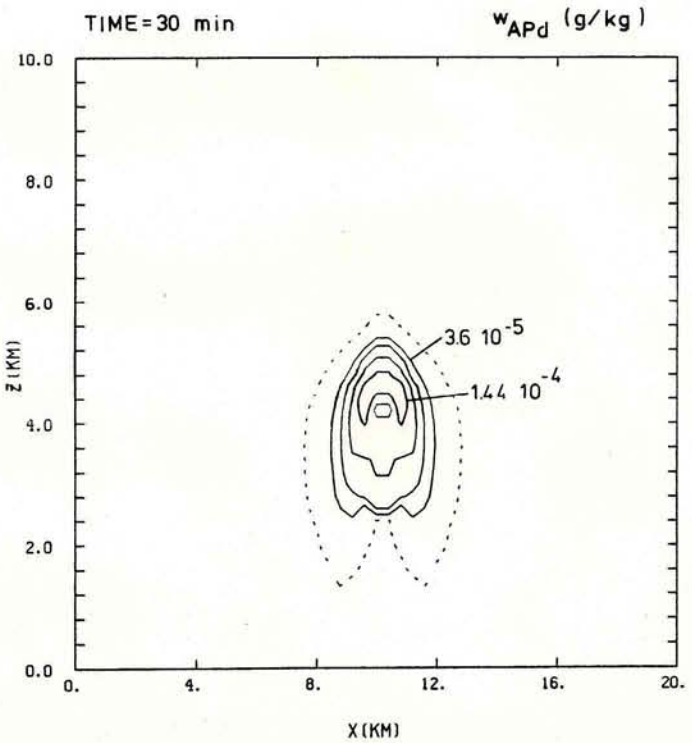

Fig.(VII-28k): Field of the total uptaken aerosol particle mass in drops w_{APd} in g/kg after 30 minutes (dashed line: 10^{-6} g/kg, spacing of the curves: $3.6\ 10^{-5}$ g/kg).

still most drops are confined to the small drop size categories and only few larger drops have formed. A similar behavior can be found for the aerosol particle mass density distribution function g_{APd} for aerosol material inside the drops (Fig.(VII-28g)). A corresponding function is displayed in Fig.(VII-28h) for the loss of unactivated aerosol particles in air. Our computations show that in the domain of the cloud most large aerosol particles became scavenged by nucleation (compare case 3 of chapter VII.1.3). At the edge of the cloud entrainment brought into the cloud aerosol particles from outside. This is stated by the two peaks in some aerosol particle spectra. Even outside the cloud defined by the nucleation scavenging region of Fig.(VII-28h) cloud drops exist. A comparison of Fig.(VII-28f) with (VII-28g) reveals that these drops have left the cloud through turbulent mixing. Fig.(VII-28i) and Fig.(VII-28k) summarize the information of Fig.(VII-28f) and Fig.(VII-28h). Fig.(VII-28i) shows the total mass of unactivated aerosol material in the air. This figure was obtained by an integration over all the particle sizes of the aerosol particle distribution of Fig.(VII-28h). The figure illustrates the depletion of the initial aerosol particle mass of about 90µg/kg through nucleation scavenging. Correspondingly the total mass of captured aerosol inside the drops w_{APd} increased to a maximum of about 144 µg/kg in the middle of the cloud due to turbulent mixing (Fig.(VII-28k)).

Figs.(VII-29a) to (VII-29k) display the situation after 40 minutes of model time. Fig.(VII-29a) represents the relative humidity field which now has a T-shaped form. This is due to the divergence in the horizontal velocity field u (compare Fig.(VII-29d)) in the domain between 4 and 6km altitude. Fig.(VII-29b) illustrates the potential temperature field θ. We notice from this figure that surface heating is still active. Fig.(VII-29c) displays the vertical velocity field w, and shows that vertical velocities of up to 16m/sec are reached. The horizontal velocity field u (Fig.(VII-29d)) reaches a maximum value at about 8m/sec. Fig.(VII-29d) also illustrates that waves are reaching the upper lid of the domain. This is an unwanted effect which only could have been circumvented by increasing the height of the computational domain. However, this measure would have made the model unduly expensive if we consider that there are other reasons why the dynamics of

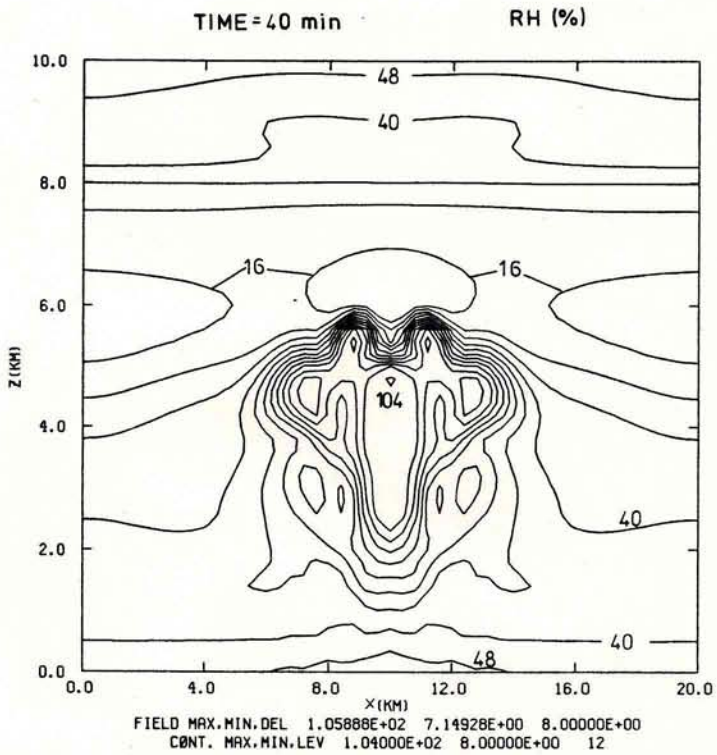

Fig.(VII-29a): Field of the relative humidity RH in % after 40 minutes (spacing of the curves: 8%).

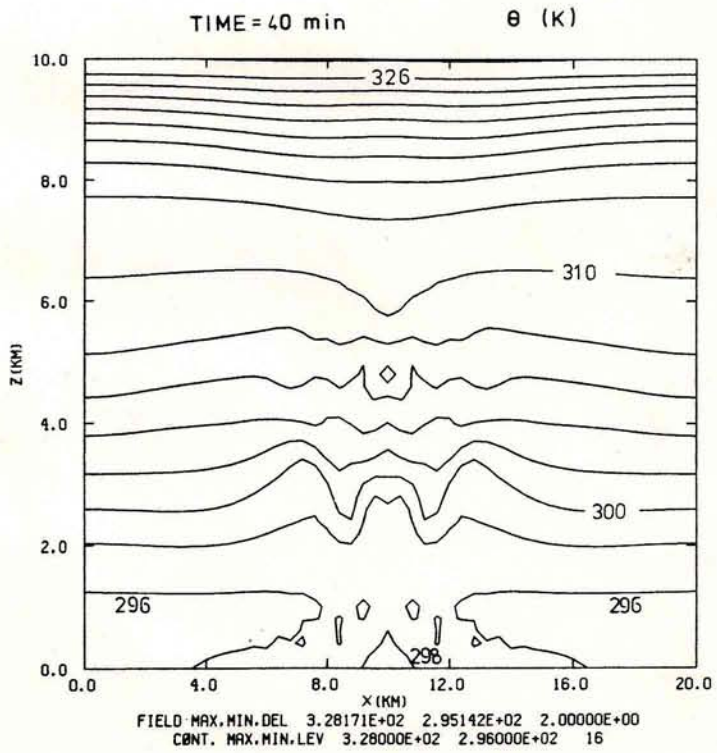

Fig.(VII-29b): Field of the potential temperature θ in K after 40 minutes (spacing of the curves: 2K).

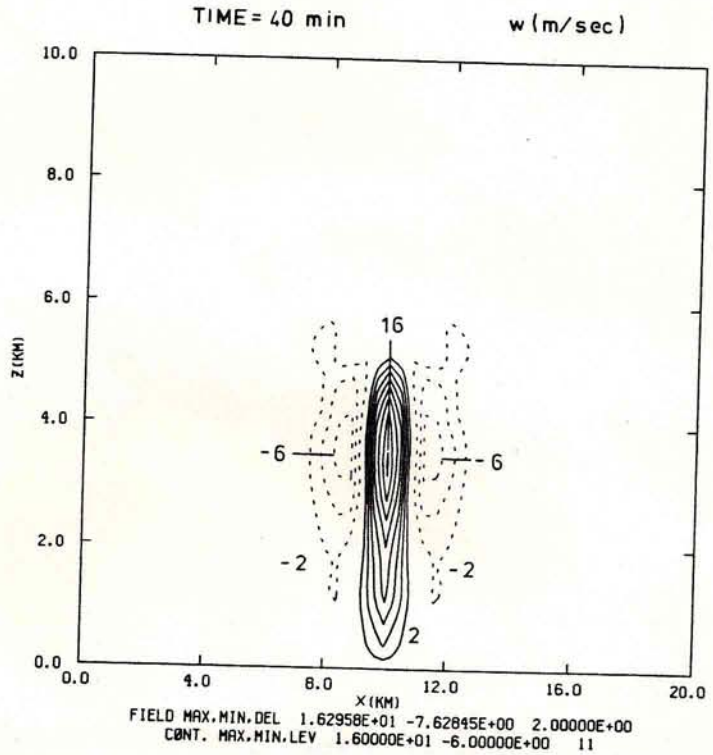

Fig.(VII-29c): Field of the vertical velocity w in m/sec after 40 minutes (solid lines: updraft, dashed lines: downdraft, spacing of the curves: 2m/sec).

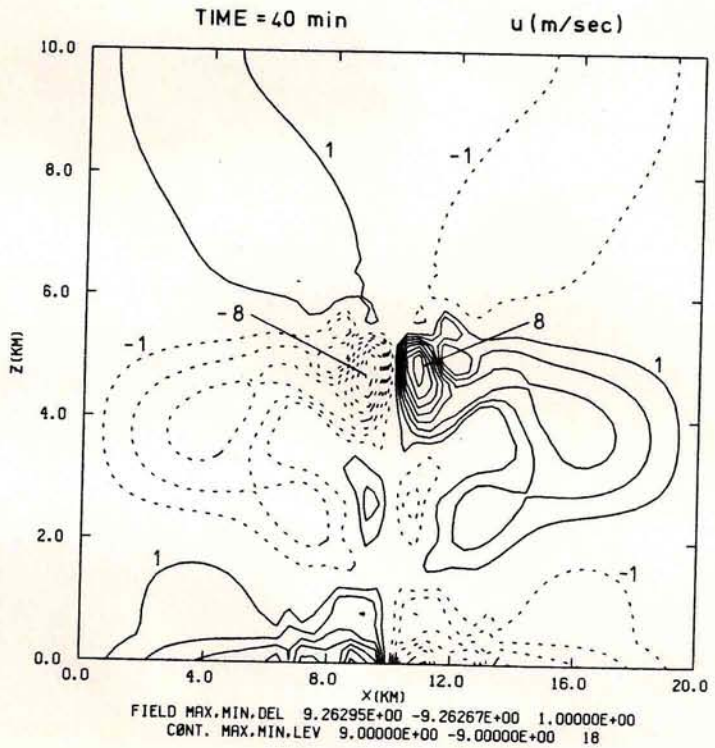

Fig.(VII-29d): Field of the horizontal velocity u in m/sec after 40 minutes (solid lines: u in positive x-direction, dashed lines: u in negative x-direction, spacing of the curves: 1 m/sec).

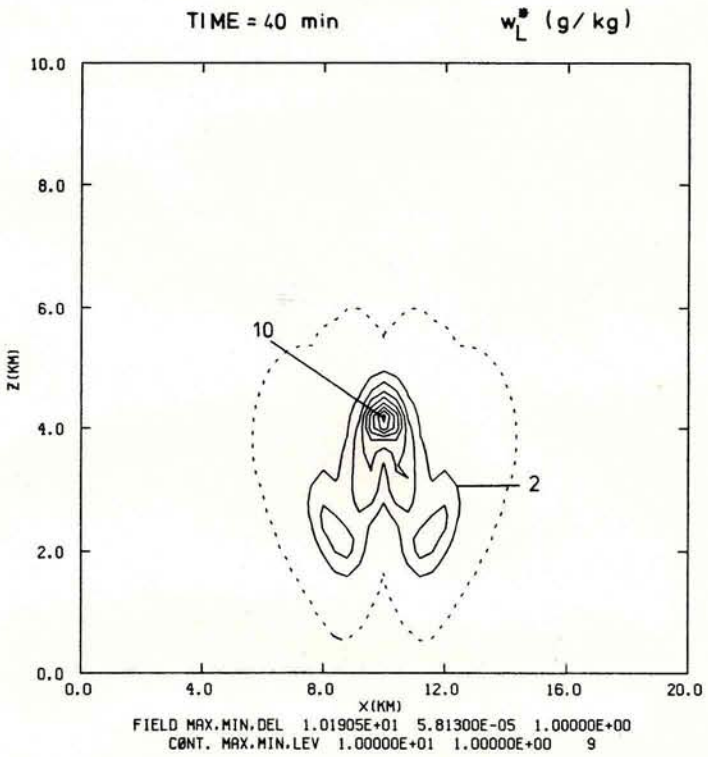

Fig.(VII-29e): Field of the total liquid water content w_L^* in g/kg after 40 minutes (dashed line: outer boundary of liquid water region = 10^{-2} g/kg, spacing of the curves: 1 g/kg).

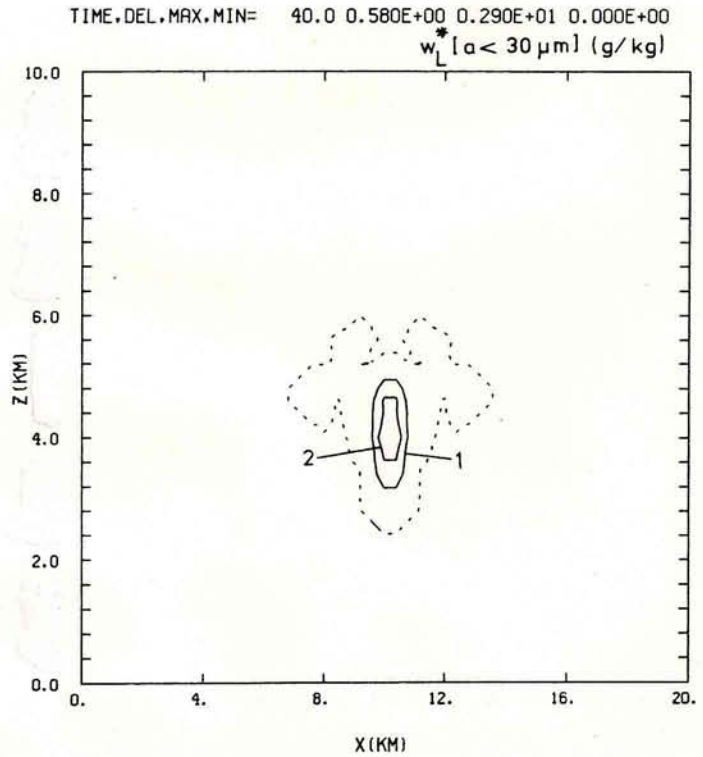

Fig.(VII-29f): Field of the liquid water content that is contained in drops smaller than 30µm radius in g/kg after 40 minutes (dashed line: outer boundary of the cloud = 10^{-2} g/kg, spacing of the curves: 1 g/kg).

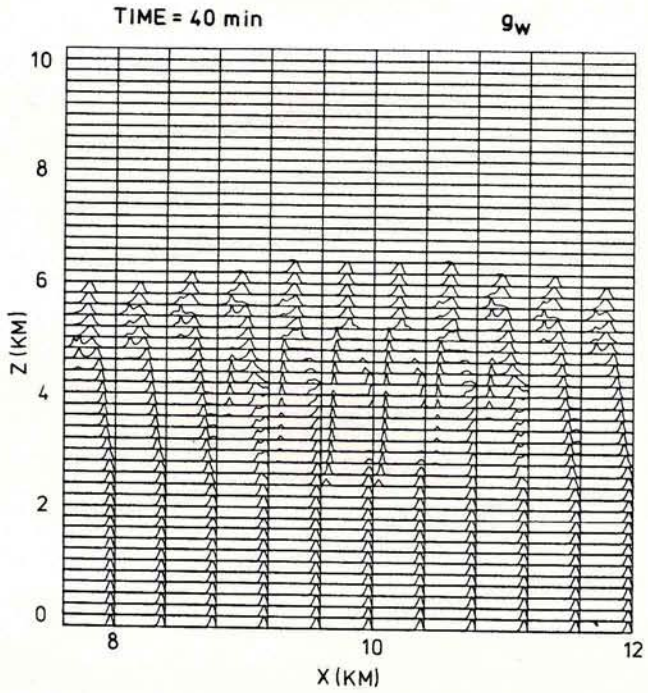

Fig.(VII-29g): Spectra of the drop water mass density distribution function g_w as a function of drop radius at each grid point in the middle section of the computational domain after 40 minutes (spectra adjusted to the maximum occuring value).

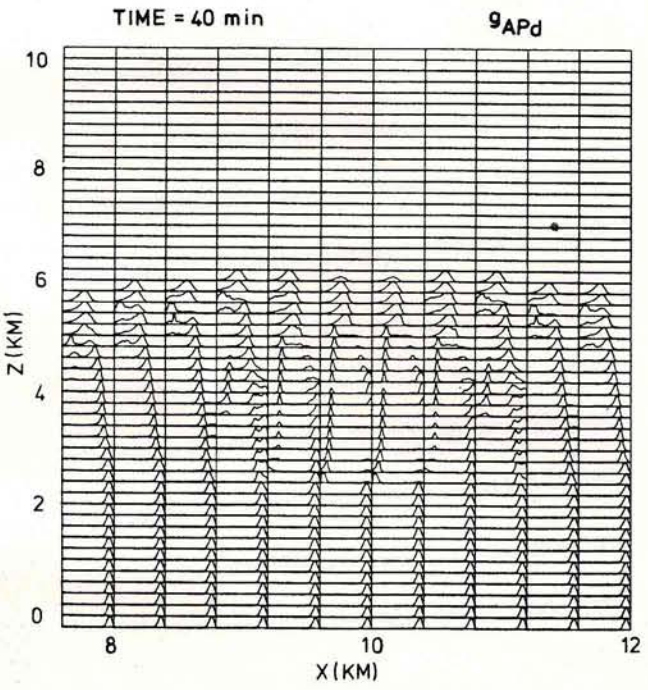

Fig.(VII-29h): Spectra of the aerosol particle mass density distribution function g_{APd} for aerosol material inside the drops as a function of drop radius at each grid point in the middle section of the computational domain after 40 minutes (spectra are adjusted to the maximum occuring value).

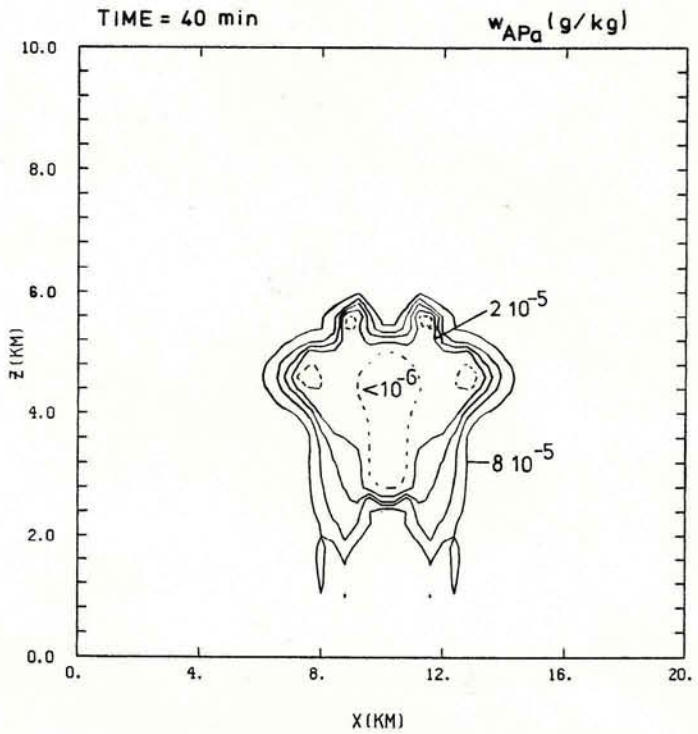

Fig.(VII-29i): Field of the total unactivated aerosol particle mass w_{APa} in air in g/kg after 40 minutes (dashed line: 10^{-6} g/kg, spacing of the curves: 2 10^{-5} g/kg).

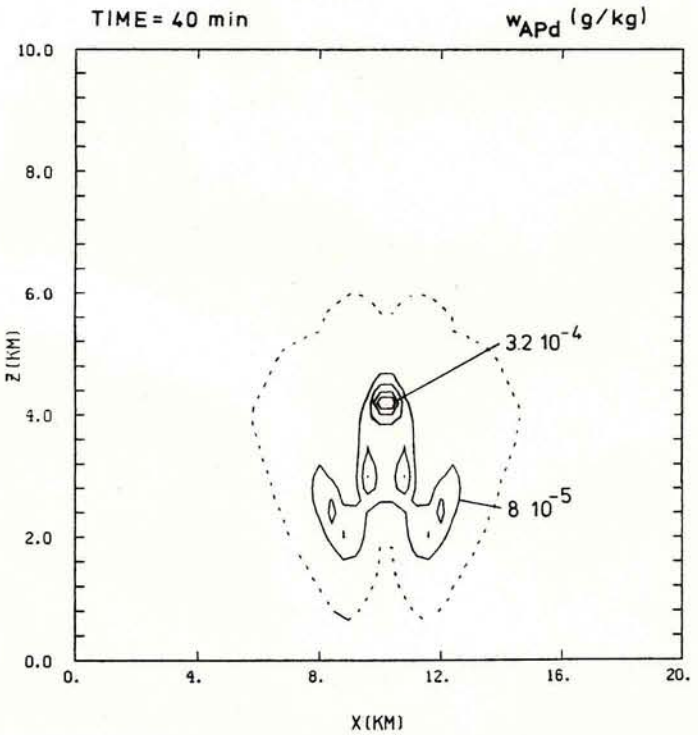

Fig.(VII-29k): Field of the total uptaken aerosol particle mass in drops w_{APd} in g/kg after 40 minutes (dashed line: 10^{-6} g/kg, spacing of the curves: 8 10^{-5} g/kg).

the model is still quite unrealistic with respect to the real clouds in the atmosphere. This is further illustrated if we take a look at the field of the total liquid water content w_L^* in Fig.(VII-29e). This field shows two 'legs' that propagate towards the ground and a 'dent' in the middle. The reason for this feature is that w_L^* also includes the rain water which falls to the ground in the left and right 'leg'. In the middle the updraft is strong and transports warm, moist air upwards so that this region represents the center of condensation. This behavior reflects the bell shaped sensible and latent heat flux producing a strong cloud in the middle of the computational domain. Fig.(VII-29f) displays that fraction of the total liquid water content which contributes to the visible cloud consisting of drops smaller than 30µm radius. This figure reflects a cloud with an even base, a form which is typical for clouds we observe in the atmosphere. This proves that the 'legs' of Fig.(VII-29e) are only due to the precipitation-sized drops. This also becomes clear from Figs.(VII-29g) and (VII-29h) which display the water mass distribution function g_w and the aerosol particle mass distribution function g_{APd} for aerosol mass inside the drops. We see from these figures that the drops in the region between the ground and 2km altitude are large. Since the plots of these mass distribution functions are adjusted with regard to the occuring maximum no information about the total mass can be drawn from the curves. So we cannot verify, as Fig.(VII-29e) hints, that the liquid water content below cloud base in the updraft region is very small. But we do notice the condensation region with the small drops right above cloud base. Figs.(VII-29g) and (VII-29h) demonstrate the similar behavior of the water mass and the aerosol particle mass in the drops. Fig.(VII-29i) summarizes the information about the interstitial aerosol particles. We notice the aerosol depletion in the region of the cloud caused by nucleation scavenging. We also notice a similar aerosol depletion in the precipitating 'legs' of the cloud caused by impaction scavenging. The corresponding aerosol mass inside the drops is displayed in Fig.(VII-29k) which integrates the information of Fig.(VII-29h) over the drop radius. We see here that the maximum of captured aerosol material is around 320µg/kg which is about 3 times the amount offered to the drops in the ambient air. This maximum, located at the upper end of the updraft region (Fig.(VII-29c)),

also corresponds to the region of the maximum liquid water content of 10g/kg in Fig.(VII-29e). So it must be due to the strong advection and turbulent mixing.

After about 43 minutes of model time the rain reaches the ground. Figs.(VII-30a) to (VII-30f) display the situation after 50 minutes of model time, that is after 7 minutes of rainfall. Fig.(VII-30a) illustrates the relative humidity. We see here that the region with supersaturated air is separated in an upper portion which belongs to the main cloud and a lower portion which is associated with the evaporating rain. Fig.(VII-30b) represents the field of the potential temperature. From these figures we notice the effect of evaporative cooling as in the rainfall region the temperature at the surface decreases to 294K. The sensible and latent heat flux at the surface are still active but have no influence on the atmosphere. The reason gets clear from Fig.(VII-30c) which displays the field of the vertical velocity and we see that in the rainfall region a downdraft with about 4m/sec developed. So the heat and moisture source at the ground are cut off from the upper region of the domain. Fig.(VII-30d) illustrates the total liquid water content w_L^* . The maximum of the rainfall reaches the ground between x=8 and 12km and the maximum liquid water content decreased already to 2.5g/kg. Fig.(VII-30e) displays the interstitial aerosol mass. We see here that the domain where impaction scavenging takes place has already migrated to the ground. The captured aerosol material in the drops (Fig.(VII-30f)) is correlated to the liquid water content in Fig.(VII-30d).

Ten minutes later, the situation is displayed in Figs.(VII-31a) to Fig.(VII-31f). We notice that the region of the supersaturated air (Fig.(VII-31a)) shrunk to 4 separate small regions, the largest at about 5 km altitude where the remaining cloud is located. Fig.(VII-31b) gives the field of the potential temperature, which shows that the low temperature values of 10 minutes earlier disappeared as the evaporative cooling decreased. Fig.(VII-31c) illustrates the field of the vertical velocity w which again shows a strong downdraft in the center of the domain. However, the downdraft region is located only in the lower 2km of the rainfall region. These

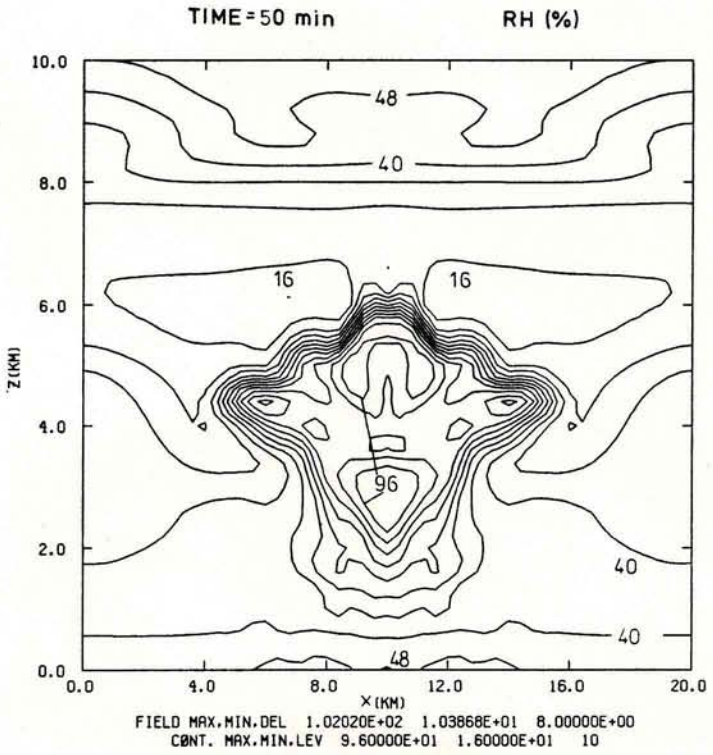

Fig.(VII-30a): Field of the relative humidity RH in % after 50 minutes (spacing of the curves: 8%).

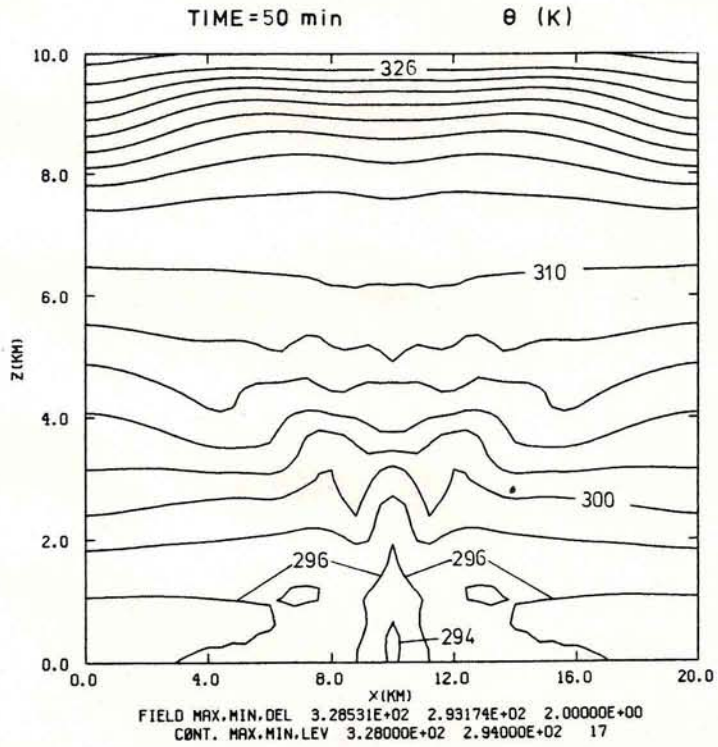

Fig.(VII-30b): Field of the potential temperature θ in K after 50 minutes (spacing of the curves: 2K).

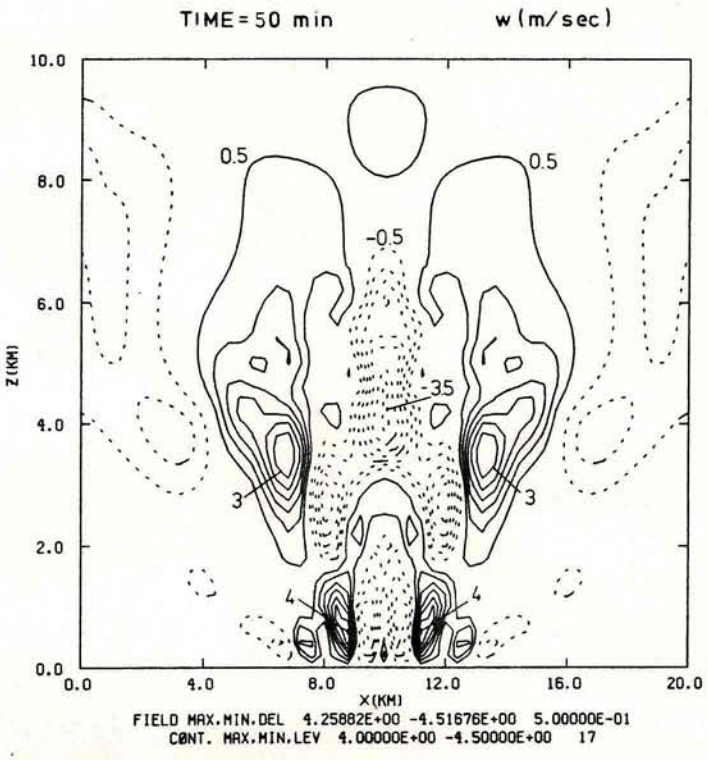

Fig.(VII-30c): Field of the vertical velocity w in m/sec after 50 minutes (solid lines: updraft, dashed lines: downdraft, spacing of the curves: 0.5m/sec).

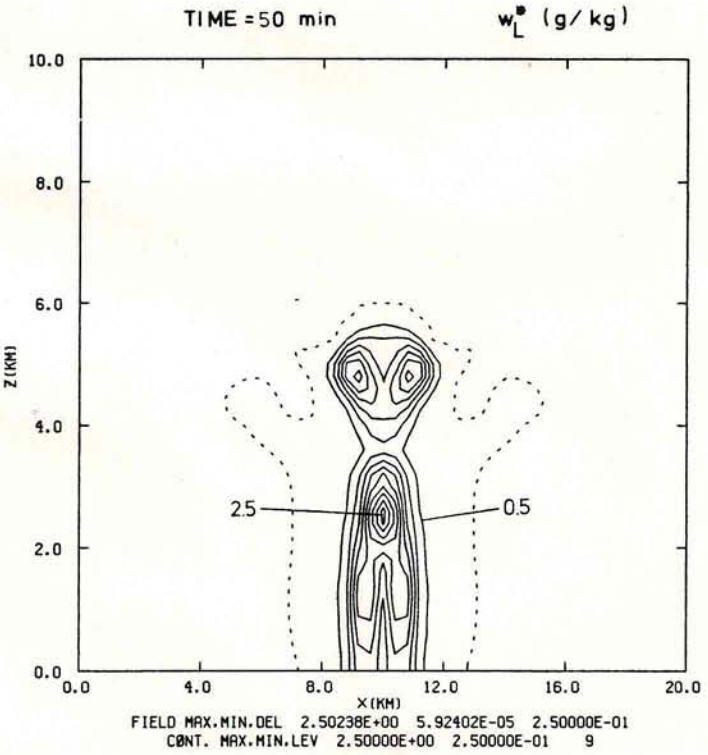

Fig.(VII-30d): Field of the total liquid water content w_L^* in g/kg after 50 minutes (dashed line: outer boundary of liquid water region = 10^{-2} g/kg, spacing of the curves: 0.25 g/kg).

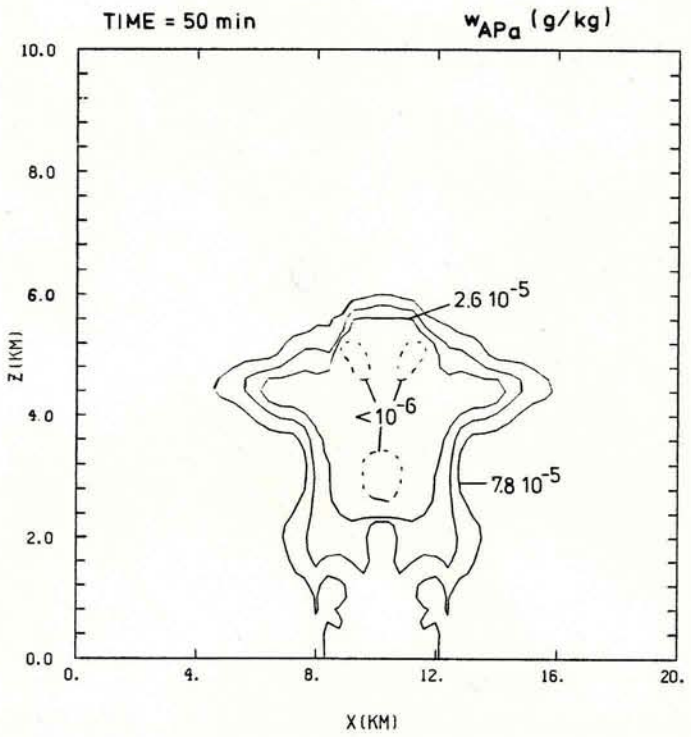

Fig.(VII-30e): Field of the total unactivated aerosol particle mass w_{APa} in air in g/kg after 50 minutes (dashed line: 10^{-6} g/kg, spacing of the curves: 2.6 10^{-5} g/kg).

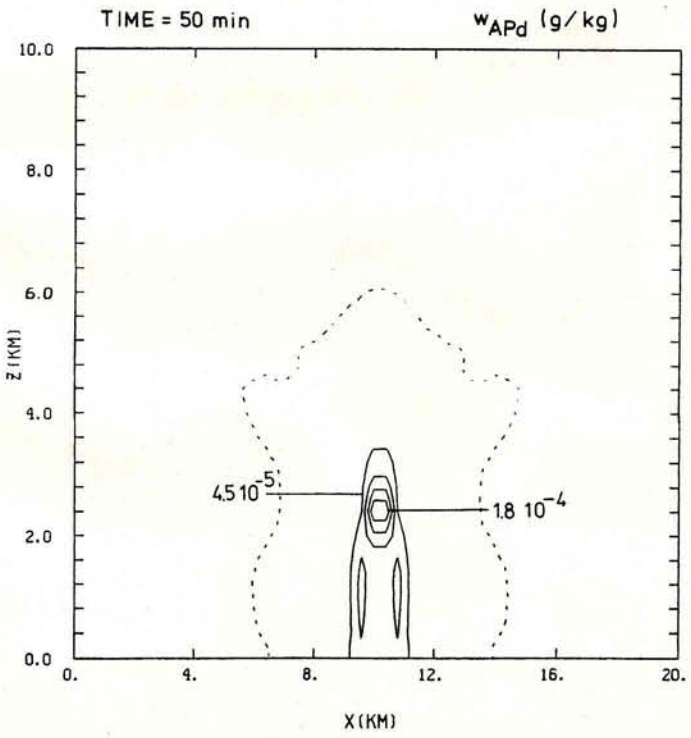

Fig.(VII-30f): Field of the total uptaken aerosol particle mass in drops w_{APd} in g/kg after 50 minutes (dashed line: 10^{-6} g/kg, spacing of the curves: 4.5 10^{-5} g/kg).

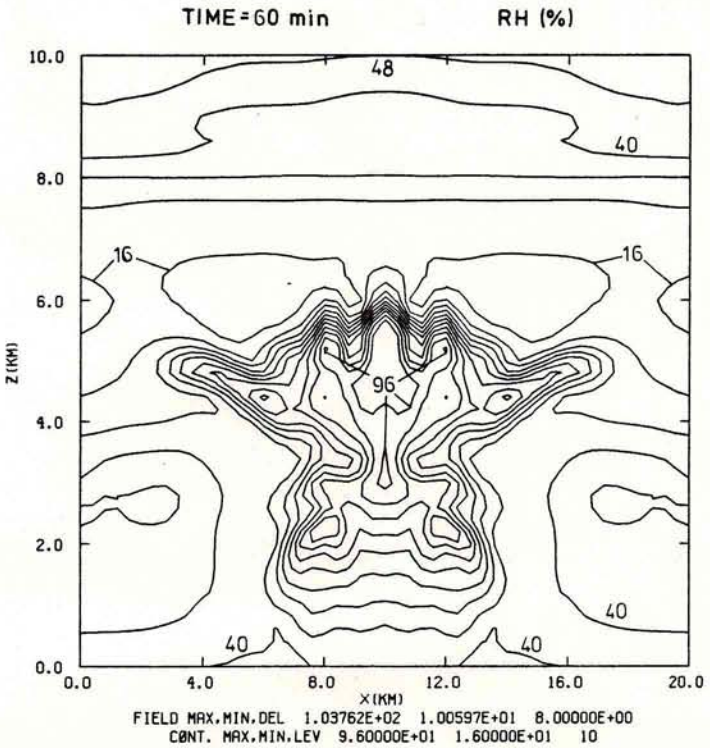

Fig.(VII-31a): Field of the relative humidity RH in % after 60 minutes (spacing of the curves: 8%).

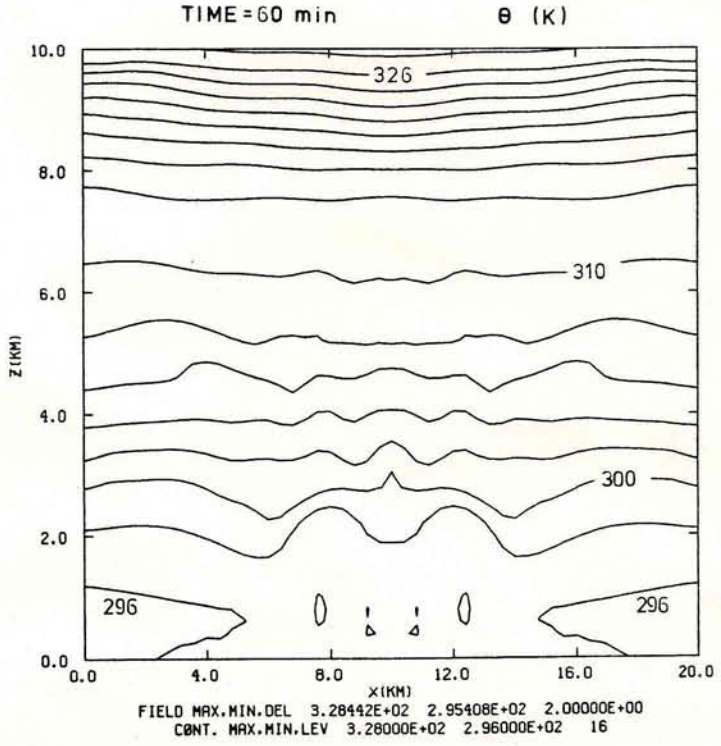

Fig.(VII-31b): Field of the potential temperature θ in K after 60 minutes (spacing of the curves: 2K).

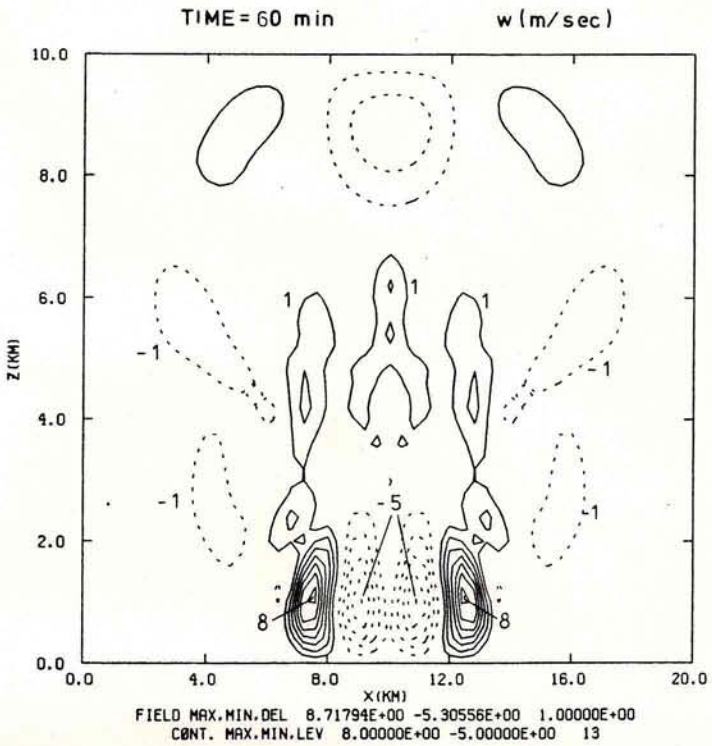

Fig.(VII-31c): Field of the vertical velocity w in m/sec after 60 minutes (solid lines: updraft, dashed lines: downdraft, spacing of the curves: 1m/sec).

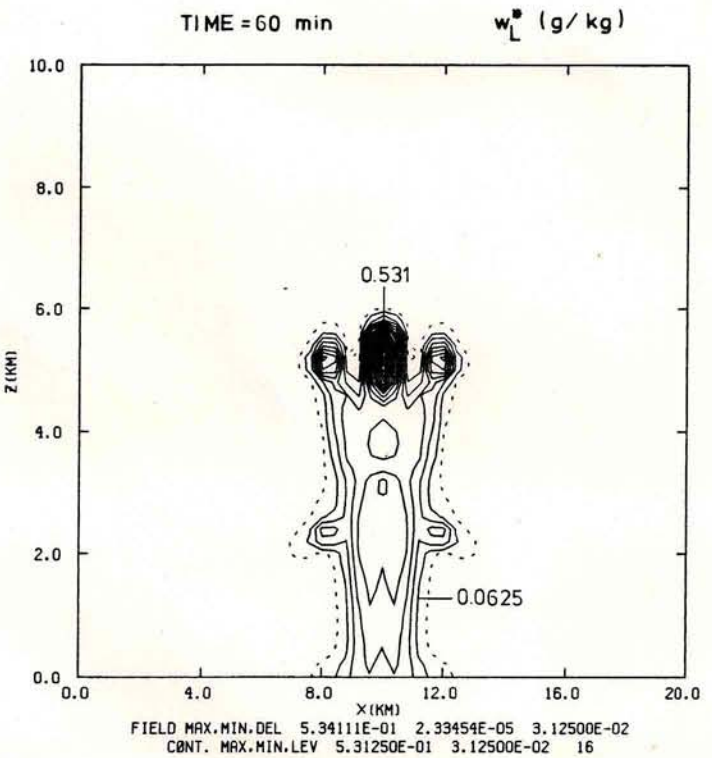

Fig.(VII-31d): Field of the total liquid water content w_L^* in g/kg after 60 minutes (dashed line: outer boundary of liquid water region = 10^{-2} g/kg, spacing of the curves: 0.03125 g/kg).

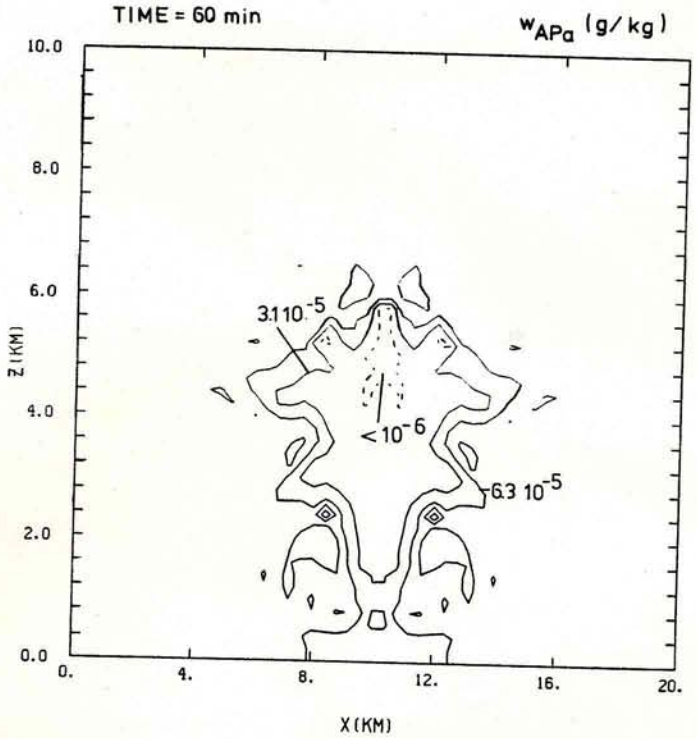

Fig.(VII-31e): Field of the total unactivated aerosol particle mass w_{APa} in air in g/kg after 60 minutes (dashed line: 10^{-6} g/kg, spacing of the curves: $3.1\ 10^{-5}$ g/kg).

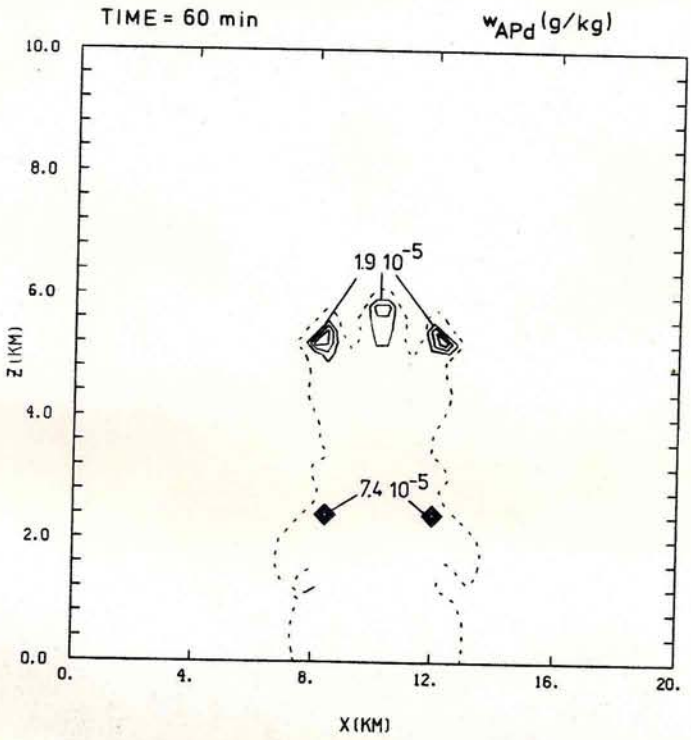

Fig.(VII-31f): Field of the total uptaken aerosol particle mass in drops w_{APd} in g/kg after 60 minutes (dashed line: 10^{-6} g/kg, spacing of the curves: $1.9\ 10^{-5}$ g/kg).

findings are indicating that the convective cell is losing its intensity and is dying. Fig.(VII-31d) displays the total liquid water content w_L^* which already decreased to 0.5g/kg in the remaining cloud. The rainfall region has a maximum liquid water content of only 0.2g/kg. Fig.(VII-31e) illustrates the interstitial aerosol particles in the domain. A comparison to Fig.(VII-30e) shows that the depleted region shrinks as it fills up again due to turbulent mixing. Fig.(VII-31f) displays the mass of captured aerosol particles whose maxima again are correlated to the maxima in the liquid water content (Fig.(VII-31d)). By this time the cloud has lost all its intensity, and after 65 minutes the rain stops. The cloud left over has a flat base and a liquid water content of about 1g/kg consisting only of small non-precipitating drops (Fig.(VII-32)). At this time we stopped

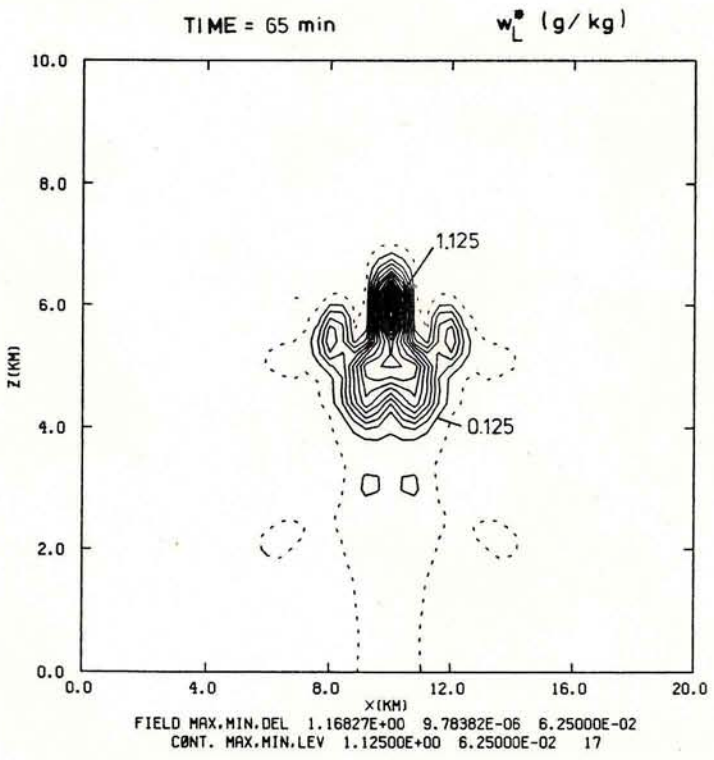

Fig.(VII-32): Field of the total liquid water content w_L^* in g/kg after 65 minutes (dashed line: outer boundary of liquid water region = 10^{-2} g/kg, spacing of the curves: 0.0625 g/kg).

our calculations.

Fig.(VII-33) and Fig.(VII-34) summarize the important features of the evolution of the water and aerosol mass over the whole computation period. Fig.(VII-33) displays the behavior of the liquid water mass in the domain. Curve (1) illustrates the mass of cumulative condensed water, while curve (2) represents the total water mass in the air, and curve (3) gives the cumulative water mass on the ground, which is the total rainfall. We notice that up to about 25 minutes of computation time the total liquid water mass doesn't change much. It represents the water attached to the aerosol particles in the air. After 25 minutes a cloud forms and the liquid water mass increases more than 4 orders of magnitude. After 43 minutes the rain reaches the ground and thus the liquid water in the atmosphere decreases. After 65 minutes the rain stops and our calculation was terminated. The sum of curves (2) and (3) give the total liquid water in the domain and the difference between this sum and curve (1) represents the evaporated water. Fig.(VII-34) displays similar quantities for the aerosol particle mass in the domain. Curve (1) illustrates the mass of interstitial aerosol particles in the air, curve (3) displays the total mass of aerosol particles in the drops in the air, and curve (4) gives the cumulative mass of aerosol particles in the drops at the ground, i.e. in the rainfall. Curve (4) thus represents the wet deposition. Curve (2) gives the cumulative aerosol particle mass scavenged by nucleation, and curve (5) illustrates the cumulative aerosol particle mass scavenged by impaction. The curves indicate when the cloud forms at 25 minutes and when the rain starts at 43 minutes. The sum of curves (2) and (5) represents the cumulative scavenged aerosol material. This sum is higher than the sum of curves (3) and (4) since some aerosol particles are deactivated again as drops completely evaporate. Furthermore we see that most aerosol particle mass enters the drops through nucleation scavenging in the cloud formation stage, and that impaction scavenging only begins to work when precipitation-sized drops are formed. But even at the end of the whole computation period impaction scavenging only has contributed 20% to the overall scavenged material. What strikes from Figs.(VII-33) and (VII-34) is what was already hinted by the other presented results of the model: the simi-

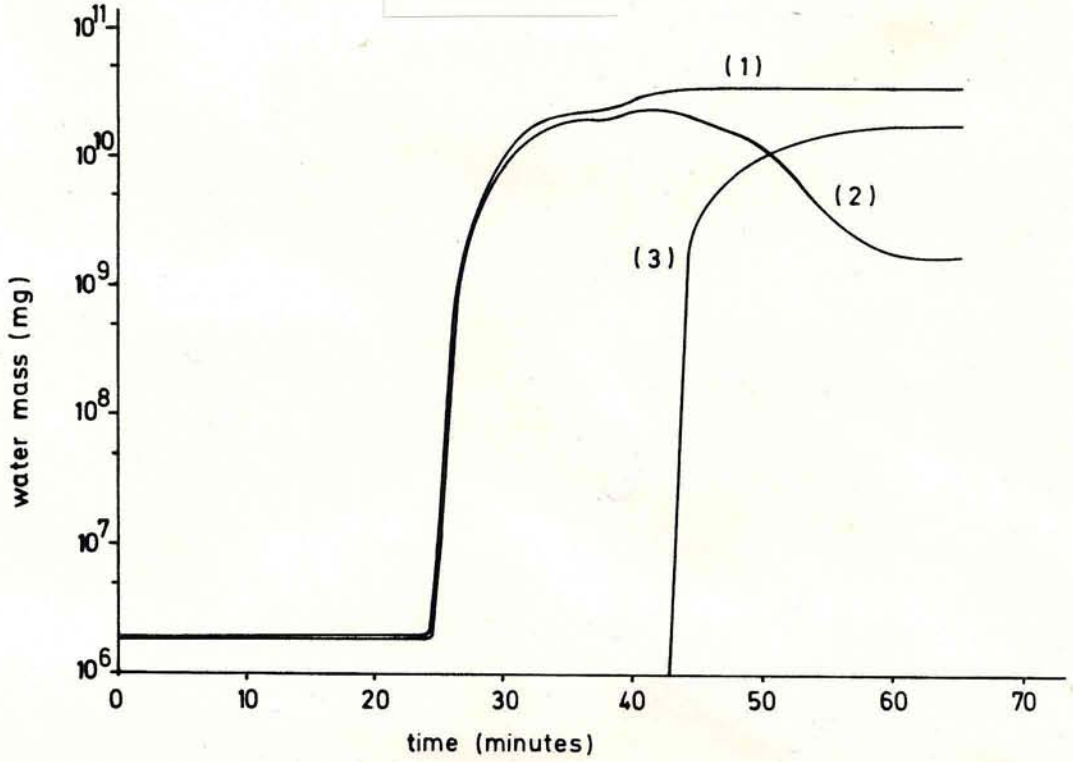

Fig.(VII-33): Liquid water mass in mg in the domain (20km*10km*1m) as a function of cloud evolution time: (1) mass of cumulative condensed water; (2) total water drop mass in air; (3) cumulative water mass on the ground.

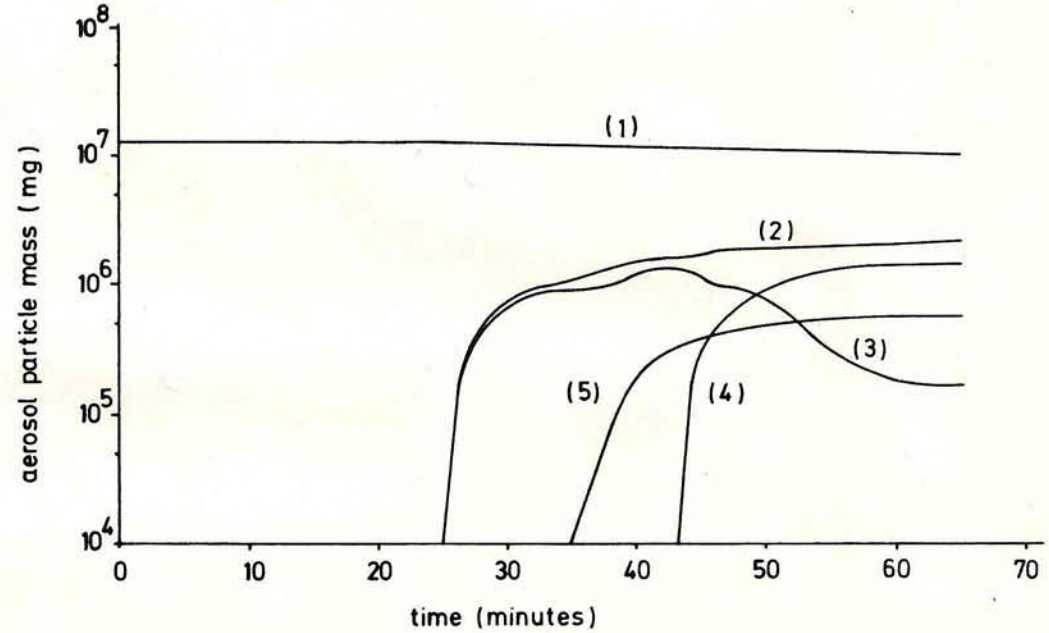

Fig.(VII-34): Aerosol particle mass in mg in the domain (20km*10km*1m) as a function of cloud evolution time: (1) mass of aerosol particles left in air as interstitial aerosol; (2) cumulative aerosol particle mass scavenged by nucleation; (3) total mass of aerosol particles in cloud water; (4) cumulative aerosol particle mass deposited on the ground by rain; (5) cumulative aerosol particle mass scavenged by impaction.

larity of the curves for the liquid water mass and the scavenged aerosol material. To further illustrate this result we calculated some efficiencies:

From Fig.(VII-33):

$$E_1 = \frac{\text{cumulative rainfall at the ground}}{\text{total liquid water in the domain}} = \frac{\text{curve (3)}}{\text{curves (3) + (2)}} \qquad \text{(VII-1)}$$

$$E_2 = \frac{\text{cumulative rainfall at the ground}}{\text{cumulative condensed water mass}} = \frac{\text{curve (3)}}{\text{curve (1)}}$$

From Fig.(VII-34):

$$E_3 = \frac{\text{cumulative aerosol particle mass in rainfall}}{\text{total aerosol particle mass in the drops}} = \frac{\text{curve (4)}}{\text{curves (3) + (4)}}$$

$$E_4 = \frac{\text{cumulative aerosol particle mass in rainfall}}{\text{cumulative nucleation scavenging}} = \frac{\text{curve (4)}}{\text{curve (2)}} \qquad \text{(VII-2)}$$

$$E_5 = \frac{\text{cumulative aerosol particle mass in rainfall}}{\text{cumulative scavenging}} = \frac{\text{curve (4)}}{\text{curves (2) + (5)}}$$

The change with time of these efficiencies is summarized in Table VII-5. We can compare here E_1 with E_3 and E_2 with E_4 and E_5 as they are calculated analogously. A striking feature is the similar behavior of the efficiencies for the liquid water mass and the captured aerosol particle mass. All efficiencies increase with time as more and more material is deposited on the ground. Only in the later stages of the cloud they start to decrease as the rainfall ceases. Comparison of E_2 with E_4 and E_5 shows that the aerosol particle mass efficiencies are larger than the rain efficiencies. This is due to the fact that in a rainfall the drops do evaporate, however, rarely to the point that they become aerosol particles again. So the rainfall loses more water mass compared to the aerosol particle mass. Approximately 50% of the cumulative condensed water mass is deposited on the ground after the convection event and about the same fraction of the cumulative scavenged aerosol particle mass. Comparison of E_1 and E_3 shows that

time (min)	E_1(%)	E_3(%)	E_2(%)	E_4(%)	E_5(%)
43.416	0.58	0.90	0.40	0.73	0.61
45.08	15.54	22.72	10.33	18.60	15.24
46.75	27.33	36.91	17.71	30.75	24.93
48.416	36.23	44.69	22.85	37.67	30.37
50.08	46.09	53.64	27.95	45.00	35.98
51.75	60.54	64.44	35.22	53.33	42.42
53.416	73.55	74.24	41.27	60.52	48.01
55.08	82.52	82.21	44.92	65.64	51.93
56.75	86.81	85.17	45.98	66.19	52.44
58.416	88.99	87.23	46.34	65.84	52.27
60.08	90.69	88.95	46.62	65.68	52.19
61.75	91.59	89.11	46.73	64.65	51.57
63.416	90.91	89.28	46.59	63.90	51.11
65.08	89.79	88.58	46.20	63.18	50.66

Table VII-5: Precipitation efficiencies E_1 and E_2 and aerosol scavenging efficiencies E_3, E_4 and E_5 as given by eqs.(VII-1) and (VII-2) as a function of cloud evolution time.

until about 55 minutes E_3 is larger than E_1. This is analogous to the behavior of E_2, E_4 and E_5. After this time E_1 dominates. This is also due to the fact that the liquid water mass decreases stronger through evaporation than the captured aerosol particle mass. However, both the rain efficiency E_1 as well as the aerosol particle scavenging efficiency E_3 eventually reach 90%. This result proves the conclusion we drew earlier from the entraining air parcel model that the main scavenged aerosol mass follows the main water mass.

In Table VII-6 some additional results of the aerosol scavenging in the two dimensional cloud model of Clark et al. are summarized. The table displays the variation with time of the cumulative rainfall, the rainfall rate, the cumulative sulfur in the rain water, the wet deposition rate of sulfur through aerosol scavenging and the cumulative concentration of sulfur in the rainwater. All these quantities repre-

time (min)	total rainfall (mm)	R (mm/hr)	total S in rainfall (mg/m^2)	S in rainfall (mg/m^2hr)	concentration of S in rainwater (mg/l)
43.416	$2.679\ 10^{-2}$	$9.642\ 10^{-2}$	0.58	2.09	21.64
45.08	0.7047	2.440	15.11	54.38	22.27
46.75	1.236	1.915	27.22	41.57	22.02
48.416	1.622	1.388	34.93	27.70	21.53
50.08	2.000	1.362	42.08	25.81	21.04
51.75	2.527	1.895	50.59	30.56	20.02
53.416	2.968	1.585	58.35	27.95	19.66
55.08	3.237	0.9688	63.73	19.42	19.69
56.75	3.316	0.2857	65.65	6.82	19.79
58.416	3.355	0.1389	66.69	3.74	19.87
60.08	3.385	0.1089	67.47	2.87	19.93
61.75	3.408	$8.236\ 10^{-2}$	68.15	2.39	19.99
63.416	3.421	$4.617\ 10^{-2}$	68.63	1.78	20.06
65.08	3.427	$1.946\ 10^{-2}$	68.92	1.05	20.12

Table VII-6: Variation with cloud evolution time of the cumulative rainfall in mm, the rainfall rate R in mm/hr, the cumulative sulfur in the rainwater in mg/m^2, the wet deposition rate of sulfur in $mg/(m^2hr)$ and the cumulative concentration of sulfur in the rainwater in mg/l (quantities represent averages over a horizontal domain of 5km, the rates are extrapolated from 100 second intervals).

sent averages over a 5km rainfall region. The rainfall rate R and the wet deposition rate of sulfur are extrapolated from 100 seconds intervals.

Comparison of the total rainfall and the rainfall rate with field observations show that we were modeling a cloud with moderate precipitation (Pruppacher and Klett(1978)). This is due to the low vertical extension of the cloud (only 4km). So only 3.5mm of rain fell averaged over a horizontal rainfall region of 5km.

The cumulative concentration of sulfur in the rainwater varies between 19.66 and 22.27 mg/l. These values are high by about a factor of 10 as compared to field observations, as the average observed sulfur concentration in the rainwater ranges between 1 and 6 mg/l (Kins(1982), Perseke et al.(1974), Perseke(1982), Kuttler(1982), Murakami et al.(1983), Meszaros(1974), Pruppacher and Klett(1978)), though Kuttler reports a concentration of 25 mg/l from the smog alarm event Jan 1979 in the Western Ruhr District, West Germany. Our overestimate, however, is expected on the basis of what we have mentioned in section V.2 regarding the amount of sulfur offered by the air to the drops. Thus, the high sulfur concentration in the air caused by assuming that the aerosol particles consist only of ammonium sulfate (ε=1) leads invariably to the high sulfur concentration in the cloud water. Case 3 of the entraining air parcel model runs discussed in chapter VII.1.3 has the same aerosol mass input as the present 2-D run and also experiences a sulfur concentration in the liquid water phase of over 10 mg/l. However, we mentioned in section IV.2.1 that only 1 to 10% of the total aerosol material in the air consists of sulfate, and chemical analysis of the composition of the pollutants in the rainwater yields that only about 50% of the soluble material consists of sulfate (Meszaros(1974), Pruppacher and Klett(1978)) with an unknown fraction of insoluble material. Also we must stress here that only part of the sulfate found by field studies in the rainwater resulted from particle scavenging. A noticeable amount resulted from the oxidation of uptaken SO_2. Reduction of our input data to observed sulfate particle concentrations yields sulfur concentrations that agree well with the range of the observed ones. Also the high values reported by Kuttler(1982) confirm this explanation. During the smog alarm event the input must have been extremely high to introduce 25

mg/l sulfur into the rainwater.
Another quantity which has been introduced in literature as a measure of the amount of scavenged pollutants by clouds and rain is the wash-out ratio W. Scott(1981) deduced this ratio W by the relation:

$$W = \frac{\text{pollutant concentration in the rainwater}}{\text{pollutant concentration in the air}} \qquad \text{(VII-3)}$$

$$= \frac{\text{g pollutant / liter}}{\text{g pollutant / m}^3}$$

In our calculations we obtain washout ratios which have values near 1000. These values agree well with the values deduced by Scott.
To compare the total sulfur in the rainfall and the wet deposition rate of sulfur to observations is difficult as most of the values reported in the literature refer to yearly, monthly or daily periods (Perseke et al.(1974), Kuttler(1982), Perseke(1982)) rather than to periods of one hour. We therefore refrained from a comparison.
Furthermore we tried to compare the time evolution of the rainfall rate and its correlation to the sulfur concentration in the rain water as given in columns 3 and 6 of Table VII-6 with field observations. Thus, Kins(1982) reported the variation with time of atmospheric trace substances in the rainfall of a convective shower. In her Fig.2 the rainfall intensity experiences a similar behavior as compared to our results: shortly after the rain starts the rainfall rate reaches its maximum around 4 mm/hr and then decreases until the rain stops after 1.5 hours. The figure shows also that the concentrations of sulfur in the rainwater experience an inverse behavior with the rainfall rate: at the maximum of the rainfall rate it reaches its minimum of 1mg/l and then increases to about 3mg/l at the end of the rainfall. This inverse relationship is due to the fact that during the initial stages of the rainfall the rain intensity was low due to the presence of small drops which experienced evaporation during their fall from the cloud to the ground, thus concentrating the pollution mass in the precipitation water. As the rainfall rate increases later large drops fall which carry comparatively more water and thus lower pollutant concentrations. This inverse correlation agrees with the results of

our parcel model (compare section VII.1.4) which show that the small drops are more contaminated than the larger ones which carry the main water mass and are prevalent in high rainfall rates.
The cumulative sulfur concentrations obtained with our two dimensional model express a somewhat different behavior. As the rainfall rate increases the sulfur concentration also increases, thus representing a direct correlation. Such correlations only 500m or 5 min apart from inverse correlations are also reported in the literature (e.g. Gatz and Dingle(1971)). In our model this direct relationship between rainfall rate and sulfur concentration is most likely due to two facts. First, our values represent averages over a horizontal region of 5km and a time span of 100 seconds. So it includes regions of low rainfall rate and presumably high sulfur concentrations and vice versa. The average then might result in a medium high rainfall rate correlated to a medium high sulfur concentration. Secondly, Fig.(VII-34), curve (5) illustrates that 2 to 5 minutes before the maximum sulfur content at the ground is reported impaction scavenging contributes its maximum amount to the uptaken aerosol material. At 45 minutes already 70% of the overall impaction scavenging took place. This obviously results in an enhancement of the concentration. At later times the concentration of the pollutants in the rain water in our model decreases as the rainfall rate and thus the impaction scavenging decrease. However, after 55 minutes the concentration increases again due to evaporation effects and thus results in an inverse correlation as also measured by Kins(1982).

VII.3.2 Conclusions

In order to study the scavenging of particles in a convective cloud model we have linked our aerosol scavenging model described in chapter II to the two dimensional cloud model of Clark et al. described in chapter V. We confined ourselves to the removal of $(NH_4)_2 SO_4$ particles and intended to study the mass of uptaken material into the drops, the relative importance of the nucleation scavenging as compared to impaction scavenging, the concentration of aerosol material in the rainwater and the efficiency of the aerosol scavenging.

Our study with the two dimensional cloud model of Clark et al. led to the following conclusions:

1.) It is possible to simulate aerosol particle scavenging by a detailed microphysical model embedded in a two dimensional cloud model, and to keep track of the aerosol mass in the air, in the drops, and at the ground.

2.) The calculated concentrations of sulfur in the rain water are reasonable, if one considers that natural aerosol spectra do not solely consist of ammonium sulfate as was assumed in this run. The reduction of our results to real conditions yields values that agree well with field observations.

3.) As predicted by our air parcel model, it is verified that the aerosol mass is always associated with the main water mass so that drops which precipitate carry with them the main pollution mass to the ground. Thus, it is possible to formulate an aerosol scavenging efficiency analogously to the commonly used precipitation efficiencies. These efficiencies experience the same behavior.

4.) As predicted by our air parcel model it is verified that nucleation scavenging is practically identical with in-cloud scavenging, and is more important to the overall scavenging than impaction scavenging, which uniquely represents below-cloud scavenging. Thus, in the present calculation the impaction scavenging (i.e. below-cloud scavenging) of $(NH_4)_2SO_4$ particles contributes only about 20% to the overall scavenged mass. Together with our conclusion stated in chapter VII.2.7 that below-cloud scavenging of SO_2 gas contributes less than 30% to the total amount of sulfur scavenged from SO_2, we can now draw the general conclusion that below-cloud scavenging of gaseous and particulate sulfur contributes only about 20-30% to the total sulfur scavenging. This result agrees well with the observations of Murakami et al.(1983).

5.) The entraining air parcel model is a very useful tool in studying some specific problems of microphysics. Within certain limitations it gives insight into a variety of interactions between the drop size spectrum and the pollutants, as the main conclusions regarding the aerosol particle scavenging were verified by the two dimensional model.

VIII Final remarks and suggestions for future research

In the present study we have developed a theoretical model in which the condensation process, the collision-coalescence process, the process of impaction scavenging, and the process of gas scavenging are coupled in such a manner that for a given uniform aerosol type and particle size distribution, and for a given SO_2 concentration in the air the evolution in time of the drop size distribution, the pollutant mass inside the drops, the aerosol mass remaining in the air as drop-interstitial aerosol, and the environmental gas concentration can be determined.
We have linked the scavenging model to an entraining air parcel model and deduced the results summarized in chapter VII.1.4 and VII.2.7.
In a second attempt we incorporated our aerosol scavenging model in a two dimensional dynamic model for convective clouds and came to the conclusions summarized in section VII.3.2.
The results we gained are very encouraging as they represent a first attempt to shed more light on a number of questions regarding the scavenging of pollutants. Though there is still a lot of work to be done as there are many questions still left unanswered. We therefore shall attempt below to suggest a few important extensions of our work.

Firstly, more model runs with the two dimensional cloud model are needed to do sensitivity studies concerning different aerosol particle distributions and compositions. Also, it would be desirable to model 'outer' mixtures of aerosol particles as well as 'inner' mixtures with different soluble and insoluble compounds.

Secondly, gas scavenging needs to be included into the two dimensional cloud model. At that time one would be able to determine the relative importance of nucleation and impaction scavenging of aerosol particles as compared to gas scavenging, depending on various oxidation rates inside the cloud drops. Also the model could be extended to include other gases than SO_2.

After the completion of a sufficient number of sensitivity studies one could begin to formulate a parameterization scheme for the aerosol and

gas scavenging going on inside and below a convective cloud. The scheme should have the purpose of eliminating the expensive numerical treatment of aerosol particle and drop size evolution without losing too much of the physics. A helpful clue in doing this could be that the scavenged material experiences a similar cycle than the liquid water. This parameterization would allow to include the scavenging mechanism in a three dimensional cloud model which is a more realistic description of the cloud dynamics.

All the suggestions for future research thus far given above are confined to warm clouds. In our latitudes, however, most clouds contain ice. Simple considerations show that the presence of ice particles grown by diffusion from the vapor and by collision with supercooled drops may significantly affect the scavenging and deposition of pollutants. It is therefore suggested that future models take into account the water as well as the ice phase in clouds.

As shown above there is still a considerable amount of research to be carried out in the field of modeling wet deposition. At present, progress in this field will most likely be limited by the capacity of the computers. The limited computer space will require to confine ourselves to simplified problems considering only one or two different species of pollutants or cloud constituents and leave the complex evaluations to future generations.

Appendix A1

Interactions between the dynamics and condensation/evaporation

A1.1 The saturation vapor pressure

In order to determine the saturation vapor pressure with respect to water we follow Hall(1980) by integrating the Clausius-Clapeyron equation

$$\frac{d\, e_{sat,w}(T)}{dT} = \frac{L_v}{R_v T^2} \qquad \text{(A1-1)}$$

assuming the latent heat of vaporization to vary linearly with temperature. The latent heat of vaporization L_v is expressed as

$$L_v(T) = L_{vo} + \beta (T - T_o) \qquad \text{(A1-2)}$$

With this assumption of $L_v(T)$ the saturated vapor pressure over water can be expressed by integration of (A1-1) and expansion of the resulting logarithm as

$$e_{sat,w}(T) = e_{sat,w}(T_o) \exp\left\{\frac{(T-T_o)}{R_v T T_o}\left(L_{vo} + \beta (T-T_o)\frac{2T_o - T}{2T_o}\right)\right\} \qquad \text{(A1-3)}$$

The above equation can be described also in terms of perturbation variables for the temperature by letting

$$T = \overline{T} + T' \qquad T' \ll \overline{T} \qquad \text{(A1-4)}$$

Eq.(A1-3) then reduces to

$$e_{sat,w}(T) = e_{sat,w}(\overline{T_o}) \exp\{A_e\} \exp\left\{B_e \frac{T'}{\overline{T}}\right\} \qquad \text{(A1-5)}$$

where

$$A_e = \frac{L_{vo}(\overline{T} - T_o)}{R_v T_o \overline{T}} + \frac{\beta}{R_v}\left(\frac{\overline{T} - T_o}{T_o}\right)^2 \left(\frac{2T_o - \overline{T}}{2\overline{T}}\right) \qquad \text{(A1-6)}$$

$$B_e = \frac{L_{vo}}{R_v \bar{T}} + \frac{\beta}{R_v} \frac{(\bar{T} - T_o)}{2T_o} \left\{ \frac{(2T_o - \bar{T})(\bar{T} + T_o)}{\bar{T}\ T_o} - \frac{(\bar{T} - T_o)}{T_o} \right\} \qquad \text{(A1-7)}$$

A_e and B_e are now only a function of $\bar{T}$.
This formulation of the saturation vapor pressure has proven to be extremely accurate when compared to the Smithsonian Meteorological Tables (List(1947)).

A1.2 The supersaturation

The supersaturation is a quantity that can be found from the knowledge of the water vapor and the temperature; therefore any numerical treatment of the supersaturation should be consistent with existing treatments of thermodynamics.
The method used by Hall(1980) breaks the time integration up into separate treatments of advection and the microphysical processes. The advection of temperature and water vapor define the dynamic tendencies of the supersaturation field. The dynamic tendencies and the spectrum of hydrometeors are used to determine the average supersaturation over the given time step. This supersaturation is then directly applied to the diffusional growth equation for the drops (II-59) and for the aerosol particles (II-38).
The dynamic processes of advection and turbulent mixing of water vapor and temperature are calculated from:

$$\tilde{w}_v = w_v^{\tau} - \Delta t \left\{ \nabla \cdot (v\, w_v) - \nabla \cdot (K_m \nabla w_v) \right\} \qquad \text{(A1-8)}$$

$$\widetilde{(\varrho_a T)} = (\varrho_a T)^{\tau} - \Delta t \left\{ \nabla \cdot (v\, \varrho_a T) - \nabla \cdot (K_m \nabla \varrho_a T) - \frac{1}{c_{pa}} \frac{dp}{dt} \right\} \qquad \text{(A1-9)}$$

compare eqs.(II-2) and (II-6).
The quantities $\tilde{(\ )}$ denote an intermediate time level and remain constant over the time step during the microphysical calculations. From these quantities we can derive:

$$\tilde{S}_{v,w} = \frac{\tilde{w}_v}{w_{v,sat}(\tilde{T})} - 1 \qquad \text{(A1-10)}$$

It is important to point out this value of $\tilde{s}_{v,w}$ should not be directly applied to the diffusional growth equations (II-38) and (II-59) or the nucleation scavenging because it only represents the dynamic forcing component and doesn't take into account yet the opposing microphysical processes.

At the end of the condensation time step the supersaturation will be:

$$s_{v,w}^{\tau+1} = \frac{w_v^{\tau+1}}{w_{v,sat}(T^{\tau+1})} - 1 \qquad \text{(A1-11)}$$

with

$$w_v^{\tau+1} = \tilde{w}_v - C_{Ph}\,\Delta t \qquad \text{(A1-12)}$$

and

$$w_{v,sat}(T^{\tau+1}) \approx \varrho_a \frac{R_d}{R_v} \frac{e_{sat,w}(T^{\tau+1})}{p} \qquad \text{(A1-13)}$$

To evaluate $e_{sat,w}(T^{\tau+1})$ we can use eq.(A1-5) and with

$$T^{\tau+1} = \tilde{T} + \frac{L_v C_{Ph}\,\Delta t}{c_{pa}\,\varrho_a} \qquad \text{(A1-14)}$$

(ϱ_a is assumed to be constant during this process) we can identify

$$\overline{T} = \tilde{T} \quad ; \quad T' = \frac{L_v C_{Ph}\,\Delta t}{c_{pa}\,\varrho_a} \qquad \text{(A1-15)}$$

With eqs.(A1-15), (A1-13), (A1-3) and (A1-12) eq.(A1-11) becomes now:

$$s_{v,w}^{\tau+1} = \frac{\tilde{w}_v - C_{Ph}\,\Delta t}{w_{v,sat}(\tilde{T})\,\exp\left\{Be\,\frac{L_v C_{Ph}\,\Delta t}{c_{pa}\,\varrho_a\,\tilde{T}}\right\}} - 1 \qquad \text{(A1-16)}$$

To calculate $s_{v,w}^{\tau+1}$ we assume:

$$C_{Ph} = C_{Ph}'\,\overline{s_{v,w}} = C_{Ph}'\,(s_{v,w}^{\tau} + s_{v,w}^{\tau+1})\,0.5 \qquad \text{(A1-17)}$$

A1.3 Treatment of nucleation and condensation/evaporation

The next step of the integration scheme is to implicitly solve for the average supersaturation over the time step Δt, apply this to nucleation scavenging and the diffusional growth of drops and aerosol particles, and update T and w_v due to the phase change processes.

To accomplish this the following procedure is used:
C_{Ph}' is calculated assuming a unit (i.e. 1%) supersaturation in four steps:
First a preliminary advection is calculated with $\overline{s}_{v,w} = \tilde{s}_{v,w}$. Then the diffusional growth of drops is calculated with an assumed $\overline{s}_{v,w} = 1\%$ according eqs.(II-57) and (II-59). From this

$$C_{Ph} = \frac{w_L^{new} - w_L^{old}}{\Delta t} \tag{A1-18}$$

and the old values of $f_d(m)$ are restored. From eq.(A1-17) we get

$$C_{Ph}' = \frac{C_{Ph}}{\overline{s}_{v,w}} = \frac{C_{Ph}}{0.01} = 100\, C_{Ph} \tag{A1-19}$$

So we gained a value for C_{Ph}', which is now introduced into eq.(A1-16):

$$s_{v,w}^{\tau+1} = \frac{\tilde{w}_v - C_{Ph}' \left(s_{v,w}^{\tau+1} + s_{v,w}^{\tau} \right) 0.5\, \Delta t}{w_{v,sat}(\tilde{T}) \exp\left\{ \frac{Be}{2} \frac{L_v \Delta t}{c_{pa} g_a \tilde{T}} C_{Ph}' \left(s_{v,w}^{\tau+1} + s_{v,w}^{\tau} \right) \right\}} - 1 \tag{A1-20}$$

Eq.(A1-20) can be solved iteratively using for example Newton-Ralphson method which requires

$$F\left(s_{v,w}^{\tau+1}\right) := s_{v,w}^{\tau+1} + 1 - \frac{\tilde{w}_v - 0.5\, C_{Ph}' \left(s_{v,w}^{\tau+1} + s_{v,w}^{\tau} \right) \Delta t}{w_{v,sat}(\tilde{T}) \exp\left\{ \frac{Be}{2} \frac{L_v \Delta t}{c_{pa} g_a \tilde{T}} C_{Ph}' \left(s_{v,w}^{\tau+1} + s_{v,w}^{\tau} \right) \right\}} \tag{A1-21}$$

to be zero to solve for

$$\left(s_{v,w}^{\tau+1}\right)_{n+1} = \left(s_{v,w}^{\tau+1}\right)_n - \frac{F\left\{\left(s_{v,w}^{\tau+1}\right)_n\right\}}{\frac{\partial F\left\{\left(s_{v,w}^{\tau+1}\right)_n\right\}}{\partial s_{v,w}^{\tau+1}}} \tag{A1-22}$$

For the first guess we set $(s_{v,w}^{\tau+1})_o = 1\%$ then the expression converges after four iterations towards the true value $s_{v,w}^{\tau+1}$.
Knowing $s_{v,w}^{\tau+1}$ we can calculate the average supersaturation over the given time step

$$\overline{s_{v,w}} = \frac{1}{2} \left(s_{v,w}^{\tau} + s_{v,w}^{\tau+1} \right) \qquad \text{(A1-23)}$$

With this we now determine the nucleation scavenging (see chapter II.5) and the diffusional growth of drops according chapter II.6. This gives us C_{Ph} and from that a new intermediate value $s_{v,w}^{\tau+1}$ (see eq.(A1-11)) and a new $\overline{s_{v,w}}$ (as in eq.(A1-23)) is calculated. This serves as new input for the diffusional growth of the aerosol particles according chapter II.4 so that we now finally get

$$C_{Ph} = \frac{w_L^{*\,\tau+1} - \tilde{w}_L^{*}}{\Delta t} \qquad w_v^{\tau+1} = \tilde{w}_v - C_{Ph}\,\Delta t$$

$$T^{\tau+1} = \tilde{T} + \frac{L_v\, C_{Ph}}{c_{pa}\, \varrho_a}\,\Delta t \qquad s_{v,w}^{\tau+1} = \frac{w_v^{\tau+1}}{w_{v,sat}\,(T^{\tau+1})} \qquad \text{(A1-24)}$$

A measure for the accuracy of this approach is how close the values for $s_{v,w}^{\tau+1}$ from eqs.(A1-22) and (A1-24) are.

In the above paragraphs we have described how the processes of condensation/evaporation and activation/deactivation are modeled in conjunction with a dynamic framework.

Appendix A2

Conservation of aerosol particle mass inside the drops during collision and coalescence

Due to the collision and coalescence of drops the aerosol particle mass inside the drop spectrum should not change:

$$\int_0^\infty \left.\frac{\partial g_{APd}(m)}{\partial t}\right|_{d,coal} dm \doteq 0 \qquad \text{(A2-1)}$$

or with eq.(II-73)

$$\int_0^\infty \int_0^{m/2} \{Q_{APd}(m')\, m' + Q_{APd}(m-m')\{m-m'\}\} f_d(m-m')\, f_d(m')\, K_d(m-m', m')\, dm'\, dm \qquad \text{(A2-2)}$$

$$- \int_0^\infty dm\, g_{APd}(m) \int_0^\infty f_d(m')\, K_d(m,m')\, dm' \doteq 0$$

In the first integral the expression is symmetric between m' and m-m'. That's why we can write:

$$\frac{1}{2}\int_0^\infty dm \int_0^m Q_{APd}(m')\, m'\, f_d(m')\, f_d(m-m')\, K_d(m-m', m')\, dm'$$

$$+\frac{1}{2}\int_0^\infty dm \int_0^m Q_{APd}(m-m')\{m-m'\} f_d(m')\, f_d(m-m')\, K_d(m-m', m')\, dm' \qquad \text{(A2-3)}$$

$$- \int_0^\infty g_{APd}(m) \int_0^\infty f_d(m')\, K_d(m,m')\, dm'\, dm$$

$$= \underline{\mathrm{I}} + \underline{\mathrm{II}} + \underline{\mathrm{III}} \doteq 0$$

Focussing our attention on the first integral on the left hand side of eq.(A2-3) we note that the domain of integration covers the range between the line m=m' and the upper half of the m-axis, as shown on the shaded portion of Fig.(A2-1)(Thompson (1968)). Thus we can transform the first integral by using:

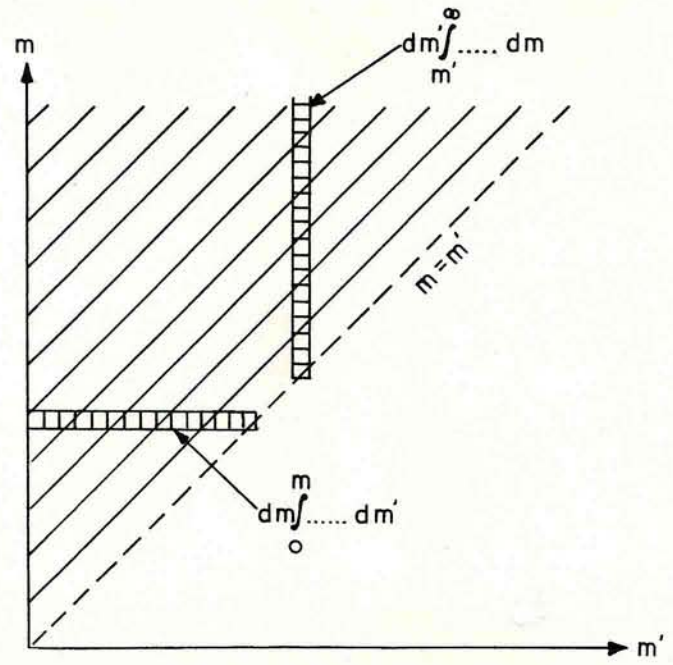

Fig.(A2-1): Illustration of the collision-coalescence integral (Thompson (1968)).

$$\int_0^\infty dm \int_0^m \ldots dm' = \int_0^\infty dm' \int_{m'}^\infty \ldots dm \qquad \text{(A2-4)}$$

Therefore the first integral becomes

$$I = \frac{1}{2} \int_0^\infty dm' \int_{m'}^\infty Q_{APd}(m')\, m' \{d(m')\, \{d(m-m')\, K_d(m-m', m')\, dm$$

Substituting $\tau = m-m'$, $m = \tau + m'$, $dm = d\tau$ results in:

$$I = \frac{1}{2} \int_0^\infty dm' \int_0^\infty Q_{APd}(m')\, m' \{d(m')\, \{d(\tau)\, K_d(\tau, m')\, d\tau$$

Renaming $m' = m$, $\tau = m'$

$$I = \frac{1}{2} \int_0^\infty \int_0^\infty Q_{APd}(m)\, m \{d(m)\, \{d(m')\, K_d(m, m')\, dm'\, dm$$

The second integral of eq.(A2-3) can be transformed in a similar way by using eq.(A2-4)

$$II = \frac{1}{2} \int_0^\infty dm' \int_{m'}^\infty Q_{APd}(m-m')\, \{m-m'\}\, \{d(m-m')\, \{d(m')\, K_d(m-m', m')\, dm$$

Substituting $\tau = m - m'$, $m = \tau + m'$, $dm = d\tau$ gives

$$\underline{\underline{II}} = \frac{1}{2} \int_0^\infty dm' \int_0^\infty Q_{APd}(\tau)\, \tau\, f_d(\tau)\, f_d(m')\, K_d(\tau, m')\, d\tau$$

Renaming $\tau = m$

$$\underline{\underline{II}} = \frac{1}{2} \int_0^\infty \int_0^\infty Q_{APd}(m)\, m\, f_d(m)\, f_d(m')\, K_d(m, m')\, dm'\, dm$$

Putting the integrals together we obtain:

$$\int_0^\infty \left.\frac{\partial g_{APd}(m)}{\partial t}\right|_{d,coal} dm = \underline{I} + \underline{\underline{II}} + \underline{\underline{III}} = 0$$

$$= \frac{1}{2} \int_0^\infty \int_0^\infty Q_{APd}(m)\, m\, f_d(m)\, f_d(m')\, K_d(m, m')\, dm'\, dm$$

$$+ \frac{1}{2} \int_0^\infty \int_0^\infty Q_{APd}(m)\, m\, f_d(m)\, f_d(m')\, K_d(m, m')\, dm'\, dm$$

$$- \int_0^\infty \int_0^\infty Q_{APd}(m)\, m\, f_d(m)\, f_d(m')\, K_d(m, m')\, dm'\, dm$$

This implies that the aerosol particle mass inside the drops is conserved during this process.

Table of collection efficiencies for drops from radius a=1μm to 4096μm colliding with aerosol particles from radius $r=10^{-3}$μm to 6.5μm for a relative humidity of 100%.

relative humidity=100.0 %

	0.1000E+01	0.1587E+01	0.2520E+01	0.4000E+01	0.6350E+01	0.1008E+02	0.1600E+02	0.2540E+02	0.4032E+02
0.1000E-02	0.5220E+05	0.1390E+05	0.3280E+04	0.7750E+03	0.1830E+03	0.4320E+02	0.1020E+02	0.2910E+01	0.1080E+01
0.1587E-02	0.1260E+05	0.3730E+04	0.9850E+03	0.2600E+03	0.6870E+02	0.1820E+02	0.4800E+01	0.1500E+01	0.5360E+00
0.2520E-02	0.3380E+04	0.1070E+04	0.3060E+03	0.8720E+02	0.2490E+02	0.7100E+01	0.2030E+01	0.6760E+00	0.2390E+00
0.4000E-02	0.1140E+04	0.3720E+03	0.1090E+03	0.3220E+02	0.9500E+01	0.2800E+01	0.8240E+00	0.2820E+00	0.1020E+00
0.6350E-02	0.3660E+03	0.1250E+03	0.3860E+02	0.1200E+02	0.3700E+01	0.1140E+01	0.3540E+00	0.1280E+00	0.4770E-01
0.1008E-01	0.1130E+03	0.4100E+02	0.1350E+02	0.4470E+01	0.1470E+01	0.4870E+00	0.1610E+00	0.6300E-01	0.2450E-01
0.1600E-01	0.3650E+02	0.1400E+02	0.4960E+01	0.1750E+01	0.6180E+00	0.2180E+00	0.7720E-01	0.3080E-01	0.1290E-01
0.2540E-01	0.1340E+02	0.5410E+01	0.2020E+01	0.7520E+00	0.2800E+00	0.1040E+00	0.3900E-01	0.1600E-01	0.6940E-02
0.4032E-01	0.5480E+01	0.2310E+01	0.8970E+00	0.3490E+00	0.1360E+00	0.5280E-01	0.2050E-01	0.8770E-02	0.3780E-02
0.6400E-01	0.4280E-02	0.3870E-02	0.3470E-02	0.3100E-02	0.2780E-02	0.2490E-02	0.2230E-02	0.1820E-02	0.1210E-02
0.1016E+00	0.4450E-07	0.1430E-06	0.5130E-06	0.1840E-05	0.6580E-05	0.2360E-04	0.8420E-04	0.1990E-03	0.2750E-03
0.1613E+00	0.2130E-07	0.7440E-07	0.2920E-06	0.1140E-05	0.4490E-05	0.1760E-04	0.6880E-04	0.1440E-03	0.1840E-03
0.2560E+00	0.8090E-07	0.2160E-06	0.6300E-06	0.1840E-05	0.5370E-05	0.1570E-04	0.4570E-04	0.1130E-03	0.3020E-03
0.4064E+00	0.8630E-11	0.6920E-10	0.6720E-09	0.6530E-08	0.6350E-07	0.6170E-06	0.5990E-05	0.5910E-04	0.2090E-03
0.6451E+00	0.1540E-08	0.5460E-08	0.2170E-07	0.8640E-07	0.3440E-06	0.1370E-05	0.5440E-05	0.2170E-04	0.9380E-04
0.1024E+01	0.6670E-16	0.1280E-14	0.3230E-13	0.8150E-12	0.2050E-10	0.5170E-09	0.1300E-07	0.3280E-06	0.8270E-05
0.1625E+01	0.9310E-24	0.1420E-21	0.3430E-19	0.8290E-17	0.2000E-14	0.4830E-12	0.1170E-09	0.2820E-07	0.6820E-05
0.2580E+01	0.8990E-37	0.7920E-33	0.1600E-28	0.3230E-24	0.6530E-20	0.1320E-15	0.2670E-11	0.5390E-07	0.8160E-03
0.4096E+01	0.2750E-30	0.1360E-26	0.1460E-22	0.1560E-18	0.1670E-14	0.1780E-10	0.1910E-06	0.2020E-02	0.2030E+00
0.6502E+01	0.1360E-33	0.2380E-29	0.1020E-24	0.4360E-20	0.1860E-15	0.7970E-11	0.3410E-06	0.1430E-01	0.7220E+00

0.6400E+02	0.1016E+03	0.1613E+03	0.2560E+03	0.4064E+03	0.6451E+03	0.1024E+04	0.1625E+04	0.2580E+04	0.4096E+04
0.4390E+00	0.2010E+00	0.1100E+00	0.6330E-01	0.3660E-01	0.8150E-02	0.1680E-02	0.3940E-03	0.5910E-04	0.1320E-04
0.2240E+00	0.1070E+00	0.6080E-01	0.3640E-01	0.2360E-01	0.7310E-02	0.1670E-02	0.3950E-03	0.5920E-04	0.1330E-04
0.1050E+00	0.5200E-01	0.2980E-01	0.1860E-01	0.1230E-01	0.5950E-02	0.1660E-02	0.3960E-03	0.5940E-04	0.1330E-04
0.4750E-01	0.2430E-01	0.1360E-01	0.8850E-02	0.5450E-02	0.4460E-02	0.1640E-02	0.3990E-03	0.5970E-04	0.1340E-04
0.2330E-01	0.1200E-01	0.6730E-02	0.4480E-02	0.2660E-02	0.3890E-02	0.1640E-02	0.4020E-03	0.6040E-04	0.1350E-04
0.1240E-01	0.6350E-02	0.3590E-02	0.2400E-02	0.1450E-02	0.3930E-02	0.1650E-02	0.4060E-03	0.6120E-04	0.1380E-04
0.6760E-02	0.3480E-02	0.2010E-02	0.1310E-02	0.9780E-03	0.3980E-02	0.1680E-02	0.4150E-03	0.6280E-04	0.1420E-04
0.3670E-02	0.1930E-02	0.1150E-02	0.7260E-03	0.5650E-03	0.4080E-02	0.1730E-02	0.4300E-03	0.6570E-04	0.1490E-04
0.1970E-02	0.1080E-02	0.6800E-03	0.4100E-03	0.2790E-03	0.4220E-02	0.1800E-02	0.4520E-03	0.6980E-04	0.1600E-04
0.7160E-03	0.3500E-03	0.2380E-03	0.2670E-03	0.3890E-03	0.4460E-02	0.1930E-02	0.4910E-03	0.7710E-04	0.1790E-04
0.2070E-03	0.8290E-04	0.6220E-04	0.2010E-03	0.1270E-02	0.4860E-02	0.2130E-02	0.5540E-03	0.8910E-04	0.2110E-04
0.1700E-03	0.9360E-04	0.7490E-04	0.1850E-03	0.2480E-02	0.5630E-02	0.2550E-02	0.6860E-03	0.1160E-03	0.2830E-04
0.2120E-03	0.1210E-03	0.1000E-03	0.1320E-03	0.2600E-02	0.6940E-02	0.3270E-02	0.9300E-03	0.1670E-03	0.4290E-04
0.2310E-03	0.1650E-03	0.1380E-03	0.1130E-03	0.1580E-02	0.9730E-02	0.4900E-02	0.1520E-02	0.3030E-03	0.8420E-04
0.2340E-03	0.2290E-03	0.2100E-03	0.1740E-03	0.6440E-03	0.1670E-01	0.9400E-02	0.3350E-02	0.7910E-03	0.2490E-03
0.2030E-03	0.5270E-03	0.7130E-03	0.9270E-03	0.2980E-02	0.4130E-01	0.2770E-01	0.1240E-01	0.3890E-02	0.1520E-02
0.1580E-02	0.1980E-01	0.3640E-01	0.4800E-01	0.7890E-01	0.1830E+00	0.1650E+00	0.1080E+00	0.5360E-01	0.2950E-01
0.4820E-01	0.2450E+00	0.3720E+00	0.4360E+00	0.4730E+00	0.4930E+00	0.4970E+00	0.4140E+00	0.2990E+00	0.2250E+00
0.4270E+00	0.5860E+00	0.6690E+00	0.7080E+00	0.7300E+00	0.7460E+00	0.7380E+00	0.6790E+00	0.5880E+00	0.5200E+00
0.8050E+00	0.8690E+00	0.9020E+00	0.9150E+00	0.9320E+00	0.1040E+01	0.9270E+00	0.9040E+00	0.8710E+00	0.8420E+00

Table of collection efficiencies for drops from radius a=1μm to 4096μm colliding with aerosol particles from radius $r=10^{-3}$ μm to 6.5μm for a relative humidity of 95%.

relative humidity= 95.0 %

	0.1000E+01	0.1587E+01	0.2520E+01	0.4000E+01	0.6350E+01	0.1008E+02	0.1600E+02	0.2540E+02	0.4032E+02
0.1000E-02	0.5220E+05	0.1390E+05	0.3280E+04	0.7750E+03	0.1830E+03	0.4320E+02	0.1020E+02	0.2910E+01	0.1080E+01
0.1587E-02	0.1260E+05	0.3730E+04	0.9850E+03	0.2600E+03	0.6870E+02	0.1820E+02	0.4800E+01	0.1500E+01	0.5360E+00
0.2520E-02	0.3410E+04	0.1090E+04	0.3110E+03	0.8900E+02	0.2550E+02	0.7300E+01	0.2090E+01	0.7000E+00	0.2470E+00
0.4000E-02	0.1170E+04	0.3860E+03	0.1150E+03	0.3430E+02	0.1020E+02	0.3040E+01	0.9060E+00	0.3140E+00	0.1130E+00
0.6350E-02	0.4390E+03	0.1500E+03	0.4630E+02	0.1430E+02	0.4440E+01	0.1370E+01	0.4250E+00	0.1540E+00	0.5700E-01
0.1008E-01	0.1880E+03	0.6610E+02	0.2110E+02	0.6720E+01	0.2140E+01	0.6840E+00	0.2180E+00	0.8230E-01	0.3190E-01
0.1600E-01	0.1490E+03	0.5010E+02	0.1530E+02	0.4650E+01	0.1420E+01	0.4320E+00	0.1320E+00	0.4770E-01	0.1890E-01
0.2540E-01	0.1390E+03	0.4460E+02	0.1290E+02	0.3740E+01	0.1080E+01	0.3130E+00	0.9070E-01	0.3040E-01	0.1190E-01
0.4032E-01	0.1450E+03	0.4440E+02	0.1220E+02	0.3350E+01	0.9200E+00	0.2530E+00	0.6950E-01	0.2120E-01	0.7880E-02
0.6400E-01	0.1160E+03	0.3370E+02	0.8770E+01	0.2280E+01	0.5940E+00	0.1550E+00	0.4030E-01	0.1100E-01	0.3650E-02
0.1016E+00	0.7850E+02	0.2190E+02	0.5420E+01	0.1340E+01	0.3330E+00	0.8250E-01	0.2040E-01	0.5050E-02	0.1430E-02
0.1613E+00	0.1090E+03	0.3060E+02	0.7630E+01	0.1900E+01	0.4740E+00	0.1180E+00	0.2950E-01	0.7350E-02	0.2060E-02
0.2560E+00	0.1270E+03	0.3580E+02	0.9010E+01	0.2270E+01	0.5710E+00	0.1440E+00	0.3610E-01	0.9130E-02	0.2560E-02
0.4064E+00	0.1090E+03	0.3110E+02	0.7870E+01	0.1990E+01	0.5040E+00	0.1280E+00	0.3230E-01	0.8190E-02	0.2290E-02
0.6451E+00	0.7770E+02	0.2210E+02	0.5590E+01	0.1410E+01	0.3580E+00	0.9060E-01	0.2290E-01	0.5730E-02	0.1560E-02
0.1024E+01	0.5550E+00	0.2480E+00	0.1020E+00	0.4220E-01	0.1740E-01	0.7210E-02	0.2970E-02	0.1060E-02	0.3060E-03
0.1625E+01	0.1270E-18	0.5750E-17	0.3680E-15	0.2350E-13	0.1500E-11	0.9610E-10	0.6140E-08	0.3730E-06	0.2070E-04
0.2580E+01	0.9010E-37	0.7940E-33	0.1600E-28	0.3240E-24	0.6550E-20	0.1320E-15	0.2670E-11	0.5400E-07	0.8160E-03
0.4096E+01	0.2750E-30	0.1360E-26	0.1460E-22	0.1560E-18	0.1670E-14	0.1780E-10	0.1910E-06	0.2020E-02	0.2030E+00
0.6502E+01	0.1360E-33	0.2380E-29	0.1020E-24	0.4360E-20	0.1860E-15	0.7970E-11	0.3410E-06	0.1430E-01	0.7220E+00

0.6400E+02	0.1016E+03	0.1613E+03	0.2560E+03	0.4064E+03	0.6451E+03	0.1024E+04	0.1625E+04	0.2580E+04	0.4096E+04
0.4390E+00	0.2010E+00	0.1100E+00	0.6330E-01	0.3660E-01	0.8150E-02	0.1680E-02	0.3940E-03	0.5910E-04	0.1320E-04
0.2240E+00	0.1070E+00	0.6080E-01	0.3640E-01	0.2360E-01	0.7310E-02	0.1670E-02	0.3950E-03	0.5920E-04	0.1330E-04
0.1090E+00	0.5430E-01	0.3140E-01	0.1950E-01	0.1310E-01	0.5950E-02	0.1660E-02	0.3960E-03	0.5940E-04	0.1330E-04
0.5390E-01	0.2750E-01	0.1600E-01	0.1020E-01	0.6510E-02	0.4460E-02	0.1640E-02	0.3990E-03	0.5970E-04	0.1340E-04
0.2800E-01	0.1440E-01	0.8430E-02	0.5540E-02	0.3700E-02	0.3890E-02	0.1640E-02	0.4020E-03	0.6040E-04	0.1350E-04
0.1540E-01	0.7780E-02	0.4630E-02	0.3130E-02	0.2350E-02	0.3930E-02	0.1650E-02	0.4060E-03	0.6120E-04	0.1380E-04
0.8770E-02	0.4360E-02	0.2700E-02	0.1760E-02	0.1290E-02	0.3980E-02	0.1680E-02	0.4150E-03	0.6280E-04	0.1420E-04
0.5280E-02	0.2600E-02	0.1620E-02	0.1020E-02	0.7250E-03	0.4080E-02	0.1730E-02	0.4300E-03	0.6570E-04	0.1490E-04
0.3340E-02	0.1650E-02	0.9980E-03	0.6110E-03	0.4210E-03	0.4220E-02	0.1800E-02	0.4520E-03	0.6980E-04	0.1600E-04
0.1500E-02	0.6880E-03	0.3980E-03	0.3850E-03	0.5360E-03	0.4460E-02	0.1930E-02	0.4910E-03	0.7710E-04	0.1790E-04
0.5710E-03	0.2330E-03	0.1270E-03	0.2640E-03	0.1320E-02	0.4860E-02	0.2130E-02	0.5540E-03	0.8910E-04	0.2110E-04
0.7840E-03	0.3190E-03	0.1680E-03	0.2650E-03	0.2590E-02	0.5630E-02	0.2550E-02	0.6860E-03	0.1160E-03	0.2830E-04
0.9490E-03	0.3820E-03	0.2070E-03	0.2170E-03	0.2880E-02	0.6940E-02	0.3270E-02	0.9300E-03	0.1670E-03	0.4290E-04
0.8500E-03	0.3500E-03	0.2200E-03	0.1650E-03	0.1740E-02	0.9730E-02	0.4900E-02	0.1520E-02	0.3030E-03	0.8420E-04
0.6330E-03	0.3360E-03	0.2640E-03	0.2090E-03	0.6830E-03	0.1670E-01	0.9400E-02	0.3350E-02	0.7910E-03	0.2490E-03
0.4920E-03	0.6180E-03	0.7720E-03	0.9890E-03	0.3080E-02	0.4130E-01	0.2770E-01	0.1240E-01	0.3890E-02	0.1520E-02
0.2060E-02	0.2080E-01	0.3730E-01	0.4890E-01	0.7960E-01	0.1830E+00	0.1650E+00	0.1080E+00	0.5360E-01	0.2950E-01
0.4820E-01	0.2450E+00	0.3720E+00	0.4360E+00	0.4730E+00	0.4930E+00	0.4970E+00	0.4140E+00	0.2990E+00	0.2250E+00
0.4270E+00	0.5860E+00	0.6690E+00	0.7080E+00	0.7300E+00	0.7460E+00	0.7380E+00	0.6790E+00	0.5880E+00	0.5200E+00
0.8050E+00	0.8690E+00	0.9020E+00	0.9150E+00	0.9320E+00	0.1040E+01	0.9270E+00	0.9040E+00	0.8710E+00	0.8420E+00

Table of collection efficiencies for drops from radius a=1μm to 4096μm colliding with aerosol particles from radius $r=10^{-3}$ μm to 6.5μm for a relative humidity of 75%.

relative humidity= 75.0 %

	0.1000E+01	0.1587E+01	0.2520E+01	0.4000E+01	0.6350E+01	0.1008E+02	0.1600E+02	0.2540E+02	0.4032E+02
0.1000E-02	0.5210E+05	0.1390E+05	0.3280E+04	0.7740E+03	0.1830E+03	0.4320E+02	0.1020E+02	0.2910E+01	0.1080E+01
0.1587E-02	0.1250E+05	0.3700E+04	0.9800E+03	0.2590E+03	0.6860E+02	0.1820E+02	0.4810E+01	0.1500E+01	0.5360E+00
0.2520E-02	0.3700E+04	0.1180E+04	0.3370E+03	0.9660E+02	0.2770E+02	0.7920E+01	0.2270E+01	0.7350E+00	0.2560E+00
0.4000E-02	0.1530E+04	0.5030E+03	0.1490E+03	0.4420E+02	0.1310E+02	0.3880E+01	0.1150E+01	0.3620E+00	0.1250E+00
0.6350E-02	0.8660E+03	0.2840E+03	0.8440E+02	0.2510E+02	0.7440E+01	0.2210E+01	0.6550E+00	0.2070E+00	0.7070E-01
0.1008E-01	0.6830E+03	0.2180E+03	0.6260E+02	0.1800E+02	0.5170E+01	0.1490E+01	0.4270E+00	0.1380E+00	0.4700E-01
0.1600E-01	0.8810E+03	0.2640E+03	0.7070E+02	0.1900E+02	0.5080E+01	0.1360E+01	0.3650E+00	0.1080E+00	0.3540E-01
0.2540E-01	0.1040E+04	0.2980E+03	0.7660E+02	0.1970E+02	0.5060E+01	0.1300E+01	0.3340E+00	0.9210E-01	0.2910E-01
0.4032E-01	0.1080E+04	0.3060E+03	0.7760E+02	0.1970E+02	0.4980E+01	0.1260E+01	0.3200E+00	0.8440E-01	0.2570E-01
0.6400E-01	0.7570E+03	0.2120E+03	0.5290E+02	0.1320E+02	0.3290E+01	0.8210E+00	0.2050E+00	0.5230E-01	0.1510E-01
0.1016E+00	0.4140E+03	0.1150E+03	0.2820E+02	0.6940E+01	0.1710E+01	0.4210E+00	0.1040E+00	0.2590E-01	0.7060E-02
0.1613E+00	0.5390E+03	0.1520E+03	0.3800E+02	0.9540E+01	0.2390E+01	0.5990E+00	0.1500E+00	0.3790E-01	0.1060E-01
0.2560E+00	0.6210E+03	0.1770E+03	0.4490E+02	0.1140E+02	0.2890E+01	0.7340E+00	0.1860E+00	0.4720E-01	0.1340E-01
0.4064E+00	0.5400E+03	0.1550E+03	0.3950E+02	0.1010E+02	0.2580E+01	0.6590E+00	0.1680E+00	0.4260E-01	0.1220E-01
0.6451E+00	0.3880E+03	0.1110E+03	0.2830E+02	0.7210E+01	0.1840E+01	0.4680E+00	0.1190E+00	0.3060E-01	0.8680E-02
0.1024E+01	0.2000E+01	0.9380E+00	0.4100E+00	0.1790E+00	0.7830E-01	0.3420E-01	0.1500E-01	0.6450E-02	0.2970E-02
0.1625E+01	0.1910E-18	0.8770E-17	0.5720E-15	0.3730E-13	0.2440E-11	0.1590E-09	0.1040E-07	0.6730E-06	0.4460E-04
0.2580E+01	0.9020E-37	0.7940E-33	0.1600E-28	0.3240E-24	0.6550E-20	0.1320E-15	0.2670E-11	0.5400E-07	0.8160E-03
0.4096E+01	0.2750E-30	0.1360E-26	0.1460E-22	0.1560E-18	0.1670E-14	0.1780E-10	0.1910E-06	0.2020E-02	0.2030E+00
0.6502E+01	0.1360E-33	0.2380E-29	0.1020E-24	0.4360E-20	0.1860E-15	0.7970E-11	0.3410E-06	0.1430E-01	0.7220E+00

0.6400E+02	0.1016E+03	0.1613E+03	0.2560E+03	0.4064E+03	0.6451E+03	0.1024E+04	0.1625E+04	0.2580E+04	0.4096E+04
0.4390E+00	0.2010E+00	0.1100E+00	0.6330E-01	0.3660E-01	0.8150E-02	0.1680E-02	0.3940E-03	0.5910E-04	0.1320E-04
0.2240E+00	0.1070E+00	0.6080E-01	0.3640E-01	0.2360E-01	0.7310E-02	0.1670E-02	0.3950E-03	0.5920E-04	0.1330E-04
0.1120E+00	0.5540E-01	0.3200E-01	0.1970E-01	0.1330E-01	0.5950E-02	0.1660E-02	0.3960E-03	0.5940E-04	0.1330E-04
0.5760E-01	0.2930E-01	0.1690E-01	0.1060E-01	0.6920E-02	0.4460E-02	0.1640E-02	0.3990E-03	0.5970E-04	0.1340E-04
0.3230E-01	0.1680E-01	0.9340E-02	0.5810E-02	0.4050E-02	0.3890E-02	0.1640E-02	0.4020E-03	0.6040E-04	0.1350E-04
0.1990E-01	0.1040E-01	0.5430E-02	0.3290E-02	0.2630E-02	0.3930E-02	0.1650E-02	0.4060E-03	0.6120E-04	0.1380E-04
0.1380E-01	0.6780E-02	0.3460E-02	0.2030E-02	0.1570E-02	0.3980E-02	0.1680E-02	0.4150E-03	0.6280E-04	0.1420E-04
0.1030E-01	0.4820E-02	0.2440E-02	0.1400E-02	0.1050E-02	0.4080E-02	0.1730E-02	0.4300E-03	0.6570E-04	0.1490E-04
0.8140E-02	0.3680E-02	0.1880E-02	0.1080E-02	0.7910E-03	0.4220E-02	0.1800E-02	0.4520E-03	0.6980E-04	0.1600E-04
0.4680E-02	0.1990E-02	0.1010E-02	0.7360E-03	0.8930E-03	0.4470E-02	0.1930E-02	0.4910E-03	0.7710E-04	0.1790E-04
0.2300E-02	0.9000E-03	0.4500E-03	0.4850E-03	0.1470E-02	0.4860E-02	0.2130E-02	0.5540E-03	0.8910E-04	0.2110E-04
0.3490E-02	0.1370E-02	0.6710E-03	0.5740E-03	0.2940E-02	0.5630E-02	0.2550E-02	0.6860E-03	0.1160E-03	0.2830E-04
0.4440E-02	0.1750E-02	0.8440E-03	0.5650E-03	0.3500E-02	0.6940E-02	0.3270E-02	0.9300E-03	0.1670E-03	0.4290E-04
0.4030E-02	0.1580E-02	0.7510E-03	0.4350E-03	0.2200E-02	0.9730E-02	0.4900E-02	0.1520E-02	0.3030E-03	0.8420E-04
0.2890E-02	0.1120E-02	0.5480E-03	0.3750E-03	0.8600E-03	0.1670E-01	0.9400E-02	0.3350E-02	0.7910E-03	0.2490E-03
0.1570E-02	0.1030E-02	0.1030E-02	0.1260E-02	0.3480E-02	0.4130E-01	0.2770E-01	0.1240E-01	0.3890E-02	0.1520E-02
0.2980E-02	0.2420E-01	0.4060E-01	0.5250E-01	0.8250E-01	0.1830E+00	0.1650E+00	0.1080E+00	0.5360E-01	0.2950E-01
0.4820E-01	0.2450E+00	0.3720E+00	0.4360E+00	0.4730E+00	0.4930E+00	0.4970E+00	0.4140E+00	0.2990E+00	0.2250E+00
0.4270E+00	0.5860E+00	0.6690E+00	0.7080E+00	0.7300E+00	0.7460E+00	0.7380E+00	0.6790E+00	0.5880E+00	0.5200E+00
0.8050E+00	0.8690E+00	0.9020E+00	0.9150E+00	0.9320E+00	0.1040E+01	0.9270E+00	0.9040E+00	0.8710E+00	0.8420E+00

relative humidity= 50.0 %

	0.1000E+01	0.1587E+01	0.2520E+01	0.4000E+01	0.6350E+01	0.1008E+02	0.1600E+02	0.2540E+02	0.4032E+02
0.1000E-02	0.5220E+05	0.1390E+05	0.3280E+04	0.7750E+03	0.1830E+03	0.4320E+02	0.1020E+02	0.2910E+01	0.1080E+01
0.1587E-02	0.1260E+05	0.3730E+04	0.9850E+03	0.2600E+03	0.6870E+02	0.1820E+02	0.4800E+01	0.1500E+01	0.5360E+00
0.2520E-02	0.4450E+04	0.1390E+04	0.3900E+03	0.1100E+03	0.3080E+02	0.8640E+01	0.2430E+01	0.7830E+00	0.2700E+00
0.4000E-02	0.2590E+04	0.8100E+03	0.2270E+03	0.6390E+02	0.1790E+02	0.5030E+01	0.1410E+01	0.4400E+00	0.1460E+00
0.6350E-02	0.1960E+04	0.6022E+03	0.1660E+03	0.4570E+02	0.1260E+02	0.3460E+01	0.9530E+00	0.2800E+00	0.9270E-01
0.1008E-01	0.1920E+04	0.5690E+03	0.1510E+03	0.4010E+02	0.1060E+02	0.2820E+01	0.7490E+00	0.2060E+00	0.6890E-01
0.1600E-01	0.2080E+04	0.6043E+03	0.1560E+03	0.4050E+02	0.1050E+02	0.2710E+01	0.7030E+00	0.1850E+00	0.5720E-01
0.2540E-01	0.2230E+04	0.6360E+03	0.1620E+03	0.4100E+02	0.1040E+02	0.2640E+01	0.6710E+00	0.1740E+00	0.5130E-01
0.4032E-01	0.2350E+04	0.6590E+03	0.1650E+03	0.4120E+02	0.1030E+02	0.2570E+01	0.6430E+00	0.1680E+00	0.4900E-01
0.6400E-01	0.1650E+04	0.4570E+03	0.1120E+03	0.2770E+02	0.6800E+01	0.1670E+01	0.4120E+00	0.1060E+00	0.3040E-01
0.1016E+00	0.8990E+03	0.2460E+03	0.5970E+02	0.1450E+02	0.3520E+01	0.8560E+00	0.2080E+00	0.5240E-01	0.1450E-01
0.1613E+00	0.1170E+04	0.3260E+03	0.8070E+02	0.2000E+02	0.4960E+01	0.1230E+01	0.3050E+00	0.7770E-01	0.2190E-01
0.2560E+00	0.1300E+04	0.3710E+03	0.9380E+02	0.2370E+02	0.6010E+01	0.1520E+01	0.3850E+00	0.9790E-01	0.2760E-01
0.4064E+00	0.1180E+04	0.3330E+03	0.8420E+02	0.2130E+02	0.5370E+01	0.1360E+01	0.3420E+00	0.8760E-01	0.2500E-01
0.6451E+00	0.7740E+03	0.2233E+03	0.5720E+02	0.1470E+02	0.3780E+01	0.9700E+00	0.2490E+00	0.6360E-01	0.1800E-01
0.1024E+01	0.3720E+01	0.1770E+01	0.7810E+00	0.3450E+00	0.1530E+00	0.6750E-01	0.2990E-01	0.1300E-01	0.6240E-02
0.1625E+01	0.2340E-18	0.1080E-16	0.7050E-15	0.4620E-13	0.3020E-11	0.1980E-09	0.1290E-07	0.8440E-06	0.5680E-04
0.2580E+01	0.9020E-37	0.7940E-33	0.1600E-28	0.3240E-24	0.6550E-20	0.1320E-15	0.2670E-11	0.5400E-07	0.8160E-03
0.4096E+01	0.2750E-30	0.1360E-26	0.1460E-22	0.1560E-18	0.1670E-14	0.1780E-10	0.1910E-06	0.2020E-02	0.2030E+00
0.6502E+01	0.1360E-33	0.2380E-29	0.1020E-24	0.4360E-20	0.1860E-15	0.7970E-11	0.3410E-06	0.1430E-01	0.7220E+00

	0.6400E+02	0.1016E+03	0.1613E+03	0.2560E+03	0.4064E+03	0.6451E+03	0.1024E+04	0.1625E+04	0.2580E+04	0.4096E+04
0.4390E+00	0.2010E+00	0.1100E+00	0.6330E-01	0.3660E-01	0.8150E-02	0.1680E-02	0.3940E-03	0.5910E-04	0.1320E-04
0.2240E+00	0.1070E+00	0.6080E-01	0.3640E-01	0.2360E-01	0.7310E-02	0.1670E-02	0.3950E-03	0.5920E-04	0.1330E-04
0.1170E+00	0.5640E-01	0.3250E-01	0.2030E-01	0.1360E-01	0.5950E-02	0.1660E-02	0.3960E-03	0.5940E-04	0.1330E-04
0.6620E-01	0.3090E-01	0.1770E-01	0.1150E-01	0.7280E-02	0.4460E-02	0.1640E-02	0.3990E-03	0.5970E-04	0.1340E-04
0.4100E-01	0.1830E-01	0.9900E-02	0.6550E-02	0.4440E-02	0.3890E-02	0.1640E-02	0.4020E-03	0.6040E-04	0.1350E-04
0.2800E-01	0.1190E-01	0.5800E-02	0.3840E-02	0.3040E-02	0.3930E-02	0.1650E-02	0.4060E-03	0.6120E-04	0.1380E-04
0.2170E-01	0.9030E-02	0.4620E-02	0.2800E-02	0.2080E-02	0.3980E-02	0.1680E-02	0.4150E-03	0.6280E-04	0.1420E-04
0.1840E-01	0.7470E-02	0.3840E-02	0.2220E-02	0.1610E-02	0.4080E-02	0.1730E-02	0.4300E-03	0.6570E-04	0.1490E-04
0.1680E-01	0.6610E-02	0.3260E-02	0.1880E-02	0.1400E-02	0.4220E-02	0.1800E-02	0.4520E-03	0.6980E-04	0.1600E-04
0.9990E-02	0.3860E-02	0.1860E-02	0.1240E-02	0.1400E-02	0.4470E-02	0.1930E-02	0.4910E-03	0.7710E-04	0.1790E-04
0.4660E-02	0.1790E-02	0.8600E-03	0.7190E-03	0.1650E-02	0.4860E-02	0.2130E-02	0.5540E-03	0.8910E-04	0.2110E-04
0.7200E-02	0.2810E-02	0.1370E-02	0.9410E-03	0.3300E-02	0.5630E-02	0.2550E-02	0.6860E-03	0.1160E-03	0.2830E-04
0.9260E-02	0.3640E-02	0.1730E-02	0.1010E-02	0.4060E-02	0.6940E-02	0.3270E-02	0.9300E-03	0.1670E-03	0.4290E-04
0.8410E-02	0.3300E-02	0.1530E-02	0.8010E-03	0.2600E-02	0.9730E-02	0.4900E-02	0.1520E-02	0.3030E-03	0.8420E-04
0.6060E-02	0.2380E-02	0.1100E-02	0.6580E-03	0.1070E-02	0.1670E-01	0.9400E-02	0.3350E-02	0.7910E-03	0.2490E-03
0.3460E-02	0.1790E-02	0.1420E-02	0.1640E-02	0.4010E-02	0.4130E-01	0.2770E-01	0.1240E-01	0.3890E-02	0.1520E-02
0.3860E-02	0.2860E-01	0.4480E-01	0.5690E-01	0.8590E-01	0.1830E+00	0.1650E+00	0.1080E+00	0.5360E-01	0.2950E-01
0.4820E-01	0.2450E+00	0.3720E+00	0.4360E+00	0.4730E+00	0.4930E+00	0.4970E+00	0.4140E+00	0.2990E+00	0.2250E+00
0.4270E+00	0.5860E+00	0.6690E+00	0.7080E+00	0.7300E+00	0.7460E+00	0.7380E+00	0.6790E+00	0.5880E+00	0.5200E+00
0.8050E+00	0.8690E+00	0.9023E+00	0.9150E+00	0.9320E+00	0.1040E+01	0.9270E+00	0.9040E+00	0.8710E+00	0.8420E+00

Table of collection efficiencies for drops from radius a=1μm to 4096μm colliding with aerosol particles from radius r=10^{-3} μm to 6.5μm for a relative humidity of 50%.

Appendix B2:

Table of collection efficiencies for drops from radius a=0.5μm to 600μm colliding with drops as a function of the radius ratio (= collected drops radius / collector drop radius)

radius ratio	0.0500	0.1000	0.1500	0.2000	0.2500	0.3000	0.3500	0.4000	0.4500	0.5000
collector drop radius (μm)										
600.0	1.0000	1.0000	1.0000	1.0000	1.0000	1.0000	1.0000	1.0000	1.0000	1.0000
500.0	1.0000	1.0000	1.0000	1.0000	1.0000	1.0000	1.0000	1.0000	1.0000	1.0000
400.0	1.0000	1.0000	1.0000	1.0000	1.0000	1.0000	1.0000	1.0000	1.0000	1.0000
300.0	0.9700	1.0000	1.0000	1.0000	1.0000	1.0000	1.0000	1.0000	1.0000	1.0000
200.0	0.8700	0.9600	0.9800	1.0000	1.0000	1.0000	1.0000	1.0000	1.0000	1.0000
150.0	0.7700	0.9300	0.9700	0.9700	1.0000	1.0000	1.0000	1.0000	1.0000	1.0000
100.0	0.5000	0.7900	0.9100	0.9500	0.9500	0.9500	1.0000	1.0000	1.0000	1.0000
70.0	0.2000	0.5800	0.7500	0.8400	0.8800	0.9000	0.9200	0.9400	0.9500	0.9500
60.0	0.0500	0.4300	0.6400	0.7700	0.8400	0.8700	0.8900	0.9000	0.9100	0.9100
50.0	0.0050	0.4000	0.6000	0.7000	0.7800	0.8300	0.8600	0.8800	0.9000	0.9000
40.0	0.0010	0.0700	0.2800	0.5000	0.6200	0.6800	0.7400	0.7800	0.8000	0.8000
30.0	0.0001	0.0020	0.0200	0.0400	0.0850	0.1700	0.2700	0.4000	0.5000	0.5500
20.0	0.0001	0.0001	0.0050	0.0160	0.0220	0.0300	0.0430	0.0520	0.0640	0.0720
10.0	0.0001	0.0001	0.0001	0.0140	0.0170	0.0190	0.0220	0.0270	0.0300	0.0330
5.0	0.0005	0.0005	0.0005	0.0005	0.0005	0.0005	0.0005	0.0005	0.0005	0.0005
1.0	0.0005	0.0005	0.0005	0.0005	0.0005	0.0005	0.0005	0.0005	0.0005	0.0005
0.5	0.0005	0.0005	0.0005	0.0005	0.0005	0.0005	0.0005	0.0005	0.0005	0.0005

0.5500	0.6000	0.6500	0.7000	0.7500	0.8000	0.8500	0.9000	0.9500	1.0000
1.0000	1.0000	1.0000	1.0000	1.0000	1.0000	1.0000	1.0000	1.0000	1.0000
1.0000	1.0000	1.0000	1.0000	1.0000	1.0000	1.0000	1.0000	1.0000	1.0000
1.0000	1.0000	1.0000	1.0000	1.0000	1.0000	1.0000	1.0000	1.0000	1.0000
1.0000	1.0000	1.0000	1.0000	1.0000	1.0000	1.0200	1.0400	2.0300	4.0000
1.0000	1.0000	1.0000	1.0000	1.0000	1.0000	1.0200	1.0400	2.3000	4.0000
1.0000	1.0000	1.0000	1.0000	1.0000	1.0000	1.0200	1.0400	2.3000	4.0000
1.0000	1.0000	1.0000	1.0000	1.0000	1.0000	1.0200	1.0400	2.3000	4.0000
0.9500	0.9500	0.9500	0.9500	0.9700	1.0000	1.0200	1.0400	2.3000	4.0000
0.9100	0.9100	0.9100	0.9200	0.9300	0.9500	1.0000	1.0300	1.7000	3.0000
0.9000	0.9000	0.8900	0.8800	0.8800	0.8900	0.9200	1.0100	1.3000	2.3000
0.8000	0.7800	0.7700	0.7600	0.7700	0.7700	0.7800	0.7900	0.9500	1.4000
0.5800	0.5900	0.5800	0.5400	0.5100	0.4900	0.4700	0.4500	0.4700	0.5200
0.0790	0.0820	0.0800	0.0760	0.0670	0.0570	0.0480	0.0400	0.0330	0.0270
0.0350	0.0370	0.0380	0.0380	0.0370	0.0360	0.0350	0.0320	0.0290	0.0270
0.0005	0.0005	0.0005	0.0005	0.0005	0.0005	0.0005	0.0005	0.0005	0.0005
0.0005	0.0005	0.0005	0.0005	0.0005	0.0005	0.0005	0.0005	0.0005	0.0005
0.0005	0.0005	0.0005	0.0005	0.0005	0.0005	0.0005	0.0005	0.0005	0.0005

Appendix B3:

category in parcel model runs	category in 2-D model run	radius (μm)	percentage
44	32	143.7	0.0
45	33	161.3	0.2
46	34	181.0	0.3
47	35	203.2	0.5
48	36	228.1	1.0
49	37	256.0	1.5
50	38	287.4	2.0
51	39	322.5	2.5
52	40	362.0	4.0
53	41	406.4	5.5
54	42	456.1	7.5
55	43	512.0	9.0
56	44	574.7	10.0
57	45	645.1	12.0
58	46	724.1	10.0
59	47	812.7	9.0
60	48	912.3	7.5
61	49	1024.0	5.5
62	50	1149.4	4.0
63	51	1290.2	2.5
64	52	1448.2	2.0
65	53	1625.5	1.5
66	54	1824.6	1.0
67	55	2048.0	0.5
68	56	2298.8	0.3
69	57	2580.3	0.2

Table of percentage of drop break up mass placed in each category

List of symbols:

a	drop radius
a_c	critical drop radius for deactivation
a_s	staggered drop radius
a_w	equivalent radius of the drop water mass
A	parameter in the drop growth equation
A_D	parameter in Deirmendijan size distribution
A_e	parameter in equation for saturation vapor pressure
B	parameter in the drop growth equation
B_D	parameter in Deirmendijan size distribution
B_e	parameter in equation for saturation vapor pressure
c	concentration
c_G	concentration of sulfur in drops
c_4	concentration of sulfur (IV) in drops
c_6	concentration of sulfur (VI) in drops
c_{pa}	specific heat of air (p=const)
c_{pd}	specific heat of dry air (p=const)
C	parameter in equation for turbulent eddy mixing coefficient
C_{ph}	rate of phase change
C_1, C_2, C_3	constants
D	parameter in equation for activation size
Def	total deformation
D_g	diffusion coefficient for gas in air $=0.136+5.64\ 10^{-4}\ (T-T_o)$ $cm^2\ sec^{-1}$ for SO_2
D_{ij}	components of deformation tensor
D_v^*	diffusivity of water vapor in air
e_a	water vapor pressure
$e_{sat,w}$	saturation water vapor pressure

$\mathbf{e}$	unit vector
E	parameter in equation for activation size
E_{AP}	collection efficiency for drops colliding with unactivated aerosol particles
E_d	collection efficiency for drops colliding with drops
$E_1, .., E_5$	rain and aerosol scavenging efficiencies
f_{APa}	aerosol particle number density distribution function for aerosol particles in air
f_d	cloud drop number density distribution function
F	dummy function
F_v	ventilation coefficient
g	acceleration of gravity
g_{APa}	aerosol particle mass density distribution function for aerosol mass in unactivated aerosol particles
g_{APd}	aerosol particle mass density distribution function for aerosol particles in cloud water
g_{Ga}	mass of sulfur dioxide in air
g_{G4AP}	mass density distribution function for sulfur (IV) inside the water on an unactivated aerosol particle
g_{G6AP}	mass density distribution function for sulfur (VI) inside the water on an unactivated aerosol particle
g_{G4d}	mass density distribution function for sulfur (IV) in cloud water
g_{G6d}	mass density distribution function for sulfur (VI) in cloud water
g_{Gd}	$= g_{G4d} + g_{G6d}$
g_w	drop water mass density distribution function
g_{wa}	mass density distribution function of water attached to unactivated aerosol particles
h_d	hour of the day
H	surface sensible heat flux
J	discretion parameter of the drop radius

JRS	resolution parameter of the drop radius
J_{max}	maximum J
$\mathbb{J}^L$	flux of total liquid water content
$\mathbb{J}^q$	heat flux
$\mathbb{J}^v$	flux of water vapor
$\mathbb{J}$	dissipation stress tensor
k_a^*	thermal conductivity of air
K	discretion parameter of the aerosol particle radius
KRS	resolution parameter of the aerosol particle radius
K_{max}	maximum K
K_{AP}	collection kernel of drops colliding with unactivated aerosol particles
K_d	collection kernel of drops colliding with drops
KK	alignment factor
K_H	Henry constant
K_H'	partition coefficient
K_m	turbulent eddy mixing coefficient
K'	oxidation rate
K_o	parameter in equation for turbulent eddy mixing coefficient
K_1, K_2, K_3	first, second and third dissociation constant
$\mathbb{k}$	vertical unit vector
L_v	latent heat of evaporation
L_{vo}	$=L_v(T_o)$
m	total mass of drop
m_{AP}	total mass of unactivated aerosol particle
$(m_{AP})_{eq}$	equilibrium mass of unactivated aerosol particle
m_N	nucleus mass in drop
m_s	mass of water-soluble component in dry aerosol particle

m_w	drop water mass
M_a	molecular weight of air
M_s	molecular weight of salt
M_w	molecular weight of water
M_{SO_2}	molecular weight of sulfur dioxide
n	number of iterations
n_d	number of day of the year
N_m	number of moles
N_{APa}	total number of unactivated aerosol particles in air per unit volume (*)
N_d	total number of drops per unit volume (*)
p	pressure
p_o	= 1000mb
pH	$=-\log [H^+]$
P_H	average surface sensible heat flux
P_Q	average surface latent heat flux
q_v	water vapor mixing ratio
Q	surface latent heat flux
Q_{APa}	mixing ratio of aerosol particle mass in unactivated aerosol particles
$\overline{Q}_{APa}$	total mass mixing ratio of aerosol particle mass in unactivated aerosol particles
Q_{APd}	mixing ratio of aerosol particle mass in drops
$\overline{Q}_{APd}$	total mass mixing ratio of aerosol particle mass in cloud water
Q_{G4d}	mixing ratio of sulfur (IV) in drops
Q_{G6d}	mixing ratio of sulfur (VI) in drops
r	radius of unactivated aerosol particle
r_c	critical radius of unactivated aerosol particle
r_{eq}	equilibrium radius of unactivated aerosol particle

r_N	equivalent radius of dry aerosol particle nucleus
r_{Nc}	nucleus radius of the particle with critical radius r
r_{100}	critical radius at 100% relative humidity
r_s	staggered aerosol particle radius
R	radius of air parcel
$\mathcal{R}$	universal gas constant
RH	relative humidity
R_v	gas constant of water vapor
R_d	gas constant of dry air
Ri	local Richardson number
$s_{v,w}$	supersaturation of water vapor = $e_a / e_{sat,w} - 1$
S	shortwave solar flux
S_o	solar constant
t	time
T	temperature
T_o	= 273.15K
T_v	virtual temperature
u	horizontal velocity
$\tilde{u}$	correction diffusion velocity
U	updraft velocity in parcel model
v	vertical velocity
w	velocity field
V	volume of drop
V_{AP}	volume of unactivated aerosol particle
V_N	volume of dry aerosol nucleus
V_w	volume of water mass on drop
V_∞	terminal velocity
w_{APa}	total aerosol particle mass in unactivated aerosol particles per unit volume (*)

w_{APd}	total aerosol particle mass in drops per unit volume (*)
w_{G4d}	total sulfur (IV) mass in drops per unit volume (*)
w_{G6d}	total sulfur (VI) mass in drops per unit volume (*)
w_{Gd}	$= w_{G4d} + w_{G6d}$ (*)
w_L	liquid water content of drops (*)
w_{LAP}	liquid water content of unactivated aerosol particles (*)
w_L^*	$= w_L + w_{LAP}$ (*)
w_v	water vapor content
$w_{v,sat}$	saturation water vapor field
W	washout ratio
x	horizontal coordinate
x_o	middle of computational domain (x-direction)
y	dummy variable
z	vertical coordinate
Z	zenith angle
α_D	parameter in Deirmendijan size distribution
α_H	parameter in equation for surface sensible heat flux
α_Q	parameter in equation for surface latent heat flux
β	parameter in equation for latent heat of evaporation
β_H	fraction of total energy that goes into Gaussian perturbation of the surface sensible heat flux
β_Q	fraction of total energy that goes into Gaussian perturbation of the surface latent heat flux
γ	parameter in equation of motion in parcel model
γ_D	parameter in Deirmendijan size distribution
Γ	gamma function
δ_g	gas film thickness
δ_{ij}	Kronecker delta function

Δy	numerical increment of y
Δ	$=\sqrt{\Delta x\, \Delta z}$
ε	composition of aerosol particle = m_s/m_N
θ	potential temperature
λ	sun declination angle
μ	entrainment factor
ν	number of ions
π	$=3.1415....$
ϱ	actual density of the drop
ϱ_a	density of air
ϱ_{AP}	actual density of unactivated aerosol particles
ϱ_{moist}	density of moist air
ϱ_N	density of dry aerosol particle nucleus
ϱ_w	density of water
σ_H	half-width of Gaussian perturbation in surface sensible heat flux
σ_Q	half-width of Gaussian perturbation in surface latent heat flux
$\sigma_{w,a}$	surface tension of water
τ	model time
τ_{ij}	components of stress tensor
φ	latitude
Φ	acceleration potential of gravity
Φ_r	hour angle
Φ_s	osmotic coefficient
ψ	dummy function
Ω	angular velocity vector of the earth

Subscripts:

a	air
AP	aerosol particle
d	drop
G	gas
G4	sulfur (IV)
G6	sulfur (VI)
$( )\|_{act}$	change due to activation of aerosol particles to drops
$( )\|_{con/eva}$	change due to condensation and/or evaporation
$( )\|_{AP,coll}$	change due to aerosol particle collection
$( )\|_{d,coal}$	change due to collision and coalescence of drops
$( )\|_{d,break}$	change due to drop break up
$( )\|_{uptake}$	change due to uptake of gas
$( )\|_{ox}$	change due to oxidation of uptaken gas
$\overline{\psi}$	mean value
ψ'	perturbation around the mean value $= \psi - \overline{\psi}$
$\widetilde{\psi}$	intermediate value
ψ^e	environmental value
[ ]	concentration
f	number (N) density distribution function $=dN/dy$ with y=mass in all equations with y=ln(radius) in all graphs
g	mass (w) density distribution function $=dw/dy$ with y=mass in all equations with y=ln(radius) in all graphs

(*) In some of the diagrams these quantities are displayed per unit mass of air

List of references:

Baboolal, L.B., H.R. Pruppacher, and J.H. Topalian, 1981: A sensitivity study of a theoretical model of SO_2 scavenging by water drops in air. J. Atmos. Sci., 38, 856-870

Barlow, A.K., and J. Latham, 1983: A laboratory study of the scavenging of sub-micron aerosol by charged raindrops. Quart. J. Roy. Meteor. Soc., 109, 763-770

Beard, K.V., and S.N. Grover, 1974: Numerical collision efficiencies for small raindrops colliding with micron size particles. J. Atmos. Sci., 31, 543-550

Berry, E.X., and R.L. Reinhardt, 1974a: An analysis of cloud drop growth by collection: Part I. Double distributions. J. Atmos. Sci., 31, 1814-1824

Berry, E.X., and R.L. Reinhardt, 1974b: An analysis of cloud drop growth by collection: Part II. Single initial distributions. J. Atmos. Sci., 31, 1825-1831

Berry, E.X., and R.L. Reinhardt, 1974c: An analysis of cloud drop growth by collection: Part III. Accretion and self-collection. J. Atmos. Sci., 31, 2118-2126

Berry, E.X., and R.L. Reinhardt, 1974d: An analysis of cloud drop growth by collection: Part IV. A new parameterization. J. Atmos. Sci., 31, 2127-2135

Best, A.C., 1950: The size distribution of raindrops. Quart. J. Roy. Meteorol. Soc., 76, 16-36

Brosset, C., 1978: Water soluble sulphur compounds in aerosols. Atmos. Envir., 12, 25-38

Carstens, J.C., and J.J. Martin, 1982: In-cloud scavenging by thermophoresis, diffusiophoresis and Brownian diffusion. J. Atmos. Sci., 39, 1124-1129

Chaumerliac, N., 1984: Evaluation des termes de captation dynamique dans un modele tridimensionnel a mesochelle de lessivage de l'atmosphere. Ph.D. thesis. Univ. Clermont. U.E.R. de Recherche Scientifique et Technique, 82pp

Clark, T.L., 1977: A small-scale dynamic model using a terrain-following coordinate transformation. J. Comput. Phys., 24, 186-215

Clark, T.L., 1979: Numerical simulations with a three-dimensional cloud model: lateral boundary condition experiments and multi-cellular severe storm simulations. J. Atmos. Sci., 36, 2191-2215

Clark, T.L., and R.D. Farley, 1984: Severe downslope windstorm calculations in two and three spatial dimensions using anelastic interactive grid nesting: a possible mechanism for gustiness. J. Atmos. Sci., 41, 329-350

Clark, T.L., and R. Gall, 1982: Three-dimensional numerical model simulations of airflow over mountainous terrain: a comparison with observations. Mon. Wea. Rev., 110, 766-791

Danielsen, E.F., R. Bleck and D.A. Morris, 1972: Hail growth by stochastic collection in a cumulus model. J. Atmos. Sci., 29, 135-155

Davis, M.H., 1972: Collisions of small droplets: Gas kinetic effects. J. Atmos. Sci., 29, 911-915

Deirmendijan, D., 1969: Electromagnetic Scattering on Spherical Polydispersions. American Elsevier, 290pp.

Flossmann, A.I., W.D. Hall and H.R. Pruppacher, 1985: A theoretical study of the wet removal of atmospheric pollutants. Part I: Redistribution of aerosol particles captured through nucleation and impaction scavenging by growing cloud drops. J. Atmos. Sci., 42, 583-606

Flossmann, A.I., and H.R. Pruppacher, 1986: A theoretical study of the wet removal of atmospheric pollutants. Part II: The uptake and redistribution of $(NH_4)_2SO_4$ particles and SO_2 gas simultaneously scavenged by growing cloud drops. submitted for publication J. Atmos. Sci.

Gatz, D.F. and A.N. Dingle, 1971: Trace substances in rain water: concentration variations during convective rains, and their interpretation. Tellus, 23, 14-27

Georgii, H.W., 1982: Global distribution of the acidity in precipitation. Deposition of Atmospheric Pollutants, H.W. Georgii and J. Pankrath eds., D. Reidel Publ. Co., Dordrecht, 55-66

Georgii, H.W., 1985: Atmospheric Pollution by SO_2 and Oxidants. Pollutants and Their Ecotoxicological Significance, H.W. Nuernberg ed., Wiley Publ., 3-10

Georgii, H.W., D. Jost, and W. Vitze, 1971: Konzentration und Groessenverteilung des Sulfataerosols in der unteren und mittleren Troposphaere. Berichte Inst. Meteor. Univ. Frankfurt, 23, 1-84

Georgii, H.W., and D. Woetzel, 1970: On the relation between drop size and concentration of trace gas elements in rainwater. J. Geophys. Res., 75, 1727-1731

Grover, S.N., H.R. Pruppacher and A.E. Hamielec, 1977: A numerical determination of the efficiency with which spherical aerosol particles collide with spherical water drops due to inertial impaction and phoretic and electric forces. J. Atmos. Sci., 34, 1655-1663

Hall, W.D., 1980: A detailed microphysical model within a two-dimensional dynamic framework: Model description and preliminary results. J. Atmos. Sci., 37, 2486-2507

Hampl, V., M. Kerker, D.D. Cooke and E. Matijevic, 1971: Scavenging of aerosol particles by a falling water droplet. J. Atmos. Sci., 28, 1211-1221

Hegg, D.A., and P.V. Hobbs, 1978: Oxidation of sulfur dioxide in aqueous systems with particular reference to the atmosphere. Atmos. Envir., 12, 241-253

Hegg, D.A., and P.V. Hobbs, 1981: Cloud water chemistry and the production of sulfates in clouds. Atmos. Envir., 15, 1597-1604

Hegg, D.A., and P.V. Hobbs, 1982: Measurements of sulfate production in natural clouds. Atmos. Envir., 16, 2663-2668

Hegg, D.A., and P.V. Hobbs, 1983: Preliminary measurements on the scavenging of sulfate and nitrate by clouds. Precipitation Scavenging, Dry Deposition, and Resuspension, Vol. I, Pruppacher et al. eds. Elsevier Publ. Co., New York, 78-89

Hegg, D.A., P.V. Hobbs, and L.F. Radke, 1980: A preliminary study of cloud chemistry. Preprints Cloud Phys. Conf., Clermont Ferrand, France, 7-10

Hegg, D.A., P.V. Hobbs, and L.F. Radke, 1984: Measurements of the scavenging of sulfate and nitrate in clouds. Atmos. Envir., 18, 1939-1946

Hidy, G.M., P.K. Mueller, and E.Y. Tong, 1978: Spatial and temporal distributions of airborne sulfate in parts of the United States. Atmos. Envir., 12, 735-752

Hindman, E.E., P.V. Hobbs, and L.F. Radke, 1977: Cloud condensation nucleus size distribution and their effect on cloud droplet size distribution. J. Atmos. Sci., 34, 951-956

Jonas, P.R., 1972: The collision efficiency of small drops. Quart. J. Roy. Meteor. Soc., 98, 681-683

Junge, C.E., 1963: Air chemistry and Radioactivity. Academic Press, New York, 382pp

Kerker, M., and V. Hampl, 1974: Scavenging of aerosol particles by a falling water drop and calculation of washout coefficients. J. Atmos. Sci., 31, 1368-1376

Kins, L., 1982: Temporal variation of chemical composition of rainwater during individual precipitation events. Deposition of Atmospheric Pollutants, H.W. Georgii and J. Pankrath eds., D. Reidel Publ. Co., Dordrecht, 87-96

Klett, J.D., and M.H. Davis, 1973: Theoretical collision efficiencies of cloud droplets at small Reynolds numbers. J. Atmos. Sci., 30, 107-117

Kuttler, W., 1982: Investigations about wet deposition of pollutants in an urban ecosystem. Deposition of Atmospheric Pollutants, H.W. Georgii and J. Pankrath eds., D. Reidel Publ. Co., Dordrecht, 97-113

Lai, K.Y., N. Dayan, and M. Kerker, 1978: Scavenging of aerosol particles by a falling water drop. J. Atmos. Sci., 35, 674-682

Lee, I.Y., G. Haenel, and H.R. Pruppacher, 1980: A numerical determination of the evolution of cloud drop spectra due to condensation on natural aerosol particles. J. Atmos. Sci., 37, 1839-1853

Leong, K.H., K.V. Beard, and H.T. Ochs, 1982: Laboratory measurements of particle capture by evaporating cloud drops. J. Atmos. Sci., 39, 1130-1140

Lilly, D.K., 1962: On the numerical simulation of buoyant convection. Tellus, 14, 148-172

Lin, C.L., and S.C. Lee, 1975: Collision efficiency of water drops in the atmosphere. J. Atmos. Sci., 32, 1412-1418

List, R.J., 1951: Smithsonian Meteorological Tables, 6th rev. ed. Smithsonian Institution Press, Washington, DC, 527pp

Martin, L.R., 1984: Kinetic studies of sulfite oxidations in aqueous solutions. SO_2, NO and NO_2 oxidation mechanisms, J.G. Calvert ed., 63-100, Butterworth Publ., London, 254pp

Mason, B.J., and P.R. Jonas, 1974: The evolution of droplet spectra and large droplets by condensation in cumulus clouds. Quart. J. Roy. Meteor. Soc., 100, 23-38

Meszaros, E., 1974: On the spring maximum of the concentration of trace constituents in the atmospheric precipitation. Tellus, 26, 402-407

Meszaros, E., 1978: Concentration of sulfur compounds in remote continental and oceanic areas. Atmos. Envir., 12, 699-705

Meszaros, E., 1981: Atmospheric Chemistry, Elsevier Publ. Co., New York, 201pp

Murakami, M., T. Kimura, Ch. Magono and K. Kikuchi, 1983: Observations of precipitation scavenging for water-soluble particles. J. Meteor. Soc. Japan, 61, 346-357

Ogura, Y., and N.A. Phillips, 1962: Scale analysis of deep and shallow convection in the atmosphere. J. Atmos. Sci., 19, 173-179

Perseke, C., 1982: Die trockene und feuchte Deposition saeurebildender atmosphaerischer Spurenelemente. Berichte Inst. Meteor. Univ. Frankfurt, 48, 174pp

Perseke, C., S. Beilke, and H.W. Georgii, 1980: Die Gesamtschwefeldeposition in der Bundesrepublik Deutschland auf der Grundlage von Messdaten des Jahres 1974. Berichte Inst. Meteor. Univ. Frankfurt, 40, 52pp

Pielke, R.A., 1984: Mesoscale meteorological modeling. Academic Press, 612pp

Pruppacher, H.R., and K.V. Beard, 1970: A wind tunnel investigation of the internal circulation and shape of water drops falling at terminal velocity in air. Quart. J. Roy. Meteor. Soc., 96, 247-256

Pruppacher, H.R., and R.L. Pitter, 1971: A semi-empirical determination of the shape of cloud and rain drops. J. Atmos. Sci., 28, 86-94

Pruppacher, H.R., and J.D. Klett, 1978: Microphysics of clouds and precipitation. D. Reidel, 714pp

Radke, L.F., 1983: Preliminary measurements of the size distribution of cloud interstitial aerosol. Precipitation Scavenging, Dry Deposition and Resuspension, Vol. I, Pruppacher et al. eds., Elsevier Publ. Co., New York, 71-78

Radke, L.F., P.V. Hobbs, and M.W. Eltgroth, 1980: Scavenging of aerosol particles by precipitation. J. Appl. Meteor., 19, 715-722

Schlamp, R.J., S.N. Grover, H.R. Pruppacher and A.E. Hamielec, 1976: A numerical investigation of the effect of electric charges and vertical external electric fields on the collision efficiency of cloud drops. J. Atmos. Sci., 33, 1747-1755

Scott, B.C., 1981: Sulfate Washout ratios in winter storms. J. Appl. Meteor., 20, 619-625

Shafrir, U., and T. Gal-Chen, 1971: A numerical study of collision efficiencies and coalescence parameters for droplet pairs with radii up to 300 microns. J. Atmos. Sci., 28, 741-751

Shaw, R.W., and R.J. Paur, 1983: Measurements of sulfur in gases and particles during sixteen months in the Ohio river valley. Atmos. Envir., 17, 1431-1438

Sillen, L.G., 1964: Stability constants of metal-ion complexes, Section 1-inorganic ligands, 2nd ed., J. Chem. Soc. (London), Special Publication No.17, 229-232

Silverman, B.A., and M. Glass, 1973: A numerical simulation of warm cumulus clouds: Part I. Parameterized vs non-parameterized microphysics. J. Atmos. Sci., 30, 1620-1637

Smagorinsky, J., 1963: General circulation experiments with the primitive equations. I:The basic experiment. Mon. Wea. Rev., 91, 99-164

Smolarkiewicz, P.K., 1983: A simple positive definite advection scheme with small implicit diffusion. Mon. Wea. Rev., 111, 479-486

Smolarkiewicz, P.K., 1984: Personal communications.

Spiegel, E.A., and G. Veronis, 1960: On the boussinesq approximation for a compressible fluid. The Astrophysical Journal, 131, 442-447

Thompson, P.D., 1968: A transformation of the stochastic equation for droplet coalescence. Proceedings of the International Conference on cloud physics, Aug.26-30, 1968, Toronto, Canada, 115-126

Walcek, C.J., and H.R. Pruppacher, 1984a: On the scavenging of SO_2 by cloud and raindrops: I. A theoretical study of SO_2 absorption and desorption by water drops in air. J. Atmos. Chem., 1, 269-289

Walcek, C.J., and H.R. Pruppacher, 1984b: On the scavenging of SO_2 by cloud and raindrops: III. A theoretical study of SO_2 washout by rain falling through a pollution plume, J. Atmos. Chem., 1, 307-324

Walcek, C.J., H.R. Pruppacher, J.H. Topalian, and S.K. Mitra, 1984: On the scavenging of SO_2 by cloud and raindrops, II. An experimental study of SO_2 absorption and desorption for water drops in air. J. Atmos. Chem., 1, 291-306

Wang, P.K., and H.R. Pruppacher, 1977: An experimental determination of the efficiency with which aerosol particles are collected by water drops in subsaturated air. J. Atmos. Sci., 34, 1664-1669

Wang, P.K., S.N. Grover, and H.R. Pruppacher, 1978: On the effect of electric charges on the scavenging of aerosol particles by clouds and small raindrops. J. Atmos. Sci., 35, 1735-1743